UNIVERSITY OF SOUTHAMPTON

FACULTY OF ENGINEERING, SCIENCE & MATHEMATICS

School of Ocean & Earth Science

Emiliania huxleyi and climate change: a genetic and biogeographic investigation of bloom dynamics for a key phytoplankton species in the global carbon cycle

by

Daria J. Hinz

Thesis for the degree of Doctor of Philosophy

October, 2010

ABSTRACT

FACULTY OF ENGINEERING, SCIENCE & MATHEMATICS
SCHOOL OF OCEAN & EARTH SCIENCES

Doctor of Philosophy

***EMILIANIA HUXLEYI* AND CLIMATE CHANGE: A GENETIC AND BIOGEOGRAPHIC INVESTIGATION OF BLOOM DYNAMICS FOR A KEY PHYTOPLANKTON SPECIES IN THE GLOBAL CARBON CYCLE**

by Daria J. Hinz

Emiliania huxleyi is a ubiquitous coccolithophore present throughout the global ocean and capable of forming large blooms with significant effects on the global carbon cycle. Developing our understanding of *E. huxleyi* ecology is necessary in order to better quantify *E. huxleyi*'s role in the present carbon cycle, and to predict its role in the future carbon cycle under climate change scenarios. Major gaps in the understanding of *E. huxleyi* ecology were addressed using (1) controlled mesocosm experiments in June 2008 in Raunefjord, Norway, to map population genetics of *E. huxleyi* blooms in relation to ecological pressures (viruses and rapid growth), (2) biogeographic sampling of nannoplankton (2 - 20 µm) in the SO, including *E. huxleyi*, to determine ecological pressures on *E. huxleyi* blooms *in situ* (environmental gradients), and (3) controlled iron (Fe) addition bioassay experiments in the SO to establish the role of Fe gradients in the nannoplankton community relative to the phytoplankton community.

During the mesocosm experiments, 279 individual *E. huxleyi* cells were isolated to establish clonal cultures, of which 143 were successfully genotyped using 5 microsatellite molecular markers. Both high gene diversity and two distinct genotypic populations were detected over the bloom time series and are strong evidence for a large reservoir of genetic variability within the *E. huxleyi* species concept, which may translate into phenotypic plasticity, such as differing levels of viral resistance. In the SO, the spatial and temporal biogeography of the three most numerous mineralizing nannoplankton groups, the coccolithophore *E. huxleyi*, the smaller (<20 µm) species of the diatom genus *Fragilariopsis,* and chrysophytes of the genus *Tetraparma* were defined using scanning electron microscopy (SEM) analysis in conjunction with an array of biological, physical, and chemical variables during two successive cruises to the Scotia Sea. Multivariate statistical analyses were used to identify the most influential environmental variables controlling mineralizing nannoplankton biogeography. Sea surface temperature (SST) and salinity were identified as primary variables and removed from the analysis, leaving frontal boundaries, macronutrient, and dFe concentrations significantly associated with a northern *E. huxleyi*-dominated community (group I; higher nutrients) and a southern *Tetraparma*- and *Fragilariopsis*-dominated community (group II; lower nutrients). Estimates of biomass indicated that the Scotia Sea mineralizing nannoplankton community formed a substantial part (on average 13%) of the total phytoplankton community. The results of bioassay Fe incubations indicated a response in medium and large diatoms and *E. huxleyi*, and a number of microplankton (20 – 200 µm) diatom species. Overall, the work contributes substantially to our understanding of the molecular population structure, extent of phenotypic plasticity, and environmental parameters affecting the key phytoplankton *E. huxleyi*.

List of Contents

List of Figures

Chapter 1

Chapter 2

Chapter 3

Chapter 4

List of Tables

List of Accompanying Materials

DECLARATION OF AUTHORSHIP

I, Daria J. Hinz

declare that the thesis entitled

Emiliania huxleyi and climate change: a genetic and biogeographic investigation of bloom dynamics for a key phytoplankton species in the global carbon cycle

and the work presented in the thesis are both my own, and have been generated by me as the result of my own original research. I confirm that:

- this work was done wholly or mainly while in candidature for a research degree at this University;
- where any part of this thesis has previously been submitted for a degree or any other qualification at this University or any other institution, this has been clearly stated;
- where I have consulted the published work of others, this is always clearly attributed;
- where I have quoted from the work of others, the source is always given. With the exception of such quotations, this thesis is entirely my own work;
- I have acknowledged all main sources of help;
- where the thesis is based on work done by myself jointly with others, I have made clear exactly what was done by others and what I have contributed myself;
- none of this work has been published before submission

Signed: ……..

Date:…….

Acknowledgements

Foremost I would like to thank my main supervisor Tom Bibby for his much appreciated support and advice throughout the course of this PhD. This research would also not have been possible without the direction and feedback provided by my PhD panel chair, Duncan Purdie, and my PhD co-supervisor, Débora Iglesias-Rodríguez.

Many thanks to the wonderful team at University of Bergen for all of their help with field work: Aud Larsen, Dale Evensen, Evy Foss Skjoldal, Jorun Egge, and Agnes Aadnesen. Thanks also to Lesley Hinks and Sylvia Diaper at the Human Genetics Division (University of Southampton) for their timely and expert assistance with the microsatellite analyses, to Joanna Craggs at Beckman Coulter UK for her microsatellite input, to Tatiana Rynearson for her extensive help and advice with population genetic analysis of phytoplankton populations using microsatellites, and to William Wilson for organizing and leading the 2008 Bergen mesocosm experiments. Financial support for the Bergen work was provided by a Worldwide Universities Network (WUN) International Research Mobility Scheme (IRMS) grant.

The work in the Southern Ocean would not have been possible without the expert support of the officers and crew of the RRS James Clark Ross. Thanks also to Richard Pearce (NOCS) for his SEM expertise and guidance, to Alex Poulton (NOCS) for his unparalleled support in identification of SEM samples and the application of multivariate statistical analyses to phytoplankton populations, to Mark Moore (NOCS) for his advice on analysis of FRRf data and Southern Ocean phytoplankton communities, and to Eric Achterberg for leading the collaboration between NOCS and the British Antarctic Survey (BAS). I am also grateful for the data provided in advance of publication by Elizabeth Jones, Hugh Venables, Rebecca Korb, Maria Nielsdóttir, and Geraint Tarling. Financial support for the Southern Ocean work was provided by a CGS grant (Antarctic Funding Initiative), a National Oceanography Centre PhD studentship, and an ORSAS grant (Higher Education Funding Council for England).

Finally, I cannot thank my family enough for their unrelenting support over the last four years. And to my colleagues and friends in Southampton thank you for all of the tea.

Abbreviations

AASW	Antarctic Surface Water
ACC	Antarctic Circumpolar Current
AFC	analytical flow cytometry
AZ	Antarctic Zone
BAS	British Antarctic Survey
BD	below detectable limit
$CaCO_3$	calcium carbonate
CCN	cloud condensation nuclei
Chl-*a*	chlorophyll-*a*
CMM	coccolith morphology motif
CO_2	carbon dioxide
COD-FISH	$CaCO_3$ optical detection with fluorescent *in situ* hybridization
CPC	coccolith-production compartment
CZ	Continental Zone
dFe	dissolved iron
DIC	dissolved inorganic carbon
DMS	dimethyl sulphide
DMSP	dimethylsulfoniopropionate
DNA	deoxyribonucleic acid
DSG	downstream of South Georgia Island
Fe	iron
FRR	fast repetition rate
FRRf	fast repetition rate fluorometry
F_{ST}	proportion of total genetic variance contained in a subpopulation
F_v/F_m	maximum PSII photochemical efficiency
G: N	clonal diversity
HCO_3^-	bicarbonate
H_E	expected number of heterozygotes given the HWE
HNLC	high nutrient low chlorophyll
H_O	observed number of heterozygotes given the HWE
HWE	Hardy-Weinberg Equilibrium
LGM	last glacial maximum
MDS	multidimensional scaling
MLD	mixed layer depth
Mya	million years ago
N	Nitrogen
NA	not applicable
NH_4^+	ammonium
NO_3^-	nitrate
NPP	net primary production
P	phosphorous
PCA	principal components analysis
pCO_2	partial pressure of carbon dioxide
PCR	polymerase chain reaction
PF	Polar Front
PFZ	Polar Front Zone
PIC	particulate inorganic carbon

PO_4^{3-}	phosphate
POC	particulate organic carbon
PSI	Photosystem I complex
PSII	Photosystem II complex
RAPD	Random Amplification of Polymorphic DNA
RCII	O_2-evolving reaction centre
SACCF	Southern Antarctic Circumpolar Current Front
SAF	sub-Antarctic Front
SALH	silicic acid leakage hypothesis
SAMS	Scottish Association for Marine Science
SAZ	sub-Antarctic Zone
SEM	scanning electron microscopy
SG	South Georgia
Si	silica
Si(OH)4	silicate
S-MAX	salinity maximum
S-MIN	salinity minimum
SOI	South Orkney Islands
SST	sea surface temperature
STF	Subtropical Front
TEP	transparent exopolymer particles
TPB	total phytoplankton biomass
TSA-FISH	tyramide signal amplification with fluorescent *in situ* hybridization
UCDW	Upper Circumpolar Deep Water
USG	upstream of South Georgia Island
Θ-MAX	temperature maximum
Θ-MIN	temperature minimum
Ω-aragonite	saturation state with respect to aragonite
Ω-calcite	saturation state with respect to calcite
σ_{PSII}	maximum PSII effective absorption cross section

1 Introduction

The marine system is the most expansive environment on Earth, with a volume 300 times greater than that of terrestrial and freshwater environments combined. This vast ocean territory hosts a plethora of life and plays a fundamental role in the biogeochemical processes which shape the Earth and its climate. The ocean's dominant primary producers are the phytoplankton, a group of unicellular photosynthetic organisms that are transported passively through the water column. Phytoplankton, which make up 1% of Earth's biomass, carry out more than 45% of the Earth's annual net primary production (Field et al., 1998; Falkowski et al., 2004) in the narrow euphotic zone, the depth to which sufficient light penetrates to power the reduction of carbon dioxide (CO_2) to organic carbon compounds (typically 200 m in the open ocean). Phytoplankton are responsible for producing an estimated 48.5 petagrams of carbon per year, or the equivalent of approximately half the annual global net primary production (NPP) (Field et al., 1998). Approximately 5,000 species of marine phytoplankton have been characterized in the ocean, and though many contribute to marine primary production, only a relatively small number of species contribute significantly to export production, i.e. production that escapes recycling in the surface ocean and is transported to depth (section 1.1). The relatively few species contributing to export production are usually divided into two functional groups of shell-forming phytoplankton, siliceous or silica-producing diatoms, and calcareous or calcium carbonate ($CaCO_3$)-producing coccolithophores, and one group of flagellated phytoplankton forming organic plates and mucilaginous colonies (including dinoflagellates and *Phaeocystis*) (Rost and Riebesell, 2004). Diatoms, coccolithophores, and dinoflagellates are responsible for the majority of export production. These three phytoplankton functional groups are all eukaryotes (cells with their genetic material (DNA) in a distinct nucleus) and contain plastids (a membrane-bound photosynthetic cell organelle similar to the chloroplast in plant cells). Each of these functional groups is derived from the red algae lineage (rhodophytes) that evolved approximately 1.5 billion years ago; however, they rose to ecological prominence approximately 250 to 65 million years ago (Falkowski et al., 2004).

The following chapters will consider the ecology and potential impacts on climate of several shell-forming phytoplankton functional groups, referred to from this point

forward as mineralizing phytoplankton, from the coccolithophore, diatom, and chrysophyte groups. These mineralizing species are of particular interest for two reasons: (1) because the efficient sinking of biogenic matter with mineralized skeletons is a major consideration in global biogeochemical cycles (McCave, 1975; Honjo, 1980; Honjo, 1996), and (2) because of their biogeography, certain species are either highly ubiquitous (for example the coccolithophore, *Emiliania huxleyi*) or they dominate in certain areas of the world's oceans (for example diatoms in iron-fertilized regions of the Southern Ocean; chapter 3). Changes in distribution patterns of mineralizing phytoplankton in the modern ocean can therefore be indicators of environmental change that may have impacts on global biogeochemical cycles.

1.1 Marine phytoplankton and climate

Levels of CO_2 and other greenhouse gases have increased dramatically in the atmosphere since 1750, resulting in a global temperature increase of 0.74°C (IPCC, 2007a). Between 1800 and 1994, an estimated 48% of anthropogenic emissions were absorbed by the oceans; consequently, the observed increase in atmospheric CO_2 concentration from 281 ppm in 1800 to 359 ppm in 1994 is two thirds less than it would be with no ocean CO_2 sink (Sabine et al., 2004). Concern about the extent to which the ocean will continue to absorb anthropogenic CO_2 and, as a result, serve as a negative feedback on global warming has led to an avid interest among politicians and scientists in the marine carbon cycle.

The ocean regulates atmospheric CO_2 through two processes, the solubility pump and the biological pump, both of which transport carbon species from the euphotic zone (upper ocean) to the deep ocean. The deep ocean is only exposed to the upper ocean approximately every 1,000 years, thus carbon species exported there can remain sequestered from interaction with the atmosphere for millennia (Sigman and Boyle, 2000; Figure 1). To put the importance of this export into perspective, the amount of inorganic carbon stored in the deep ocean is over 10 times larger than the combined reservoirs of atmospheric CO_2 (excluding recent anthropogenic changes), terrestrial biosphere CO_2, soil carbon CO_2, and upper ocean inorganic carbon (Holmen, 1992; Sigman and Boyle, 2000).

The solubility pump is related to the chemistry and circulation of the oceans: sea water cooled at high latitudes absorbs more CO_2 than warm sea water. Because this cold water is dense it sinks to the deep ocean, and the dissolved CO_2 is removed from the

surface ocean (IPCC, 2007b). In addition to this purely physico-chemical process, the biological pump, or the net sum of the biological processes that act to mediate any given element (in this case carbon), also sequesters CO_2 from the atmosphere, and it is this process which involves phytoplankton. The biological pump involves CO_2 fixation into organic carbon by photosynthesizing phytoplankton (Equation 1).

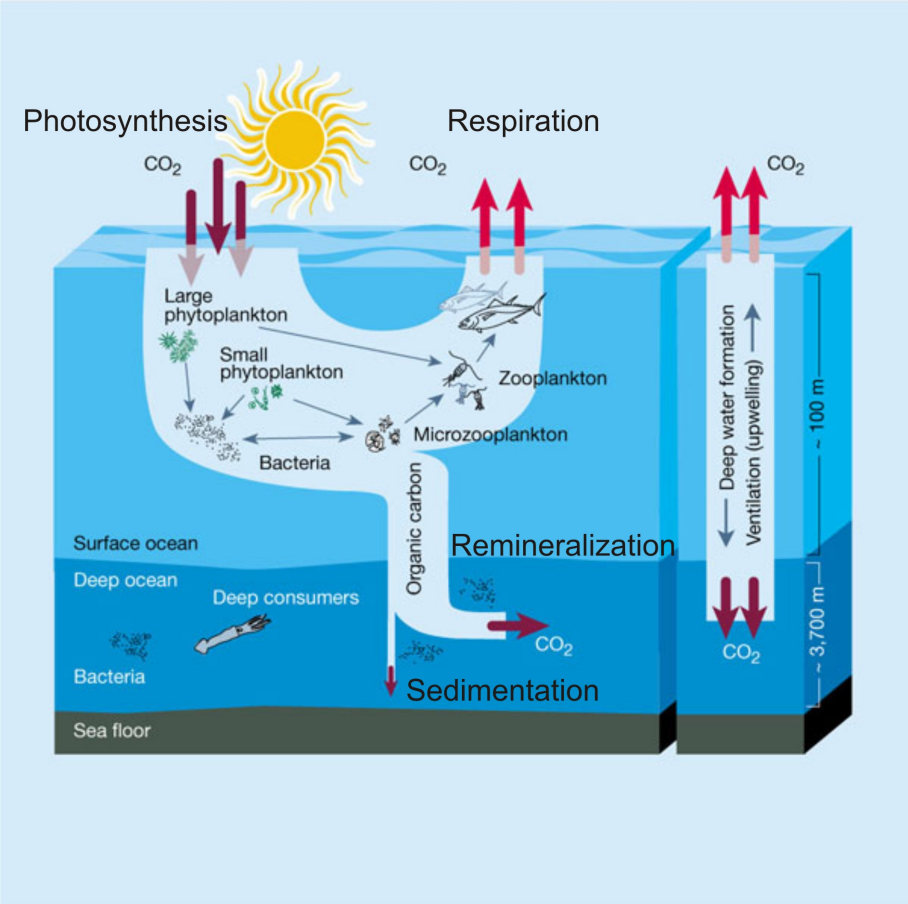

Figure 1. Schematic diagram of the ocean carbon cycle showing photosynthesis, respiration in the upper ocean, respiration at depth (remineralization), and burial in sediments (sedimentation) (modified from figure 1 in Chisholm et al. (2000)).

$$6CO_{2(g)} + 12H_2O_{(l)} + photons \xrightarrow{PHOTOSYNTHESIS} C_6H_{12}O_{6(aq)} + 6O_{2(g)} + 6H_2O_{(L)}$$
$$\xleftarrow{RESPIRATION}$$

Equation 1. Balanced equation showing the chemical reaction involved in photosynthesis.

Organic carbon particles result from phytoplankton fixation of inorganic carbon. Those that are not respired by heterotrophic organisms in the surface and intermediate ocean layers sink to the deep ocean. In the deep ocean, organic carbon compounds are either respired by heterotrophic organisms and remain for millennia in inorganic form, or they are buried in sediments and remain for geological time scales. Over time, the net result of photosynthesis, export and respiration at depth (remineralization), and export and burial at depth (sedimentation) is a reduction in the amount of dissolved CO_2 in the surface ocean (Figure 1). Because it is a highly soluble gas, a reduction of dissolved CO_2 in the surface ocean draws down CO_2 from the atmosphere and the ocean acts as a CO_2 sink. Over geological time scales, phytoplankton photosynthesis has been responsible for massive changes in global climate, with the evolution of photosynthesis approximately 2.8 billion years ago in the cyanobacteria and other groups of photosynthetic bacteria precipitating the switch from an anoxic (low-oxygen) to an oxic (oxygen-rich) environment (Morel et al., 1991; Des Marais, 2000).

1.1.1 **Mineralizing phytoplankton and the carbon cycle**

Mineralizing phytoplankton are an effective means of transporting organic carbon to the ocean floor due to the efficient sinking of their dense inorganic shells and any associated particulate organic carbon (POC) (McCave, 1975; Honjo, 1980; Honjo, 1996). This 'ballast effect' has been observed for diatoms, which possess dense siliceous skeletons and produce large amounts of transparent exopolymer particles (TEP), a group of particulate extracellular polysaccharides that drive aggregation of sinking POC (Passow, 2002; De La Rocha and Passow, 2007), and for coccolithophores, which produce dense calcareous skeletons in the form of calcareous liths which aggregate in zooplankton faecal pellets and feeding structures (De La Rocha and Passow, 2007). The ballast effect is more pronounced in the marine sediment record for biogenic calcite (the type of $CaCO_3$ produced by coccolithophores) than biogenic opal (from siliceous phytoplankton) (Armstrong et al., 2001; Francois et al., 2002; Klaas and Archer, 2002). De La Rocha et al. (2007), however, suggest the lack of correlation between biogenic silica and POC export is the result of variable biogenic silica to POC production ratios.

Uniquely, production of $CaCO_3$ by coccolithophores and other calcareous phytoplankton also produces particulate inorganic carbon (PIC), which sinks with POC and is buried in the deep ocean through the action of the biological pump. The

production of PIC, however, both removes and releases carbon from the surface ocean. The dissociation of aqueous CO_2 produces bicarbonate (HCO_3^-), which is the source of carbon for calcareous marine phytoplankton (Equation 2). The production of $CaCO_3$ in turn produces more aqueous CO_2 (Equation 3), such that for an idealized parcel of sea water, one unit of carbon fixed in the form of $CaCO_3$ releases 0.63 units of CO_2 (Rost and Riebesell, 2004).

$$CO_{2(g)} \leftrightarrow CO_{2(aq)} + H_2O_{(l)} \leftrightarrow H_2CO_3 \leftrightarrow H^+ + HCO_3^- \leftrightarrow H^+ + CO_3^{2-}$$

Equation 2. Dissociation of CO_2 produces bicarbonate (HCO_3^-) and carbonate (CO_3^{2-}) ions (Sarmiento and Gruber, 2006).

$$2HCO_3^- + Ca^{2+} \leftrightarrow CO_{2(aq)} + CaCO_3 + H_2O$$

Equation 3. Production of $CaCO_3$ results in the production of CO_2 (Sarmiento and Gruber, 2006).

The CO_2 production associated with calcification is called the carbonate counter pump and acts in opposition to the biological pump discussed in section 1.1 (Figure 2).

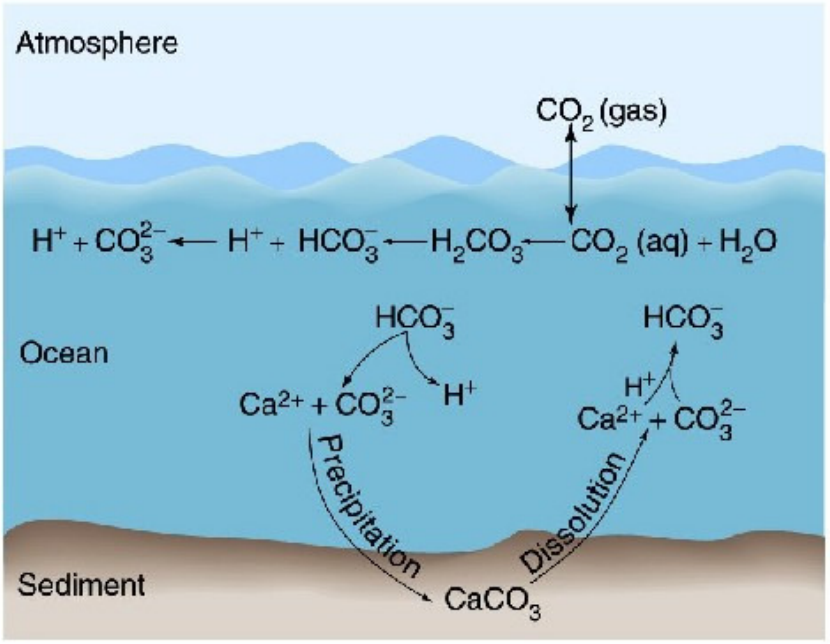

Figure 2. Schematic diagram of the carbonate counter pump, taken from F.J. Jochem (2007).

Determining the relative strengths of the biological pump and the carbonate counter pump is an important consideration in both local and global predictions of ocean atmosphere CO_2 exchange, and of particular relevance given the growing evidence that anthropogenic CO_2 inputs could fundamentally alter the ecology of calcareous phytoplankton, and as a result, their role in the global carbon cycle.

1.1.1.1 *Emiliania huxleyi*: a model calcareous phytoplankton

In order to better understand how calcareous phytoplankton affect the carbon cycle and are affected by changes in climate, it is necessary to consider specific ecological examples. Most of the recent work studying interactions between atmospheric CO_2, the organic carbon pump, and the carbonate counter pump has focused on *Emiliania huxleyi* (Lohmann, 1902). *E. huxleyi* is a species of coccolithophore (Order *Haptophyta*; Class *Prymnesiophyceae*), a group of eukaryotic autotrophs that dominate marine calcification (Rost and Riebesell, 2004) and are characterized by the formation of $CaCO_3$ scales called liths (Figure 3).

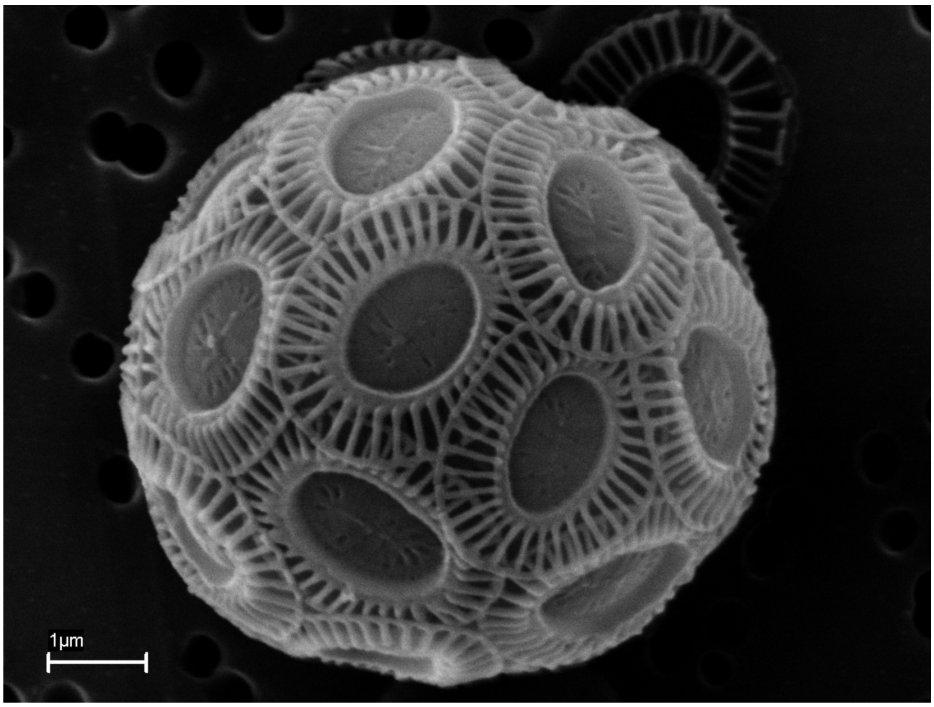

Figure 3. Scanning Electron Microscopy (SEM) image of *E. huxleyi* isolate DJB608 (Plymouth Culture Collection, MBA) showing the $CaCO_3$ exterior liths. SEM is a standard microscopy technique that uses a beam of electrons to measure surface topography (image taken by D. J. Hinz). The isolate was collected by D. J. Hinz during the mesocosm experiments detailed in chapter 2 (C-replete, day 14).

E. huxleyi first appeared approximately 270,000 years ago and came to dominate the coccolithophore assemblage in the world ocean approximately 85,000 to 73,000 years ago (Thierstein et al., 1977). Today, *E. huxleyi* is present in all the world's oceans, save the Arctic and high-latitude Southern Ocean, and forms huge blooms in subpolar nutrient-rich waters (Figure 4; Winter et al., 1994; Tyrell and Merico, 2004), and as such is considered a model organism.

Figure 4. SeaWiFS satellite image of an *E. huxleyi* bloom off Newfoundland on 21st July 1999, courtesy of *NERC Earth Observation Data Acquisition and Analysis Service (NEODAAS).*

E. huxleyi can be classified into five morphotypes: A, B, B/C, C, and R, based on physiology, immunological properties, and coccolith morphology (Young and Westbroek, 1991; Young et al., 2003). Although the distributions, and even the characterization of these morphotypes, are the subject of much debate, Young and Westbroek (1991) reported that morphotype A is a warm water variety and morphotype B is a North Sea and fjord variety. Morphotype B/C has been observed primarily in temperate and subpolar regions of the Southern hemisphere (Cubillos et al., 2007), while morphotype C has been observed primarily in cold polar waters (McIntyre and Bé, 1967; Findlay and Giraudeau, 2000). The range of the R morphotype is particularly

ambiguous, with very few observations recorded. Of these morphotypes, A and B are the best represented both in culture and in the literature (Medlin et al., 1996; Schroeder et al., 2005).

Emiliania huxleyi has the potential to form large blooms with cell concentrations of up to 115 x 10^6 cells L^{-1} in temperate and coastal regions during the spring and summer (Berge, 1962). Empirical studies of *E. huxleyi* blooms have shown an increase in the partial pressure of CO_2 (pCO_2) in surface waters (Holligan et al., 1993; Purdie and Finch, 1994; Robertson et al., 1994). The authors suggest that *E. huxleyi* blooms can act as sources of CO_2 to the atmosphere through outgassing of aqueous CO_2, and that the ability of *E. huxleyi* to act as a net sink of CO_2 relative to its noncalcareous counterparts is limited by the carbonate counter pump. *E. huxleyi*'s role in transporting organic carbon to depth as a ballast material (section 1.1.1), however, remains integral to the biological pump and the species remains prominent in carbon export studies.

1.1.1.1.1 ***Genetic diversity***

Many questions still exist regarding the dynamics of *E. huxleyi* blooms, and by extension regarding the role of *E. huxleyi* in future climate scenarios. To explore the genetic makeup of this model organism, a draft genome measuring 167.7 MB (megabases) has been constructed for a single *E. huxleyi* strain from the North Pacific, CCMP 1516 (morphotype A) (Steinke et al., 1998; JGI, 2008). While the genome, once completed, may reveal genes regulating important *E. huxleyi* cellular processes such as calcification, it is biased toward the isolate and morphotype used in genome construction, and therefore fails to encompass genetic variability within the species (intraspecific diversity). Genetic variability has been shown to improve survival in changing environments and reduce susceptibility to parasites and pathogens (Gadagkar, 1998), and is therefore a key consideration in understanding mechanisms of *E. huxleyi* bloom formation and demise. This intraspecific variability is potentially responsible for (1) *E. huxleyi*'s ability to rapidly take advantage of nutrient inputs, (2) the adaptive ability of *E. huxleyi* to photoacclimate (Suggett et al., 2007), and (3) the resistance of some cell lines to *E. huxleyi*-specific virus (EhV), the principal factor causing *E. huxleyi* bloom demise when nutrient concentrations are non-limiting (Bratbak et al., 1993; Bratbak et al., 1996; Castberg et al., 2001; Wilson, W. H. et al., 2002; Wilson et al., 2005; Frada et al., 2008), and forms the basis for hypotheses 1 and 2 (section 1.3).

A study by von Dassow et al. (2009) of expressed sequence tags (ESTs), short (200 to 500 nucleotide) sequences of DNA corresponding to an expressed gene, found that only 47% of ESTs matched between a coastal New Zealand *E. huxleyi* strain, RCC1216 (morphotype R), and the genome strain, CCMP1516. From this point, the term 'strain' will be replaced with the term 'isolate' to emphasize that each strain derives from an individual cell isolate which was clonally cultured. The variability in the transcriptome (portion of the genome transcribed into mRNA molecules) between isolates of different morphotypes and from different locations is not apparent in the DNA sequences of the two isolates, which are >99% identical. The study, therefore, suggests that different isolates adapt to a range of ocean environments through changes in gene regulation, rather than sequence mutations.

This mechanism is consistent with *E. huxleyi*'s relatively recent evolution (section 1.1.1.1), however, in isolated, rapidly mutating regions of the genome, mutations may have occurred which differentiate genetically between *E. huxleyi* isolates. A number of molecular techniques have been employed over the past two decades to test intraspecific *E. huxleyi* genetic variability, using both specific genes which have a functional role, and non-functional regions which track the relatedness of *E. huxleyi* isolates. Here, three different molecular markers (a gene or sequence that can be used to distinguish between organisms) are discussed in more detail. Random Amplification of Polymorphic DNA (RAPD) analysis is a type of genetic fingerprinting technique that uses arbitrarily chosen primers to amplify segments of DNA at random. The sequences of the amplified segments from different individuals are then compared to determine relatedness. A 1996 study using RAPD revealed different banding patterns throughout the isolates studied, suggesting a high degree of intraspecific diversity on both a geographically large (i.e. between geographically well-separated isolates) and small scale (i.e. between individuals isolated from the same *E. huxleyi* bloom; Medlin et al., 1996). The experiments have been difficult to repeat, however, due to the potential for contaminating sequences (from bacteria or viruses for example) to appear in the results.

A more recent study by Schroeder et al. (2005) found sequence variation between A and B morphotypes in a gene thought to be related to calcium binding, called GPA. A one-base-pair substitution within the translated region of the GPA gene differentiated the two morphotypes, while differences in the 3' untranslated region (UTR), designated the coccolith morphology motif, or CMM, produced a total of four

different genotypes. CMM has been used to test intraspecific diversity in two separate time series from mesocosm experiments (mesocosms are presented in more detail in section 1.2.1) separated by three years. Both time series produced a single genotype upon analysis, morphotype A CMM I (Martinez et al., 2007). The lack of variation in this case seems to suggest that, at least in the Norwegian coastal area, *E. huxleyi* blooms are made up of identical genotypes year after year; however, CMM is a functional molecular marker, which is likely to mutate more slowly than a non-functional marker and therefore is not as useful in tracking population relatedness.

A third set of molecular markers, microsatellites, are more reproducible than RAPD and appear more variable than CMM. Microsatellites are regions of non-coding DNA where a repeated sequence motif of one to six bases occurs. They are found throughout the genomes of all analyzed organisms (Zane et al., 2002) and have been used in a wide range of genetic assays, from archaeology, to forensics, to population genetics and biological resource management (see Jarne and Lagoda (1996) for an excellent review) to track population relatedness. These non-functional microsatellite regions mutate rapidly, causing variations in the length of the repeated region (length polymorphisms) that can be used to determine very small differences between individuals within a population (Iglesias-Rodríguez et al., 2006). Mutation rates vary significantly between microsatellite loci (Di Rienzo et al., 1998) and can range from 10^{-2} to 10^{-6} mutations per locus per generation (Li et al., 2002).

Figure 5 shows a schematic diagram of a microsatellite locus with three DNA strands of differing repeat numbers, each corresponding to a different microsatellite fragment length. For example, if the microsatellite region was characterized by a dinucleotide repeat, a five-repeat microsatellite region would measure 10 bp in length, a three-repeat region would measure 6 bp in length, and a seven-repeat region would measure 14 bp in length. This length polymorphism can be identified through polymerase chain reaction (PCR) amplification of microsatellite markers followed by DNA sequencing. Microsatellite molecular markers are developed using unique flanking sequences on either side of a microsatellite region to design primers for PCR amplification. Although the mechanism causing length polymorphisms in microsatellite regions is still disputed, the most likely explanation is that DNA slippage occurs during replication, resulting in the addition or deletion of a repeat (Schlotterer and Tautz, 1992).

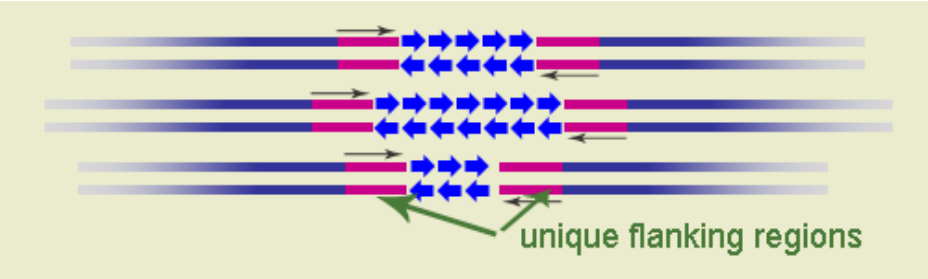

Figure 5. Schematic diagram of a microsatellite region (from NCBI) showing 3 DNA strands with variable microsatellite fragment lengths. The blue arrows represent the repeat region, thus the top individual contains 5 repeats, the middle contains 7, and the bottom contains 3. Unique flanking regions refer to the sequences bordering the microsatellite region used to design PCR primers.

Investigations into phytoplankton intraspecific diversity using microsatellite markers have been expanding throughout the past decade, with studies targeting diatoms (Rynearson and Armbrust, 2000; Evans et al., 2004; Evans and Hayes, 2004; Rynearson and Armbrust, 2004; Evans et al., 2005), dinoflagellates (Nagai et al., 2004), and coccolithophores (Iglesias-Rodríguez et al., 2002; Iglesias-Rodríguez et al., 2006) all revealing a high degree of intraspecific diversity. The intraspecific diversity over the massive ecological shifts of rapid growth and viral attack during the time series of an *E. huxleyi* bloom, however, has not been addressed in previous *E. huxleyi* microsatellite studies and motivated the development of hypotheses 1 and 2 (section 1.3). An understanding of relatedness between theoretically clonal individuals in an *E. huxleyi* bloom and overall population responses to ecological pressures could provide a wealth of information regarding how individual *E. huxleyi* isolates could vary so widely in their gene expression depending on isolation location.

1.1.1.1.2 ***Life cycle***

One principle means of generating genetic variability is sexual reproduction, which allows recombination of parent genotypes, resulting in unique progeny genotypes and potentially an improved ability to adapt to changing environments (Gadagkar, 1998). Although the main method of reproduction observed in *E. huxleyi* cultures is asexual cell division, nuclear (Green et al., 1996) and molecular (Frada et al., 2006) staining have illuminated a complicated life cycle involving phenotypically distinct life cycle stages and, potentially, sexual reproduction. Many coccolithophores exhibit haplo-diploid life cycles, or the alternation of generation between two life cycle stages,

one containing one copy of the genome (haploid; n) and the other containing two copies (diploid; 2n) (Geisen et al., 2002). In sexually reproducing species, haploid cells from different individuals fuse to create a genetically unique diploid individual, a process that has been observed in, *Coccolithus pelagicus* (Houdan et al., 2003), but not to date in *E. huxleyi* (Klaveness, 1972; Green et al., 1996). Although sexual fusion has not been observed directly in *E. huxleyi,* pure cultures of diploid C-cells, which bear liths and are found during natural bloom events, can give rise to two other cell types: (1) haploid S-cells, which are flagellated and covered by unmineralized scales, and (2) diploid N-cells, which bear no outer covering (hence, they are called naked cells) (Figure 6). All three cell types can reproduce asexually and be maintained in pure cultures. Diploid N-cells are probably an artefact of extended growth in culture, but the haploid S-cells appear to be a motile gamete stage in the life cycle capable of directed movement either for mating purposes or for greater flexibility under stressful environmental conditions (Klaveness, 1972; Billard, 1994; Green et al., 1996).

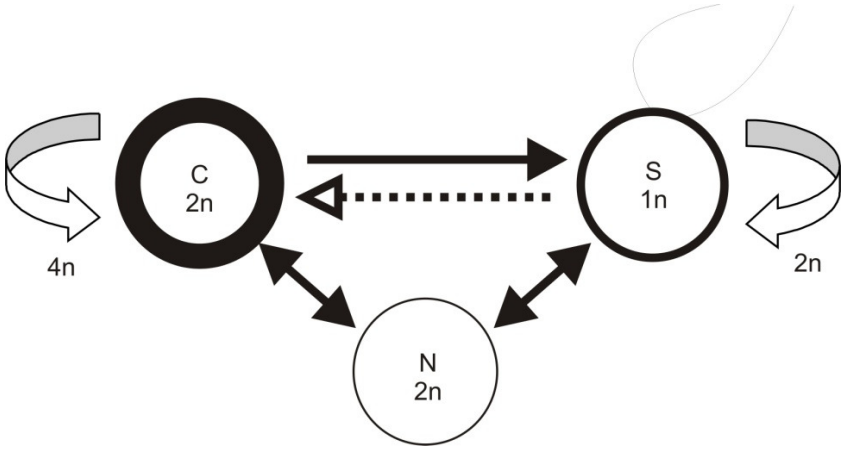

Figure 6. Life cycle proposed by Billard (1994) with additional ploidy data from Green (1996). 1n, 2n, and 4n correspond to haploid, diploid/haploid just prior to asexual cell division, and diploid just prior to asexual cell division respectively. The solid arrows indicate observed relationships while the broken arrow indicates a hypothetical relationship.

Non-calcifying *E. huxleyi* cells (including both S- and N-cells) are observable using a technique called $CaCO_3$ optical detection with fluorescent *in situ* hybridization (COD-FISH). The technique combines tyramide signal amplification with fluorescent *in situ* hybridization (TSA-FISH) and molecular staining to identify *E. huxleyi* cells and

then uses cross-polarized microscopy to differentiate between calcifying cells and non-calcifying cells (Frada et al., 2006). Recently, Frada et al. (2008) have demonstrated a further ecological function of haploid S-cells beyond their expected sexual role. In laboratory experiments comparing cultures of pure diploid (C-cells) and pure haploid (S-cells) infected with *E. huxleyi*-specific virus (EhV) (family *Phycodnaviridae*) to uninfected controls, the haploid cells were found to be resistant to infection. EhV is a lytic virus (Wilson, W. H. et al., 2002) and the major cause of bloom demise (Bratbak et al., 1993; Wilson et al., 1998; Larsen et al., 2001; Jacquet et al., 2002). Following injection of its nucleic acid into a cell and production of virus progeny therein, the host cell fatally bursts (or lyses) releasing the progeny (Fuhrman, 1999). While infected diploid cultures experienced a 96% reduction in cell density following viral addition, infected haploid cultures remained identical to controls. Furthermore, long-term assays demonstrated that infection of diploid cultures with EhV stimulated production of haploid cells after 24 days. The authors proposed a 'Cheshire Cat' escape strategy to explain the ploidy switch, i.e. that haploid *E. huxleyi* S-cells escape viral infection and survive to propagate the species. The existence of diploid-resistant *E. huxleyi* isolates in culture (Vardi et al., 2009), however, suggests that intraspecific diversity within diploid *E. huxleyi* populations may also play a role in the success of the species in the face of high lytic virulence. As such marine viruses, or virioplankton, are expected to be a major driver behind diversity in the *E. huxleyi* model system. Phosphate limitation has further been shown to inhibit development of viruses in *E. huxleyi* (Bratbak et al., 1993), suggesting that phosphate limitation may have strong effects on *E. huxleyi* virus-host interactions (Wilson et al., 1998).

The publication of the transcriptomes for the calcifying diploid, RCC1216 (C-cell; morphotype R), and its non-calcifying haploid progeny, RCC1217 (S-cell), further highlighted the large physiological differences between the two cell types, with overlap in ≤50% of ESTs (von Dassow et al., 2009). The authors found that the haploid isolate was differentiated by signal transduction and motility functional genes, while the diploid isolate was differentiated by calcium, hydrogen, and bicarbonate functional genes with a richer transcriptome overall. They suggest that the greater transcriptome richness of the diploid isolate allows it more versatility suited to a wide range of environments, and that the haploid isolate is genetically more 'streamlined,' raising interesting possibilities for identification of intraspecific genetic diversity in diploid

cells isolated from the dynamic selective environment of an *E. huxleyi* bloom (hypotheses 1 and 2; section 1.3).

1.1.1.2 Siliceous phytoplankton: efficient exporters

While *E. huxleyi* is the major focus of this PhD thesis as a model bloom-forming mineralizing phytoplankton, an investigation of the environmental factors behind *E. huxleyi* blooms and biogeography must also consider competing phytoplankton groups. Many species of the major siliceous phytoplankton group, the diatoms (Order *Heterokonta*; Class *Bacilariophyceae*), also form extensive blooms (Smetacek, 1999), and are responsible for ~40% of net ocean primary production (Dugdale and Wilkerson, 1998). Diatoms are characterized by an external skeleton made up two inter-locking silica cases, called frustules. As discussed in section 1.1.1, these siliceous skeletons provide effective ballast material, and as a result, >50% of organic carbon export is carried out by diatoms (Dugdale and Wilkerson, 1998).

Like coccolithophores, diatoms are eukaryotic single-celled autotrophs and evolved in the middle Triassic period following secondary symbiosis of an ancestral rhodophyte plastid. One of the most important physiological differences between diatoms and other phytoplankton groups is the evolution of a nutrient storage vacuole, which allows diatoms to sequester nitrate and phosphate. Storage of macronutrients in the vacuole both sustains diatoms through periods of low ambient macronutrient concentrations and deprives other phytoplankton of macronutrients during pulses of high ambient macronutrient concentrations, thus providing a competitive advantage over other phytoplankton groups in unstable environments such as coastal upwelling regions and turbulent high latitude seas (Falkowski et al., 2004; Tozzi et al., 2004).

Although not a major phytoplankton clade in terms of marine global production and export, a final functional group containing siliceous, bloom-forming representatives which can be dominant at the local level in marine environments is the chrysophyte clade, or golden-brown algae (Order *Heterokonta*; Class *Chrysophyceae*). Members of this eukaryotic lineage are typically flagellated, mixotrophic (capable of both autotrophy and heterotrophy), and dominant in moderate to low-productivity freshwater environments (Sandgren et al., 1995). The chrysophyte group is highly diverse, however, and marine species are also present. The Parmales, a tiny (2-5 µm) single-celled marine taxa within the *Chrysophyceae*, are characterized by an external skeleton of relatively large silica plates (8 or 5 plates for the families *Triparmarceae* and

Pentalaminaceae respectively; (Ichinomiya et al., 2010) and no flagellate stage (Booth and Marchant, 1987; Andersen, 2004). Parmales have been observed from tropical to polar regions, and are most abundant in subpolar and polar regions (Andersen, 2004). The order Parmales has only been recognized since 1987 (Booth and Marchant, 1987) and the group's ecology is still not very well understood. It has been suggested that due to its worldwide distribution, the group may be of greater importance in marine foodwebs than current research suggests (Kosman et al., 1993).

1.1.2 Environmental regulation of mineralizing phytoplankton growth

Each of the mineralizing phytoplankton functional groups investigated in this thesis research, the coccolithophores, diatoms, and chrysophytes, demonstrate different ecological strategies which maximize the species' growth under different nutrient, light, temperature, and carbon chemistry regimes. These diverse ecological strategies are responsible for the differing biogeography of the groups in the modern ocean and will largely determine their biogeography in the future ocean as a result of climate change. Biologists use the terms r-strategists and K-strategists to classify ecological types (MacArthur and Wilson, 1967) based on the Verhulst equation of population growth (Verhulst, 1838). K-strategists typically produce fewer offspring and live longer, while r-strategists typically have a high fecundity and a short generation time. The two strategies are the results of differing evolutionary pressures applied in different environments. K-strategists are selected in stable environments favouring highly adapted competitors, while r-strategists are selected in unstable environments favouring opportunists (Pianka, 1970).

In 1978, Margalef proposed an expression for predicting marine phytoplankton ecological strategies (known as Margalef's Mandala) based on turbulence and nutrient concentration which still forms the basis of biologists' understanding of phytoplankton ecology. According to Margalef's Mandala, diatoms are r-strategists which possess a competitive advantage under conditions of high nutrient availability and high turbulence, while *E. huxleyi* is intermediate between K-strategists (including dinoflagellates) and r-strategists (including diatoms) (Margalef, 1978; Figure 7). In effect, *E. huxleyi* can adopt either a K-strategy in nutrient-poor oceanic waters (a relatively stable environment) or an r-strategy in nutrient-rich subpolar waters (a relatively unstable environment). This plasticity derives from *E. huxleyi*'s resilience to nutrient limitation (K-strategy), and its fast growth rates during blooms (r-strategy)

(Brand, 1994). Very little is known about marine chrysophyte ecology, however, evidence from freshwater species which thrive in low- to moderate-productivity lakes (Sandgren et al., 1995) suggests that they are more likely K-strategists or intermediate strategists. The differences in ecological strategy between *E. huxleyi*, diatoms, and chrysophytes have important implications for the growth and dominance of these organisms under different present-day environmental conditions and in future climate scenarios, and form the basis for hypotheses 3 and 4 (section 1.3), findings summarized in Table 1.

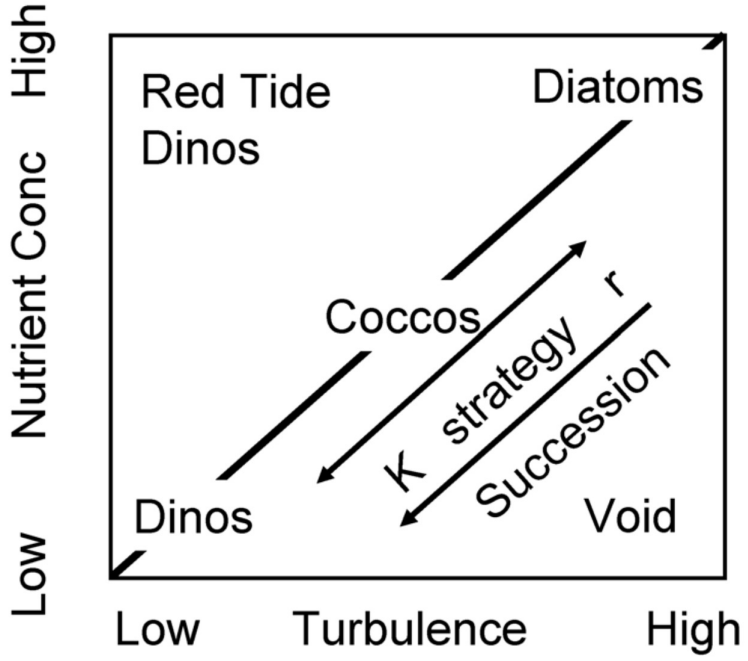

Figure 7. Adapted version of Margalef's Mandala (Fig. 2; Margalef, 1978) taken from Balch (Fig. 1; 2004) and showing the relationships between diatoms, coccolithophores (coccos), dinoflagellates (dinos), turbulence, and nutrient concentrations.

Table 1. Relationships between environmental factors, the predicted effects of climate change, and three mineralizing phytoplankton groups.

Environmental Factors	*E. huxleyi*	Diatoms	Chrysophytes	Future Climate Scenario	Favoured mineralizing phytoplankton
Ecological strategy	Intermediate	r-strategist	Not well understood, possibly K-strategist		
Macronutrients	Low nitrate (N) and phosphate (P) requirement No Si requirement	Competitive advantage under high nutrient conditions - nutrient storage vacuole	Not well understood, but mixotrophy suggests low inorganic N and P requirement	Increasing stratification in low to mid-latitudes slows vertical mixing, reducing nutrient flux	*E. huxleyi* and potentially chrysophytes in low to mid-latitudes.
Temperature	Global distribution, but higher abundances in temperate regions	Global distribution	Global distribution, but higher abundances in subpolar and polar regions	Increasing SST	See macronutrients, iron, and light.
Iron (Fe)	Low Fe requirement	Medium & large – high Fe requirement. Small – low Fe requirement	Parmales - Low Fe requirement	Increasing stratification in low to mid-latitudes slows vertical mixing, reducing Fe availability in some regions, while increased upwelling may occur locally, increasing Fe availability in other regions	*E. huxleyi* and potentially chrysophytes in low to mid-latitudes. Diatoms where local Fe upwelling occurs.
Light	Negative effects of supraoptimal light intensities are dependent on the species distribution rather than phylogeny			Increased growth season and shallower mixed layer depth in high latitudes	Diatoms in high latitudes.
Partial pressure of CO_2 (pCO_2)	Sensitive to changes in calcite saturation state	No predicted effect of calcite saturation state	No predicted effect of calcite saturation state	Increasing atmospheric CO_2 lowers ocean pH	Predictions are conflicting regarding *E. huxleyi*. Diatoms and chrysophytes unlikely to be affected directly.

1.1.2.1 Nutrients, Turbulence, and Temperature

E. huxleyi is considered a low-nutrient taxa and maintains its low nutrient requirements by using ammonium, nitrate, nitrite, and urea as nitrogen sources, and both phosphate and various organic phosphates as phosphate sources (Brand, 1994). Diatoms in contrast, are more abundant in high-nutrient conditions and combat nutrient limitation through storage of nitrate and phosphate in a nutrient storage vacuole. Diatoms growth, however, is also limited by silicate availability, a nutrient which is not limiting for *E. huxleyi*. These differing strategies typically result in the rapid proliferation of diatoms following a mixing event (i.e. a pulse of nutrients in a turbulent environment) as they sequester nutrients and deny them to competing taxa, followed by gradual succession to coccolithophore dominance and finally dinoflagellate dominance as nutrients become depleted and the environment stabilizes (Margalef, 1978; Balch, 2004; Figure 7). As mixotrophs able to use organic complexes to supply nutrients, chrysophytes are likely to be resilient to nutrient limitation and more able to compete with nutrient-sequestering diatoms. Siliceous chrysophytes, however, like diatoms are subject to silicate limitation. All three organisms require iron (Fe) for intracellular reduction-oxidation (redox) reactions and photosynthesis, and this requirement is discussed in detail in section 1.1.2.1.1.

At present, the biogeography of these species reflects their differing nutrient requirements, with diatoms typically dominating in neritic environments and turbulent open ocean environments (Falkowski et al., 2004), and in temperate seas during the spring and early summer when nutrients are readily available due to winter mixing. In environments where silicate and other nutrients are less available, often due to heavy nutrient drawdown during preceding diatom blooms, however, low-nutrient-adapted *E. huxleyi* proliferate rapidly (Brand, 1994; Tyrell et al., 1999; Tyrell and Merico, 2004). Numerous hypotheses have been suggested to explain the formation of *E. huxleyi* blooms; however, one of the most important triggers in productive, high-nutrient areas is probably silicate limitation which restricts diatom competition (Tyrell and Merico, 2004). The higher abundance of the marine chrysophyte Parmales in subpolar and polar regions is, however, less well-understood.

Past competition between diatoms and coccolithophores has been recorded on geological time scales through mineral deposits and roughly corresponds to periods of varying upper ocean turbulence and corresponding nutrient availability (Tozzi et al.,

2004). In the fossil record, coccolithophores reached a maximum species richness in the relatively warm and quiescent Cretaceous Period (146 - 65.5 Million years ago; Mya) when global winds and ocean circulation were sluggish (Huber et al., 1995). They have, however, declined in diversity to the present, while diatoms have increased in diversity throughout the Cenozoic Era (65.5 Mya - present) (Falkowski et al., 2004; Tozzi et al., 2004). The shift in dominance has been attributed to the onset of the major polar ice caps (~32 Mya) which resulted in more intense thermohaline circulation and therefore an increase in nutrient availability (Tozzi et al., 2004).

The close relationship between global temperature, ocean circulation, and nutrient availability suggests that the current trend of global warming may have far-reaching effects on phytoplankton biogeography and productivity. A recent study of coupling between global climate and NPP found that changes in NPP between 1997 and 2006 were driven by changes occurring in warm (over 15 °C), permanently stratified areas of the ocean (roughly between 40 °N and 40 °S) (Behrenfeld et al., 2006). The study found that warmer conditions resulted in a global decrease in NPP, due to increased stratification, or an increase in the density difference between the surface layer where phytoplankton photosynthesize and the underlying nutrient-rich layer, and a corresponding decrease in vertical mixing which sustains phytoplankton growth through nutrient exchange. When atmosphere-ocean general circulation models are coupled to ocean ecosystem models and forced by rising CO_2 concentrations, the resulting changes in NPP for stratified areas of the ocean are consistently similar to the Behrenfeld et al. (2006) data, with an increase in sea surface temperature (SST) and water-column stratification driving a decrease in NPP. In high latitudes, however, the models predict an increase in NPP due to an extension in the phytoplankton growing season and shallower mixed layers (Bopp et al., 2001; Boyd and Doney, 2002; Sarmiento et al., 2004). The predicted increases in temperature, upper ocean stratification, and corresponding decreases in vertical mixing of nutrients could potentially favour low-nutrient taxa globally. With lower frequencies of nutrient pulses, and lower nutrient concentrations overall, the competitive advantage currently experienced by diatoms may decrease, potentially allowing a greater dominance of *E. huxleyi* and chrysophytes as lower turbulence conditions correlated to a greater dominance of *E. huxleyi* in the Cretaceous. The past effects of differing phytoplankton responses to nutrient pulses motivated the comparison of neighbouring nutrient-limited (static) and nutrient-replete (subject to nutrient pulses) regions in the Southern Ocean (hypothesis 3; section 1.3).

Other than those tied to stratification and nutrients, the effects of increasing ocean temperature on *E. huxleyi*, diatoms, and chrysophytes are unclear, however their present global distributions suggest the potential of all three to exploit a wide range of temperatures.

1.1.2.1.1 *Oceanic Fe and photosynthesis*

To cope with low dFe concentrations, phytoplankton have already developed several strategies to minimize Fe requirements. Using nitrogen (N) sources which require less Fe in their reduction, such as NH_4^+, is one strategy. Another is to reduce cell size. A cell's Fe requirement decreases as a function of volume (r^3; where r refers to radius), while its available surface area for uptake molecules only reduces as a function of area (r^2) and the diffusion-limited rate by r (Morel et al., 1991). The phenomenon is partly supported by field observations of large nannoplankton (phytoplankton 2–20 µm in size) populations in High Nutrient Low Chlorophyll (HNLC) regions, where phytoplankton are unable to make use of excess surface nitrate and phosphate, due to Fe limitation (Martin, 1990; Morel et al., 1991; Blain et al., 2008), and motivated the development of hypotheses 3 and 4 (section 1.3).

Although Fe requirements in marine phytoplankton are extremely low compared with nitrogen, phosphorous, and silica , the low solubility of the predominant form of Fe in oxygenated seawater, oxidized FeIII, makes Fe a limiting nutrient in many areas of the modern ocean (Martin, 1990). The dependence of marine phytoplankton on Fe is an artefact from evolution in anoxic environments where Fe was readily available in the past (Morel et al., 1991). Typically, phytoplankton Fe requirements range from 1 µmol Fe: 1 mol carbon (C), to 10 µmol Fe: 1 mol C (depending on which species are analyzed, Fe-limited oceanic ones or Fe-replete coastal ones, respectively; Raven, 1988; Brand, 1991). In oceanic Fe-limited phytoplankton, up to 150,000 times less Fe is required than N and silica (Si) (for siliceous taxa), and 6,000 times less Fe than phosphorous (P) – thus Fe is termed a micronutrient, while N, Si, and P are macronutrients (Redfield, 1958; Brzezinski, 1985). Dissolved Fe (dFe) concentrations in the deep Atlantic and Pacific Oceans are on the order 10^{-3} µmol dFe (Gordon et al., 1982; Symes and Kester, 1985), meaning that upwelling of deep water alone resupplies very little dFe to the photic zone. Fe limitation, therefore, occurs primarily in oceanic areas that do not receive supplemental Fe from continental Fe input (resuspended

bottom sediments) nor from atmospheric dust deposition, including most of the Southern Ocean and equatorial Pacific (Martin and Gordon, 1988; Martin, 1990).

Fe limitation affects intracellular redox reactions, including the reduction of inorganic nitrogen species and photosynthesis, due to their relatively high Fe demands. With respect to inorganic nitrogen species, Fe is required both for the reduction of nitrogen (N) and nitrate (NO_3^-) to ammonium (NH_4^+), and for the assimilation of NH_4^+. Approximately 101 more mol Fe are required to process N than NH_4^+ and 1.6 more mol Fe are required to process NO_3^- than NH_4^+ (Raven, 1988), leading to reduced N uptake, and in some cases a switch from NO_3^- to NH_4^+ utilization when Fe is limiting (Morel et al., 1991; Price et al., 1991). The other key cellular process affected by Fe limitation in phytoplankton is photosynthesis, due to the significant quantities of Fe used in the catalytic complexes Photosystem I (PSI), Photosystem II (PSII), and cytochrome b_6-f-FeS (Raven, 1990).

Emiliania huxleyi and marine chrysophytes of the order Parmales fall into the nannoplankton size fraction, and are therefore expected to have low Fe requirements, while medium and large diatoms are expected to have higher Fe requirements, a fact which forms the basis for hypothesis 4 (section 1.3). This prediction has been supported by Fe-addition experiments, which tend to favour growth of medium and large diatoms (Martin, 1990; de Baar et al., 2005; Boyd et al., 2007) as the result of relief from Fe limitation combined with low grazing pressure (Morel et al., 1991), although some small increases in nannoplankton (2–20 µm) abundance have also been observed (Gall et al., 2001); chapter 4). The responses of small diatoms within the nannoplankton size class are less well-studied, however, their Fe requirements are also expected to be relatively low due to small cell size. *E. huxleyi* also possess a competitive advantage in low-Fe environments due to its ability to utilize various compounds as nitrogen sources, including NH_4^+ (section 1.1.2.1). Like the macronutrients, the availability of Fe in future climate scenarios will be affected by changes in upper ocean stratification, however, the effects of atmospheric dust deposition and changes to Fe availability in HNLC regions are poorly constrained in current models (Bopp et al., 2001; Boyd and Doney, 2002; Sarmiento et al., 2004). It is likely that Fe availability will vary widely at the local level, with some areas experiencing greater upwelling which favours larger diatoms (Boyd and Doney, 2002).

1.1.2.1.2 ***Measuring nutrient stress***

Over the past 17 years the measurement of active chlorophyll-*a* fluorescence has become an important technique for assessing the physiological state of phytoplankton in nature through photosynthetic physiology (Kolber et al., 1990; Geider et al., 1993; Greene et al., 1994; Suggett et al., 2009). These measurements quantify the amount of absorbed light not utilized by PSII, which is reflected as chlorophyll-*a*. When phytoplankton are subjected to 'stressful' growth conditions, their maximum PSII photochemical efficiency decreases, allowing the effects of excessive light or nutrient starvation to be assessed across entire communities *in situ* through photosynthetic physiology. Fast repetition rate (FRR) fluorometers are particularly useful because of their high sensitivity, a necessary feature in oligotrophic open ocean waters where chlorophyll-*a* concentrations are very low, and because of their ability to simultaneously measure two important photosynthetic physiological parameters: the maximum PSII effective absorption cross section (σ_{PSII}), and the normalized active fluorescence (F_v/F_m) (Suggett et al., 2009). Nutrient limitation results in a decrease in F_v/F_m and an increase in σ_{PSII} (Kolber et al., 1988; Bibby et al., 2008; Suggett et al., 2009) as the proportion of functional oxygen-evolving reaction centres (RCIIs) decreases, leading to the use of both factors as important indicators of nutrient stress, including Fe limitation (Greene et al., 1991; Kolber et al., 1994; Suggett et al., 2009). F_v/F_m and σ_{PSII} can also be an indication of the taxonomic structure of the phytoplankton community, however, an effect referred to as a taxonomic 'signature', which often exceeds that of nutrient limitation (Suggett et al., 2009). Interpretation of physiology results, therefore, must include an assessment of whether nutrient stress, taxonomic shifts, or a combination of the two, are driving changes in F_v/F_m and σ_{PSII}.

1.1.2.2 Light

Phytoplankton growth is heavily dependent on light availability, with high light intensities potentially producing both negative and positive effects. Increased irradiance through the spring and summer has a positive effect on growth and is one of the major triggers of phytoplankton blooms in seasonally changing latitudes. In combination with reduced diatom growth following stripping of nutrients, high light intensities are known to produce *E. huxleyi* blooms (Brand, 1994; Tyrell et al., 1999; Tyrell and Merico, 2004). The retardation of photosynthesis caused by excessive light is called photoinhibition, and is caused by damage to RCIIs in phytoplankton cells (Long et al.,

1994; Suggett et al., 2009). The amount of irradiance experienced by phytoplankton is closely tied to the amount of vertical mixing occurring in the water column, with photoinhibition at the surface higher from mid-day to sunset and in stratified regions where vertical mixing is negligible during the day (Long et al., 1994). The ability of phytoplankton to prevent and recover from photoinhibition varies widely depending the environment, with cells subjected to continuously low irradiance more susceptible to photoinhibition (Long et al., 1994; Ragni et al., 2008; Alderkamp et al., 2010). Coastal species generally experience equal or higher growth rates under continuous light conditions, while oceanic species generally are photoinhibited under continuous light conditions, independent of phylogenetic affiliation (Brand and Guillard, 1981). Even within a species, different strains can demonstrate differing photoacclimation 'strategies', such as that between *E. huxleyi* calcifying and non-calcifying strains (strain B11 – isolated in Norwegian mesocosm experiments, 1992; strain 92A – isolated in the English Channel, 1957; Suggett et al., 2007).

The degree of photoinhibition experienced by diatoms, *E. huxleyi*, and chrysophytes is expected to vary, therefore, according to the environment previously experienced by that organism. Maximum growth rates under optimal regional light conditions, however, are highly dependent on phylogeny, with diatoms growing fastest and coccolithophores growing at intermediate rates between diatoms and slower-growing dinoflagellates (section 1.1.2); Brand and Guillard, 1981). The slower growth rates of *E. huxleyi* may in part be due to the fact that calcification is strongly light-dependent and coccolith production occurs primarily during the day (Paasche, 1966). Growth rates of the Parmales are not well studied, however, evidence that freshwater varieties may be K-selected or intermediate (section 1.1.2) indicates that even under optimal light conditions their growth rates will be slower than diatoms.

The implications from climate models are that light limitation at the higher latitudes will be relieved as global temperatures increase due to longer growing seasons and shallower mixed layers (section 1.1.2.1). Given the ability of shallow-dwelling phytoplankton to adapt to higher light intensities (Long et al., 1994), these changes at the high latitudes would favour dominance by fast-growing diatoms, as photoinhibition is unlikely to be a long-term challenge once organisms acclimate.

1.1.2.3 Ocean Acidification

Calcium carbonate forms the skeletons of many marine organismsn, with aragonite found in corals and in foraminifera, and calcite found in coccolithophores. These two crystalline forms of $CaCO_3$ are highly susceptible to changes in ocean pH. Higher pH causes the dissolution of $CaCO_3$ structures by shifting the equilibrium outlined in Equation 3 towards dissolution of $CaCO_3$ into its component ions (i.e. the left). Due to increases in atmospheric levels of CO_2, the pH of the oceans has decreased over the past 200 years by 0.1 units (Raven et al., 2005), and is expected to decrease by a total of 0.3 to 0.4 units by 2100 (Orr et al., 2005). As atmospheric levels of CO_2 increase, a greater portion of soluble CO_2 enters the surface ocean, decreasing the pH of sea water, a phenomenon called ocean acidification. Ocean acidification reduces sea water's saturation state with respect to calcite (Ω-calcite) and (Ω-aragonite).

The largest effects of ocean acidification, therefore, will be felt in the low latitudes, where reef-building corals proliferate, and in the high latitudes, where cold surface waters have a higher carrying capacity for pCO_2. Large areas of the Southern Ocean are predicted to become undersaturated with respect to aragonite within the next 50 years and undersaturated with respect to calcite starting in isolated areas in 2100 (Orr et al., 2005). The potential ecological upheaval posed by ocean acidification has motivated a wave of studies on the effects of increased pCO_2 on the major marine taxa affected: coccolithophores (Riebesell et al., 2000; Feng et al., 2008; Iglesias-Rodríguez et al., 2008), foraminifera (Bijma et al., 1999), and corals (Gattuso et al., 1998; Kleypas et al., 1999; Langdon et al., 2000). Diatoms and chrysophytes are unlikely to be affected directly by ocean acidification due to their Si-based skeletons.

Zondervan et al. (2001) showed in laboratory experiments that, under conditions of increased atmospheric CO_2, the amount of POC produced by the coccolithophores *E. huxleyi* and *Gephyrocapsa oceanica* increased while the amount of PIC decreased. The phenomenon of decreasing PIC occurred as a result of inhibiting the formation of $CaCO_3$ liths. The authors' resulting model demonstrated *E. huxleyi's* ability to act as a negative feedback mechanism on increasing atmospheric CO_2 through decreased calcification, which in turn decreased the amount of CO_2 produced by the calcification process (Zondervan et al., 2001).

Although the trend in the study of Zondervan et al. (2001) on coccolithophores, and many of the studies on other calcareous organisms to date (Gattuso et al., 1998;

Bijma et al., 1999; Kleypas et al., 1999; Langdon et al., 2000; Riebesell et al., 2000), has been reduction in calcification rates and dissolution of $CaCO_3$ structures under high pCO_2, some instances of increased or unchanged calcification have been reported in studies of *E. huxleyi*. The inconsistency appears to be dependent on the species studied and the methods of pCO_2 manipulation used. When pCO_2 levels are adjusted by changing media pH, *E. huxleyi* calcification is greatly reduced (Zondervan et al., 2001), but when pCO_2 levels are adjusted by directly bubbling CO_2 gas, more variable results are observed. A strong case can be made that CO_2 bubbling is a better representation of the natural situation because it alters the two fundamental regulators of Ω-calcite, pH and dissolved inorganic carbon (DIC), while merely altering pH does not affect DIC (Iglesias-Rodríguez et al., 2008).

Two studies in 2008 used CO_2 bubbling to increase pCO_2 and measured the effects on *E. huxleyi* calcification. The first, by Feng et al (2008), varied temperature and irradiance as well as pCO_2 and found no change in calcification under low-light conditions regardless of pCO_2. Only under high-light conditions was high pCO_2 found to have a negative effect on calcification, suggesting other physiological factors were involved. A second study by Iglesias-Rodriguez et al. (2008), demonstrated an *increase* in calcification for *E. huxleyi* at high pCO_2 levels, a finding that was supported by fossil evidence. These results contradict the assumption that calcification will act as a negative feedback mechanism on increasing pCO_2 and instead suggest the opposite; calcification could in fact act as a positive feedback mechanism, whereby an increase in pCO_2 stimulates an increase in calcification, which in turn stimulates a further increase in pCO_2. Before a prediction can be made about the negative or positive feedback effect of anthropogenic CO_2 on calcification in *E. huxleyi*, however, a better understanding is required of what other physiological factors may be affecting these types of studies and how POC changes relative to PIC. It seems likely that a single prediction will not apply to all calcareous taxa, and that *E. huxleyi,* and possibly other coccolithophores, may demonstrate a unique response. More *in situ* experiments are necessary to complement these laboratory experiments, however, the later laboratory experiments, which used CO_2 bubbling to alter carbon chemistry, motivated the prediction of pCO_2's role in nannoplankton bioageography (hypothesis 3; section 1.3).

1.2 Field observations

Given *E. huxleyi's* important role as a model organism in studies of carbon cycling, it is vital to support an understanding of its responses to changes in carbon chemistry, nutrient availability, temperature, and light with the best possible understanding of *E. huxleyi* physiology and ecology both with studies of model systems (hypotheses 1 and 2; section 1.3) and field observations (hypothesis 3; section 1.3). Field observations further provide the opportunity to study *E. huxleyi* ecology and plasticity in the wider ecological context of the mineralizing phytoplankton community and environmental heterogeneity, where differing ecological strategies are expected to affect the dominance of specific taxa. The major aspect of *E. huxleyi* ecology addressed in this thesis research are the dynamics and biogeography of *E. huxleyi* blooms. *E. huxleyi* blooms are usually defined by cell concentrations of at least 1 x 10^6 cells L^{-1} and appear on satellite images as patches of white water (Figure 4). This bloom signal is due to the high number of reflective shed coccoliths within the bloom region that increase water albedo (reflectance). Interestingly, *E. huxleyi* blooms are often associated with areas of low concentrations of chlorophyll-*a*, which confirms the importance of *E. huxleyi's* role in local carbon cycling (Tyrell et al., 1999). Blooms are known to occur in the North Atlantic, North Sea, Black Sea, and Bering Sea. Unconfirmed blooms have also been observed via satellite in the North Pacific, Barents Sea, and in the Southern Ocean off the Patagonian Shelf and in the vicinity of South Georgia Island (Tyrell and Merico, 2004; Holligan et al., 2010).

1.2.1 The Bergen mesocosms: a controlled model system

Mesocosm systems have been used to extensively study bloom dynamics of *E. huxleyi* (Bratbak et al., 1993; Bratbak et al., 1996; Wilson et al., 1998; Jacquet et al., 2002; Martinez et al., 2007) because they allow experimental conditions to be manipulated on a large scale with high reproducibility through enclosure of *in situ* sea water in transparent bags (Martínez-Martínez et al., 2006). These mesocosm experiments have been carried out at the Espeland Marine Biological Station in a bay adjacent to Raunefjord, a Norwegian fjord 20 km south of Bergen (Figure 8). Between May and July, *E. huxleyi* blooms occur annually in Norwegian coastal waters and fjords, with typical concentrations of 2 to 3 x 10^4 cells ml^{-1} (Bratbak et al., 1993), and maximum observed concentrations of 1.2 x 10^5 cells ml^{-1} (Berge, 1962). Though

coastal, surface salinity at the station is ≥30 units due to low inputs of fresh water and temperatures remain below 15 °C even in summer. This highly controlled environment, where *E. huxleyi* blooms are known to naturally occur, provided the ideal model system for investigating genetic diversity of *E. huxleyi* blooms (hypotheses 1 and 2; section 1.3), a key gap in scientists' understanding of *E. huxleyi* ecology.

Figure 8. Map of the location of Raunefjord, Norway produced using Google Earth®.

1.2.2 The Southern Ocean: a case study for climate change

The Southern Ocean is an important natural laboratory for studying the effects of nutrient availability, temperature changes, light availability, and ocean acidification on all phytoplankton, and particularly the calcareous taxa. Due to upwelling and the action of the solubility pump (section 1.1), the Southern Ocean is an area of intense interaction between the ocean interior, where carbon is stored, and the ocean surface, where aqueous carbon interacts with the atmosphere as CO_2 (Sigman and Boyle, 2000). This interaction and the cold temperatures of the Southern Ocean mean that it is both an area highly susceptible to climate change (section 1.1.2.3) and an area with a large potential to influence global climate (Martin, 1990; Sigman and Boyle, 2000; Watson et al., 2000; Bopp et al., 2003). Natural gradients in nutrients, temperature, and pCO_2 occurring in the Southern Ocean provide an ideal case study environment to compare

phytoplankton communities experiencing different ecological pressures (hypotheses 3 and 4; section 1.3)

One very important nutrient gradient in the Southern Ocean is that of Fe. In contrast to the last glacial maximum (LGM) 18,000 years ago, when ice sheets reached their maximum extent, the modern Southern Ocean is the world's largest HNLC region due to Fe limitation (Martin, 1990; Morel et al., 1991; Blain et al., 2008). In areas of natural Fe fertilization in the Southern Ocean, however, intense phytoplankton blooms occur during the short summer growing season (Blain et al., 2001; Korb and Whitehouse, 2004; Moore et al., 2007a; Korb et al., 2008). These natural blooms are more representative of conditions during the LGM, where increased utilization of nutrients in the Southern Ocean was possible due to 50-fold higher atmospheric Fe dust inputs than today (Martin, 1990). Modelling conclusions suggest that this increased Fe availability led to: (1) an increase in diatom export in the sub-Antarctic, (2) an increase in the N:Si uptake ratio in the Antarctic, which relieved Si limitation for diatoms, and possibly (3) an increase in export by non-siliceous phytoplankton groups in the Antarctic (difficult to assess as these groups are not as well-preserved in the sediment record) which collectively acted to raise atmospheric CO_2 (Sigman and Boyle, 2000). A more far-ranging effect whereby excess silicic acid in the Antarctic, resulting from increased Fe availability and a corresponding reduction in the amount of Si required by siliceous organisms (modelling conclusion 2), was transported to lower latitudes where it fuelled further increases in production (silicic acid leakage hypothesis; SALH) may also have acted to reduce atmospheric CO_2 (Matsumoto et al., 2002). Following the LGM, atmospheric CO_2 increased from approximately 200 ppm (in the glacial period) to a preindustrial level of 280 ppm (in the present interglacial period) (Barnola et al., 1987; Martin et al., 1989; Martin, 1990). This change, representing 170 Gt of C input to the Earth's atmosphere, is now widely accepted to be in part (approximately 30%) the result of decreased Southern Ocean production and phytoplankton nutrient utilization as a result of Fe limitation, called the 'iron hypothesis' (Martin, 1990; Sigman and Boyle, 2000; Watson et al., 2000; Bopp et al., 2003).

In the present day, the Southern Ocean continues to experience rapid climate change as the result of the vigorous action of the biological pump (Orr et al., 2005). Recently, Cubillos et al. (2007) suggested that an extension in the *E. huxleyi*'s range southwards detected between 1995 and 2002 in the Pacific sector of the Southern Ocean is evidence of a response to climate perturbation. Dominance of the two morphotypes

found (A, highly calcified, and B/C, weakly calcified) was closely tied to Ω-calcite, which is changing rapidly in the high latitude southern hemisphere due to more rapid ocean acidification in cold waters (section 1.1). This preliminary data, as well as the high intraspecific genetic diversity (section 1.1.1.1.1) and phenotypic plasticity (section 1.1.2) demonstrated by *E. huxleyi*, suggest that the species may be an important factor in phytoplankton community shifts related to environmental changes in the future ocean. A better understanding of the current state of Southern Ocean phytoplankton communities and species biogeography, especially calcareous taxa which are heavily influenced by ocean acidification and adapted to stratified Fe-limited environments; and smaller siliceous phytoplankton taxa, which are poorly studied, but proliferate in Fe-deplete conditions, will improve oceanographers' ability to predict future climate scenarios which may have knock-on effects on biogeochemical cycles and on higher trophic levels within the delicate Southern Ocean food web.

1.2.2.1 Physical oceanography

1.2.2.1.1 *Southern Ocean circulation*

Southern Ocean phytoplankton communities are constrained by the well-defined frontal boundaries of the region (Deacon, 1982; Eynaud et al., 1999), a factor included in the development of hypothesis 3 (section 1.3). According to the seminal work of Orsi et al. (1995), the Subtropical Front (STF) marks the boundary between the colder, fresher Southern Ocean to the south and the subtropical circulations to the north. South of the STF, in the Southern Ocean, the Antarctic Circumpolar Current (ACC) flows eastwards circumnavigating the globe and connecting all the major oceans. South of the ACC, in the subpolar region, clockwise cyclonic eddies dominate in areas removed from the Antarctic continent (Deacon, 1933; Deacon, 1979; Rodman and Gordon, 1982) and westward flows in the region of the continental slope are driven by wind and buoyancy effects (Orsi et al., 1995). The flow of the ACC is controlled by major bottom ridges (Gordon et al., 1978), including the Southwest Indian Ridge (Deacon, 1979; Orsi et al., 1993), the Pacific-Antarctic Ridge (Patterson and III, 1990), and the Scotia Arc (Gill, 1973; Gordon, 1988).

Three major circumpolar fronts lie within the ACC, defining distinct water masses with unique physical properties (Figure 9). The Sub-Antarctic Front (SAF) is the most northward front and separates the deeper salinity minimum (S-MIN) of 400 m

found in the sub-Antarctic Zone (SAZ) from the near-surface S-MIN found in the Polar Frontal Zone (PFZ) (Whitworth and Nowlin, 1987). Polewards of the PFZ, the Polar Front (PF) separates the deeper temperature minimum (θ-MIN) waters of the PFZ from the shallower θ-MIN waters of the Antarctic Zone (AZ) (Gordon, 1967). Finally, the southernmost front of the ACC, called the Southern Antarctic Circumpolar Current Front (SACCF), is defined by a maximum temperature (θ-MAX) shoaling in the Upper Circumpolar Deep Water (UCDW) of over 1.8°C. These changes in the UCDW used to define the SACCF contrast with the changes in the Antarctic Surface Water (AASW) used to define the PF and the SAF and to separate the AZ from the Continental Zone (CZ) (Orsi et al., 1995) (Figure 10).

The properties of the zones separated by the major ACC fronts as well as the subpolar region south of the ACC are defined in Table 2 as they represent the case study region used in chapters 3 and 4. Generally, S-MIN is deeper in the SAZ than it is further south. The salinity maximum (S-MAX) also shoals polewards and decreases overall. θ-MIN decreases (becomes colder) overall in the top 100 m moving southwards, while θ-MAX both decreases and shoals (Orsi et al., 1995). These contrasting and sharply defined zones produce unique and biologically-isolated phytoplankton communities.

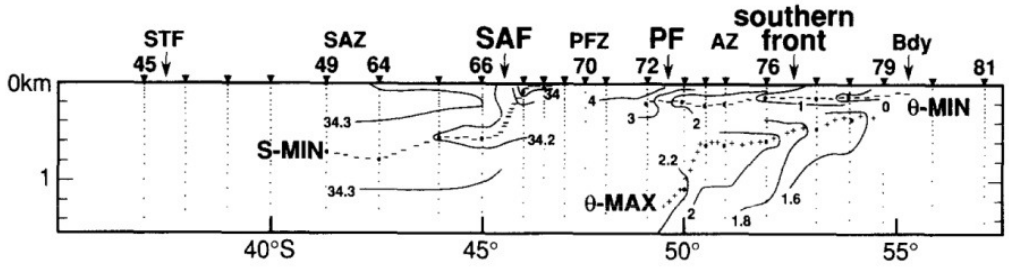

Figure 9. Figure taken from Orsi et al. (1995) showing selected isohalines and isotherms used in defining the 3 major ACC fronts: SAF, PF, and southern front (here called the SACCF), as well as the two ACC boundaries (labelled STF to the north and Bdy to the South) and 3 of the 4 ACC zones (SAZ, PFZ, and AZ).

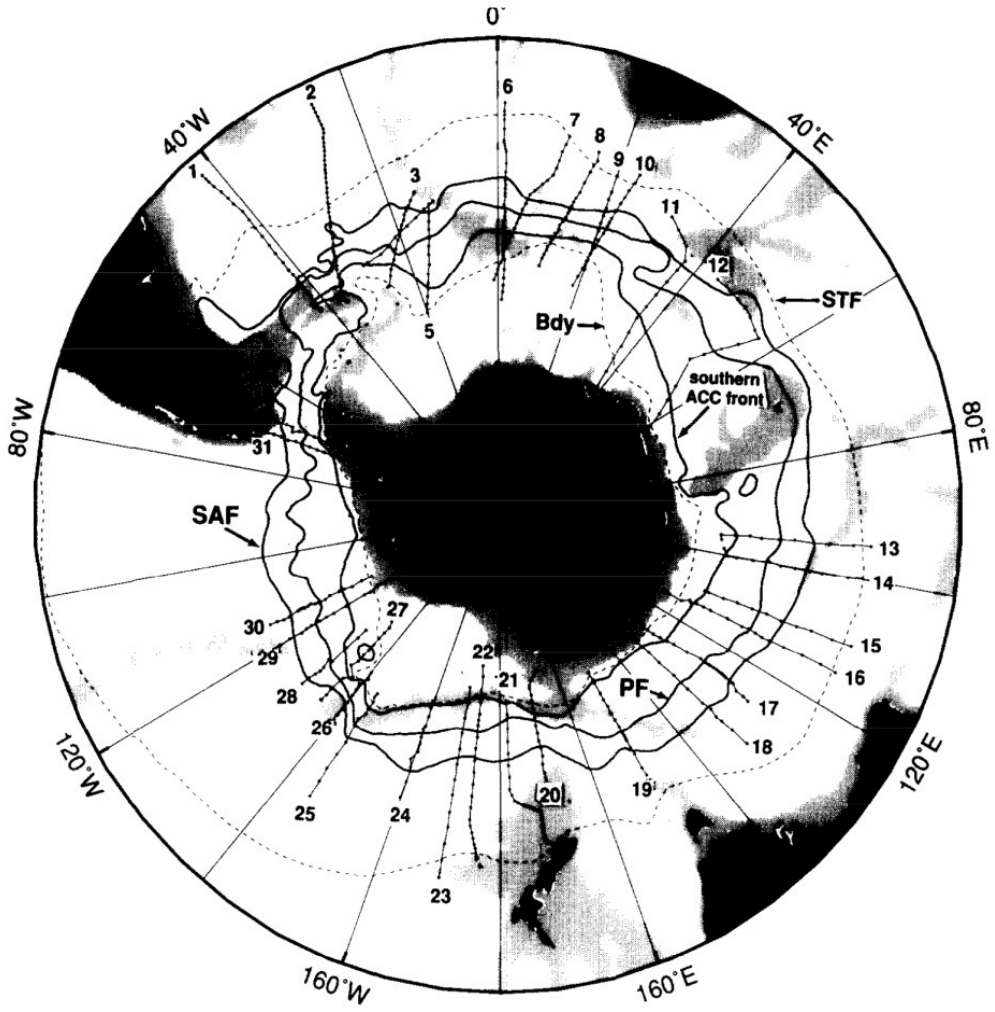

Figure 10. Figure taken from Orsi et al. (1995) mapping the circumpolar distribution of the fronts defined in Figure 9, with ACC boundaries shown by dashed lines and fronts within the ACC shown by solid lines. Numbers refer to transects used to extrapolate the circumpolar distribution shown , and are detailed further in the original article (Orsi et al., 1995).

Table 2. Table modified from Orsi et al. (1995) showing average values for the characteristic water masses within the ACC zones and the subpolar region. Depth (Z) in m, Temperature (θ) in °C, Salinity (S), and oxygen concentration O_2) in ml l^{-1}.

		SAZ	PFZ	AZ	Southern (CZ)	Subpolar
Θ-min	Z			125	100	100
(100 m)	Θ	(6.749)	(3.635)	0.805	-0.184	-0.875
	S	(34.219)	(33.967)	34.078	34.172	34.264
S-min	Z	400				
	S	34.275				
	Θ	4.968				
Θ-max	Z			600	400	400
	Θ			1.998	1.653	0.926
	S			34.619	34.673	34.676
S-max	Z	2400	1900	1400	900	700
	S	34.754	34.746	34.734	34.724	34.699
	Θ	1.770	1.579	1.485	1.302	0.785

1.2.2.1.2 ***Southern Ocean mineralizing nannoplankton biogeography***

Three mineralizing nannoplankton groups have been found south of the SAF in previous studies in the Southern Ocean (Table 3). The following chapters focus on the diatom genus *Fragilariopsis*, the chrysophyte genus *Tetraparma*, and the coccolithophores including, but not limited to *E. huxleyi* (for reasons explained therein; section 3.1). The four species of *Fragilariopsis* detected in the Southern Ocean all occurred in the Antarctic Zone (PF to SACCF) according to Hasle (1965). *Fragilariopsis curta* and *Fragilariopsis cylindricus* occurred primarily in this zone and in increasing abundance towards Antarctica. They were also the primary species recovered in samples taken under sea ice. *Fragilariopsis rhombica* occurred in small numbers in both the Antarctic and the sub-Antarctic; however it was more common in the Antarctic. *Fragilariopsis pseudonana* occurs throughout the world ocean at a broad range of temperatures, though again usually in small numbers (Hasle, 1965).

Parmales, the clade to which *Tetraparma* belongs, has only been recognized since 1987 (Booth and Marchant, 1987). Previously, members of the Parmales were thought to be cysts of an oceanic choanoflagellate; thus, much of the data on their distribution do not recognize species, but merely records “siliceous cysts”. These cysts were recorded in the sub-Arctic Pacific (Booth et al., 1980; Booth et al., 1982) and the Weddell sea both under sea ice (Silver et al., 1980) and at the ice edge (Buck and

Garrison, 1983). More recently, studies have recognized divisions at the species level, allowing a clearer picture of *Tetraparma* distributions. *Tetraparma pelagica* has been recorded in subpolar regions (Booth and Marchant, 1987; Kosman et al., 1993; Komuro et al., 2005) and was the dominant mineralizing plankton in a recent study in the sub-Arctic Pacific (Komuro et al., 2005).

The vast majority of studies of sub-Antarctic (STF to PF) and Antarctic coccolithophores have noted a decrease in overall cell numbers polewards, a decrease in coccolithophore diversity polewards, and the dominance of *E. huxleyi* in the coccolithophore community (Hasle, 1960; McIntyre and Bé, 1967; Nishida, 1986; Verbeek, 1989; Findlay and Giraudeau, 2000; Mohan et al., 2008). *E. huxleyi* has been reported south of the PF in the Atlantic (McIntyre and Bé, 1967; Eynaud et al., 1999; Winter et al., 1999) and Pacific (Hasle, 1960; Nishida, 1986; Findlay and Giraudeau, 2000; Cubillos et al., 2007) sectors of the Southern Ocean, with recent satellite evidence predicting large *E. huxleyi* blooms in the Scotia Sea off the Patagonian shelf, along the PF to the north and west of South Georgia Island, and between the PF and SACCF to the south of South Georgia (Holligan et al., 2010). The major *E. huxleyi* morphotype observed in the southern region is morphotype B/C, though a few examples of partially dissolved coccospheres (an as-yet-uncharacterized morphotype D) have also been observed (Findlay and Giraudeau, 2000; Cubillos et al., 2007).

South of the SACCF, sampling for coccolithophores has only been carried out in the Australian sector and on one transect from South Africa to the Weddell Sea. The early Australian transects (Nishida, 1986; Findlay and Giraudeau, 2000) detected no coccolithophores south of the SACCF, while later transects consistently identified *E. huxleyi* morphotype B/C (Cubillos et al., 2007), which the authors suggested indicates range expansion (section 1.2.2). The South African transect detected four species of coccolithophore, including *E. huxleyi*, at the highest latitudes ever reported (69°S and 70°S) for the species. The authors suggested, however, that the species assemblage, generally considered to be subtropical, may have been introduced to the Weddell Sea from the Agulhas Current or an eddy from the Brazil-Malvinas confluence (Winter et al., 1999).

Table 3. Summary of species distributions for the three nannoplankton groups studied.

Group	Genus	Species	Distribution	Source
Diatom	*Fragilariopsis*	*F. curta/cylindricus*	Primarily found from the PF polewards with increasing abundance towards Antarctica Dominant *Fragilariopsis* species under sea ice	(Hasle, 1965)
		F. rhombica	More common south of the PF	(Hasle, 1965)
		F. pseudonana	Found throughout the world ocean	(Hasle, 1965)
Chrysophyte	*Tetraparma*	siliceous cysts	Present in the subarctic Pacific	(Booth et al., 1980; Booth et al., 1982)
			Found in the Weddell sea under sea ice	(Silver et al., 1980)
			Found in the Weddell sea at the ice edge	(Buck and Garrison, 1983)
		T. pelagica	Present in subpolar regions	(Booth and Marchant, 1987; Kosman et al., 1993; Komuro et al., 2005)
Coccolithophore	*Emiliania*	*E. huxleyi* (primarily morphotype B/C)	Found from the STF to south of the PF. Occur with decreasing abundance polewards	(Hasle, 1960; McIntyre and Bé, 1967; Nishida, 1986; Verbeek, 1989; Findlay and Giraudeau, 2000; Mohan et al., 2008; Holligan et al., 2010)
			Found south of the SACCF *in situ**	(Cubillos et al., 2007)
			Found south of the SACCF in satellite images**	(Holligan et al., 2010)
			Found in the Weddell Sea †	(Winter et al., 1999)
	Gephyrocapsa	*G. oceanica*	Found south of the SAF up to the PF	(Verbeek, 1989)
		G. ericsonii	Found south of the SAF up to the PF	(Verbeek, 1989)
	Calcidiscus	*C. leptoporus*	Found south of the SAF up to the PF	(Findlay and Giraudeau, 2000)
	Syracosphaera	*S. anthos,*	Found south of the SAF up to the PF	(Eynaud et al., 1999)
		S. sp. Type D	Found south of the SAF up to the PF	(Eynaud et al., 1999)
	Acanthoica	*A. quattrospina*	Found south of the SAF up to the PF	(Eynaud et al., 1999)
	Papposphaera	*P. sagitifera*	Found south of the PF	(Findlay and Giraudeau, 2000)
		P. obypyramidalis	Found south of the PF	(Findlay and Giraudeau, 2000)
	Wigwamma	*W. antarctica*	Found south of the PF	(Findlay and Giraudeau, 2000)
		W. triradiata	Found south of the PF	(Findlay and Giraudeau, 2000)
	Umbellosphaera	*U. irregularis*	Found south of the PF †	(Eynaud et al., 1999; Winter et al., 1999)
		U. tunuis	Found south of the PF †	(Winter et al., 1999)
		U. hulburtiania	Found south of the PF †	(Winter et al., 1999)

***** in earlier transects along the same cruise track, *E. huxleyi* were not present south of the SACCF (Nishida, 1986; Findlay and Giraudeau, 2000)

**satellite evidence supports the occurrence of *E. huxleyi* South of the SACCF in some years, and constraint by the SACCF in others (Holligan et al., 2010).

† the authors suggested that the subtropical coccolithophore assemblage found, including may have been introduced by physical mixing

Other coccolithophores found south of the SAF include *Gephyrocapsa oceanica*, *Gephyrocapsa ericsonii* (Verbeek, 1989), *Calcidiscus leptoporus* (Eynaud et al., 1999; Findlay and Giraudeau, 2000), *Papposphaera sagitifera, Papposphaera obpyramidalis, Wigwamma antarctica,* and *Wigwamma triradiata* (Findlay and Giraudeau, 2000), *Umbellosphaera irregularis, Umbellosphaera tunuis* (Eynaud et al., 1999; Winter et al., 1999)*, Umbellosphaera hulburtiania* (Winter et al., 1999)*, Syracosphaera anthos, Syracosphaera* sp. type D*,* and *Acanthoica quattrospina* (Eynaud et al., 1999). These coccolithophores always occurred at relatively low abundances compared to *E. huxleyi* and only a few were present south of the PF (*P. sagitifera, P. obpyramidalis, W. antarctica, W. triradiata, U. irregularis, U. tunuis,* and *U. hulburtiania*).

1.2.2.1.3 ***The Scotia Sea and its islands***

The Scotia Sea is a region of the Southern Ocean between the Drake Passage to the west and the Antarctic Peninsula to the east (Figure 11) where large phytoplankton blooms regularly occur in the vicinity of island chains (Korb and Whitehouse, 2004; Korb et al., 2004; Korb et al., 2008; Korb et al., 2010). The Scotia Ridge borders the Scotia Sea, and it is on this relatively shallow rise that the islands of the Scotia Sea are located: the South Orkney Islands, the South Sandwich Islands, and South Georgia. Areas of strong reflective signal corresponding to potential coccolithophore blooms have been observed via satellite in this region: on the Falkland Island shelf, in the PF region north and west of South Georgia, and between the PF and the SACCF south of South Georgia in the central Scotia Sea (Holligan et al., 2010), predictions which are investigated by hypothesis 3 (section 1.3).

South Georgia lies on a deep, narrow shelf on the North Scotia Ridge. The ACC flows eastwards towards the island, where its flow is perturbed by the island's topography (Orsi et al., 1995). The current is deflected northwest through a narrow channel between South Georgia Island and Shag Rocks, before being deflected east again by the PF. Waters from the SACCF are deflected south by South Georgia, but then follow the northern island shelf before continuing eastwards (Korb et al., 2004). The complicated physical oceanography in the region produces a chemical and biological gradient from south of South Georgia (upstream of the island from the perspective of the ACC) to north of South Georgia (downstream of the island), which creates an ideal natural laboratory for comparative studies of phytoplankton

communities in Fe-deplete and Fe-replete environments, (hypotheses 3 and 4; section 1.3).

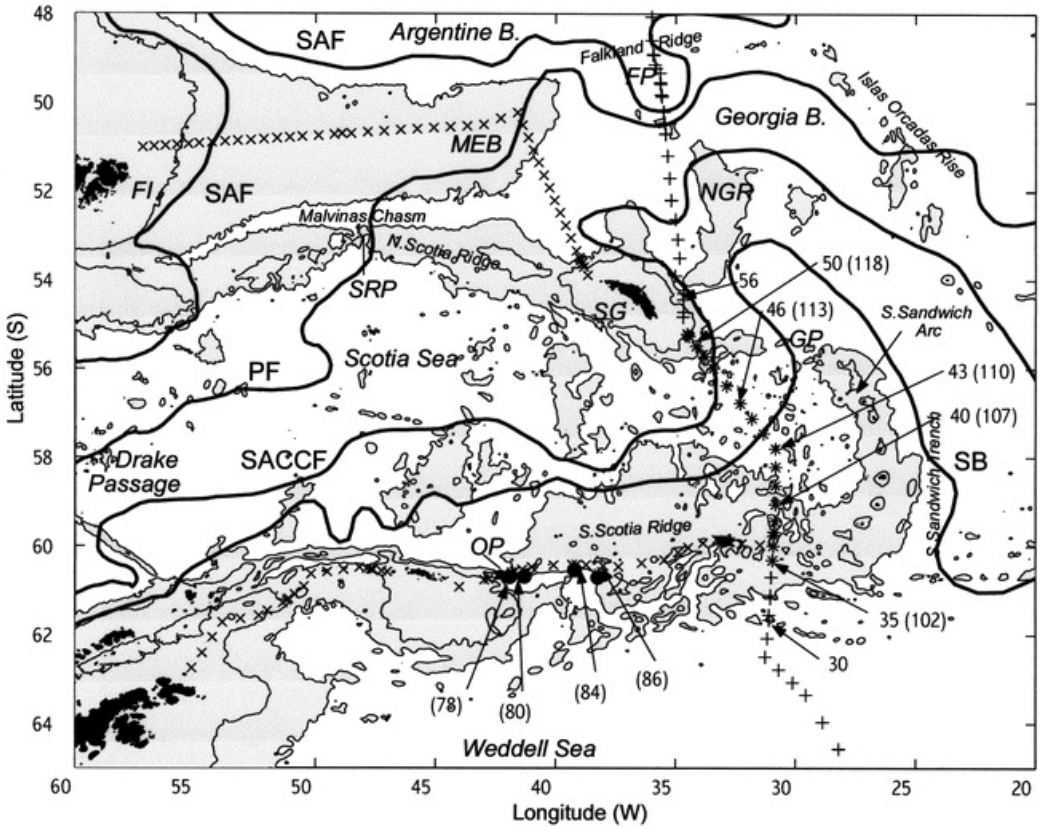

Figure 11. Figure taken from Meredith et al (2001) showing the Scotia Sea, the major circumpolar fronts, and the underlying bathymetry. Various topographic features are labelled by their initials, FP: Falkland Passage; MEB: Maurice Ewing Bank; FI: Falkland Islands; NGR: Northeast Georgia Rise; SRP: Shag Rocks Passage; SG: South Georgia; GP: Georgia Passage; OP: Orkney Passage. The 1000-m and 3000-m isobaths are marked; regions shallower than 3000 m are shaded. Dots, pluses, and numbers represent various cruise stations, which are detailed in the original article .

1.2.2.1.4 ***Southern Ocean Fe enrichment observational studies and experiments***

SOIREE, in February 1999, was the earliest mesoscale Fe addition experiment in the Southern Ocean (experiments summarized in Table 4). The study detected an increase in medium and large diatoms (large diatoms containing >1000 pg C $cell^{-1}$; medium diatoms containing between 100 and 1000 pg C $cell^{-1}$; these definitions will be used throughout the thesis) in the Fe-treated patch (most conspicuously *Fragilariopsis kerguelensis*) after an initial increase in haptophytes with pigment signatures

characteristic of *Phaeocystis* spp. and coccolithophores. CARUSO/EisenEX closely followed in November 2000 and found an increase in both small (diatoms containing <100 pg C cell^{-1}; this definition of 'small' will be used throughout the chapter) and large diatoms in an Antarctic eddy treated with successive Fe infusions. The large diatoms were dominated by *Rhizosolenia* spp., *Thalassiothrix* spp., and *Corethron pennatum*. Nitrate concentrations decreased in the treated patch, by 1.61 mmol m^{-3} (Gervais et al., 2002). Medium and large diatoms, including *Thalassiothrix antarctica*, *Corethron inerme*, *Guinardia* spp., *Proboscia* spp., and *Rhizosolenia* spp., were again the main group to respond to Fe addition in the most recent mesoscale Fe enrichment in the Atlantic, EIFEX, which also showed a large increase in chlorophyll-*a* (Chl-*a*) in the Fe-treated patch (0.5 mg m^{-3} to 2.9 mg m^{-3}) (Hoffmann et al., 2006).

Complementary studies using natural areas of Fe enrichment and high phytoplankton biomass close to Antarctic island chains, the "island mass effect" (Doty and Oguri, 1965), have been carried out in the Kerguelen Islands, Crozet Islands, and South Georgia Island (Table 4; bottom half). In austral spring 1995, the occurrence of Fe-rich waters (>2 nM) with low biomass, and moderate Fe waters (0.45 nM to 0.7 nM) with higher biomass was explained in the Kerguelen Islands by a more favourable light-mixing regime in the latter region. Though not the maximum values observed, the Fe present in the high biomass region was sufficient to support a phytoplankton community of large diatoms and of dinoflagellates (Blain et al., 2001). A summer 2005 Kerguelen study, KEOPS, analyzed the large bloom southeast of the island above the Kerguelen plateau. Although dFe values on the plateau were relatively low (0.09 nM), higher values close to the seafloor (0.6 nM) were indicative of a constant Fe supply fertilizing and maintaining the high production at the surface.

While the Kerguelen Islands studies were based solely on *in situ* measurements, the CROZEX study was the most similar to the study presented in chapter 4 as it combined *in situ* measurements with measurements from bioassay Fe enrichment experiments, and utilized F_v/F_m to assess nutrient stress in the phytoplankton population. The Crozet experiments demonstrated that the phytoplankton community in the *in situ* phytoplankton bloom associated with the Crozet Islands, which it was estimated exported a significant 25.0 mmol C m^{-2} y^{-1} to deep water (3.5 times more C than was exported in the surrounding HNLC waters; (Pollard et al., 2009), was dominated by *Phaeocystis antarctica* and medium diatoms. Depending on the *in situ* phytoplankton community, medium diatoms such as *Eucampia antarctica* and *Guinardia* spp., as well

as the small diatom *Pseudonitzschia* spp. and the large diatom *Chaetoceros criophilius,* all responded to Fe enrichment in bioassays (Moore et al., 2007a; Moore et al., 2007b). The authors showed that F_v/F_m was consistently higher in the phytoplankton bloom (0.47 to 0.6 inside bloom versus 0.3 to 0.44 outside bloom), as was Chl-*a* concentration.

Table 4. Summary of previous Fe fertilization experiments and observational studies in the Southern Ocean (SO) detailing the species which responded to artificial Fe enrichment (mesoscale Fe enrichment; bioassay Fe enrichment) or were more abundant at higher Fe concentrations *in situ* (natural Fe fertilization). Size specifications, small (S), medium (M), and large (L), were added according to the conventions used in this work.

Experiment	Date	Type	Responding Species	Reference
SOIREE (Australian sector SO)	Feb. 1999	Mesoscale Fe enrichment	Large diatoms *Fragilariopsis kerguelensis* (M)	(Gall et al., 2001)
CARUSO/EisenEX (Atlantic sector SO)	Nov. 2000	Mesoscale Fe enrichment	*Rhizosolenia* spp. (L) *Thalassiothrix* spp. (L) *Corethron pennatum* (L)	(Gervais et al., 2002)
EIFEX (Atlantic Sector SO)	Jan. to Mar. 2004	Mesoscale Fe enrichment	*Thalassiothrix antarctica* (L) *Corethron inerme* (L) *Guinardia* spp. (M) *Proboscia* spp. (L) *Rhizosolenia* spp. (L)	(Hoffmann et al., 2006)
Kerguelen Islands (Indian sector SO)	Oct. 1995	Natural Fe fertilization	Large diatoms Dinoflagellates	(Blain et al., 2001)
KEOPS (Kerguelen Islands)	Jan. to Feb. 2005	Natural Fe fertilization	Not specified	(Blain et al., 2007; Blain et al., 2008)
CROZEX (Crozet Islands; Indian sector SO)	Nov. 2004 to Jan. 2005	Natural Fe fertilization	*Phaeocystis antarctica* Medium diatoms	(Moore et al., 2007a)
		Bioassay Fe enrichment	Depended on initial phytoplankton community structure: *Phaeocystis antarctica* OR *Pseudonitzschia* spp. (S) *Eucampia antarctica* (M) *Guinardia* spp. (M) *Chaetoceros criophilus* (L)	
South Georgia Island (Scotia Sea; Atlantic Sector SO)	Jan. 2003	Natural Fe fertilization	*Eucampia antarctica* (L)	(Korb et al., 2010)
	Jan. to Feb. 2008*	Natural Fe fertilization	*Melosira adele* (S) *Thalassiothrix antarctica* (L)	

* This data was collected on the same cruise (North-west of South Georgia región) as the summer 2008 data in the current study.

The high F_v/F_m values were usually, but not always associated with high concentrations of dissolved Fe (dFe). In Moore et al.'s (2007a; 2007b) bioassay incubations, F_v/F_m, a fast-response physiological change, generally increased in Fe-treated bottles within 24

hours, while phytoplankton community shifts, representing slower biomass changes, were measured after 5-6 days.

Previous studies in the island chains of the Scotia Sea, the region of interest in chapter 4 have been observational. Phytoplankton blooms develop seasonally north and northwest of South Georgia (Korb and Whitehouse, 2004; Korb et al., 2004; Korb et al., 2008; Korb et al., 2010), downstream from where the ACC is deflected through a narrow channel between South Georgia and Shag Rocks. The region is referred to as Downstream of South Georgia (DSG), as opposed to the region south of South Georgia that supports smaller, shorter phytoplankton blooms and is referred to as Upstream of South Georgia (USG) (Korb et al., 2008). Korb et al. (2008) found that DSG is characterized by higher NO_3^-:PO_4^{3-} depletion ratios and lower $Si(OH)_4$:NO_3^- depletion ratios, which are consistent with an Fe-fertilized ecosystem. The authors also found that the DSG blooms exhibit higher F_v/F_m and a predominance of large diatoms (>63%), further suggesting Fe-fertilized conditions. In summer 2003 and 2008 (the summer 2008 data were collected on the same cruise as the summer 2008 data reported in the current study), blooms observed in the DSG region (referred to as north-west of South Georgia; NW-SG in the paper) were characterized by dominance of the diatoms *Melosira adele* (S) and *Thalassiothrix antarctica* (L) in 2008 and *Eucampia antarctica* (M) in 2003 (Table 4; (Korb et al., 2010). These DSG blooms persisted until March, in stark contrast to the less productive bloom in the USG region in 2008 (referred to as south-west of South Georgia; SW-SG in the paper), which peaked in December 2007 and had virtually disappeared by February 2008. The authors suggest that the observed regional differences in the longevity of blooms was due to a continuous resupply of macronutrients and Fe in the DSG region capable of sustaining prolonged bloom growth, and a seasonal resupply in the USG region that was soon depleted, leading to bloom demise (Korb et al., 2010). Another high chlorophyll region of the Scotia Sea is north of the South Orkney Island chain (as observed by satellite observations). Few direct measurements have been made in this region; however, in summer 2008, Korb et al. (2010) recorded high cryptophyte numbers in the region (referred to as Southern Scotia Sea; S-SCOT in the paper).

1.3 **Aims and objectives**

The aim of the research undertaken during this PhD is to expand the understanding of ecological processes for the model coccolithophorid, *E. huxleyi*

through filling two major gaps in current knowledge: the population structure and genetic outcome of *E. huxleyi* blooms, and the environmental and biological factors which determine the extent of *E. huxleyi* blooms at the edge of its known range. A better understanding of *E. huxleyi* ecology in these key areas will allow better predictions to be made regarding both the potential of *E. huxleyi* to adapt to future climate scenarios (by measuring variability within a bloom at the genetic level), and the possible future range of *E. huxleyi* (by identification of current limits). These two aims were accomplished with (1) a fine-scale analysis of population genetic diversity in the model system of a Norwegian mesocosm bloom and (2) a broad-scale analysis of phytoplankton community dynamics in the case study of the Southern Ocean. The Southern Ocean is considered a key oceanic region, as it allows the opportunity to test predictions regarding phytoplankton and mineralizing nannoplankton community dynamics within the context of variable macronutrient concentrations, Fe regimes, and pCO_2 concentrations at the limit of the species' current range. An analysis of *E. huxleyi* population diversity in the Southern Ocean, the logical combination of these two research aims was not possible in the timeframe of the PhD due to the logistical requirements for isolating large numbers of *E. huxleyi* cells, but remains an exciting area for future research and is addressed in section 5.2. The specific hypotheses tested through the PhD research and their groundings in the literature and previous work were the following:

Given the phenotypic plasticity found in *E. huxleyi* both in its ecological strategy and morphological diversity (sections 1.1.2 and 1.1.1.1), the genetic diversity of *E. huxleyi* is expected to be high (section 1.1.1.1.1). While previous work has produced this result in geographically wide-ranging samples, the opposite result is expected in *E. huxleyi* blooms due to the selective pressures of rapid bloom proliferation and viral-induced bloom demise (section 1.1.1.1.2), both of which are expected to reduce intraspecific genetic diversity. Intraspecific diversity is instead expected to be renewed through events following the bloom, including haploid cell recombination (section 1.1.1.1.2). These predictions were tested using the following hypotheses:

1. Intraspecific genetic diversity varies over an *E. huxleyi* bloom time series, starting high at the outset of the bloom, and reducing as the bloom progresses through exponential growth and a virally-mediated crash.

2. Population differentiation occurs at the molecular level during an *E. huxleyi* bloom time series following the selection of faster-growing individuals during rapid bloom proliferation and the selection of viral-resistant individuals during bloom demise.

Given the differing ecological strategies of coccolithophores, diatoms, and chrysophytes, the biogeography of these mineralizing phytoplankton species is expected to be limited by environmental factors including nutrient availability, temperature, and pCO_2 (section 1.1.2). In addition, diatoms are expected to exert a biological effect on the other groups, outcompeting them when growth conditions are favourable (section 1.1.2). Previous work in the Southern Ocean, where *E. huxleyi*'s range terminates and environmental gradients are strong, has found that phytoplankton communities are constrained by the strong fronts in the region (section 1.2.2.1), with nannoplankton (2-20 µm) succeeding in Fe-deplete HNLC regions, as expected due to their low dFe requirements (sections 1.1.2.1.1 and 1.2.2.1.2). The range of *E. huxleyi*, small diatoms, and chrysophytes in the region, therefore, is expected to be limited not by dFe as with medium and large diatoms, but by limiting macronutrients and competition within the nannoplankton size fraction. Small diatoms are expected to out-compete slower-growing *E. huxleyi* and chrysophytes where silica is non-limiting, while *E. huxleyi* is expected to dominate in silica-limited regions as it does not require the nutrient. Thus the *E. huxleyi* blooms which have been predicted using satellite imagery are expected in low silica regions where competition from diatoms is relieved. Although some research suggests that high pCO_2 would restrict *E. huxleyi* blooms, the latest results of increased calcification under high pCO_2 suggest that pCO_2 gradients will not affect *E. huxleyi* bloom distributions (section 1.1.2.3). The SACCF, however, is expected to be a stable boundary to the southern range of *E. huxleyi* (section 1.2.2.1). These predictions were tested using the following hypotheses:

3. Mineralizing nannoplankton biogeography is determined by silicate concentrations, with fast-growing small diatoms dominating when silica is non-limiting and slower-growing *E. huxleyi* dominating and forming blooms when silica is limiting. *E. huxleyi* distributions and blooms are further affected by the position of the SACCF, which generally forms a southern boundary to its range, however, the partial pressure of CO_2 does not affect distributions.

4. Adding Fe to phytoplankton communities in controlled experiments will produce a response in medium and large diatoms, but not in the nannoplankton size fraction. Thus *E. huxleyi*, small diatoms, and chrysophyte abundances will not increase in Fe treatments.

In order to pursue these research aims, several objectives first had to be met:

- Assessment of the ability of microsatellite molecular markers (Iglesias-Rodríguez et al., 2002; Iglesias-Rodríguez et al., 2006) to track genetic diversity within an *E. huxleyi* bloom time series.
- Development of a method capable of isolating large numbers of single *E. huxleyi* cells with low mortality.
- Stimulation of large-scale *E. huxleyi* blooms in an easily manipulated, yet relatively natural environmental setting.
- Description of phytoplankton community structure in regions of the Southern Ocean where *E. huxleyi* blooms are suspected to occur as well as neighbouring regions where they do not.
- Sampling of all possible environmental parameters throughout the Southern Ocean study area for comparison to species biogeography.
- Manipulation of dFe concentrations in incubation experiments to assess the effect of dFe availability on the total phytoplankton community.

The hypotheses are tested and the objectives are met in the following chapters following the structure outlined below:

Chapter 2: "Using microsatellites to track population dynamics in blooms of the marine coccolithophorid *E. huxleyi*." This chapter explores the first two hypotheses, studying the population dynamics of *E. huxleyi* blooms at the molecular level using microsatellite molecular markers and flow cytometry single-cell sorting during controlled mesocosm experiments in a Norwegian fjord.

Chapter 3: “Seasonal biogeography of mineralizing nannoplankton in the Scotia Sea.” This chapter explores the third hypothesis, quantifying mineralizing nannoplankton abundances and biomass, assessing potential *E. huxleyi* blooms, and describing mineralizing nannoplankton community structure in relation to environmental and biological controls using scanning electron microscopy (SEM) and multivariate statistics.

Chapter 4: “Seasonal iron control of phytoplankton community structure in the Scotia Sea.” This chapter further explores the fourth hypothesis, describing the experimentally-controlled effects of dFe availability on both the larger phytoplankton and nannoplankton communities.

Chapter 5: “Synthesis and future work.” This chapter summarizes the findings of the previous three chapters, discusses the implications of the results, and presents avenues for future research.

2 Using microsatellites to track population dynamics in blooms of the marine coccolithophorid *Emiliania huxleyi*

2.1 Introduction

Within the *E. huxleyi* species concept (i.e. the collection of organisms defined as *E. huxleyi*), functional DNA sequences appear highly conserved, however, high variability between *E. huxleyi* isolates in the transcriptome (von Dassow et al., 2009), some variability in the calcium-binding gene GPA (Schroeder et al., 2005), and high variability in non-coding microsatellite regions (Iglesias-Rodríguez et al., 2002; Iglesias-Rodríguez et al., 2006), suggest high intraspecific genetic diversity. If a positive relationship between genetic diversity and functional diversity exists (as suggested by Gadagkar (1998)), this genetic diversity may drive *E. huxleyi*'s adaptability to changing environments and its morphological plasticity, with correspondingly large implications for future *E. huxleyi* ecology as the effects of climate change alter marine environments. The most striking and biogeochemically important example of *E. huxleyi* phenotypic plasticity, however, the *E. huxleyi* bloom, is expected to reduce *E. huxleyi* genotypic diversity. This chapter seeks to quantify *E. huxleyi* genetic diversity through an analysis of intraspecific population dynamics in the highly selective bloom environment.

Previous experiments during *E. huxleyi* blooms have investigated variation in the GPA gene, called the coccolith morphology motif (CMM) over the course of an *E. huxleyi* bloom (Martinez et al., 2007). Although this functional marker showed no variation either within a bloom or between blooms in 2000 and 2003 in the same location, the ability of more highly variable microsatellite markers to detect genotypic variation over the course of an *E. huxleyi* bloom remains to be tested. The precedent for this work has been set by previous microsatellite studies which have detected a high level of genetic diversity in a diatom bloom over time and differentiated diatom populations and dinoflagellate populations over small spatial scales (Rynearson and Armbrust, 2004; Rynearson and Armbrust, 2005; Rynearson et al., 2006; Nagai et al., 2007). *E. huxleyi* genetic diversity has also been investigated using microsatellites, however, the study focused on isolates from a wide geographic range and did not

analyze enough isolates from different stages of a single bloom to analyze population structure over a bloom time series (Iglesias-Rodríguez et al., 2006).

Here, microsatellites were used to assess genetic variation and population differentiation throughout blooms of *E. huxleyi* in mesocosm experiments in Raunefjord, Bergen, Norway. The isolation of a large number of cell lines was accomplished using analytical flow cytometry (AFC), a method previously used to identify *E. huxleyi* cells and EhV based on light scattering and fluorescence characteristics (Larsen et al., 2001; Jacquet et al., 2002; Wilson, William H. et al., 2002; Larsen et al., 2004), but not previously used to live-sort single *E. huxleyi* cells. Samples from different mesocosm experiments were compared with each other and with historical samples dating back to 1991 to address the first two hypotheses outlined in section 1.3:

1. Intraspecific genetic diversity varies over an *E. huxleyi* bloom time series, starting high at the outset of the bloom, and reducing as the bloom progresses through exponential growth and a virally-mediated crash.

2. Population differentiation occurs at the molecular level during an *E. huxleyi* bloom time series following the selection of faster-growing individuals during rapid bloom proliferation and the selection of viral-resistant individuals during bloom demise.

2.2 Methods

2.2.1 Field sampling and cell isolation

Sampling was carried out during a mesocosm experiment at Espeland Marine Biological Field Station (University of Bergen), Norway (Figure 12) in June 2008 as a collaborative project with US (Bigelow Laboratory for Ocean Sciences, Rutgers University), UK (Plymouth Marine Laboratory, Marine Biological Association of the UK), and Norwegian (University of Bergen) partners. Each of the six mesocosm enclosures set up at the floating dock contained 11 m^3 of fjord water, two of which were used for *E. huxleyi* sampling, labelled bags 1 and 2. Both bags were enriched with 1.5 µmol L^{-1} $NaNO_3$ daily; however, bag 1 was also enriched with 0.1 µmol L^{-1} KH_2PO_4 (phosphate-replete treatment; P-replete) daily and bag 2 was also enriched with 0.02 µmol L^{-1} KH_2PO_4 (phosphate-deplete treatment; P-deplete) daily. An airlift was

employed in each bag to circulate the enclosed sea water. Due to the collaborative nature of the project, all of the experimental setup was performed in cooperation with the scientific group, and ancillary data to the *E. huxleyi* sampling, including phytoplankton counts, viral counts, and nutrient concentrations were collected by Kimmance et al. (manuscript in preparation). All other work was carried out by D. J. Hinz, unless otherwise stated.

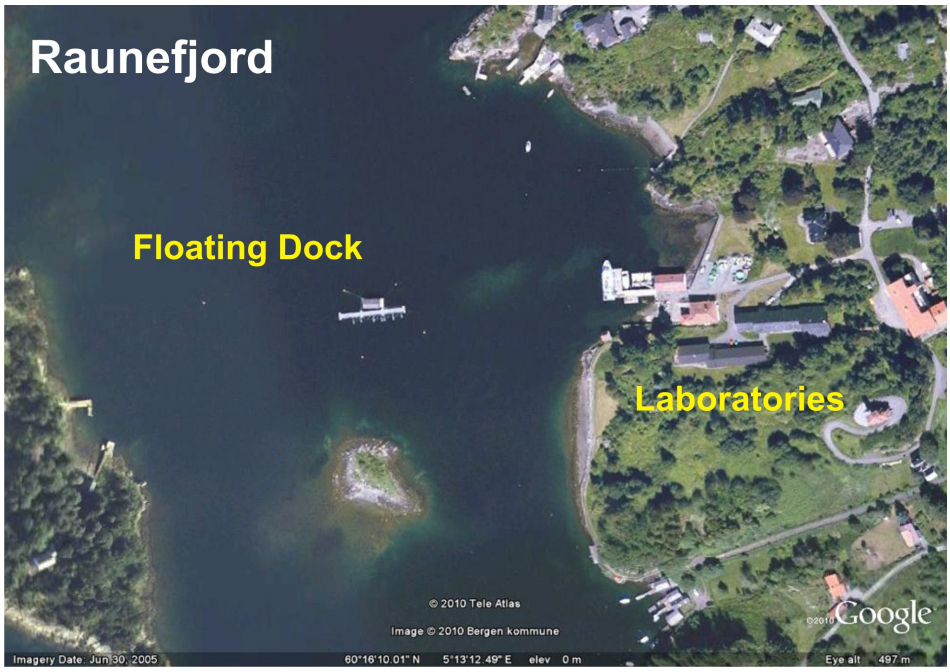

Figure 12. Mesocosm study site, showing the floating dock where mesocosm bags were moored, and onshore laboratories, where *E. huxleyi* cultures were initially maintained. Image produced using Google Earth ®.

The two bloom used were monitored for 17 days and sampled at a frequency of 2 to 7 days (on days 2, 4, 11, 14, and 16) to include the initiation, peak, and end of the blooms (section 2.3.1). Temperature and salinity were measured using a mini STD/CTD (SAIV A/S Bergen, Norway model SD 204) cast by hand. Global solar radiation data (daily total) were obtained from the 2008 Radiation Yearbook (Olseth et al., 2008). The yearbook records data collected using a CM11 pyranometer mounted at a height of 45 m on the roof of the University of Bergen's Geophysical Institute. The institute is located 20 km north of the study site.

Subsurface (0.5 m) water was collected on days 2, 4, 11, 14, and 16 from the two mesocosm bags in 2 L borosilicate bottles. If stored, bottles were kept in the dark

for up to 3 hours at 8°C before transport to the Molecular Imaging Center (University of Bergen). Cells were sorted into 24-well (Sarstedt Ltd. 83.1836.500) and 96-well tissue culture plates (Sarstedt Ltd. 83.1835.500) using a FACSAria® flow cytometer (BD Biosciences) equipped with Octagon (488-nm) blue laser 488 nm with standard filter set-up. *Emiliania huxleyi* cells were discriminated from other phytoplankton species based on dot plots of side-scatter signal (SSC) versus red (chlorophyll-*a*) fluorescence signal (695/40). Only *E. huxleyi* cells from the centre of the population grouping, expected to be healthy cells, were sorted. The Single Cell sorting mode protocol was used as recommended by the manufacturer (BD FACSAria User´s guide) with Purity Mask set to a maximum (32; only drops containing a target particle are sorted), Phase Mask set at half the maximum (16; only particles centred within the sorted drop are deflected) and Yield Mask disabled (drop trajectory and count accuracy are optimized at the expense of yield.) Culture plates were soaked overnight in MilliQ water to remove static charge (which can cause cells to stick to well walls), air dried, and pre-loaded with 2 ml or 200 µl of sterilized f/100 media (Guillard, 1975) depending on well size. Some 96-well plate media was also treated with 1.3 U ml^{-1} catalase (Sigma-Aldrich®), a chemical known to reduce H_2O_2 and improve growth in previously uncultured *Acidobacteria* species (Stevenson et al., 2004), and in *Prochlorococcus* strain MIT 9215 (Stevenson et al., 2004; Morris et al., 2008).

After sorting plates were stored in a constant temperature room at 8°C on a 12 hour day/night cycle (*in situ* temperatures ranged from 13 °C to 15 °C and day length ranged from 18.5 to 19 hours during the experiment). Light levels were maintained at approximately 20 W m^{-2} (~100 µE m^{-2} s^{-1}). Plates were then housed with the Bergen phytoplankton culture collection (Institute for Biology, University of Bergen, Norway) until visible growth was detected by eye. Plate wells were examined using light microscopy to confirm *E. huxleyi* growth. In all cases the observed growth was confirmed to be exclusively *E. huxleyi*. Inoculae from growing wells were subcultured into sterile 15 ml glass tubes at the Bergen culture collection laboratory. They were transported in ice pack-cooled Styrofoam containers from Bergen to Southampton, where clonal cultures were established. In Southampton, semicontinuous cultures were maintained under the same conditions in sterile 50 ml glass tubes. During the exponential growth phase (9 days following subculture), culture biomass had reached 10^6 to 10^7 cells ml^{-1} and cultures were pelleted via centrifugation and stored at -80°C. Although growth conditions and cell densities between cell isolation and culture

pelleting were not representative of *in situ* conditions, the DNA of cells is not affected by growth conditions (unlike RNA and protein synthesis), thus these conditions were satisfactory for the DNA-based genetic analyses employed. A selection of sixty cultures were given to the Plymouth Algal Culture Collection (accession numbers DHB600-DHB659). *E. huxleyi* morphotype was assessed according to Young et al. (2003) for a subset of the cultures using scanning electron microscopy (SEM).

2.2.2 PCR and fragment analyses

Genomic DNA was obtained using a standard phenol-chloroform extraction on culture pellets (Sambrook and Russell, 2001) followed by an ethanol precipitation, as described in Iglesias-Rodriguez et al. (2002). Microsatellite regions were PCR amplified using 5 previously developed primers (P02B12, EHMS37, P02E11, P01E05, and P02F11; Table 5; Iglesias-Rodríguez et al., 2002; Iglesias-Rodríguez et al., 2006) on either a PTC-200 DNA Engine (MJ Research) or Primus 96 Plus (MWG-Biotech) thermal cycler with HotStarTaq® Plus polymerase (standard manufacturer-provided protocol; Qiagen). PCR programs were as described in Iglesias-Rodriguez et al. (Iglesias-Rodríguez et al., 2002), except the annealing temperature (T_a) for EHMS37 was increased to 66°C.

Table 5. Details of the 5 microsatellite loci used. Adapted from Iglesias-Rodriguez et al. (2006).

Locus	Primer Sequence	EMBL Accession Number	Sequence Repeat Motif	T_a (°C)
P02B12	F: GGTTAATCGCAGCAAAGAGC	AJ487309	$(GT)_{10}$	58
	R: CAGTCTTGATCGGGAACGA	AJ487311		
EHMS37	F: TGTGAGAGTGAGCACGCA	AJ494737	$(GT)_{23}$	66
	R: TTGAGGAGGATTACGAGGTC	AJ494738		
P02E11	F: CGGTGCTACGAGGTGTGTAA	AJ487312	$(GA)_7TA\ (GA)_7$	58
	R: CACGCGCTTCACAATGTAAT	AJ487313		
P01E05	F: GTGTGCCCTTTTGTGCTTTT	AJ494739	$(GA)_{14}GG\ (GA)_{21}$	57
	R: GTGATGGTGTGCCTGTGTTC	AJ494740		
P02F11	F: CTCGTGTGGCTATGCCTATG	AJ487316	$(GT)_{11}$	58
	R: TCCAAGAGCAAAGTGCAAAA	AJ487317		

Initially, the sizes of PCR products were confirmed using 2% agarose gel electrophoresis, which also allowed an initial assessment of which individuals were homozygous (i.e. contained two identical copies of the microsatellite fragment) and which were heterozygous (i.e. contained two different copies of the microsatellite fragment; Figure 13). PCR reactions were then carried out with primers labelled with

Beckman WellRED fluorescent dyes (Proligo®). The labelled products were run on a CEQ™8000 sequencer in both singleplex and multiplex reactions. Multiplex reactions were attempted first; however, interference between the fluorescent dyes occurred in many reactions and these PCR's were re-run in singleplex, which allowed unequivocal identification of microsatellite fragment peaks . Microsatellite fragment peaks (Figure 14) were identified, measured, and analyzed using CEQ™ version 8 (Beckman Coulter). Mesocosm and fjord microsatellite fragments lengths were used as alleles to define genotypes for each of the isolated *E. huxleyi* cell lines. Sampling and subsequent laboratory procedures are summarized schematically in Figure 15.

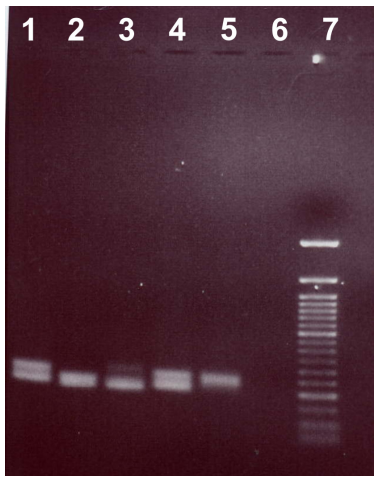

Figure 13. Image of PCR amplification products on an agarose gel for microsatellite locus P02E11 (lanes 1-5), with one band representing homozygous (lanes 2, 3, and 5) and two bands representing heterozygous individuals (lanes 1 and 4). A 50 bp ladder is shown in lane 7, and allowed an initial assessment to be made of allele sizes.

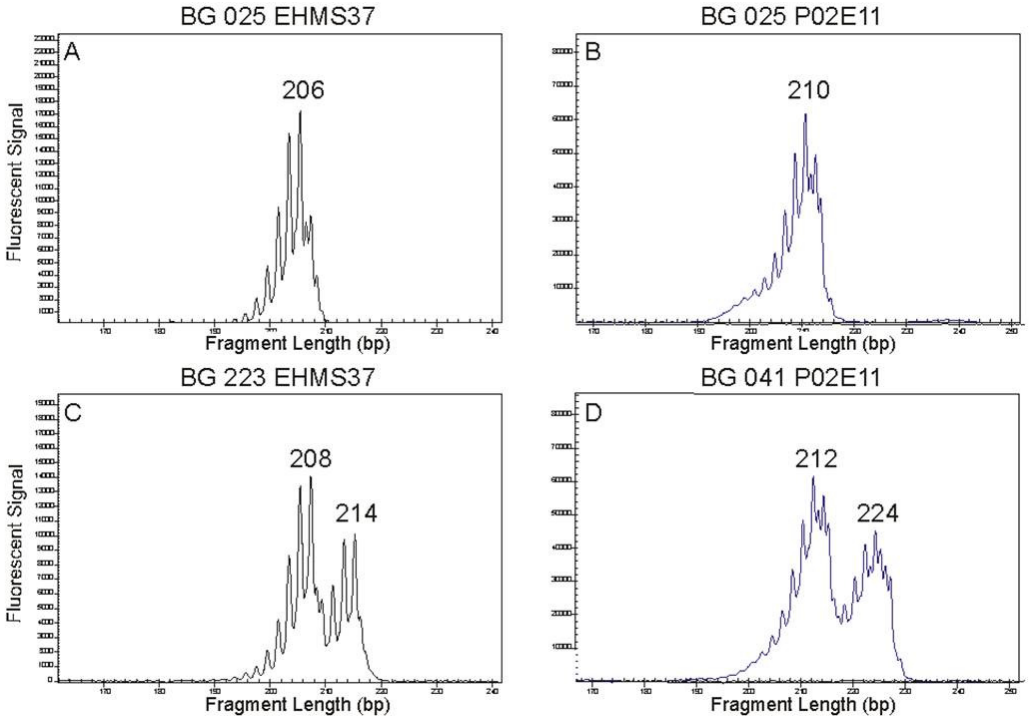

Figure 14a-d. Example of CEQ ™ fragment analysis outputs for two microsatellite loci, (a, c) EHMS37 and (b, d) P02E11. The largest peak is the true fragment peak, while the smaller peaks are artefacts. (A) EHMS37 (206 bp) and (b) P02E11 (210 bp) were both from homozygous individuals (isolates 025 and 223, respectively) and were the most commonly occurring genotypes for each locus. (C) EHMS37 (208, 214 bp) and (d) P02E11 (212, 224 bp) were both from heterozygous individuals (isolates 025 and 041, respectively) and were two of the rarest genotypes for each locus. The y-axis has no units as it is a ratio.

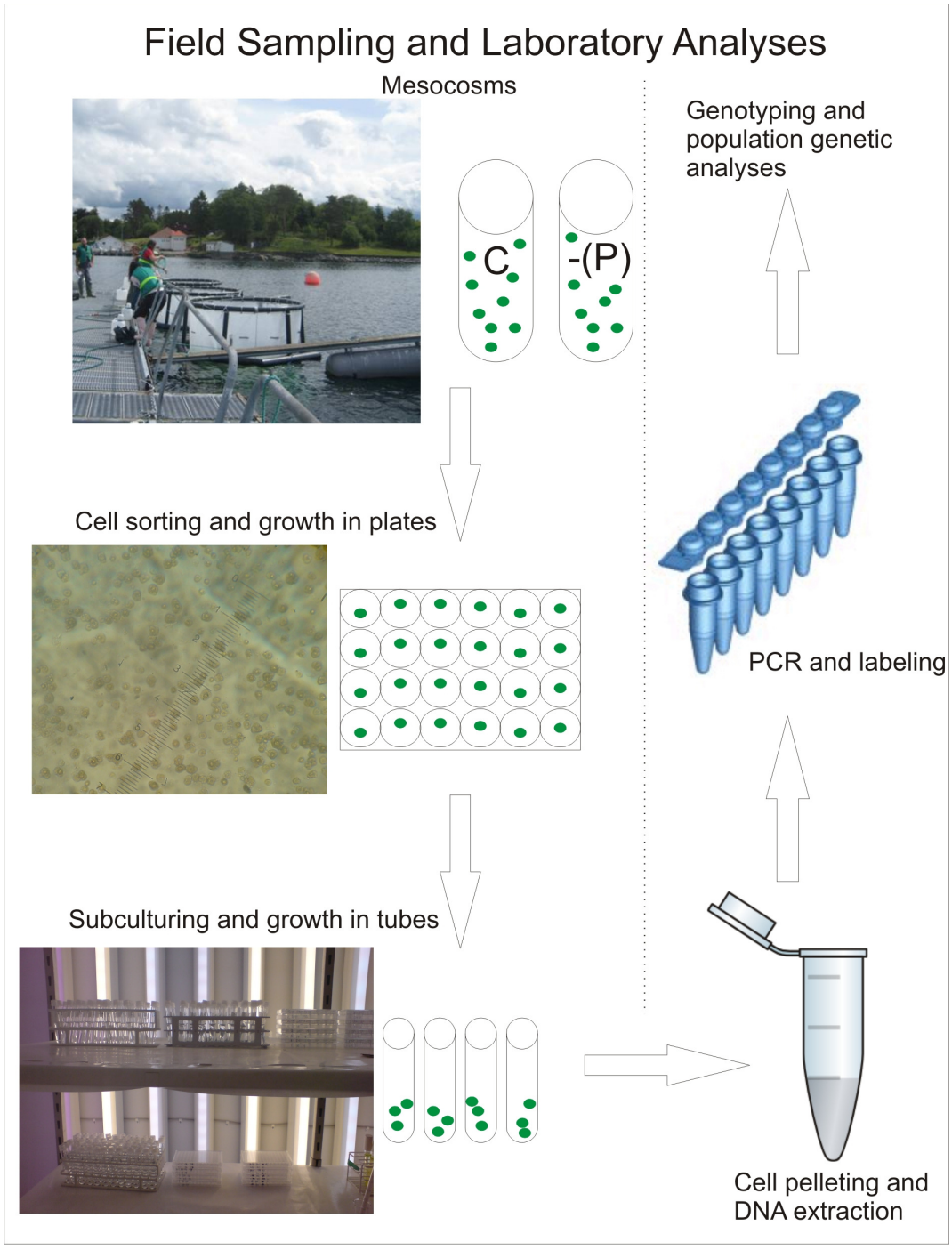

Figure 15. Schematic representation of the sampling methodology and laboratory analyses used in the mesocosm experiments.

2.2.3 **Statistical analyses**

The genotypes of single cell isolates were grouped according to isolation date (D (day)) and according to treatment (Fj (fjord), C (P-replete mesocosm), (-)P (P-deplete mesocosm)), which correspond to the 'water sample' groupings employed in previous population genetic studies of diatoms (Rynearson and Armbrust, 2005; Rynearson et al., 2006). The following groups were compared in statistical analyses: Fj D2, Fj D4, C D4, C D11, C D14, C D16, (-)P D11, (-)P D14, and (-)P D16 (statistical analyses summarized in Figure 16). In addition, two sets of data from older *E. huxleyi* cultures collected in the North Atlantic, comprised of the 42 FJ92 samples (collected in 1992) and the 22 NEA samples (collected in 1991) presented in Iglesias-Rodriguez et al. (2006), were reanalyzed as two water samples, FJ92 and NEA, and compared with the 2008 Bergen samples in a test of inter-annual genetic diversity. Because genetic diversities were calculated between isolates within each group (i.e. an individual value for Fj D4, C D11, FJ92, etc. calculated using isolates from that group), the two data sets were not combined during statistical analysis. This separation allowed the results for each group to be interpreted in terms of the differences in sampling procedure and instrumentation between the 2008 and 1991/92 datasets. The two datasets could not be used, however, to analyze inter-annual population differentiation because an estimation of genetic distance requires comparisons between isolates from different groups (i.e. Fj D4 isolates compared to FJ92 isolates) and the differences in sampling and instrumentation prevent a valid direct comparison of Bergen 2008 and 1991/92 samples.

The significance of differences in mean cell concentrations and in growth rates between different bloom phases was analyzed using a one-way ANOVA test in Minitab® 15 (Minitab, 2006), while the significance of differences between the P-replete and –deplete treatments during each phase was analyzed using an unpaired homoscedastic Student's *t*-Test. Minitab® 15 was also used to analyze the significance of methodological factors on *E. huxleyi* cell survival rates (one-way ANOVA). The extent of clonal diversity (G:N ratio), which provides an estimate of the percentage of unique genotypes relative to total genotypes in a water sample, was used first to test population genetic diversity. The ratio was determined by comparing the number of distinct five-locus genotypes (G) to the total number of five-locus genotypes analyzed (N) (Ellstrand and Roose, 1987), thus high ratios indicated a high number of unique alleles and high genetic diversity. A second measure of population genetic diversity,

called gene diversity (H_E) (Nei, 1987), was calculated in GENEPOP© version 4.0 (Raymond and Rousset, 1995; Rousset, 2008) for individual loci in each water sample and then averaged across all loci. H_E is a model-based projection of the number of heterozygote genotypes expected in a population, with high H_E values indicating a high genetic diversity in the water sample. An ANOVA test was performed on average H_E to determine whether significant differences existed between water samples using Minitab® 15. Predicted heterozygote numbers are based on the Hardy-Weinberg Equilibrium (HWE), a model used throughout population genetics to determine the equilibrium frequencies of genotypes in a randomly mating population. If the assumptions of the HWE are met, then regardless of the starting genotypes, populations will eventually reach the equilibrium values predicted by the HWE.

It was important to recognize whether HWE was achieved in the samples in this study because some tests in the next set of analyses, designed to determine whether samples segregated into distinct populations, assume HWE genotype frequencies. Samples in which genotype frequencies were significantly different from those predicted by the HWE do not meet the assumptions of the HWE, and therefore should not be judged relative to other samples solely based on tests assuming HWE. The main assumptions likely to be erroneous during an *E. huxleyi* bloom are (1) infinite populations (i.e. the sample population may not be large enough) and (2) random mating (i.e. the largely asexual reproduction that occurs during bloom growth or non-random association between loci will prevent genotypes reaching equilibrium). Departures from HWE were determined using GENEPOP© with the Hardy-Weinberg exact test (Haldane, 1954; Guo and Thompson, 1992), and significant heterozygote deficiency was determined using the U-test (Raymond and Rousset, 1995). The U-test was performed using Markov chain simulations of 200 batches and 5000 iterations with the condition that H1 = heterozygote deficit. Heterozygote deficiencies indicate that the expected number of heterozygote genotypes (H_E) is larger than the observed number of heterozygote genotypes (H_O); thus, genotypes are not in HWE and the assumptions of the HWE are not being met.

Two further tests of HWE assumptions were performed, one tested the randomness of allele recombination (fundamental to the assumption of random mating), and a second tested whether a sufficiently large portion of the population was sampled (fundamental to the assumption of infinite populations). The non-random association of loci, or linkage disequilibrium, is usually due to loci being located close together on the

chromosome, and therefore fewer breakages occurring between them during recombination. Genotypic linkage disequilibrium was tested between loci across all samples using Markov chain simulations of 100 batches and 5000 iterations in GENEPOP©. The portion of the population sampled was determined using a rarefaction curve (Heck et al., 1975), which graphically represents the accumulation of unique genotypes sampled against the total number of genotypes. A levelling off of the curve, as common genotypes are resampled, indicates that a reasonable number of genotypes has been sampled and that more intensive sampling is unlikely to yield more unique genotypes, while a continuous steep slope, as unique genotypes are found with every sampling, indicates that a large fraction of genotypic diversity remains to be discovered and that more sampling is necessary. The rarefaction curve was plotted for the P-replete treatment, as it was the most complete data set (four sampling points), using the FastGroupII web-based calculator tool (Yu et al., 2006).

Following tests of genetic diversity and conformity to the HWE, samples were tested against one another to identify whether they differentiated into distinct populations. Two methods were used to investigate population differentiation. Firstly, a pair-wise genotypic test (Goudet et al., 1996) was used to identify significant population differentiation. The test was performed using GENEPOP© with Markov chain simulations of 100 batches and 5000 iterations. The pair-wise genotypic test does not assume HWE and can therefore be applied to samples that do not conform to HWE genotype frequencies. Secondly, the estimator θ of F_{ST} (abbreviated F_{ST}) was used to quantify the degree of genetic differentiation between samples (Weir and Cockerham, 1984). F_{ST} is based on the HWE and measures the proportion of total genetic variance contained in a subpopulation relative to the total genetic variance (Foster et al., 2006). F_{ST} is a proxy for genetic distance ranging between 0 (no genetic differentiation) and 1 (total genetic differentiation; (Wright, 1965). F_{ST} values were calculated for each population pair in Genetix version 4.05 (Belkhir et al., 1996-2004) and their significance was determined using a permutation test in the same program. Significance levels for all pair-wise tests of population differentiation, both the genotypic test and F_{ST} test, were subjected to a multiple testing correction using the Dunn-Šidák method (Ury, 1976).

Principal components analyses (PCA) were performed on both the genotypic data and the environmental data to identify clusters of samples that were highly similar to each other based on genotypes and environmental conditions, respectively. F_{ST} values

were used to identify genotypic clusters in PCA-GEN version 1.2 (Goudet, 1999) and a permutation test was applied to assess significance with 10000 randomizations. Temperature, salinity, phosphate, nitrate, and daily global solar radiation (total sum of radiation from sun and sky on a horizontal surface per day; Olseth et al., 2008) were used to identify environmental condition clusters with PRIMER-E version 6.1.6 (Clarke and Gorley, 2006). The distributions of all five environmental variables were assessed using a draftsman's plot, which simultaneously displays all variable combinations in 2-dimensions. Where skewed distributions were present (salinity and nutrients), variables were transformed individually to achieve normal distributions. Salinity values were $\log_{10}$ transformed, while nutrients were increased by a constant equal to the lowest (nonzero) value for that nutrient before taking the square root. Correlation coefficients (r) were also calculated using the draftsman's plot function and used to produce r-squared values. The significance of correlations ($p \leq 0.05$) was analyzed using the regression function in Minitab® 15. All the variables were then normalized to a common scale before a resemblance matrix based on Euclidean distance was constructed. The distance matrix was then used in a CLUSTER analysis and significance of groupings was analyzed using the ANOSIM routine. The CLUSTER analysis was mapped onto a PCA ordination to visualize relationships between samples based on environmental conditions, which were then compared to those calculated using PCA-GEN based on genetic distance.

The population divisions identified using GENEPOP©, Genetix, and PCA-GEN were used to allocate samples into populations. The total number of clonal lineages, or clonal richness for each population, was calculated using EstimateS version 8.2 (Colwell, 2009) and the Chao1 (Chao, 1984; Chao, 1987) estimator. The samples that did not fall within a population were analyzed using a multi-locus likelihood function in WhichRun (Eichert, 1999) to determine the proportion of individual genotypes within the sample that derived from a differentiated population. The likelihood that a genotype derived from a given population ranged between 0 (least likely) and 1 (most likely). The allocation of genotypes to populations was based on maximum likelihood values of 1 for the source population and ≤ 0.3 for non-source populations (i.e. an approximately 100% chance the genotype derived from the source population and a less than 30% chance it derived from any other population).

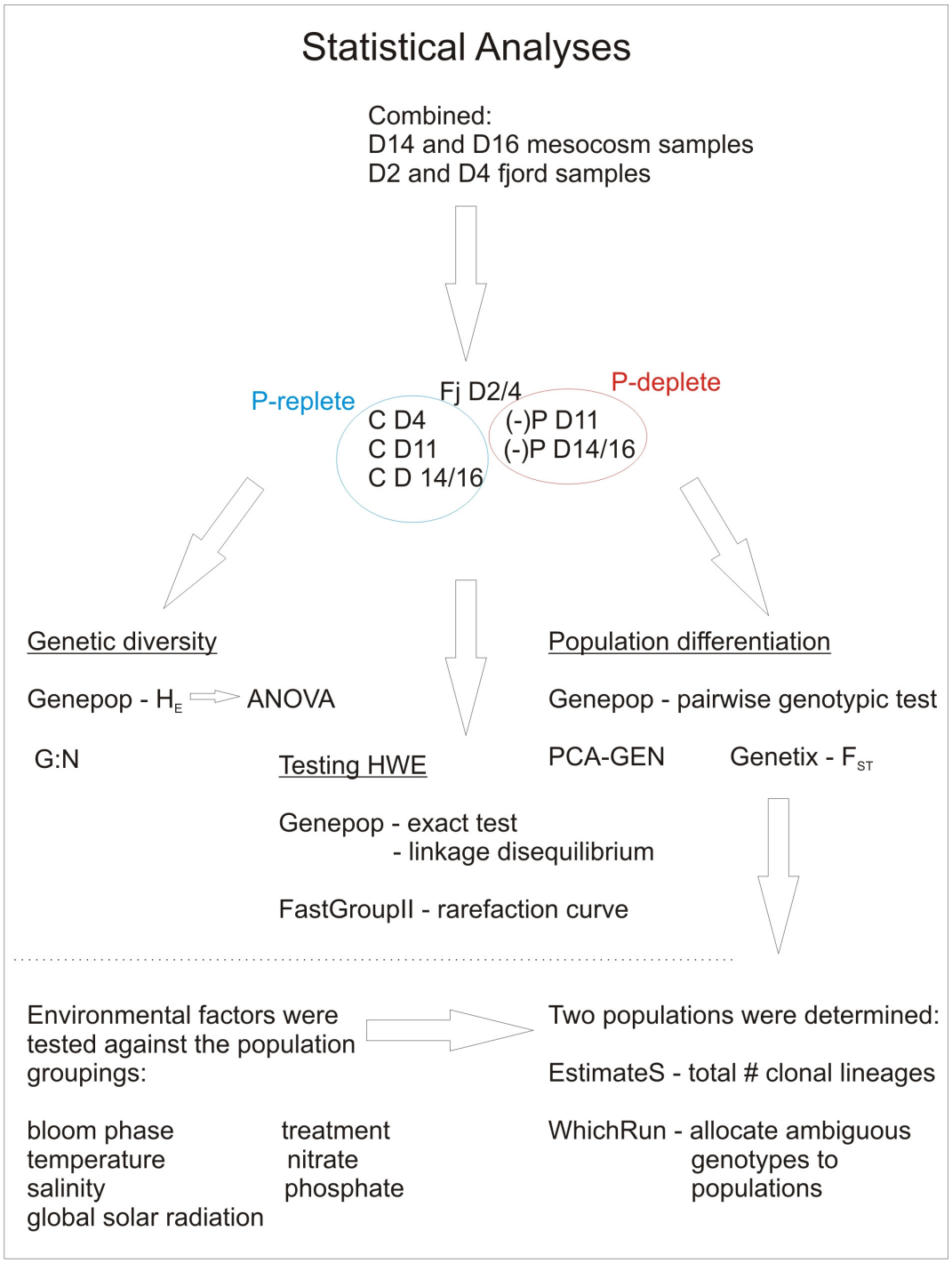

Figure 16. Schematic representation of the statistical analyses employed on the cultures resulting from the mesocosm experiments.

2.3 Results

2.3.1 Bloom structure and sample coverage

The microbial community underwent 3 distinct phases over the course of the 17-day experiment; these have been characterized by Kimmance et al. (pers. comm.). The authors identified four phytoplankton groups (*Synechococcus*, Nanoeukaryotes, Picoeukaryotes, and *E. huxleyi*) and *E. huxleyi*-specific viruses (EhV) using flow cytometry. *E. huxleyi* was the dominant photosynthetic phytoplankton; *E. huxleyi* abundance increased steadily to > 50% of total abundance (sum of abundances for all 4 photosynthetic groups) by day 6 and remained between 40% - 70% of total abundance through day 15. D. J. Hinz further identified the *E. huxleyi* population as morphotype B from a subset of isolates. Here only the results from temporal changes in *E. huxleyi* and EhV, which exhibited an inverse relationship, will be presented (Figure 17).
During *Phase 1* (days 2-7), *E. huxleyi* numbers increased exponentially from approximately 200 cells ml^{-1} to a maximum of 10,000 cells ml^{-1}, with no significant ($p \leq 0.05$) differences between P-deplete and P-replete treatments (mean cell concentrations 5,037 ±4,150 and 5,474 ±4,986 cells ml^{-1} in P-replete and –deplete treatments respectively; Student's *t*-Test). *Phase 2* (days 7-13) was primarily characterized by exponential *E. huxleyi* growth and a more visible split between phosphate treatments, however the differences were again not significant (Student's *t*-Test). Cell concentrations were higher in the P-replete treatment (averaging 88,056 ±39,152 cells ml^{-1}), with a maximum of 171,000 cells ml^{-1} towards the end of phase 2, when both treatments appeared to switch to stationary phase. In the P-deplete bags, cell concentrations averaged 51,561 ±18,525 cells ml^{-1} and only reached 70,125 cells ml^{-1} by the end of phase 2. Concentrations of EhV in both treatments also increased exponentially towards the end of phase 2, reaching a maximum of 4×10^6 EhV ml^{-1} in the P-replete treatment and a maximum of 1×10^6 EhV ml^{-1} in the P-deplete treatment.

Phase 3 (days 13-17) was primarily characterized by a crash in *E. huxleyi* numbers in both treatments correlated with an increase in EhV concentrations. In both treatments, the crash began at the beginning of phase 3 on day 13 with negative growth rates of -0.6 and -0.06 for P-replete and –deplete respectively.

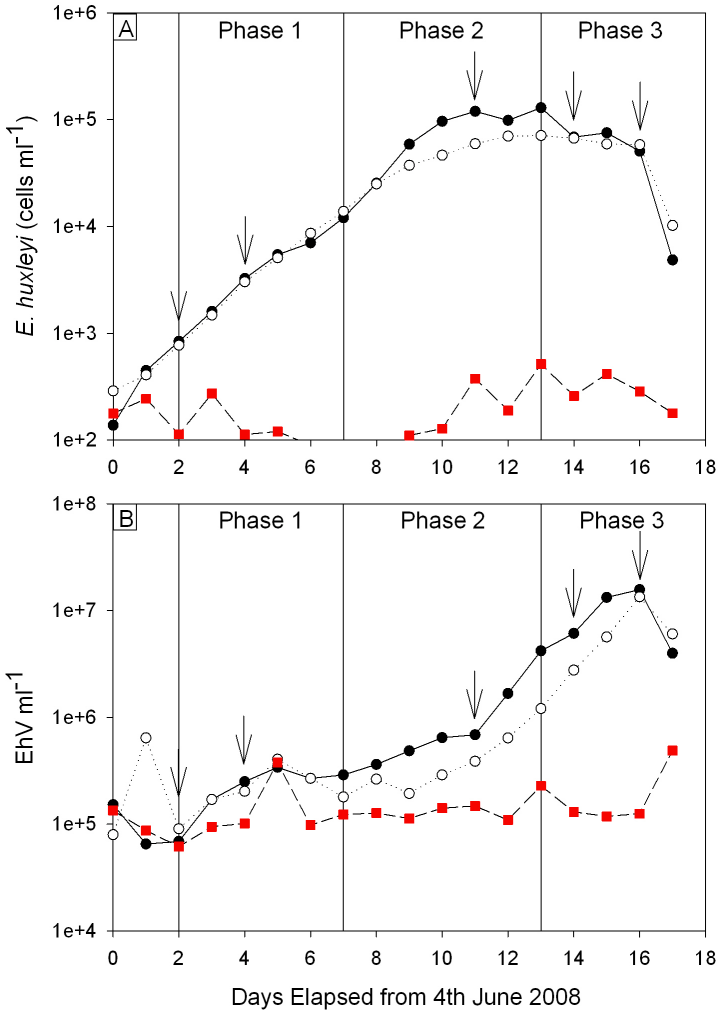

Figure 17. Log_{10}-scale flow cytometry counts of (a) *E. huxleyi* and (b) EhV for P-replete treatment, P-deplete treatment, and surrounding fjord water (filled circles, white circles, and red squares, respectively). The three bloom phases are labelled and live cell sorting sampling days are indicated by the arrows. Adapted from Kimmance et al. (pers. comm.).

E. huxleyi cell concentrations reduced by 96% by day 16 in the P-replete treatment (mean cell concentrations of 64,911 ±12,764 cells ml^{-1}), and by 82% by day 16 in the P-deplete treatment (mean cell concentrations of 61,491 ±4,853 cells ml^{-1}). Although EhV numbers were lower in the P-deplete treatment at the beginning of phase 3, after a period of exponential growth for both treatments, the P-deplete treatment reached approximately the same viral peak of 1 x 10^7 EhV ml^{-1} as the P-replete treatment on day 16. Viral populations in both treatments crashed on day 17, and analysis of nutrient and

flow cytometry data suggests that this and the precipitous drop in *E. huxleyi* numbers may have been due to the mesocosm bags being compromised (i.e. a leak; W. H. Wilson pers. comm.). For this reason, data from day 17 was not included in the statistical analyses of biological and environmental factors between phase. Though differences between treatments were not significant for any phase or for the experiment taken as a whole, both cell concentrations and growth rates (mean P-replete 0.57, 0.17, and -0.88; mean P-deplete 0.58, 0.16, and -0.63; for phases 1, 2, and 3 respectively) differed significantly between phases ($p \leq 0.05$; one-way ANOVA).

Samples were obtained from all three bloom phases in both P-replete and P-deplete treatments (the day 4 isolates from the P-replete treatment were considered to be representative for the P-deplete treatments because no differences were observed between the two treatments in phase 1; Table 6).

Table 6. Summary of surviving *E. huxleyi* cell lines and genotyping success. "Number of Surviving Cell Lines" refers to the number of cell lines which survived sorting and transfer from Bergen to Southampton. "Number genotyped" refers to the number of surviving cell lines genotyped for at least one locus. "NA" indicates not applicable.

Water sample	Year	Treatment	Day Isolated	Bloom Phase	Number Cell Lines Surviving (Total = 279)	Number Genotyped (Total = 143)
Fj D2	2008	Fjord	2	NA	2	2 (100%)
Fj D4	2008	Fjord	4	NA	6	6 (100%)
C D4	2008	P-replete	4	1	41	27 (66%)
C D11	2008	P-replete	11	2	86	33 (100%)*
C D14	2008	P-replete	14	3	17	14 (82%)
C D16	2008	P-replete	16	3	21	13 (62%)
(-)P D11	2008	P-deplete	11	2	88	28 (100%)†
(-)P D14	2008	P-deplete	14	3	2	2 (100%)
(-)P D16	2008	P-deplete	16	3	18	18 (100%)

* DNA extraction was attempted for 69 of the 86 surviving cell lines; genotyping was attempted for 33 of the DNA extractions

† DNA extraction was attempted for 66 of the 88 surviving cell lines; genotyping was attempted for 28 of the DNA extractions

Some sample sizes presented problems in downstream analysis due to low numbers of surviving cell lines ($N<20$). Samples with low sample sizes for the majority of loci were Fj D2, Fj D4, C D14, C D16, (-)P D14, and (-)P D16 (Table 7). Because days 2 and 4 both corresponded to phase 1 and days 14 and 16 both corresponded to phase 3, these samples were pooled within the fjord, P-replete, and P-deplete treatments to create the larger samples: Fj D2/4, C D14/16, and (-)P D 14/16. This adjustment produced useable sample sizes of 20 or more for the phase 3 pooled samples, but the fjord pooled sample

remained unavoidably small, and therefore this group was excluded from the population differentiation analyses.

Table 7. Summary of total genotypes sequenced for each population by locus. Bold type indicates the total number of individuals is less than 20.

Water sample	N	P02B12	EHMS37	P02E11	P01E05	P02F11
Fj D2*	**2**	**1**	**2**	**2**	**2**	**2**
Fj D4*	**6**	**1**	**6**	**6**	**6**	**6**
C D4	27	20	27	26	26	26
C D11	33	**19**	32	32	31	33
C D14†	**14**	**14**	**14**	**14**	**14**	**14**
C D16†	**13**	**9**	**13**	**13**	**13**	**13**
(-)P D11	28	**14**	27	26	26	27
(-)P D14**	**2**	**2**	**2**	**2**	**2**	**2**
(-)P D16**	**18**	**13**	**18**	**18**	**17**	**18**

*Fjord groups combined to form Fj D2/4 (N = 8)
†P-replete phase 3 treatments combined to form C D14/16 (N = 27)
**P-deplete phase 3 treatments combined to form (-)P D14/16 (N = 20)

2.3.2 **Mesocosm conditions**

In ANOVA tests comparing individual environmental factors shared by both treatments (temperature, salinity, and daily global solar radiation) for each phase, temperature was the only factor that varied significantly according to phase ($p \leq 0.001$; Figure 18). During phase 1, temperature averaged 14.5°C, during phase 2 it averaged 13.4°C, and during phase 3 it averaged 13.7°C (Table 8). Further ANOVA tests on those environmental variables which did vary between treatments (nitrate and phosphate), showed significant variation for: nitrate (NO_3^-) in the P-deplete treatment ($p \leq 0.001$), which averaged 2.9 µmol NO_3^- L^{-1}, 5.5 µmol NO_3^- L^{-1}, and 2.3 µmol NO_3^- L^{-1} in phases 1, 2, and 3 respectively; and for phosphate (PO_4^{3-}) in the P-replete treatment ($p \leq 0.045$), which averaged 0.1 µmol PO_4^{3-} L^{-1}, 0.03 µmol PO_4^{3-} L^{-1}, and 0.05 µmol PO_4^{3-} L^{-1} respectively (Figure 19).

Correlations between the environmental variables were low (draftsman's plot; Table 9). Significant correlations were tested between temperature and all variables and between nitrate and phosphate. The correlations between temperature and salinity and temperature and global solar radiation were significant ($p \leq 0.05$), though the covariation between the variables was low (r-squared 0.13and 0.16, respectively), meaning that little of the variation in one variable was explained by the other.

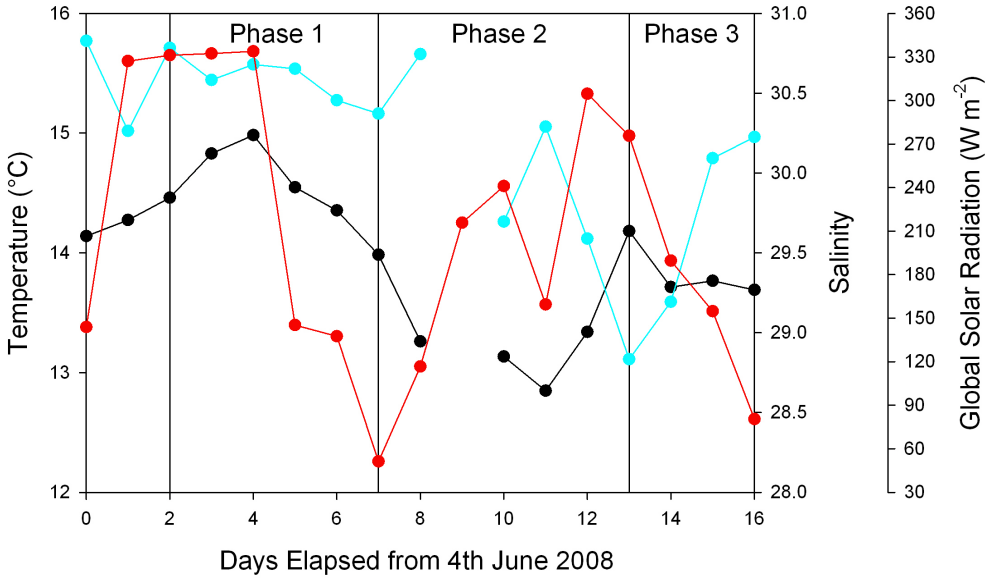

Figure 18. Environmental factors which did not vary between treatment groups: temperature (left axis; black line), salinity (near right axis; blue line), daily global solar radiation (far right axis; red line).

Table 8. Mean values ± standard deviations for environmental variables by phase.

Environmental Variable	Treatment	Phase 1	Phase 2	Phase 3
Temperature	both	14.5 ±0.4	13.4 ±0.5	13.7 ±0.04
Salinity	both	30.6 ±0.2	29.8 ±0.7	29.8 ±0.6
Global Solar Radiation	both	1917.3 ±1084.7	1890.8 ±611.8	1223.3 ±481.7
Nitrate	P-replete	0.7 ±0.7	0.2 ±0.4	0.5 ±0.5
	P-deplete	2.9 ±1.3	5.5 ±1.0	2.3 ±0.7
Phosphate	P-replete	0.1 ±0.04	0.0 ±0.04	0.0 ±0.04
	P-deplete	0	0.0 ±0.03	0

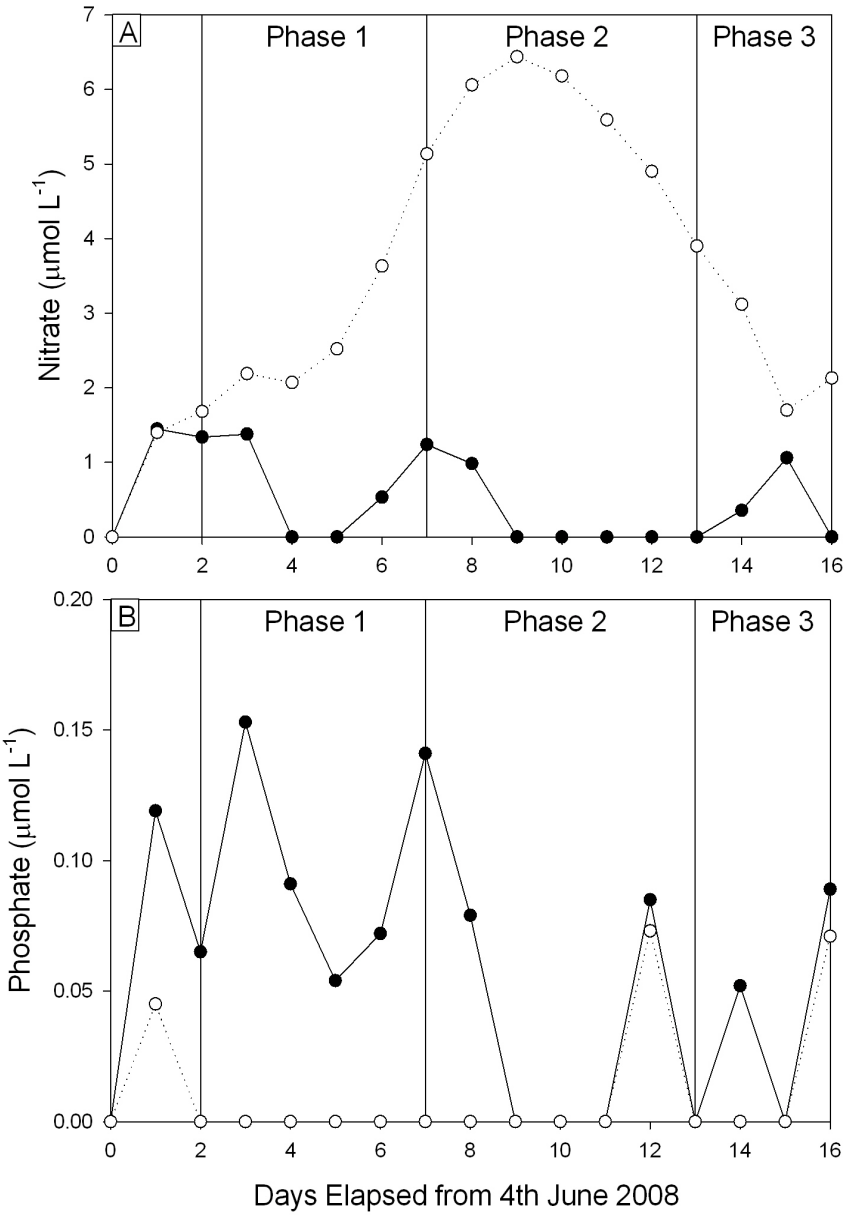

Figure 19. Environmental factors which varied between treatment groups, (a) nitrate and (b) phosphate. Filled circles are P-replete treatment; white circles are P-deplete treatment.

Table 9. Coefficient of determination (r-squared) for mesocosm environmental variables. Significant r-squared values (Minitab regression function) are shown in bold.

	SQR (Nitrate + 0.25)	SQR (Phosphate + 0.045)	Temperature	Salinity
SQR (Phosphate + 0.045)	0.07			
Temperature	0.04	0.04		
Salinity	0.00	0.00	**0.13**	
Global Solar Radiation	0.00	0.01	**0.16**	0.01

PCA analyses, therefore, which account for differences associated with both treatments and with phase, were performed on the environmental data (temperature, salinity, daily global solar radiation, nitrate, and phosphate concentrations) both with and without temperature, as constraining the effect of this potentially confounding variable was necessary. With temperature, the differences between phases and treatments for the entire period were significant ($p \leq 0.05$; ANOSIM test), while without temperature, only treatment was a significant factor ($p \leq 0.05$; ANOSIM test).

2.3.3 Single-cell sorting success

Isolated cells from the three phases of growth in mesocosm experiments were cultured in 96-well plates following single-cell sorting. The best survival rates were obtained using the catalase-treated 96-well plates. Survival rates were consistent at approximately 90% for plates sorted during phase 2; however, they dropped rapidly for plates sorted during phase 1 (between 0% and 41%) and from the fjord (between 0% and 16%). The phase 2 96-well catalase-treated plates also showed by far the most consistent success, with a standard deviation of only ±1.7% (N = 596 cells). Cultures were successfully grown in untreated 24-well plates, where survival rates varied between 8.3% and 54.2% and consistency of success was very low (Table 10; Figure 20). While it is obvious from phase 2, when the sampling methodologies overlapped, that using catalase-treated 96-well plates improved mean survival (by a factor of 3.7), survival rates were more heavily affected by the phase in which the cells were sorted (by a factor of 5.6 between phases 1 and 2). In ANOVA analyses combining all of the data, the relationship between phase and cell survival rates was significant ($p \leq 0.002$), while that between plate type and cell survival rates was not.

Table 10. Survival rates for various flow cytometry isolation methods.

Culture Vessel	Bloom Stage	Total Number of Plates Sorted	Average Percentage of Cells Surviving
24-well TC plate	Phase 2	4	25.0% ± 15.6%
	Phase 3	8	27.1% ± 18.8%
96-well TC plate, catalase treated	Fjord	3	6.6% ± 8.1%
	Phase 1	3	17.7% ± 20.8%
	Phase 2	6	91.3% ± 1.7%

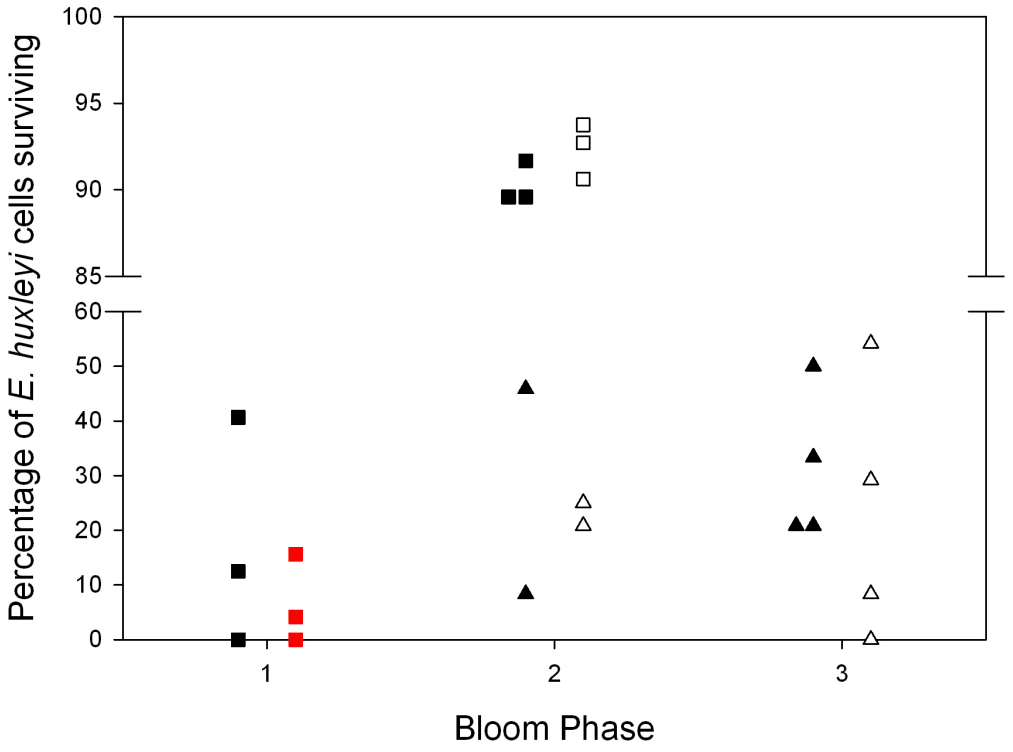

Figure 20. Results of single cell sorting for catalase-treated 96-well plates (squares) and untreated 24-well plates (triangles). P-replete treatment, P-deplete treatment, and surrounding fjord water are denoted by filled squares/triangles, white squares/triangles, and red squares, respectively.

2.3.4 **Genetic diversity and conformation to the HWE**

Out of the 279 successfully cultured cell isolates from the mesocosms and fjord, a total of 143 isolates were genotyped using microsatellite analysis. All five microsatellite loci (P02B12, EHMS37, P02E11, P01E05 and P02F11) were moderately to highly polymorphic according to 2008 data, with P02B12 showing the lowest variation at 3 allelic variants and P02E11 showing the highest at 34 allelic variants (Table 11). Of the 143 isolates, 122 unique genotypes were sampled with only ten genotypes (identical at five loci) occurring more than once. Nine of the ten genotypes occurred twice, while one occurred three times. Re-occurring genotypes were sampled from the same treatment on the same day, from the same treatment on successive days, and from different treatments; thus, they were unlikely to be due to cross-contamination.

Table 11. Summary of microsatellite loci characteristics including PCR success rates, fragment size range, and number of unique alleles for each locus. Calculated from 2008 data only

Locus	Successful PCRs	Size range (bp)	No alleles (no. isolates genotyped)
P02B12	66%	207-211	3 (94)
EHMS37	99%	200-296	13 (141)
P02E11	97%	194-241	34 (139)
P01E05	96%	118-254	21 (136)
P02F11	99%	97-192	13 (141)

Clonal diversity was consistently high (≥0.87; (Rynearson and Armbrust, 2005)) at 0.95 to 1 in all six 2008 samples and the two 1991/92 samples. Average H_E varied among sampling days in both the P-replete and P-deplete treatments, with maximum values occurring in phase 1 of the P-replete treatment (0.77) and phase 3 of the P-deplete treatment (0.78) (Table 12). Values remained high (≥0.67; Rynearson and Armbrust, 2005) both in mesocosm samples (averaging 0.67) and slightly lower in the fjord sample (0.60), however no significant differences were found comparing average H_E from all 2008 samples using an ANOVA test. Average H_E did drop sharply, however, for the two 1991/92 samples with a FJ92 value of 0.48 and a NEA of 0.39. The relationship between H_E for the 1991/92 samples, and the 2008 samples was not tested statistically, however, because the 1991/92 samples were collected on different days at nearby, but not identical locations.

Table 12. Summary of H_o and H_e for each water sample and at each locus. Also included are two diversity measures calculated across all five loci: gene diversity (± 1 S.D.) and G:N. Not applicable (NA) indicates that the data for that locus were unavailable. N indicates the total number of genotypes that could be genotyped for each sample. N_L indicates the number of isolates that could be genotyped at each locus.

	P02B12		EHMS37		P02E11		P01E05		P02F11		All loci	
Water sample (N)	Ho (N_L)	H_E	Ho (N_L)	H_E	Ho (N_L)	H_E	Ho (N_L)	H_E	Ho (N_L)	H_E	Ave. gene diversity (H_E)	Clonal diversity (G:N)
Fj D2/4 (8) †	0.00 (2)	0.00	0.88 (8)	0.78	0.75 (8)	0.90	0.13 (8)	0.59**	0.75 (8)	0.73	0.60 ± 0.35	1 (8)
C D4 (27)	0.19 (20)	0.42**	0.63 (27)	0.74	0.70 (26)	0.89**	0.26 (26)	0.81**	0.67 (26)	0.75	0.72 ± 0.18	0.96 (27)
C D11 (33)	0.03 (19)	0.34**	0.79 (32)	0.75	0.73 (32)	0.90**	0.27 (31)	0.81**	0.70 (33)	0.63	0.69 ± 0.22	1 (33)
C D14/16 (27)	0.00 (23)	0.14**	0.74 (27)	0.67	0.67 (27)	0.92**	0.56 (27)	0.87**	0.52 (27)	0.62*	0.65 ± 0.31	1 (27)
(-)P D11 (28)	0.04 (14)	0.10	0.68 (27)	0.75	0.50 (26)	0.86**	0.21 (26)	0.72**	0.46 (27)	0.63*	0.61 ± 0.30	0.96 (27)
(-)P D14/16 (20)	0.10 (15)	0.25	0.75 (20)	0.70	0.50 (20)	0.90**	0.40 (19)	0.74**	0.70 (20)	0.79**	0.68 ± 0.25	0.95 (20)
Fj 92 (42) ‡	0.19 (33)	0.18	0.38 (28)	0.48**	NA (0)	NA	0.62 (36)	0.80**	0.45 (33)	0.47	0.48 ± 0.25	1 (42)
NEA (22) ‡	0.27 (9)	0.25	0.14 (6)	0.25**	NA (0)	NA	0.59 (18)	0.69*	0.27 (11)	0.37*	0.39 ± 0.21	1 (22)

*significant heterozygote deficiency; p-value <0.05 for a Hardy-Weinberg exact test where H1=heterozygote deficit
** highly significant heterozygote deficiency; p-value <0.01 for a Hardy-Weinberg exact test where H1=heterozygote deficit
† Very few or no 5-locus genotypes due to missing allele data
‡ Reanalyzed 1991/92 samples. Original data available from Rodriguez et al. (2006)

These different sampling methodologies make a quantitative comparison of H_E values between the two datasets premature. The data are presented simply for a qualitative comparison as a first step towards more structured analyses of interannual genetic diversity.

Significant heterozygote deficiencies were observed in three or more loci for all of the mesocosm samples, with the majority highly significant, and observed in one locus (P01E05) for the Fj D2/4 sample, suggesting genotype frequencies were not in HWE. Genotypic linkage disequilibrium observed among four of the five loci, EHMS37, P02E11, P01E05, and P02F11, further indicated that allele segregation was non-random. The number of unique genotypes sampled increased linearly with the number of samples taken, and showed no signs of approaching an asymptote (levelling off) by day 16 (Figure 21), suggesting that a large amount of genotypic diversity remained unsampled.

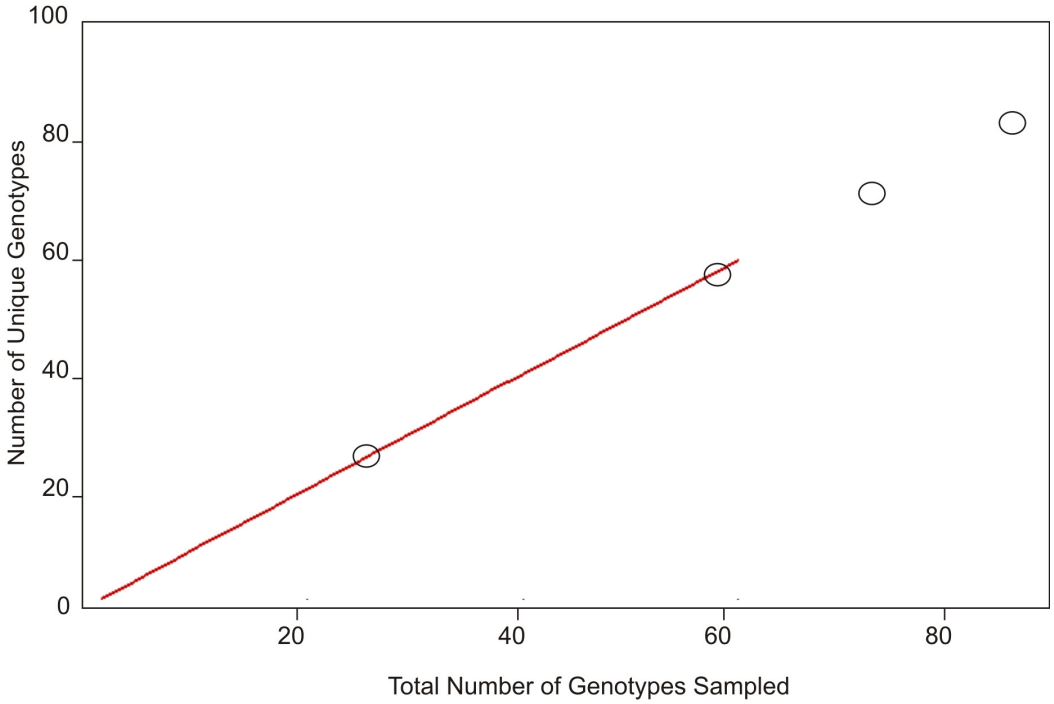

Figure 21. Genotype rarefaction curve for the P-replete treatment generated using FastGroupII. The model fit (red line) shows a continuously steep curve and no sign of approaching an asymptote. Sampling points (open circles) used as inputs into the model have been added post-analysis.

2.3.5 **Population differentiation and genetic distance**

The pair-wise genotypic test revealed significant differentiation in *E. huxleyi* populations between treatments, with one group (group 1) made up of P-replete phase 1 and 2 samples (C D4 and C D11 respectively), and a second group (group 2) made up of P-replete and -deplete phase 3 samples (C D14/16 and (-)P D14/16 respectively) (Table 13). Neither the P-deplete phase 2 sample ((-)P D11), nor the fjord sample (Fj D2/4) differentiated significantly from any other samples using a conservative Bonferroni-corrected significance level. It is worth noting that before the Bonferroni correction was applied, however, the (-)P D11 sample was placed in group 2 with the other P-deplete sample.

Table 13. P-values resulting from pair-wise tests of population differentiation.

Water Sample	C D11	C D14/16	(-)P D11	(-)P D14/16	Fj D2/4
C D4	0.97	6.47E-04**	9.42E-03	2.07E-04**	0.43
C D11		4.82E-04**	1.32E-02	1.44E-03*	0.31
C D14/16			0.26	0.52	0.30
(-)P D11				0.19	0.55
(-)P D14/16					0.14

* significant values; $p<3.41x10^{-3}$ Bonferroni corrected
**highly significant values; $p<3.41x10^{-4}$ Bonferroni corrected

The second population differentiation measure used was pair-wise F_{ST}, which showed little genetic variation (F_{ST} from 0 to 0.05) or moderate genetic variation (F_{ST} from 0.05 to 0.15) (Table 14). Significant F_{ST} values corresponded to the same samples as the pair-wise genotypic test in population group 1, but only the C D14/16 sample in group 2. The (-)P D14/16 sample was very nearly in group 2, as it differentiated significantly from one of the group 1 samples (C D11), but exceeded the conservative Bonferroni-corrected significance level with the other group 1 sample (C D4) by a very narrow margin; the (-)P D11 sample was not as close to the significance level cut-off for group 2 in the pairwise F_{ST} test as it was in the pair-wise genotypic test (Table 15).

PCA plotting of genotypic data based on F_{ST} also revealed population differentiation (Figure 22). Fj D2/4 was dropped from this analysis as it was only represented by 2 complete five-locus genotypes. Two principal component (PC) axes were sufficient to represent 82.1% of the variation (percentage inertia PC1 = 69.0%, percentage inertia PC2 = 13.1%).

Table 14. Matrix of pair-wise F_{ST} values over 5 loci. Negative values should be considered as zero values.

Water Sample	C D11	C D14/16	(-)P D11	(-)P D14/16	Fj D2/4
C D4	-0.00	5.11E-02 †	3.83E-02	4.31E-02	3.74E-02
C D11		6.18E-02 †	4.94E-02	5.64E-02 †	4.35E-02
C D14/16			-2.00E-05	8.52E-03	2.39E-03
(-)P D11				4.72E-03	-1.73E-02
(-)P D14/16					1.15E-03

† denotes moderate genetic variation

Table 15. Results of a permutation test, showing the percentage of F_{ST} values greater than the F_{ST} values given in Table 14. A value ≤5%, therefore, corresponds to p ≤0.05 for the corresponding F_{ST} value in Table 14.

Water Sample	C D11	C D14/16	(-)P D11	(-)P D14/16	Fj D2/4
C D4	86.91	0.17*	1.5	0.42	8.88
C D11		0.04*	0.63	0.25*	9.86
C D14/16			42.91	16.02	37.7
(-)P D11				29.35	69.5
(-)P D14/16					41.2

* significant values; p<0.341 Bonferroni corrected

Total F_{ST}, or genetic distance between samples, was moderate (0.048) and significant (Bonferroni-corrected; p≤0.00512). According to the broken stick model used by the PCA software, PC1 was significant, meaning that samples well-separated along the PC1 axis were genetically distinct according to F_{ST}. Two clusters of samples were well-separated on PC1, a cluster including the C D14/16, (-)P D11, and (-)P D14/16 samples (cluster 2), and a cluster including the C D4 and C D11 samples (cluster 1). Clusters 1 and 2 aligned well with the pair-wise genotypic populations groups 1 and 2, respectively. The only change, the placement of the (-)P D11 sample in cluster 2, was very similar to its placement near group 2 in the pair-wise genotypic test. Among the 3 tests of population differentiation used, the pair-wise genotypic test was deemed the most reliable because it does not assume HWE, the assumptions of which the data did not appear to meet (section 2.3.4).

Finally, the properties of the two population groups were analyzed, including clonal richness and environmental range. Group 1 was estimated to contain 316.94 ±172.23 clonal lineages, while group 2 was estimated to contain 830.33 ± 404.12. One-way ANOVA tests of individual environmental variables did not reveal any significant differences in environmental variables between groups 1 and 2.

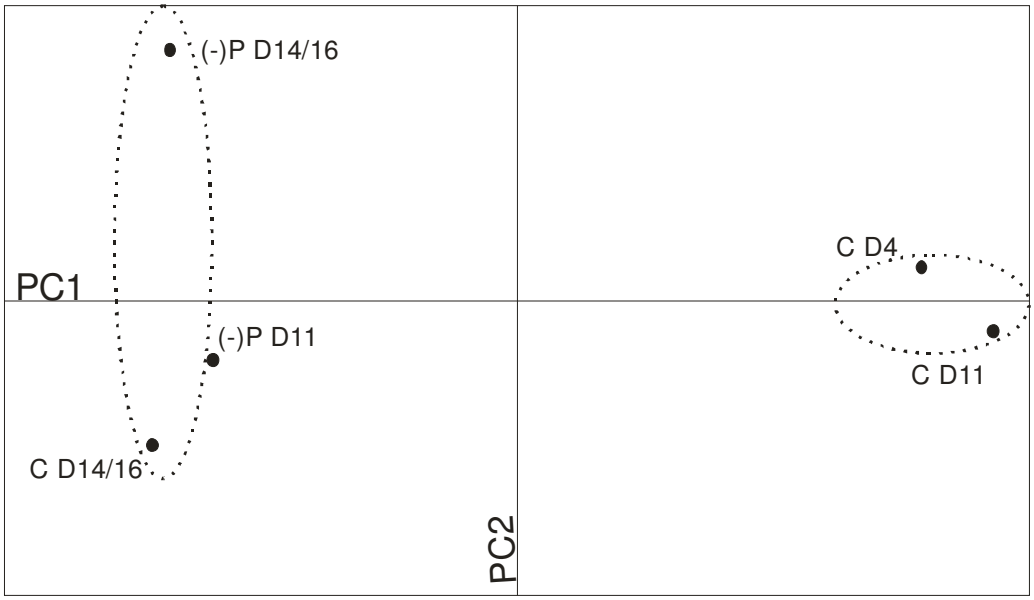

Figure 22. PCA plot based on F_{ST} (Goudet et al., 1996). Dashed circles encompass the two genetically distinct populations identified using the pair-wise genotypic test: group 1 (C D4 and C D11) and group 2 (C D14/16 and (-)P D14/16).

Because the position of the (-)P D11 sample changed in each of the three tests of population differentiation employed, the relationship between (-)P D11 and groups 1 and 2 was further investigated using WhichRun. Comparisons of individual (-)P D11 genotypes to the pooled genotypes of groups 1 and 2 showed that 25.0% were likely to be derived from the group 1 population and 57.1% were likely to be derived from the group 2 population. Five genotypes (17.9%) were not allocated to either group because the maximum likelihood estimates for both groups 1 and 2 were higher than 0.3 and the likely source population could not be determined.

2.4 Discussion

In this study, a genetic characterization of *E. huxleyi* populations sampled in controlled mesocosm experiments (both P-replete and P-deplete) and in natural *E. huxleyi* communities in Norwegian fjord waters has been presented, with the aim of quantifying *E. huxleyi* diversity and identifying distinct *E. huxleyi* populations during bloom development.

2.4.1 **High diversity at all phases of bloom development**

Clonal diversity (0.95 to 1) and average gene diversity (0.60 to 0.72) were high in all six 2008 samples, indicating a substantial pool of genetic diversity for *E. huxleyi* during bloom initiation, peak, and demise at the microsatellite level. The maintenance of high diversity through a period of rapid population growth and viral-induced bloom demise was opposite to the expectation that faster growing and viral-resistant specialist individuals would out-compete the bulk of the population and reduce genetic diversity over the course of an *E. huxleyi* bloom (hypothesis 1; section 1.3). The maintenance of genetic diversity instead suggests that the bulk of the *E. huxleyi* population is made up of highly adaptable individuals which can respond readily to strong ecological pressures, a characteristic which may underlie *E. huxleyi*'s functional diversity and success in both stable and unstable environments.

Possible mechanisms of maintaining this genetic variance include sexual reproduction, as evidenced by a haploid stage in the life cycle (Green et al., 1996; Frada et al., 2008; section 1.1.1.1.2), and environmental heterogeneity (Bell, 1997). Given the prediction that genetic diversity would decrease over a bloom, sexual reproduction was expected to maintain genetic diversity following the bloom crash (section 1.3). Contrary to these predictions, however, genetic diversity was maintained during the *E. huxleyi* bloom through the bloom crash. Over the short time scale of a single bloom in this study, and given the significant heterozygote deficiencies observed in the majority of loci, which indicate random mating is not occurring according to the HWE, environmental heterogeneity is the more likely mechanism. Sexual reproduction remains, however, a possibility for longer term maintenance of genetic variation and species success (Frada et al., 2008; section 1.1.1.1.2). EhV provides a third possible mechanism of maintaining genetic diversity through an unanticipated avenue known as 'kill the winner' (Thingstad and Lignell, 1997). This hypothesis states that because viruses are density-dependent they infect the most common organisms, and therefore rare organisms are maintained in the population through viral resistance. Although this theory has been applied to maintaining different species within communities, (Fuhrman and Schwalbach, 2003), a potential effect at the intraspecific level was unexpected, and provides an interesting new avenue for investigating host-population dynamics.

The identification of high diversity in this study was made possible by the highly polymorphic nature of the microsatellite loci employed, a polymorphism not seen with

the CMM marker used in the only previous study (to the author's knowledge) of intraspecific diversity over the course of an *E. huxleyi* bloom (Martinez et al., 2007). This polymorphism is the likely reason for the discrepancy between the findings of zero diversity in the Martinez et al. (2007) study, and the findings of high diversity in the current study. The levels of diversity in the present study, however, are consistent with another study using microsatellites to track population dynamics in a *Ditylum brightwellii* (diatom) bloom off the northwest coast of the United States by Rynearson and Armbrust (2005). Low diversity values were found for just one locus in the current study, P02B12, probably due to missing information for that locus following low rates of PCR success, possibly resulting from null alleles (mutations in the unique flanking regions used to design PCR primers; section 1.1.1.1.1). P02B12 was also the least polymorphic locus. Dropping this locus was considered; however, analyses without P02B12 (four loci) were compared to those with P02B12 (5 loci) and P02B12 was found to be highly informative despite its low polymorphism. The combination of possible null alleles and low polymorphism at the P02B12 locus, the only microsatellite locus used not to show linkage disequilibrium, suggest it may be in a different region of the *E. huxleyi* genome, possibly one that is mutating in the microsatellite primer region or has a functional component (and is therefore more highly conserved).

2.4.2 **Comparisons with 1991/92 data**

An estimate of temporal diversity at the inter-annual level was made using microsatellite data sets for two previous North Atlantic blooms. While clonal diversity remained high (G:N = 1), average gene diversity was much lower for the FJ92 and NEA samples isolated 16 and 17 years previously. The drop in gene diversity was unexpected considering the difference in sample collection between the 1991/92 samples and the 2008 Bergen samples. All of the individual cells comprising a sample in the Bergen 2008 study were collected from the same water sample on the same day, whereas this was not the case for the 1991/92 samples. The occurrence of less diversity in samples pooled from individuals experiencing greater temporal and spatial separation presents the intriguing possibility that diversity among individuals making up the FJ92 and NEA samples decreased between cell isolation (in 1992 and 1991, respectively) and DNA extraction (in approximately 2006). Using a conservative growth rate of 1.3 cell divisions day^{-1} (Half of the maximum 2.6 cell divisions day^{-1} observed in culture; Brand, 1981), the 15 years in culture would have produced 7120 generations.

Microsatellite loci vary greatly in their mutation rates, and those for the microsatellite loci used in this study are not known, however, using the typical range of 10^{-2} to 10^{-6} mutations per locus per generation (Li et al., 2002), the number of mutations per locus per generation during the 15 years in culture is expected to be between 7 x 10^{-3} and 142. With faster mutation rates, therefore, the culturing interval is theoretically sufficient for mutations in the microsatellite regions to occur and affect population composition. Differences between the methodologies for both sampling of the 1991/92 samples and analysis of the data, however, might also be responsible for the differences in genetic diversity. In fact these differences made any statistical analyses comparing the two datasets premature. While speculative, the result is interesting for researchers interested in future genome research, as the present *E. huxleyi* genome is based on a strain isolated in 1991.

2.4.3 **Population differentiation and bloom phase**

Population differentiation was assessed with three tests, two of which, the pair-wise F_{ST} test and the PCA-GEN test, were based on the assumption that genotypes were in HWE. Given the high occurrence of heterozygote deficiencies and linkage disequilibrium, indicating that the assumption of random mating was not met, and the failure of the rarefaction curve to reduce in slope, indicating the assumption of a sufficiently large population was not met, the data could not be deemed a good match to the HWE model. Samples were grouped into two significantly different populations in all three tests; however, the pair-wise genotypic test was deemed the most useful for defining the boundaries of the populations as it does not assume HWE. Both F_{ST}-based tests, however, are useful as quantitative measures of genetic distance that can be compared with other studies of phytoplankton (Rynearson and Armbrust, 2004; Rynearson and Armbrust, 2005; Nagai et al., 2007; Rynearson et al., 2009).

The main finding of the population differentiation tests was the emergence of a distinct population in phase 3 of both the P-replete and -deplete blooms following an *E. huxleyi* population crash observed in phase 2. Biological conditions differed significantly between phases in terms of both cell concentration and growth rates (section 2.3.1), however, environmental conditions were not significantly different between phases according to the conservative PCA analysis (without temperature), and the significantly higher nitrate concentrations which occurred in phase 2 were experienced by (-)P D11 (section 2.3.2). Viral attack, therefore, the major agent of *E.*

huxleyi bloom demise (Bratbak et al., 1996; Wilson, W. H. et al., 2002), appeared to be responsible for the population differentiation. This is to the author's knowledge the first evidence that, at the microsatellite level, an *E. huxleyi* population in the bloom initiation (exponential growth) and peak (stationary) phases is distinct from the healthy core population in the virally induced demise (crash) phase (only cells from the centre of the population, expected to be healthy were sorted throughout the experiments; section 2.2.1).

It is important to note that the culture media and vessels varied between phases 1 and 2 (catalase-treated 96-well plates) and phase 3 (untreated 24-well plates), however the effect of this change in methodology (necessary due to logistical field requirements) on cell mortality was expected to be minimal compared to the effect of phase on cell mortality (2.3.3). It must be stated, however, that the population differentiation measured is a combination of: (1) the effect of phase on the *in situ E. huxleyi* population, (2) the effect of phase on the survival of *E. huxleyi* isolates during single cell sorting, and (3) the effect of plate type and media on the survival of *E. huxleyi* isolates during single cell sorting, with (1) expected to be the largest effect.

The lack of population differentiation between the exponential growth and stationary phases was unexpected (hypothesis 2; section 1.3), suggesting that selection of faster-growing individuals does not occur or does not sufficiently alter the population. Population differentiation in the crash phase of the *E. huxleyi* bloom, however, was an expected outcome (hypothesis 2; section 1.3) and suggests that the subset of diploid *E. huxleyi* which avoid viral lysis, possibly through viral resistance, make up an altered population. The population shift observed in the crash phase produced a subset of the diploid population which maintained genetic diversity, and potentially functional diversity as well. The extrapolation of high functional diversity and viral resistance from high microsatellite genetic diversity and population succession is, however, speculative until direct functional experiments using the *E. huxleyi* isolates from this study can be carried out (experiments are planned for 2011). The maintenance of genetic diversity through catastrophic levels of mortality further supports the 'kill the winner' hypothesis of Thingstad and Lignell.

Further characterization of the two populations using clonal richness was inconclusive due to the large uncertainty in the estimates. Although the estimates suggested that group 2 was characterized by a larger number of genotypes (approximately 830) than group 1, the large error bounds, which are probably due to the

relatively small number of genotypes sampled (2.3.1), was not reliable. Both the clonal richness and the genetic variability estimated for *E. huxleyi* in this study, therefore, should be considered to be a minimum estimate. Interestingly, the phase 2 P-replete population and the fjord population did not fall into either the pre-crash or the crash populations. In the case of Fj D2/4, this non-differentiation was not investigated further as it was likely the result of a very small sample size (N=8), while in the case of the (-)P D11 sample, the high percentage of (-)P D11 genotypes likely to be from group 2 suggested it was closely related to that group.

Overall, F_{ST} values were similar to those of other groups of pelagic marine organisms, which are rarely larger than 0.01 (Rynearson and Armbrust, 2004). Although sample sizes in the current study were not large, significant F_{ST} values were all greater than 0.05, thus estimates for these moderate values using the sample sizes in this study ($N \geq 20$) were valid according to Kalinowski (2005). Studies of *D. brightwellii* populations have revealed much larger genetic differentiation between samples, with F_{ST} values up to 0.245 (Rynearson and Armbrust, 2004). Recent evidence, however, suggests that the two differentiated populations in that study (from different water masses) may in fact be cryptic species (Rynearson et al., 2009; Koester et al., 2010). It is perhaps more informative that, in contrast to this study, no significant differences in F_{ST} were observed between individuals within a single *D. brightwellii* bloom, a result not related to the lack of random mating found in the current study, as diatom bloom also reproduce asexually during exponential growth. The F_{ST} values suggest that, among phytoplankton, *E. huxleyi* is indeed characterized by high diversity (Rynearson and Armbrust, 2005).

2.4.4 **Sorting success with catalase treatment**

In order to genetically characterize individual cells making up a population of *E. huxleyi,* it is necessary to establish cultures from isolated cells. In this study is reported the successful use of flow cytometry single-cell sorting with catalase treatment as a viable technique for collecting large numbers of clonal *E. huxleyi* cultures. As the first sorting experiment of this kind, it is difficult to say whether the survival rates are 'normal', however the untreated 24-well plate survival rates are probably the best baseline data. Experiments in 2007 using the same technique on *E. huxleyi* with untreated 96-well plates (by D.J. Hinz; data not shown) failed to produce any viable cultures, thus without catalase, 'normal' survival rates are between 0% when small

wells (200 µL) are used and to a maximum of 54.2% when larger wells (2 mL) are used. The rates of up to 90%, therefore, for catalase-treated plates are more than triple the average baseline survival rates established with untreated 24-well plates. The finding that high success rates were not consistent between phases 1 and 2, however, highlighted a second, larger factor in cell mortality: the phase in which cells were sorted. The phase 2 cell survival rates were over 5 times higher than the phase 1 survival rates, indicating that bloom populations may be more resistant to the kinds of stress involved in single cell sorting than pre-bloom populations.

It is difficult to speculate on why this may be the case without further experiments, however, one possibility is a positive effect on survival due to increased *E. huxleyi* cell density. This speculation is partly supported by results from a set of sorting experiments carried out in Bergen prior to the 2008 fieldwork, where cells were sorted in quantities of 1, 10, or 100 cells well^{-1} into untreated 96-well plates (data not shown). Sorting 1 cell well^{-1} resulted in no surviving cells, sorting 10 cells well^{-1} resulted in a survival rate of 28%, and sorting 100 cells well^{-1} resulted in a survival rate of 94%. The experiments were not performed in triplicate and are therefore not conclusive, however, they suggest that increased cell densities in the culture plate have a positive effect, an effect which may also improve survival of sorted cells when higher densities occur prior to sorting.

2.4.5 Conclusions

To the author's knowledge, this is the first study to quantify *E. huxleyi* intraspecific genetic diversity over a bloom time series, to compare *E. huxleyi* intraspecific genetic diversity between recent isolates and culture collection isolates, to identify *E. huxleyi* population differentiation over a bloom time-series, and to sort and subsequently culture *E. huxleyi* cells using AFC. The major findings of the work were the unexpected maintenance of *E. huxleyi* genetic diversity through rapid bloom proliferation and viral bloom demise, the unexpected lack of differentiation of *E. huxleyi* populations during exponential growth, the expected differentiation of *E. huxleyi* populations as viral concentrations increased, and the ability of flow cytometry single cell sorting to produce large numbers of viable clonal *E. huxleyi* cultures.

The implications of these findings are that EhV exerts a major control, not only on *E. huxleyi* cell abundances and the fate of blooms, but also on maintenance of *E. huxleyi* genetic diversity. Rather than the predicted negative effect on diversity,

however, as would be expected if EhV acted as a classic population bottleneck, EhV may have a positive effect on the maintenance of *E. huxleyi* genetic diversity through a 'kill the winner' model acting on the intraspecific level. The questions raised by this development are two-fold; the first, whether and how this genetic diversity relates to functional diversity including viral resistance is beyond the scope of this thesis research (further experiments are planned for 2011), however, the second, how other biological and environmental factors affect *E. huxleyi* cell abundances and bloom populations will be explored in the following two chapters in natural populations in the Southern Ocean.

Finally, the additional outcome of the Bergen mesocosm studies, the success of flow cytometry single cell sorting either in 24-well plates or in 96-well plates with catalase treatment is an important result for future laboratory studies of *E. huxleyi*. Future experiments could benefit from obtaining cultures of *E. huxleyi* isolated from a larger range of ecologically diverse locations. For example, many CO_2 and other manipulation experiments motivated by concerns surrounding climate change have relied on strains of *E. huxleyi* morphotype A (Riebesell et al., 2000; Feng et al., 2008; Iglesias-Rodríguez et al., 2008), however, the responses of the ecologically distinct more weakly calcifying morphotype B/C, which dominates in the Southern Ocean (Findlay and Giraudeau, 2000; Cubillos et al., 2007), have not been tested and could provide a wealth of information.

The following chapter has been prepared as a paper and is currently in review under the same title for a Deep Sea Research Part II: Topical Studies in Oceanography special issue entitled Seasonal and spatial patterns in the Scotia Sea ecosystem.

3 Seasonal Biogeography of Mineralizing Nannoplankton in the Scotia Sea: *Emiliania huxleyi*, *Fragilariopsis,* and *Tetraparma*.

3.1 Introduction

Phytoplankton growth in the Southern Ocean is highly seasonal and is stimulated in summer by high light input and high macronutrient concentrations, which have accumulated over the dark winter. Additional factors influencing phytoplankton biomass and community dynamics in the Southern Ocean include Fe limitation, grazing (Boyd, 2002; Smetacek et al., 2004), and, if earlier laboratory experiments predicting that high pCO_2 may negatively affect calcareous taxa (section 1.1.2.3), pCO_2. The dominant bloom-forming phytoplankton in the Southern Ocean are diatoms and *Phaeocystis antarctica* (Boyd, 2002), however, recent work investigating the smaller phytoplankton suggests that a large portion of the HNLC Southern Ocean between the circumpolar fronts is dominated by both picoplankton (0.2–2 µm) and nannoplankton (2–20 µm) (Daly et al., 2001; Kang et al., 2001; Boyd, 2002). In addition, analysis of water-leaving radiance from satellite data has identified annual large-scale blooms close to the Falkland Islands and in the oceanic waters of the Scotia Sea, which have been attributed to the nannoplankton coccolithophore *E. huxleyi* (1000 to 2000 cells ml^{-1}; Holligan et al., 2010). Many previous studies in the Southern Ocean have failed to take into account nannoplankton species including *E. huxleyi* because the preservation and microscopy techniques that were used were often limited to non-calcifying phytoplankton species and a cell size of at least 10 µm (Komuro et al., 2005; Poulton et al., 2007; Korb et al., 2008), however, it appears the nannoplankton may make significant contributions to production and biomass. In addition, the contribution of phytoplankton to biomass may further increase as the effects of climate change shift phytoplankton community structure. A recent study in the Bering Sea has linked a phytoplankton community shift from diatoms to nannoplankton to a corresponding increase in temperature and CO_2 (Hare et al., 2007).

The Scotia Sea, in the Atlantic sector of the Southern Ocean (Figure 11; section 1.2.2.1.3), includes examples of many characteristic Southern Ocean ecosystems

including deep stratified water, oceanic island systems associated with shallow topological features and higher dFe concentrations, and strong nutrient gradients across circumpolar fronts. The Scotia Sea is therefore a natural laboratory of high environmental heterogeneity where the environmental and biological factors affecting *E. huxleyi* growth can be studied *in situ* in order to gain a better understanding of the ecological constraints on *E. huxleyi* biogeography. In addition to an improved understanding of current *E. huxleyi* ecology, information on the factors most influencing *E. huxleyi* biogeography at the boundary of its expected range will aid in predicting *E. huxleyi* responses towards climate change.

In this study, three mineralizing nannoplankton taxa were considered: the coccolithophores largely composed of *E. huxleyi* (Lohmann, 1902), the small diatom *Fragilariopsis* spp., (<20 µm), and the chrysophyte *Tetraparma* spp. (family *Triparmarceae*) (Figure 23). These were chosen as representative species based on their high abundance (see section 3.3.2). It was hypothesized that these groups have similar nutrient requirements (nitrate, phosphate, and Fe) and grazing pressures owing to their similar cell sizes and mineralizing skeletons; however, *Fragilariopsis* and *Tetraparma* require silicate (section 1.1.2.1), whereas *E. huxleyi* is potentially susceptible to dissolution of its $CaCO_3$ skeleton due to changes in ocean carbonate chemistry (section 1.1.2.3; Riebesell et al., 2000; Iglesias-Rodríguez et al., 2008). This chapter presents the biogeography and biomass of these three major nannoplankton groups in the Scotia Sea, as well as biogeography for some less abundant Southern Ocean coccolithophores, using scanning electron microscopy (SEM) during two phases of the Southern Ocean growing season in relation to key environmental variables to address the third hypotheses outlined in section 1.3:

3. Mineralizing nannoplankton biogeography is determined by silicate concentrations, with fast-growing small diatoms dominating when silica is non-limiting and slower-growing *E. huxleyi* dominating and forming blooms when silica is limiting. *E. huxleyi* distributions and blooms are further affected by the position of the SACCF, which generally forms a southern boundary to its range, however, the partial pressure of CO_2 does not affect distributions.

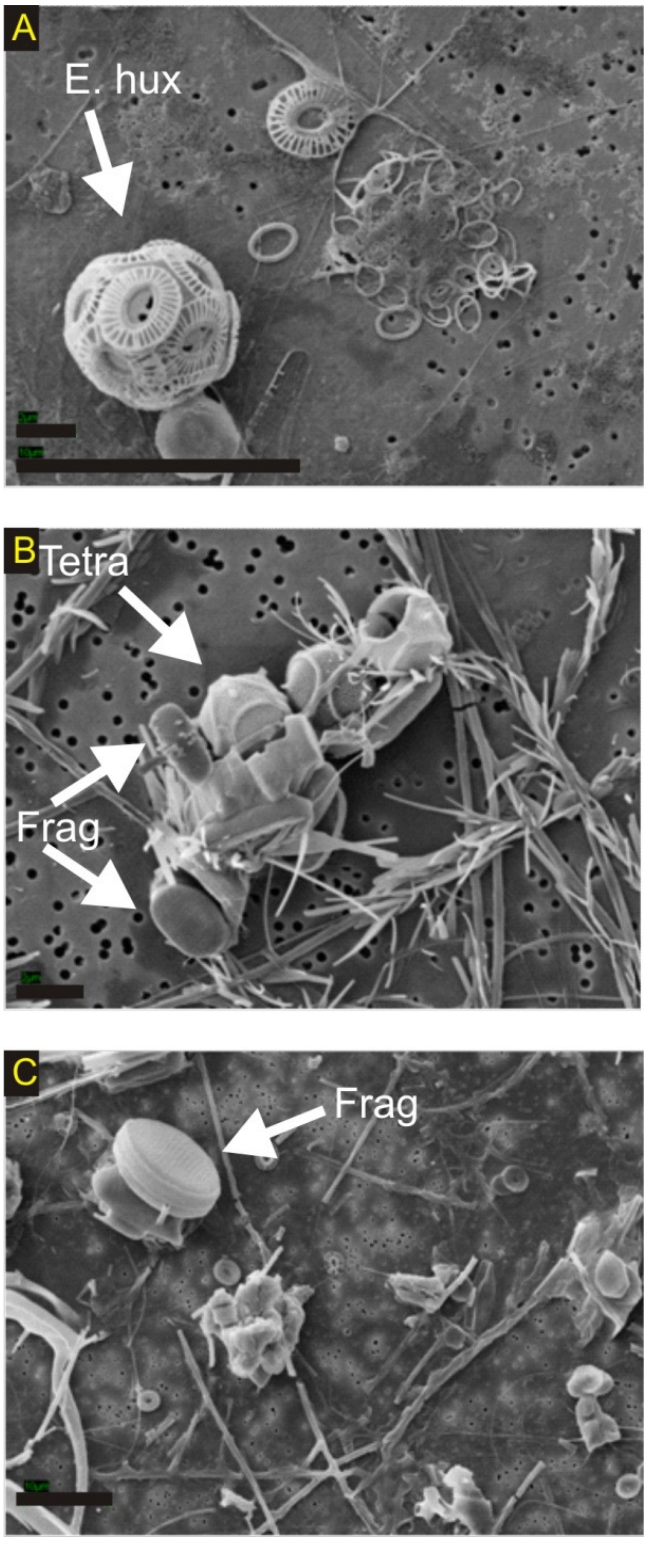

Figure 23a-b. SEM images of mineralizing nannoplankton, including (a) *E. huxleyi* (E. hux), (b) *Tetraparma* spp. (Tetra), and (b-c) *Fragilariopsis* spp. (Frag). Scale bars in (a) measure 2 µm (top) and 10µm (bottom), in (b) the scale bar measures 2 µm, and in (c) 10 µm.

3.2 Methods

3.2.1 Sampling

Phytoplankton abundance, physiology, ambient dFe concentrations, and ancillary data were measured during three successive seasons of cruises with the British Antarctic Survey (BAS) under the Discovery 2010 Antarctic FOODWEBS programme. The cruises took place during austral spring (JR161 from October 24th to December 3rd 2006), austral summer (JR177 from December 31st 2007 to February 16th 2008), and austral autumn (JR200 from March 11th to April 18th 2009; Figure 24). Due to sampling and sample analysis constraints, phytoplankton community structure data was collected and analyzed at the microplankton (20-200 µm) community level for cruises JR161 and JR177, and at the nannoplankton community level for cruises JR177 and JR200 (Table 16). Lugols analysis was not completed, however, on bioassay samples for cruise JR200, excluding the possibility of microplankton community composition analysis for those bioassays. Additional information regarding microplankton biomass was provided by R. E. Korb (pers. comm.) for cruises JR177 and JR200. The lack of both nannoplankton community data and bioassay data for JR161, of nannoplankton community data for JR177, and of microplankton bioassay data for JR200 influenced the organization of chapters 3 and 4 such that chapter 3 includes nannoplankton community composition data (JR177 and JR200) and chapter 4 includes microplankton and nannoplankton bioassay data (microplankton: JR161 and JR177; nannoplankton JR200)

Table 16. Summary of coverage and sources for microplankton and nannoplankton community data for the three cruises presented in this study. Missing data is marked by an asterisk "*".

Cruise	Source of data	Microplankton community	Nannoplankton community
JR 161 (spring)	Bioassays	T. S. Bibby and M. Nielsdottir; chapter 4	*Samples not taken
	In situ	T. S. Bibby and M. Nielsdottir; chapter 4	*Samples not taken
JR177 (summer)	Bioassays	D. J. Hinz and M. Nielsdottir; chapter 4	*Samples not taken
	In situ	Korb et al., 2010; R. E. Korb, pers. comm.; chapter 4	D. J. Hinz; chapter 3
JR200 (autumn)	Bioassays	*Data not analyzed (D. J. Hinz and S. Steigenberger)	D. J. Hinz; chapter 4
	In situ	R. E. Korb, pers. comm.; chapter 4	D. J. Hinz; chapter 3

Sampling for chapter 3 focused on gradients across the major frontal boundaries and between low and high dissolved Fe regions (Korb et al., 2005). For SEM samples, underway water supply was used to collect sub-surface (5 m) water samples, both while steaming and while conducting stationary sampling (Figure 24), from which 50 ml to 700 ml of water was gently vacuum filtered onto polycarbonate filters (25-mm diameter, 0.4-µm pore size) with a Whatmann GF/F backing filter (25-mm diameter; 0.7-µm pore size). Samples were then air-dried and stored in Petri dishes for transport. Samples for microplankton (>20 µm) community analysis and biomass estimates were preserved in 1% (JR161) or 2% (JR177, JR200) acidic Lugols iodine solution and counted on-shore by A. Poulton, using the methodology described in Poulton et al. (2007).

Ancillary biological, chemical and physical measurements were taken from concurrent underway data whenever possible, and in cases where there were no matching underway measurements, the CTD data from on-station casts (5-m Niskin bottles) of the standard stainless steel CTD with were used (General Oceanics). These ancillary measurements included: SST (H. Venables*,* pers. comm.), salinity (H. Venables*,* pers. comm.), chlorophyll-*a* (Chl-*a*) (R. E. Korb, pers. comm.), the efficiency of photosynthetic energy conversion F_v/F_m (presented in section 1.1.2.1.2), dynamic height (H. Venables, pers. comm.), bottom depth (BD) (H. Venables, pers. comm.), mixed layer depth (MLD) (H. Venables, pers. comm.), pCO_2 (E. Jones, pers. comm.), silicate ($Si(OH)_4$; R. E. Korb, pers. comm.), phosphate (PO_4^{3-}; R. E. Korb, pers. comm.), nitrate (NO^{3-}; R. E. Korb, pers. comm.), and dissolved Fe (Nielsdóttir, pers. comm.). Major frontal boundaries were determined using dynamic height according (H. Venables, pers. comm.).

Monthly composite MODIS-Aqua images for water-leaving radiance at 555 nm and particulate inorganic carbon (PIC) were obtained from the NASA Ocean Color website (http://oceancolor.gsfc.nasa.gov) to compare *E. huxleyi* concentrations *in situ* to expected concentrations (Holligan et al., 2010) and to assess the spatial extent of *E. huxleyi* blooms in the Scotia Sea during the cruise periods.

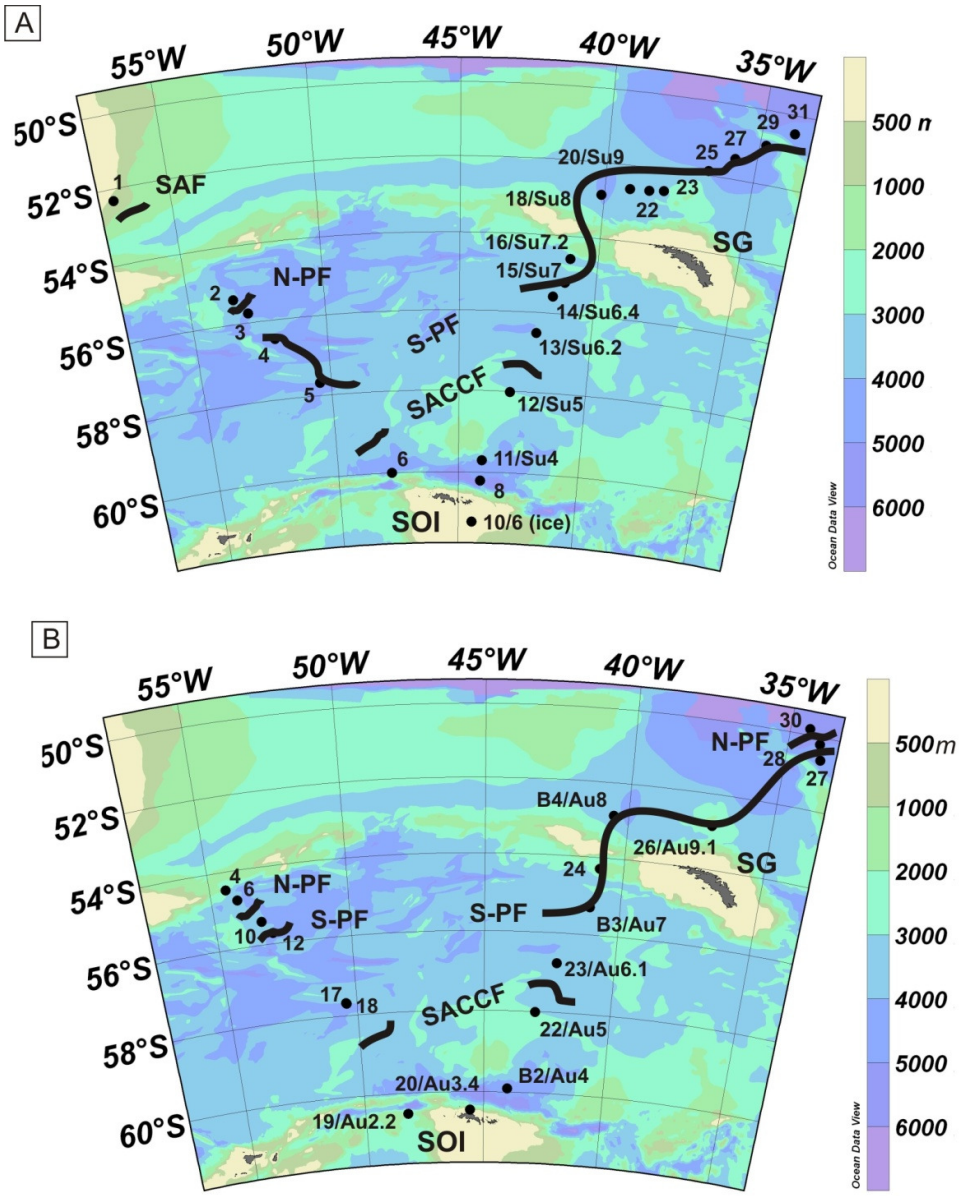

Figure 24a-b. Map of sampling stations and major fronts, for (a) JR177 austral summer and (b) JR200 austral autumn. Numbers refer to the sample number. When taken on-station the sample numbers are followed by a forward slash "/" and the official cruise station name. The major frontal boundaries are: the SAF, the Northern edge of the PF (N-PF), the Southern edge of the PF (S-PF), and the SACCF. Islands are labelled South Georgia (SG) and South Orkney Islands (SOI). Colours correspond to depth, with explanatory key at right in meters (m).

3.2.2 **Scanning electron microscopy counts and biomass estimates**

Samples were mounted on SEM pin stubs and sputter coated with 20 nm of gold. Secondary electron microscopy images of sample fragments were obtained using a LEO-1450-VP (variable pressure) SEM equipped with a Princeton Gamma Technology (PGT) light element energy dispersive X-ray microanalysis system (EDS). Imaging was undertaken using 5 kV, a probe current setting of 30 oA, and a working distance of 8 mm. For elemental spot analysis, the SEM was operated using an EHT of 15 kV and a working distance of 19 mm. For nannoplankton cell counts, a 15 by 15 frame grid was photographed and archived according to a tailored macro at a constant 5000x magnification. All 225 fields of view (FOV) per filter were counted, except for species that were very abundant. In these cases, either 300 cells or 500 coccoliths were counted per filter; if these abundances were reached before all the FOV were counted, the total number on the filter was extrapolated following Poulton et al. (2010). Species identifications of mineralizing nannoplankton were made following Hasle (1965), Young et al. (2003), and Scott and Marchant (2005).

Cell biomass (mg C m^{-3}) for *Tetraparma* spp. and *Fragilariopsis* spp. were estimated from cell shape following Poulton et al. (2007). *E. huxleyi* biomass was estimated from *in situ* measurements of inner coccosphere diameter from the Iceland Basin (Poulton et al., 2010). An extrapolation of Southern Ocean *E. huxleyi* biomass was possible from North Atlantic *E. huxleyi* data because inner coccosphere diameter does not vary between morphotypes A, B, and B/C, instead it is the thickness of the $CaCO_3$ liths which lie on the inner coccosphere which varies (A. Poulton pers. comm.). Microplankton biomass from acidic Lugols samples (2%) was provided by R. E. Korb (pers. comm.) SEM-derived nannoplankton biomass estimates were combined with Lugols-derived microplankton biomass estimates to arrive at an estimate of total phytoplankton biomass (TPB), which included *E. huxleyi, Fragilariopsis, Tetraparma* (the nannoplankton) and diatoms, dinoflagellates, planktonic ciliates, cryptophytes, and silicoflagellates (the microplankton). Small naked flagellates were not included in the microplankton counts, as they are difficult to identify in terms of taxonomy or trophic affiliation in acidic Lugols solution using only inverted light microscopy. This group can make up a significant fraction of the phytoplankton community in the Southern Ocean (Seeyave et al., 2007), however, no estimates were available for the Scotia Sea at this time.

3.2.3 **Statistical Analysis**

Multivariate statistical analysis was conducted using PRIMER-E version 6.1.6 on both biotic (species abundance) and abiotic (environmental) data. Nannoplankton counts (biotic data) were square-root transformed to reduce bias due to rare occurrences before a Bray-Curtis similarity matrix was constructed. The matrix was subjected to both CLUSTER and multidimensional scaling (MDS) analysis to identify differences in mineralizing nannoplankton community composition between samples in multivariate space. The CLUSTER routine grouped pairs of samples hierarchically based on similarity, while the MDS routine represented relationships between samples graphically. The MDS analysis was used to assess the quality of fit between the CLUSTER groupings and the data, as well as to visualize relationships between samples in two dimensions. The groupings in the CLUSTER analysis were assessed using the SIMPROF routine (1000 permutations, 5% significance level); however, significant SIMPROF groups can only be used to indicate which factors should be considered in further tests, not to identify the factors responsible for the sample groupings. A rigorous test of the factors involved in sample groupings must be *a priori,* whereas the SIMPROF test in the CLUSTER analysis is empirically derived. *A priori* groupings based on sampling year and locations relative to the major fronts were tested for significance using the ANOSIM routine.

Sea surface temperature, salinity, dynamic height, pCO_2, dFe, NO_3, PO_4, and $Si(OH)_4$ included in the set of abiotic data. Mixed layer depth, bottom depth, F_v/F_m , and Chl-*a* were excluded from the environmental analyses because (1) missing data for MLD and bottom depth reduced the number of samples available for the analysis too heavily (from 19 samples to 11 samples), and (2) F_v/F_m and Chl-*a* are not abiotic. Environmental variables included in the analysis were subjected to individual transformations to achieve normal distributions. Individual transformations and the correlation coefficients (r) following transformation were determined using the draftsman's plot function as in chapter 2 (section 2.2.3; Appendix Figure 1). Variables with right-skewed distributions were square-root transformed (dFe, and $Si(OH)_4$; Table 17). All macronutrient values were subjected to the same square-root transformation, as recommended by the software developers (Clarke and Warwick, 2001). The calculation of covariance between variables (r^2) and the significance of r^2, overall normalization of

variables, and the construction of a Euclidean distance matrix were also as in chapter 2 (section 2.2.3).

Table 17. Summary of the environmental variables included in the multivariate analysis. "Skew" refers to departures from the normal distribution observed in the draftsman's plot (R for right-skewed), while "transformation" details the function used to distribute the variable normally.

Environmental Variables	Skew	Transformation
Sea Surface Temperature (SST) (°C)		
Salinity		
Dynamic Height (Dyn Ht) (m)		
Partial pressure of CO_2 (pCO_2) (µatm)		
Dissolved Fe (dFe) (nM)*	R	sqr(*y*)
Nitrate (NO_3) (mmol m^{-3})		sqr(*y*)
Phosphate (PO_4) (mmol m^{-3})		sqr(*y*)
Silicate ($Si(OH)_4$) (mmol m^{-3})	R	sqr(*y*)

* denotes that the variable was considered in initial statistical analyses but was dropped from the final BEST comparison (see methods) due to missing data.

Following transformation, the environmental data were subject to PCA analysis. Five principal components (PCs) were analyzed and associated eigenvectors were used to provide an estimate of the relative weight of the environmental variables in the sample data (Clarke, 1993; Clarke and Warwick, 2001; Clarke and Gorley, 2006), with larger eigenvectors indicating that environmental variable had a larger effect on the sample distribution. The BEST routine was then used to compare a PCA dissimilarity matrix (based on Euclidean distance) constructed using the abiotic data to a Bray-Curtis matrix for the biotic data. The analysis compared all possible combinations of abiotic variables to the observed biotic data (from each variable individually to all variables), producing correlation coefficients that were then used to rank the variables (Clarke, 1993; Clarke and Warwick, 2001; Clarke and Gorley, 2006). A permutation test (1000 iterations) was performed to assess the significance of the correlation coefficients ($p<0.001$), with significant correlation coefficients indicating those variables were significantly related to species biogeography.

3.3 Results

3.3.1 Hydrography

The hydrography of the Scotia Sea region was dominated by strong gradients of physical, chemical and biological parameters across the major circumpolar fronts

(Figure 25; means summarized in Table 18). The SACCF was clearly defined, while the PF boundaries were more diffuse: the cruise track crossed into and out of the PF several times (Figure 25a-b). Sea surface temperature (SST) decreased sharply across the ACC fronts polewards, from a maximum of 8.3°C to a minimum of -0.6°C (Figure 25c-d). Overall SST was 0.5°C higher in austral autumn than in austral summer (average taken from overlapping sites). Salinity increased polewards in austral autumn to 34.2, but showed a sharp decrease south of the SACCF in austral summer to 33.1 in association with sea ice (Figure 25e-f). The partial pressure of CO_2 (pCO_2) generally followed an inverse pattern to SST: increasing polewards to a maximum of 395 µatm just north of the SACCF during both seasons (Figure 25g-h). Variations in the general pattern were observed, however, within the PF. During summer, pCO_2 decreased from an average of ~331 µatm within the PF to an average of ~277 µatm south of the PF. The opposite trend was observed in autumn, when pCO_2 increased from an average of ~346 µatm in the PF to an average of ~378 µatm south of the PF. The reductions in pCO_2 in and around the PF corresponded to increases in Chl-*a* concentration (from 1.1 mg m^{-3} to 2.1 mg m^{-3} in summer, and from 1.1 mg m^{-3} to 0.6 mg m^{-3} in autumn; Figure 25i-j). On average, Chl-*a* was 0.54 mg m^{-3} higher in austral summer, while pCO_2 was 42 µatm lower.

Nitrate and phosphate concentrations were highest in the south-western Scotia Sea (averaging 24.6 mmol NO_3^- m^{-3} and 2.0 mmol PO_4^{3-} m^{-3} in summer, and 25.3 mmol NO_3^- m^{-3} and 1.5 mmol PO_4^{3-} m^{-3} in autumn) and decreased to the northeast near South Georgia (averaging 18.1 mmol NO_3^- m^{-3} and 1.5 mmol PO_4^{3-} m^{-3} in summer, and 19.1 NO_3^- mmol m^{-3} and 0.9 mmol PO_4^{3-} m^{-3} in autumn; Figure 25k-n). Nitrate concentrations were higher overall in autumn, while phosphate concentrations were higher overall in summer. Silicate increased dramatically south of the SACCF during both seasons, with an average of 69.7 mmol Si m^{-3} in summer and 64.7 mmol Si m^{-3} in autumn (Figure 250-p). Dissolved Fe (dFe) generally decreased polewards in austral summer from a maximum of 1.3 nM to a minimum of 0.3 nM, with the maximum value occurring near South Georgia (Figure 25q). During austral autumn, dFe ranged from 0.08 nM to 0.4 nM, but showed no clear pattern (Figure 25r). F_v/F_m varied throughout the cruise track in both seasons, ranging from 0.16 to 0.54, without any easily extracted pattern (Figure 25s-t). Mixed layer depth was generally shallow south of the SACCF in summer (12 – 39 m), and deeper between the SACCF and PF in both seasons (Figure 25u-v).

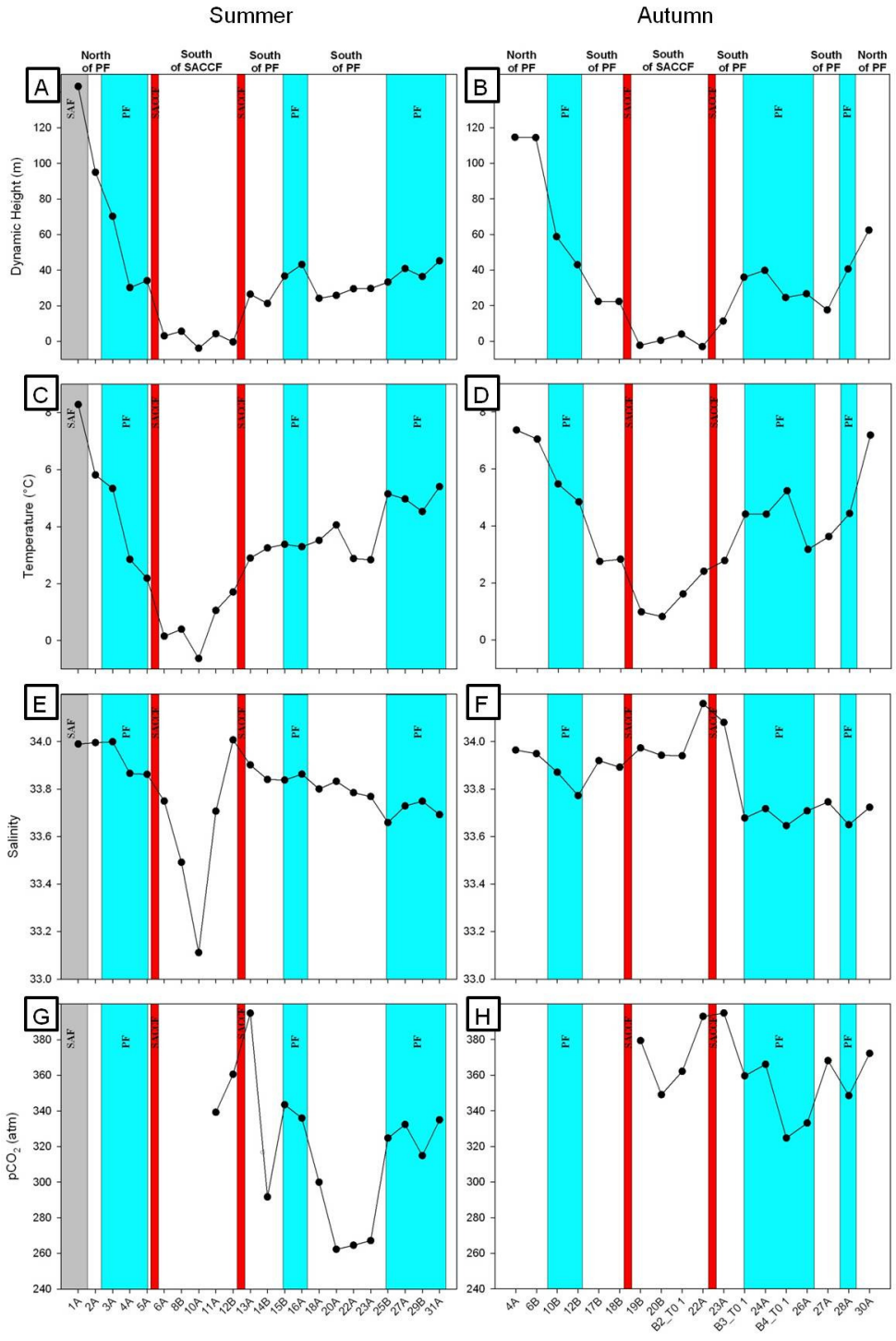

Figure 25a-h. Hydrography and sampling sites for summer (left column) and autumn (right column), showing (a-b) dynamic height, (c-d), temperature, (e-f) salinity, and (g-h) pCO_2.

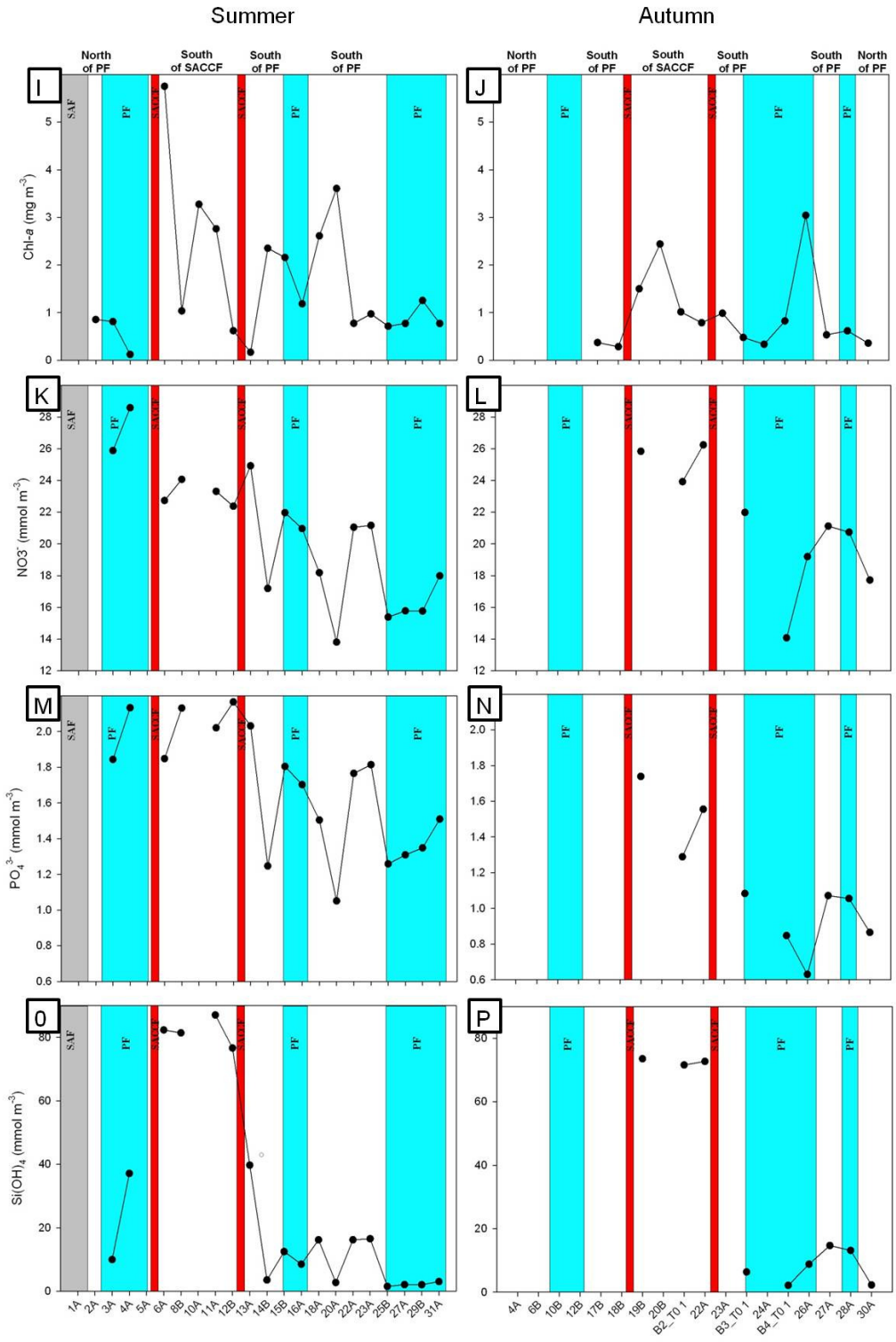

Figure 25i-p. Hydrography and sampling sites for summer (left column) and autumn (right column), showing (a-b) Chl-*a*, (c-d), nitrate, (e-f) phosphate, and (g-h) silicate.

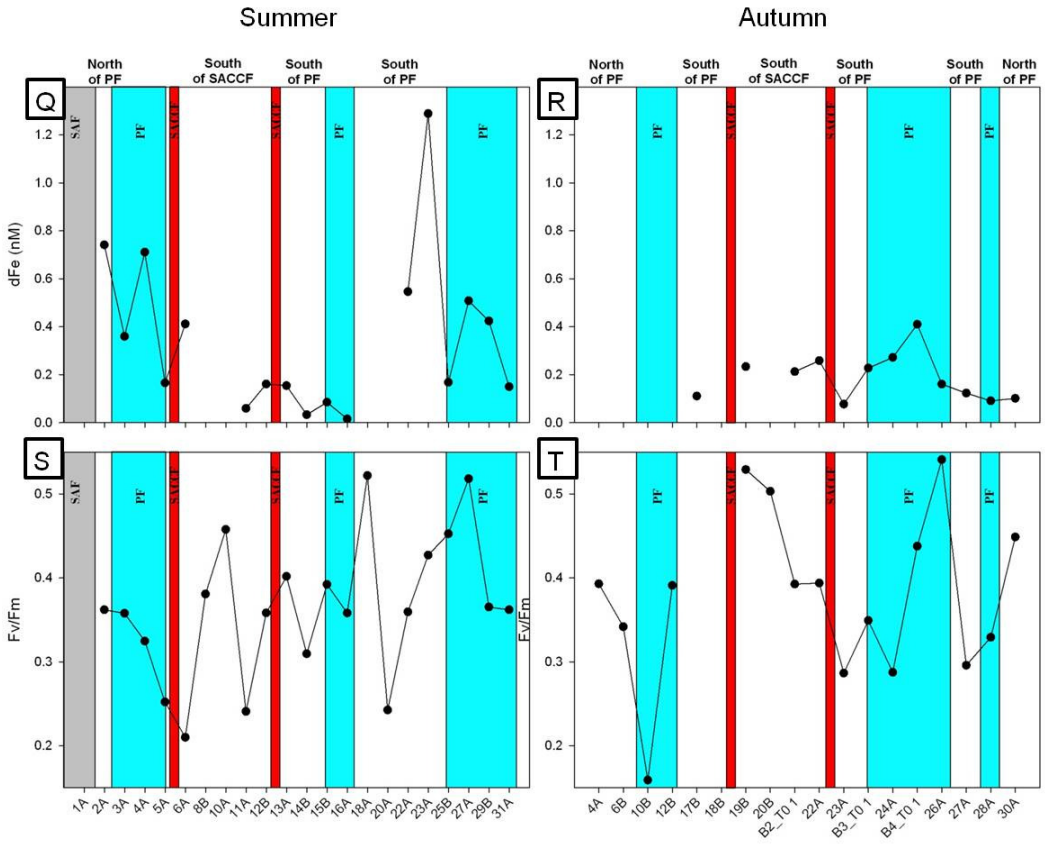

Figure 25a-t. Hydrography and sampling sites for summer (left column) and autumn (right column). Major fronts shown are as follows: gray for SAF, blue for PF, and red for SACCF.

Table 18. Hydrographic data range for all sampling stations within each physically defined oceanic region (as listed in the Front column) for summer (top half of table) and autumn (bottom half of table). Max-min data is followed by the average value in parentheses "()". Hydrographic data include: cruise number and filter label (Sample), latitude in degrees South (Lat), Sea Surface Temperature in °C (SST), Salinity (Sal.), Chlorophyll-*a* in mg m^{-3} (Chl-*a*), F_v/F_m, mixed layer depth in meters (MLD), dissolved Fe content in nM (dFe), and the macronutrient concentrations in mmol m^{-3} (nitrate - NO_3^-; phosphate - PO_4^{3-}; and silicate - $Si(OH)_4$). When underway data was not available, CTD cast station data was used instead. Blanks indicate no data was available.

Sample	Front	Lat	SST	Sal.	pCO_2	MLD	Chl-*a*	F_v/F_m	dFe	NO_3	PO_4	$Si(OH)_4$
Summer												
1A	SAF	52	8.3	34.0								
2A	N of PF	55	5.8	34.0			0.9	0.36	0.7			
3A, 16A, 31A	in PF	56 to 51	3.3-5.4 (4.7)	33.7-34.0 (33.9)	335.0- 335.9 (335.5)	63	0.8-1.2 (0.9)	0.36	0-0.4 (0.2)	18.0-25.9 (21.6)	1.5-1.8 (1.7)	3.1-10.0 (7.2)
4A, 5A, 15A, 25B, 27A, 29B	S edge PF	58 to 51	2.2- 5.1 (3.8)	33.7-33.9 (33.7)	314.9- 343.5 (328.9)	65	0.1-2.2 (1.0)	0.25-0.52 (0.38)	0.1-0.7 (0.3)	15.4-28.6 (19.5)	1.3-2.1 (1.6)	1.5-37.1 (11.1)
13A, 14B, 18A, 20B, 22A, 23A	S of PF	57 to 53	2.8- 4.1 (3.2)	33.8-33.9 (33.8)	262.3- 394.9 (296.7)	23- 61 (49)	0.2-3.6 (1.7)	0.24-0.52 (0.38)	0-1.3 (0.5)	13.8-24.9 (19.4)	1.1-2.0 (1.6)	2.7-39.7 (15.8)
6A, 8B, 10A, 11A, 12B	S of SACCF	61 to 58	-0.6- 8.3 (0.5)	33.1-34.0 (33.6)	339.2-360.5 (349.9)	12- 39 (27)	0.6-5.8 (2.7)	0.21-0.46 (0.33)	0.1-0.4 (0.2)	22.4-23.3 (22.8)	1.8-2.2 (2.0)	76.7-86.1 (82.0)
Autumn												
4A, 6A	N of PF	55	7.0- 7.4 (7.2)	33.9-34.0 (33.9)				0.34-0.39 (0.37)				
30A	N edge PF	50	7.2	33.7	372.2		0.4	0.45	0.1	17.7	0.9	2.3
10B, 28A	in PF	55 to 50	4.4- 5.5 (5.0)	33.6-33.9 (33.8)	348.5		0.6	0.16-0.33 (0.24)	0.1	20.7	1.1	13.1
12B, B3_T0 1, 24A, B4_T0 1, 26A	S edge PF	56 to 53	3.2- 5.2 (4.4)	33.6-33.8 (33.6)	324.8-366.1 (345.9)	8-67 (47)	0.3-3.0 (1.2)	0.29-0.54 (0.40)	0.2-0.4 (0.3)	14.1-22.0 (18.4)	0.6-1.1 (0.9)	2.1-8.8 (5.8)
17B, 18B, 23A, 27A	S of PF	58 to 51	2.8-3.6 (3.0)	33.7-34.1 (33.9)	368.2-394.9 (381.6)	53	0.3-1.0 (0.5)	0.29-0.30 (0.29)	0.1	21.1	1.1	14.7
19B, 20A, B2_T0 1, 22A	S of SACCF	60 to 58	0.8- 2.4 (1.5)	33.9-34.2 (33.9)	349.1-393.0 (370.9)	42- 69 (52)	0.8-2.4 (1.4)	0.39-0.53 (0.45)	0.2-0.3 (0.2)	23.9-26.2 (25.3)	1.3-1.7 (1.5)	71.6-73.6 (72.6)

3.3.2 **Mineralizing nannoplankton distribution**

In summer, areas of high reflectance and particulate inorganic carbon (PIC) concentrations occurred along the eastern coast of the Falkland Islands (FI), in the northern central Scotia Sea, and north and west of South Georgia (SG) (Figure 26). Reflectance and PIC were particularly intense in January 2008 off the SG shelf. The signals continued into February 2008, though at reduced levels and over a smaller area. Reflectance and PIC to the south of SG, however, increased. During autumn, high reflectance and PIC were found only directly on and to the east of the SG shelf in March 2009 (Figure 27). By April 2009, the signals had all but disappeared.

During *in situ* sampling, *Fragilariopsis* was the most ubiquitous nannoplankton group overall in the study area (90% of the sites sampled contained <20 µm *Fragilariopsis*) and was most widespread in summer (present at 94.4% of the sites sampled). Maximum abundances (1820 cells ml^{-1}), however, occurred in autumn at the southern end of the transect from within the PF to south of the SACCF (Figure 28a-b). *Tetraparma* also reached the highest abundances in this area, occurring at a maximum abundance of 1910 cells ml^{-1}. Its range was more restricted, however, with high abundances occurring only south of the SACCF (Figure 28c-d). Both *Fragilariopsis* and *Tetraparma* were more numerous in autumn than in summer (up to 16 and 2.5 times more numerous, respectively).

Emiliania huxleyi (morphotype B/C; some morphotype C was also detected in small numbers; according to (Young et al., 2003) occurred at abundances up to 650 cells ml^{-1}, a factor of 10 more numerous than the other coccolithophores observed (maximum 7 cells ml^{-1}). The spatial range of *E. huxleyi* extended into both western and eastern regions of the Scotia Sea, with cells and detached coccoliths found at all but two sampling sites north of the SACCF. South of the SACCF, neither cells nor coccoliths of *E. huxleyi* were observed. Generally, *E. huxleyi* numbers were highest in the PF and during the autumn cruise (Figure 28e-f).

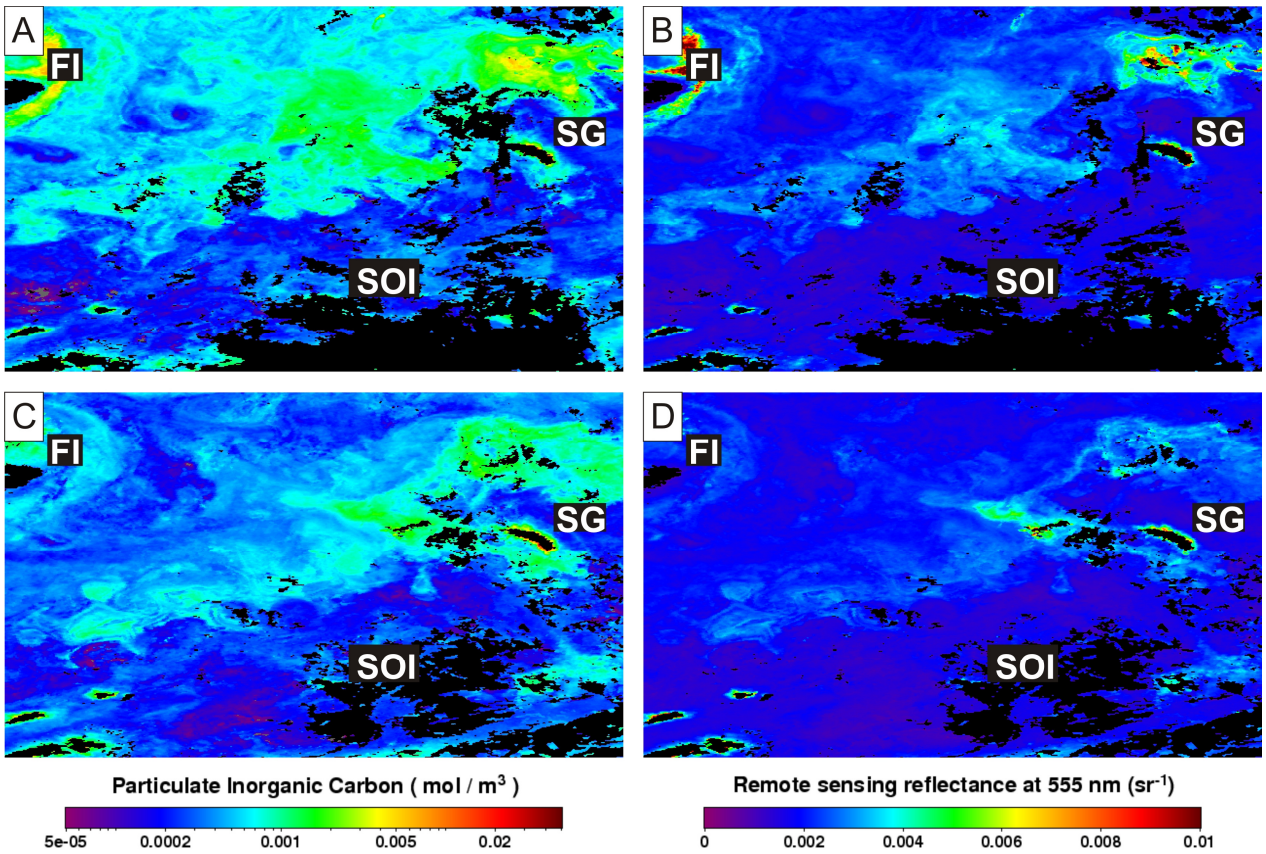

Figure 26a-d. MODIS/Aqua images (4 km resolution) of the Scotia Sea for (a-b) January 2008 and (c-d) February 2008 (the period of cruise JR177), showing (a, c) PIC (mol m^{-3}) and (b, d) reflectance at 555 nm (sr^{-1}). Labels for islands are as in Figure 24, with the addition of the Falkland Islands (FI).

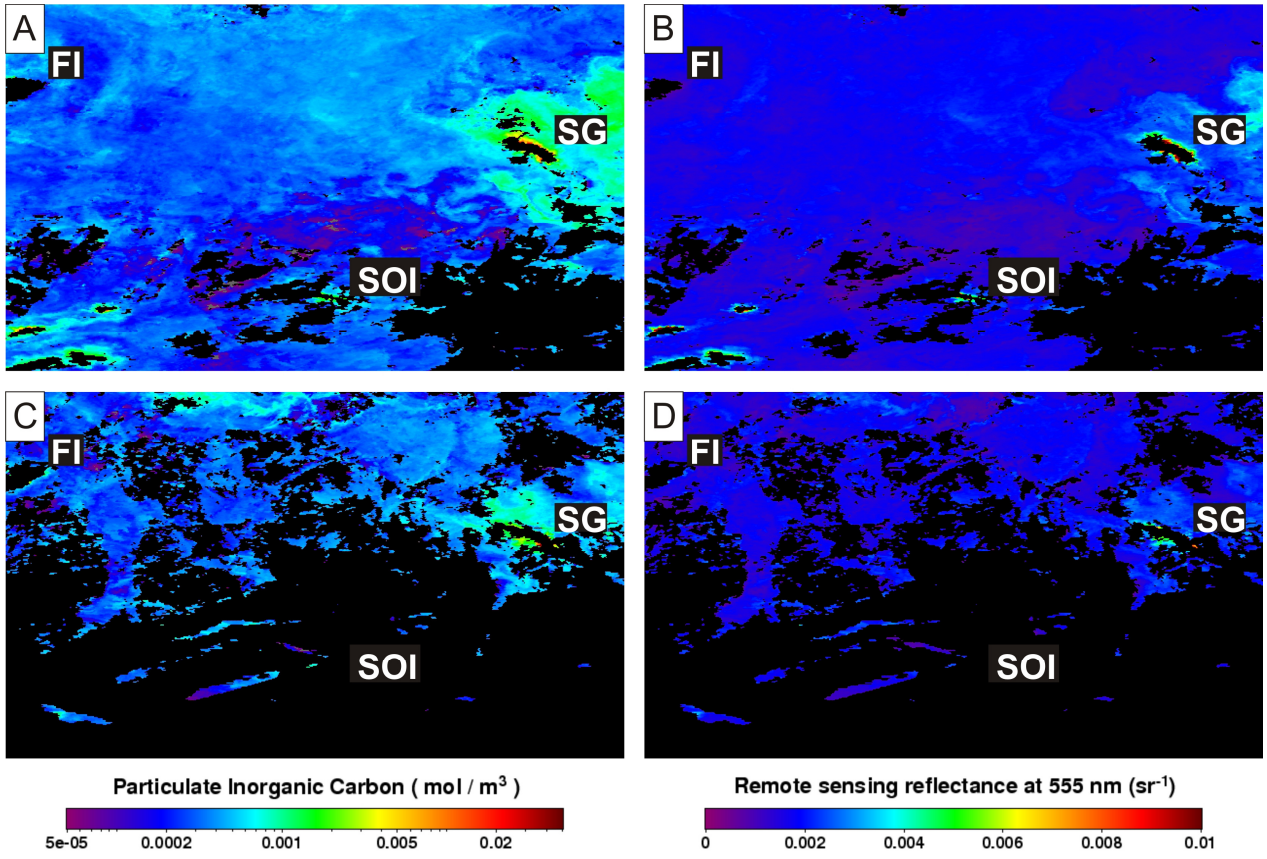

Figure 27 a-d. MODIS/Aqua images (4 km resolution) of the Scotia Sea for (a-b) March 2009 and (c-d) April 2009 (the period of cruise JR200), showing (a, c) PIC (mol m^{-3}) and (b, d) reflectance at 555 nm (sr^{-1}). Labels for islands are as in Figure 26.

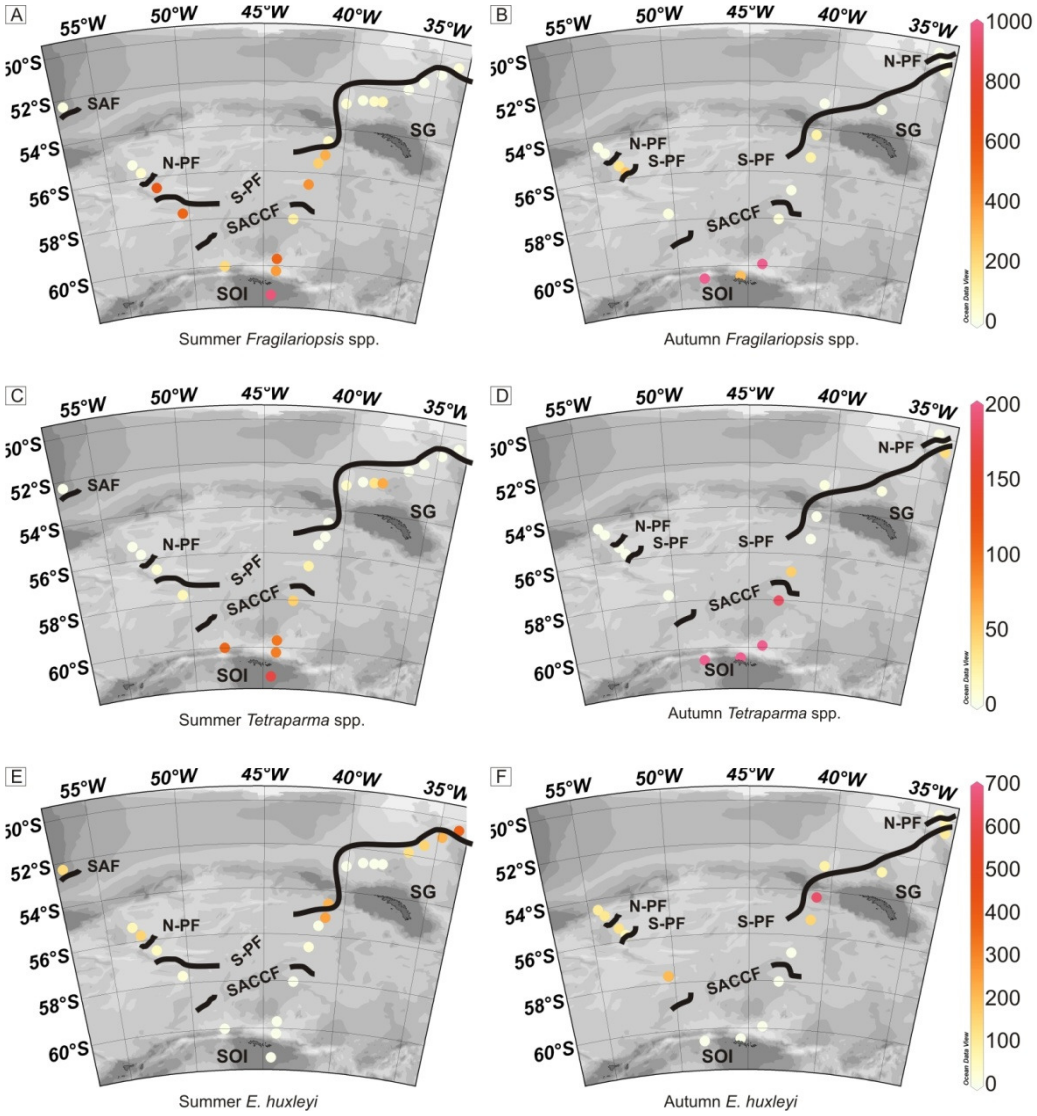

Figure 28a-f. Nannoplankton cell counts (in cells ml^{-1}) at each sampling station, where increasingly intense red colour corresponds to increasing cells ml^{-1}, according to the scale at the right, of (a-b) *Fragilariopsis* spp., (c-d) *Tetraparma* spp., and (e-f) *E. huxleyi.* Austral summer counts are shown on the left (a), (c), and (e), while austral autumn counts are shown on the right (b), (d), and (f). The major frontal boundaries and islands are as in . Large values for (b) and (d) near SOI were a factor of 2 and 10 larger respectively than the scale, actual values have been recorded in the text. Note scale changes.

The numbers of detached *E. huxleyi* coccoliths corresponded well to the abundance of *E. huxleyi* cells in the sample (r^2=0.74), with the ratio of detached coccoliths to *E. huxleyi* cells exceeding 10 in all samples in which *E. huxleyi* was

present (Figure 29). The majority of samples exhibited cell to detached coccolith ratios between 20 and 40, which are characteristic of bloom conditions (Fernández et al., 1993). In austral autumn, two samples had cell: coccolith ratios of >60 (JR200 10B and 12B; ratios of 76 and 91, respectively), strongly indicating bloom conditions. During austral summer, the coccolith: cell ratios were not as high, reaching a maximum of 47.

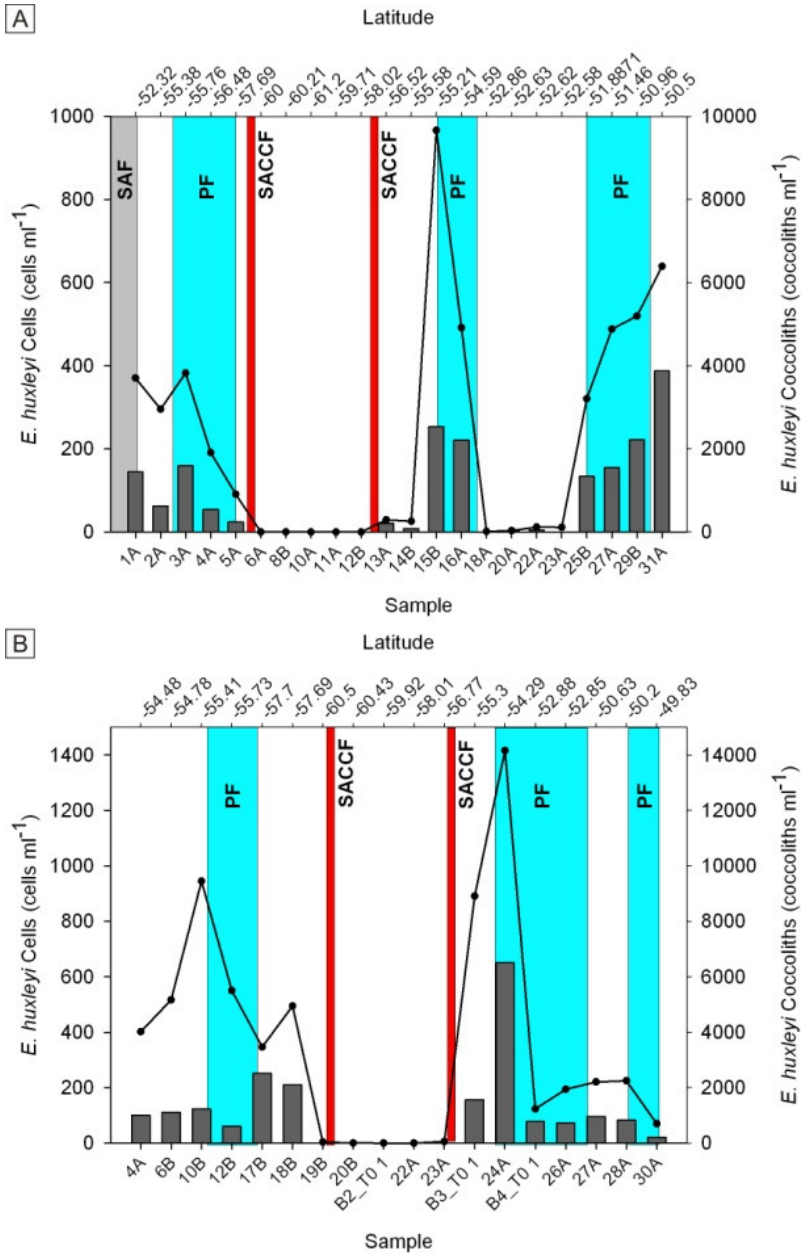

Figure 29a-b. *E. huxleyi* cell numbers (left axis, bars), coccolith numbers (right axis, solid line), and major fronts (as in Figure 25) for (a) summer and (b) autumn. Note scale change between a and b.

In addition to E. huxleyi, six other coccolithophores were identified at the genus or species level: *Gephyrocapsa* spp., *Acanthoica* spp., *Pappomonas* spp., *Papposphaera* spp., *Syracosphaera* spp., and *Wigwamma* spp. (Figure 30). The rare coccolithophores only occurred in observable numbers in austral autumn. The most common of these coccolithophores was *Acanthoica*, which appeared at 7 of the 18 austral autumn sample sites, largely in the western Scotia Sea and never south of the SACCF. The other coccolithophores occurred at four or fewer sites, again never south of the SACCF (Figure 31). One approximately spherical nannoplankton cell that could not be identified was subjected to elemental analysis. The unidentified cell, which was found on a single sample, was broken apart and appeared to be covered in basket-shaped plates (Figure 32) of approximately 3 µm diameter. The elemental structure of the plates matched that of silicate (Figure 33), and initial analyses suggest it may be of the *Heliozoa* or *Thaumatomastix* groups.

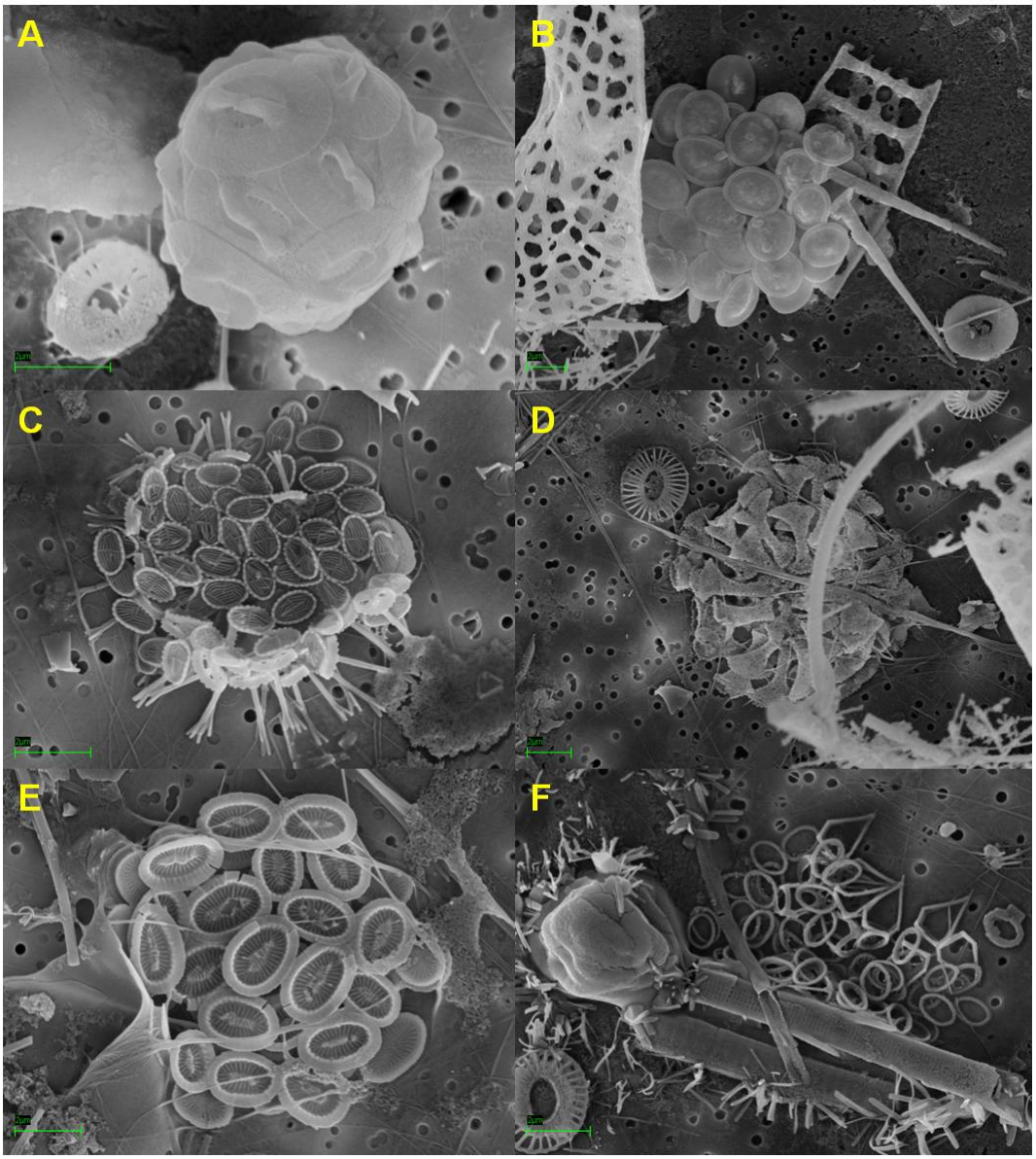

Figure 30. SEM images of the rare coccolithophores observed: (a) *Gephyrocapsa* spp., (b) *Acanthoica* spp., (c) *Pappomonas* spp., (d) *Papposphaera* spp., (e) *Syracosphaera* spp., and (f) *Wigwamma* spp. Scale bars are all 2µm.

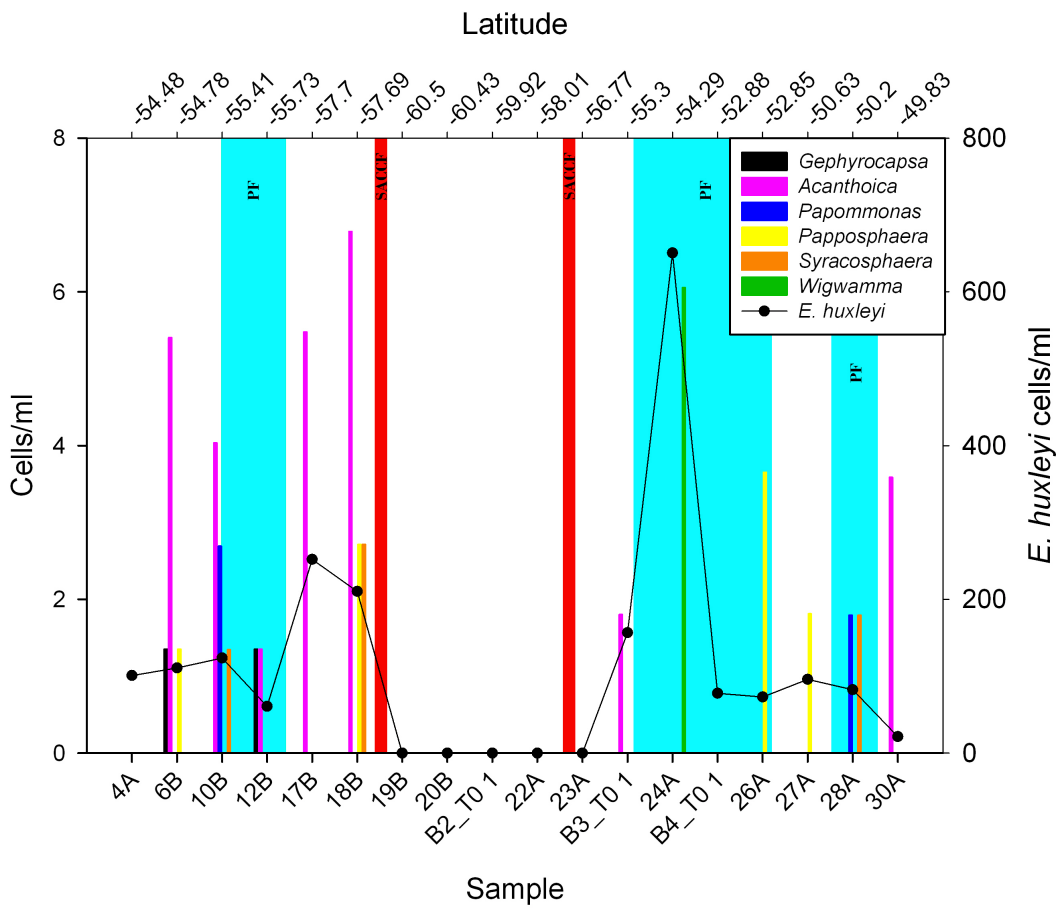

Figure 31. Autumn coccolithophore cell counts for rare coccolithophores (left axis) and *E. huxleyi* (right axis). Summer samples were counted, but no coccolithophores other than *E. huxleyi* were observed. Fronts shaded as in Figure 29.

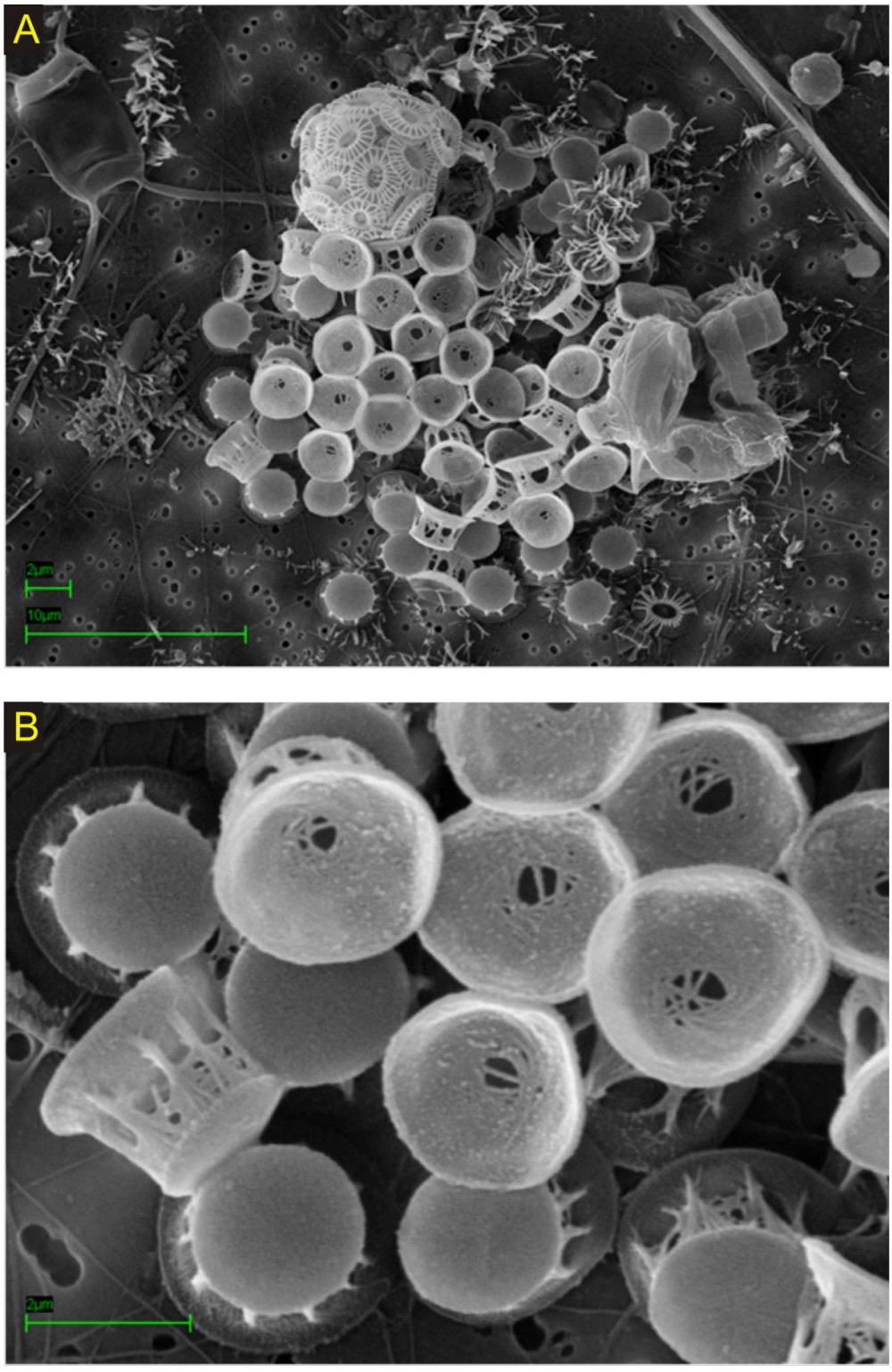

Figure 32. SEM images of liths from an unidentified siliceous nannoplankton found in JR200 sample 12B, (a) showing a wider angle of the plates and broken cell next to an E. *huxleyi* cell, and (b) a magnified image of the plates. Scale bars in (a) measure 2µm (top) and 10µm (bottom), and in (b) the scale bar measures 2µm.

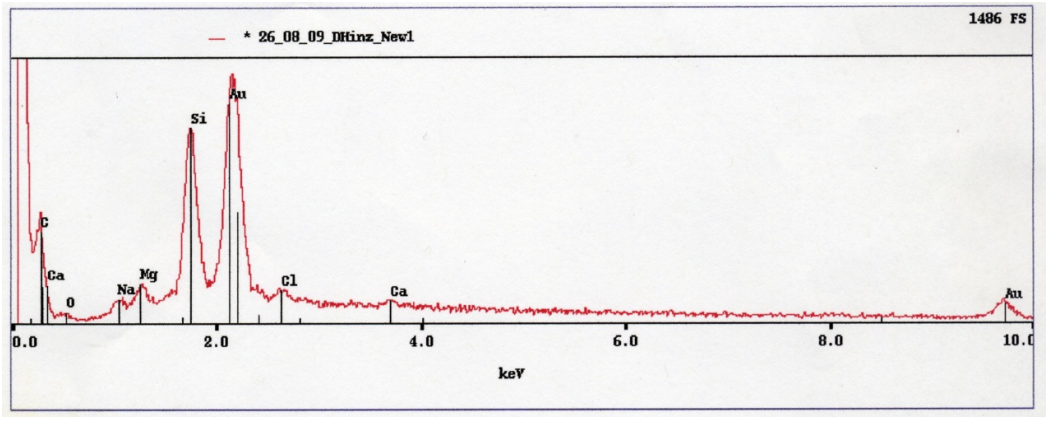

Figure 33. Elemental analysis of the unidentified cell plates shown in Figure 32. The initial peak and the Au peak are both artefacts (the Au peak is due to the gold-coating employed to fix SEM samples), while the Si peak is genuine.

3.3.3 Size-Fractionated Biomass

Nannoplankton biomass contributed 0–36% of the total phytoplankton biomass (TPB) where a comparison with microplankton counts was possible, with an average of 13% across all the stations. Microplankton biomass was highest for the diatoms (averaging 42% of TPB) and dinoflagellates (averaging 41% of TPB), with planktonic ciliates (averaging 1% of TPB), cryptophytes (averaging 4% of TPB), and silicoflagellates (averaging 0.06% of TPB) all contributing relatively little to TPB (Table 19). Southerly stations were highest in nannoplankton biomass, with three samples from south of the SACCF showing nannoplankton biomass estimates >30% of TPB (summer 11A, 30%; autumn 19B, 36%, and autumn B2T0_1, 35%). In summer the high nannoplankton biomass was due to *Fragilariopsis* (5–28%), while in autumn it was due to both *Tetraparma* (1–19%) and *Fragilariopsis* (0–17%). *E. huxleyi* biomass was high at the stations near South Georgia in autumn (4–23%).

Table 19. Biomass for all nannoplankton and microplankton counted in SEM and Lugols samples respectively, including TPB (mg C m-3), the percentage (%) of the biomass contributed by individual groups, the % of biomass contributed by the nannoplankton taxa combined, and by the % of biomass contributed by the microplankton taxa combined. Regions used as reference points in the next chapter are marked to aid cross-referencing from chapter 4 to this table, however, the regions are explained in section 4.2.2.

			Nannoplankton: Species % of TPB				Microplankton: Species % of TPB				Combined % of TPB	
Sample	Front	TPB	*E. huxleyi*	*Tetra-parma*	*Fragilari-opsis*	Diatoms	Dino-flagellates	Planktonic ciliates	Crypto-phytes	Silico-flagellates	Nanno-plankton	Micro-plankton
Summer												
8B†	S of SACCF	24	0	1	13	30	12	0	44	0	14	86
11A†	S of SACCF	16	0	2	28	19	28	0	23	0	30	70
12B	S of SACCF	19	0	1	5	29	65	1	0	0	6	94
13A	S of PF	18	1	0	18	39	36	5	0	0	20	80
15B*	S edge PF	97	2	0	3	84	12	0	0	0	4	96
16A*	in PF	66	2	0	0	77	20	0	0	0	3	97
18A**	S of PF	37	0	0	0	79	20	1	0	0	0	100
20A**	S of PF	107	0	0	0	92	8	0	0	1	0	100
Autumn												
19B†	S of SACCF	34	0	19	17	56	8	0	0	0	36	64
20B†	S of SACCF	57	0	1	0	68	31	0	0	0	2	98
B2†	S of SACCF	28	0	19	15	51	13	1	0	0	35	65
22A	S of SACCF	7	0	9	2	1	87	1	0	0	11	89
23A*	S of PF	9	0	2	1	5	92	0	0	0	3	97
B3*	S edge PF	13	8	0	7	2	82	0	0	0	16	84
24A	S edge PF	20	23	0	5	1	71	0	0	0	28	72
B4**	S edge PF	13	4	0	0	3	92	0	0	0	5	95
26A**	S edge PF	92	1	0	0	71	28	0	0	0	1	99

† SOI region in chapter 4 (section 4.2.2)
*USG region in chapter 4 (section 4.2.2)
**DSG region in chapter 4 (section 4.2.2)

3.3.4 **Biotic Grouping**

Statistical significance of the differences in community structure caused by species-specific distribution patterns was assessed using multivariate analysis. Samples were separated based on group-averaged similarity of the phytoplankton community (composed of *E. huxleyi*, *Tetraparma* spp., and *Fragilariopsis* spp.). Following CLUSTER analysis, two groups separated significantly (SIMPROF test) at the 40% Bray-Curtis similarity level and were labelled group I (including JR177 31A, 3A, 1A, 16A, 27A, 25B, 29B, 2A, 20A, and JR200 24A, 18B, 10B, 17B, 6B, 4A, 28A, 26A, 27A, 30A, B3_T0 1, and B4_T0 1) and group II (including JR177 15B, 14B, 13A, 5A, 4A, 11A, 8B, 6A, 10A, 23A, 12B, 22A, 18A, and JR200 12B, 23A, 22A, 19B, 20A, and 19B) (Figure 34). The CLUSTER results matched well with the MDS results, which fit the data in two dimensions with a low stress value of 0.09. Mapping the clusters onto the MDS plot at a similarity of 40 clearly demonstrated the same two groups appearing using both methods (Figure 35a). Group I contained all the samples taken in the PF and north of the PF, and group II contained all the samples taken south of the SACCF. Samples from the southern edge and south of the PF appeared in both groups, with group I containing the majority of southern-edge samples (64%) and group II containing the majority of southern samples (64%). Group I contained samples from both seasons (43% summer, 57% autumn), while group II predominantly comprised samples from the austral summer (68% summer, 32% autumn).The significance of season and location relative to fronts was tested *a priori* (ANOSIM test). Seasonality was not a significant factor, whereas the location relative to front was highly significant ($p<0.001$).

Overlaying species abundance data on the MDS plots allowed a graphical representation of individual species distribution patterns (Figure 35b-d). The clearest differences between groups I and II were in the distributions of *E. huxleyi* and *Tetraparma* spp. Group I contained relatively high *E. huxleyi* abundances and very low *Tetraparma* spp. abundances, while the pattern was reversed in group II. *Fragilariopsis* spp. occurred in both groups, though in higher abundances in group II.

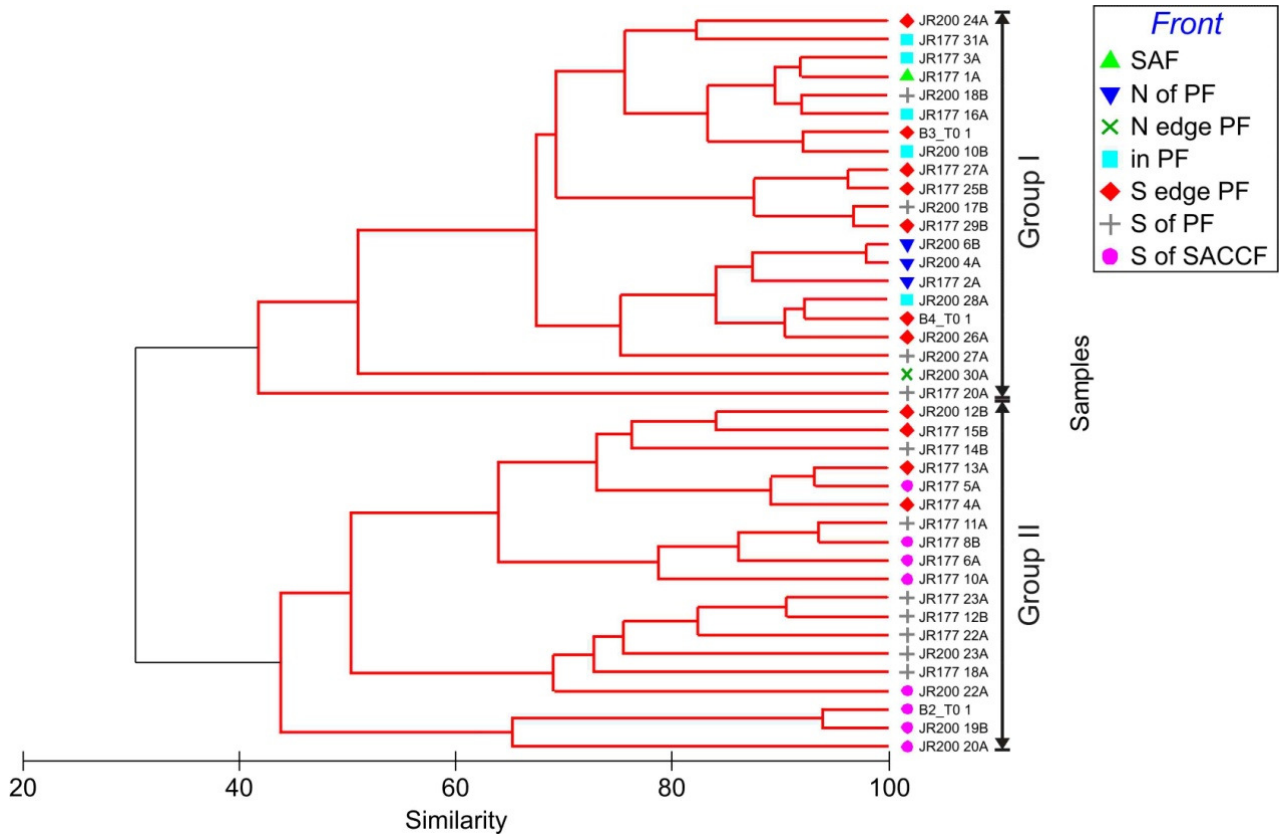

Figure 34. CLUSTER diagram showing the similarity between SEM samples based on a Bray-Curtis resemblance matrix created using cell counts from *E. huxleyi*, *Tetraparma* spp., and small *Fragilariopsis* spp. Symbols to the left of the sample name refer to the sample site's position relative to frontal boundaries (N = north/northern and S = south/southern). The black branches of the cluster tree indicate significant dissimilarity (values<40% similarity), while red branches were not significantly dissimilar.

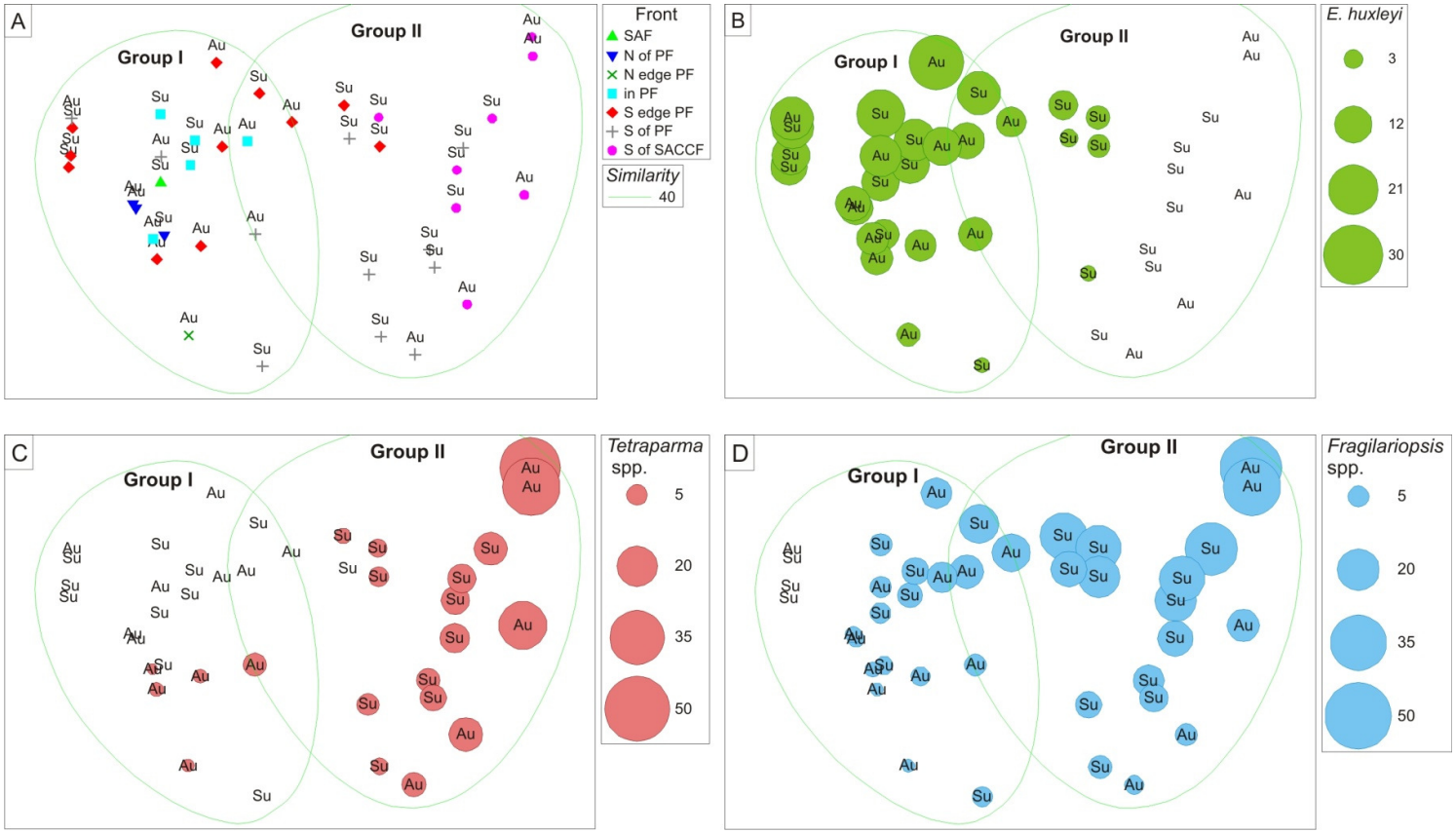

Figure 35a-d. MDS plots showing the similarity between SEM samples, created using the Bray-Curtis resemblance matrix with significant CLUSTER analysis groupings overlaid (similarity<40). (A) shows sample locations relative to fronts, while (b-d) show transformed species abundances (square root transformation of cells ml^{-1}) for (b) *E. huxleyi*, (c) *Tetraparma* spp., and (d) small *Fragilariopsis* spp. Seasons for (a-d) are labelled Su (austral summer) and Au (austral autumn).

3.3.5 **Abiotic Grouping**

To examine the environmental factors affecting the observed species distributions, the relationships between environmental variables were first considered in isolation using PCA analysis. Before the analysis could be carried out, however, the relationships between variables were assessed to determine which variables might be dependent (Table 20). Dynamic height, pCO_2, silicate, nitrate, and phosphate correlated significantly ($p \leq 0.05$) to the driving physical variables of temperature and salinity, however, only temperature and dynamic height, and temperature and silicate also demonstrated high covariation ($r^2 \geq 0.6$). Additional significant correlations between dynamic height and silicate; between silicate, nitrate and phosphate; and between pCO_2 and nutrients, are expected to be the result of the dependence of all these variables on either temperature or salinity.

Table 20. Coefficient of determination (r-squared) for environmental variables. Significant r-squared values (Minitab regression function) for are shown with an asterisk "*".

	SST	Salinity	Dyn Ht	pCO_2	SQR ($Si(OH)_4$)	SQR (PO_4)	SQR (NO_3)
Salinity	0.40						
Dyn Ht	0.79*	0.48					
pCO_2	0.03	0.23*	0.07				
SQR ($Si(OH)_4$)	0.76*	0.52*	0.71*	0.25*			
SQR (PO_4)	0.35*	0.27*	0.19	0.01	0.38*		
SQR (NO_3)	0.56*	0.46*	0.37	0.35*	0.73*	0.29*	
SQR (dFe)	0.00	0.00	0.00	0.19	0.01	0.01	0.02

The effect of removing the driving, or 'primary' variables of temperature and salinity was constrained by comparing a PCA analysis with and without those variables (Table 21). In both analyses three PCs were necessary to achieve a reasonable description of the overall structure, cumulatively accounting for >80% of the total variation (59%, 19%, and 8% for PC1, PC2, and PC3, respectively for the analysis including primary variables; 55%, 22%, and 10% for PC1, PC2, and PC3, respectively for the analysis excluding primary variables). In the analysis including all variables, eigenvectors for PC1 were highest for (1) chemical variables corresponding to a decreasing gradient of macronutrients (silicate, phosphate, and nitrate) and (2) physical variables corresponding to the frontal succession over the cruise track (increasing SST, decreasing salinity, and increasing dynamic height) (Table 21). The largest eigenvector

of PC1 was silicate, closely followed by temperature. Dissolved Fe was the largest eigenvector of PC2, followed by pCO_2. The largest eigenvector of PC3 was dFe, though PC3 accounted for only 8% of variation. When primary variables were excluded, the eigenvectors for PC1 and PC2 followed a very similar pattern to the broader analysis and phosphate became the largest eigenvector of PC3 (explaining only 10% of variation).

Table 21. Eigenvectors for each environmental variable used in the abiotic PCA analysis. Eigenvectors represent the weight of each variable in determining the PCA representation of sample relationships. Eigenvectors are provided individually for each PC, with PC1 accounting for the largest percentage of variation in the samples. The transformations undergone by each environmental variable are (Table 17) included in the environmental variable label.

	Primary variables included			Primary variables excluded		
Environmental Variables	PC1	PC2	PC3	PC1	PC2	PC3
SST	0.41*	0.21	0.38*			
salinity	-0.39*	-0.01	0.31*			
dynamic height	0.40*	0.14	0.37*	0.45*	0.19	-0.19
pCO2	-0.24	0.61*	0.47*	-0.34*	0.53*	0.36*
SQR (Si(OH)4)	-0.45**	-0.01	-0.05	-0.53**	-0.10	0.08
SQR (PO4)	-0.31*	-0.29	0.15	-0.36*	-0.40*	-0.68**
SQR (NO3)	-0.41*	0.12	0.21	-0.50*	0.02	0.15
SQR (nM Fe)	0.06	-0.68**	0.58**	0.12	-0.72**	0.59*

** indicates largest eigenvector
* indicates sizeable eigenvector (>half of the largest coefficient)

A quantitative comparison (BEST routine) between biotic data and abiotic data determined the combination of environmental variables most significantly correlated to the biotic Bray-Curtis similarity matrix for both PCA analyses. The set of best correlated variables from the 'primary values included' analysis were temperature, salinity, and silicate (0.687, $p<0.01$; Table 22), while those for the 'primary values excluded' analysis were silicate, dynamic height, nitrate, phosphate, and dFe concentrations (0.640, $p<0.01$; Table 22).

Table 22. BEST results for the 'primary variables included' and 'primary variables excluded' data sets, showing the highest correlations for 1 variable and for combinations of 2, 3, 4, and 5 variables in a comparison between biotic and abiotic data. The largest correlation coefficient is highlighted in bold, and indicates the combination of environmental variables which produced a distribution of samples that was the most similar to a distribution based on species biogeography.

# of	Primary variables included		Primary variables excluded	
Variables	Correlation	Environmental Variables	Correlation	Environmental Variables
1	0.650	SST	0.625*	Sqr [$Si(OH_4)$]
2	0.685*	SST, SQR [$Si(OH_4)$]	0.633*	Sqr [$Si(OH_4)$], Dynamic height
3	**0.687***	**SST, SQR [$Si(OH_4)$] , Salinity**	0.624*	Sqr [$Si(OH_4)$], Dynamic height, SQR [NO_3]
4	0.672*	SST, SQR [$Si(OH_4)$], Salinity, Dynamic height	0.634*	Sqr [$Si(OH_4)$], Dynamic height, SQR [NO_3], SQR [PO_4]
5	0.679*	SST, SQR [$Si(OH_4)$], Salinity, Dynamic height, SQR [dFe]	**0.640***	**Sqr [$Si(OH_4)$], Dynamic height, SQR [NO_3], SQR [PO_4], SQR [dFe]**

* indicates significant result in permutation test; $p<0.001$

3.4 Discussion

3.4.1 Biogeography of key species in relation to environmental gradients

In order to achieve a better understanding of *E. huxleyi* ecology in the Southern Ocean, the biogeography of the most numerous mineralizing nannoplankton groups was examined in the Scotia Sea, as well as potentially controlling environmental variables. CLUSTER and MDS analysis, used to describe relationships between samples based on species distributions, detected two distinct nannoplankton communities (Figure 34 and Figure 35): a northern group (group I) dominated by *E. huxleyi* (Figure 35b) and consisting of samples taken in the SAF, north of the PF, in the PF, and the majority of those taken at the southern edge of the PF; and a southern group (group II) dominated by *Fragilariopsis* and *Tetraparma* (Figure 35c-d) and consisting of samples taken south of the SACCF and the majority of those taken south of the PF. *E. huxleyi* and *Tetraparma* spp., therefore, demonstrated distinct ranges, with *E. huxleyi* dominating at the more northern stations and *Tetraparma* spp. dominating at the more southern ones. The range of *Fragilariopsis* spp. was less restricted, although the group was more numerous at the southern stations than the northern ones, and thus shared the southern end of its range with its fellow siliceous nannoplankton *Tetraparma* spp. (Figure 28).

The north to south species succession was significantly related to the sampling location relative to the major circumpolar fronts (*a priori* ANOSIM analysis), with the SAACF forming a clear southern boundary for *E. huxleyi* and a clear northern boundary for *Tetraparma* spp. Zero *E. huxleyi* abundances south of the SACCF were the expected outcome based on previous *in situ* studies (hypothesis 3; Table 3). Though predictions based on satellite images such as Figure 26 and Figure 27 suggest the SACCF is a barrier to southward penetration only in some years, this penetration has not been confirmed *in situ* (Holligan et al., 2010). It is clear using the satellite imagery from the cruise periods that both summer 2008 and autumn 2009 were examples of "SACCF-constrained" years, thus the penetration of *E. huxleyi* southward of the SACCF would not be expected from the *in situ* samples involved in this study, and the environmental factors initiating a non-constrained year, such as interaction between the SACCF and the Southern Boundary, or meteorological factors (Holligan et al., 2010) could not be investigated.

The differentiation of nannoplankton communities based on frontal boundaries was closely related to environmental gradients in the region, with initial BEST results indicating that temperature, salinity, and silicate were the largest factors affecting the biogeography of the nannoplankton groups studied (Table 22). Average high temperatures of 5.0 ± 1.5°C and low silicate concentrations of 6.0 ± 4.6 mmol $Si(OH)_4$ m^{-3} characterized group I, while lower average temperatures of 2.1 ± 1.4°C and higher average silicate concentrations of 46.6 ± 31.3 mmol $Si(OH)_4$ m^{-3} characterized group II. Salinity mean values for the two groups (33.81 ±0.13 and 33.82 ±0.23, respectively) were very similar, suggesting that other biogeographic divisions were responsible for salinity's significance in the BEST analysis. The dominance of siliceous nannoplankton in group II, which corresponded to higher silicate concentrations, and *E. huxleyi* in group I, where silicate concentrations were potentially limiting, was expected given that diatoms out-compete *E. huxleyi* when conditions are favourable (hypothesis 3; section 1.1.2) and suggests that the biogeography of *E. huxleyi* is dependent on fronts and biological factors (i.e. competition from siliceous taxa), while the biogeography of siliceous nannoplankton is dependent on environmental factors (i.e. silicate availability), and in the case of *Tetraparma* spp., fronts as well.

This simple interpretation, however, was complicated by the identification of significant correlations between silicate, a secondary variable, and temperature and salinity, the driving physical variables behind macronutrient concentrations and associated with frontal succession (Table 20). The positive relationship between temperature and *E. huxleyi* and negative relationship between temperature and the siliceous taxa may be the indirect result of the correlation between silicate and biotic distributions, or the direct result of lower temperature optima for the siliceous taxa, in which case the observed correlations to silicate could be an artefact of including dependent variables.

The importance of silicate independent of temperature was examined when the driving variables of temperature and salinity were removed from the BEST analysis. The best-correlated set of environmental variables following this second analysis were nutrient concentrations and dynamic height, suggesting that nutrient availability in general affected nannoplankton biogeography and that the high correlation between silicate and temperature was responsible for the appearance of silicate alone in the first BEST analysis. Relatively higher concentrations of dFe, nitrate, phosphate, and silicate for group 2 (0.6 ±1.1 mmol m^{-3}, 22.9 ±3.2 mmol m^{-3}, 1.8 ±0.3 mmol m^{-3}, and 46.6

±31.3 mmol m^{-3}, respectively) relative to group 1 (0.3 ±0.2 mmol m^{-3}, 18.5 ±3.6 mmol m^{-3}, 1.2 ±0.3 mmol m^{-3}, and 6.0 ±4.6 mmol m^{-3}, respectively) support an extended biological basis for the relationship between environmental factors and *E. huxleyi* biogeography, with not only higher (by a factor of 8) silicate concentrations, but also slightly elevated nitrate, phosphate, and dFe concentrations favouring fast-growing siliceous nannoplankton taxa such as the diatoms over slower-growing *E. huxleyi*. In addition to this biologically-mediated relationship to environmental factors, the appearance of dynamic height in the set of highest correlating environmental variables reiterates the point that frontal boundaries also determine nannoplankton distributions and agrees well with the evidence from the CLUSTER and MDS analyses (biotic data).With the ecological strategy of the chrysophyte *Tetraparma* poorly understood (section 1.1.2), it is difficult to say whether its dominance of group II is more likely tied to fast growth rates in favourable conditions or a close relationship to frontal geography.

As expected from more recent CO_2 manipulation experiments, pCO_2 did not appear to influence *E. huxleyi* biogeography (hypothesis 3) and was not included in the set of best-correlated variables in either BEST analysis. The significant correlation between pCO_2 and Chl-*a* ($p \leq 0.05$; $r^2=0.17$), manifesting as a reduction in pCO_2 in high Chl-*a* areas, suggests that any effect of pCO_2 in the less productive areas where nannoplankton dominate may be obscured by the relationship between pCO_2 and Chl-*a* in very productive areas where microplankton dominate. Therefore the analysis of the effect of pCO_2 on nannoplankton biogeography (336.8 ± 29.0 µatm for group I and 341.6 ± 46.8 µatm for group II) is problematic, however, the lack of relationship between pCO_2 and biogeography suggests as expected (hypothesis 3) that it is not currently limiting *E. huxleyi* distributions in the Southern Ocean (at least within the range of values found in the Scotia Sea).

The effect of Fe on nannoplankton biogeography was unexpectedly complicated, as an effect of higher dFe concentrations combination with the effect of higher macronutrients (particularly silicate) and frontal boundaries. The Fe requirements of all 3 nannoplankton groups were expected to be low (section 1.1.2.1.1) and indistinguishable (hypothesis 3). Though lower dFe concentrations may limit competition for nutrients from siliceous *micro*plankton, it was not expected to be a significant factor for *nanno*plankton biogeography. The grouping of dFe with the macronutrients could not be explained by covariance between variables, as dFe did not

correlate significantly to any other environmental variable (Table 20), suggesting that Fe-limitation may also affect nannoplankton.

3.4.2 **Biomass contribution**

For eight of the seventeen samples which could be compared using SEM and Lugols counts, mineralizing nannoplankton biomass constituted >10% of total phytoplankton biomass (TPB). On average the nannoplankton contribution (13%) was on par with the contributions made by the two most abundant microplankton groups, diatoms (42%) and dinoflagellates (41%) (Table 19). *Fragilariopsis* biomass was consistently high south of the SACCF during both seasons, while *Tetraparma* biomass was high in autumn south of the SACCF. The large biomass of both siliceous nannoplankton species in the high-latitude Southern Ocean in autumn, and in summer for *Fragilariopsis*, suggests that these understudied groups may be influential in Southern Ocean ecosystems.

High *E. huxleyi* biomass in the South Georgia shelf area in autumn and the high numbers of detached *E. huxleyi* coccoliths in and around the PF south of the Falkland Islands (in autumn), west of South Georgia (in autumn and summer) and north of South Georgia (in summer) coincide well with the previous predictions of *E. huxleyi* blooms based on satellite images (Holligan et al., 2010) and the reflectance and PIC satellite images obtained for the cruise track (Figure 26 and Figure 27); although cell numbers were lower than the expected 1000–2000 cells ml^{-1} (Holligan et al., 2010). Across all three taxa, therefore, the mineralizing nannoplankton comprise a significant component of the Southern Ocean ecosystem, potentially forming blooms in both calcareous and siliceous taxa.

3.4.3 **Conclusions**

To the author's knowledge, this is the first study to present *in situ* measurements of *E. huxleyi*, *Fragilariopsis*, and *Tetraparma* abundances in the central and eastern Scotia Sea, to estimate mineralizing nannoplankton biomass in the Southern Ocean, and to relate mineralizing biogeography in the Southern Ocean to environmental gradients and ecological strategies. The major findings of the work were the expected correlation between silicate concentrations and the nannoplankton biogeography, with siliceous taxa dominating in areas of higher silicate concentrations, the unexpected correlation between nitrate, phosphate, and dFe concentrations and nannoplankton biogeography,

with siliceous taxa dominating in areas of slightly higher nutrient concentrations, the expected correlation between frontal geography and *E. huxleyi* biogeography, with the SACCF a southern boundary for *E. huxleyi*, and the substantial biomass of all three mineralizing nannoplankton taxa in several areas.

The implications of these findings are that despite the low requirements for nitrate, phosphate, and dFe expected for all nannoplankton taxa due to their small cell size, ecological strategies favouring r-selected diatoms in higher nutrient conditions appear to be maintained in the nannoplankton of the Scotia Sea. Furthermore, the biomass results suggest that consideration of mineralizing nannoplankton communities in studies of carbon export is critical to understanding regional biogeochemical cycling as siliceous nannoplankton species make up a significant portion of the biomass south of the SACCF and as *E. huxleyi* blooms occur off the South Georgia and Falkland Island shelves. The first question raised by these outcomes, whether the very preliminary observation of a nannoplankton Fe response can be confirmed in controlled experiments, is explored in the following chapter; the second question, the extent of Southern Ocean nannoplankton blooms cannot be taken further in this thesis research, however the agreement between *in situ* high *E. huxleyi* abundances and satellite-predicted high abundances in 3 areas of the Scotia Sea suggest that addressing the question with regard to *E. huxleyi* could provide important information regarding local biogeochemical cycling.

The following chapter has been prepared as a paper and is currently in review under the same title for a Deep Sea Research Part II: Topical Studies in Oceanography special issue entitled Seasonal and spatial patterns in the Scotia Sea ecosystem.

4 Seasonal iron control of phytoplankton community structure in the Scotia Sea

4.1 Introduction

In the High Nutrient Low Chlorophyll (HNLC) Southern Ocean, iron (Fe) has been consistently demonstrated to be a major limiting element for microplankton (20–200 µm) growth, with natural Fe inputs in the vicinity of Southern Ocean island chains leading to large microplankton diatom blooms and export of carbon (Martin, 1990; de Baar et al., 2005; Boyd et al., 2007). Mesoscale Fe addition experiments carried out in polar regions of the Southern Ocean, including SOIREE (Gall et al., 2001), CARUSO/EisenEX (Gervais et al., 2002), and EIFEX (Hoffmann et al., 2006) have consistently shown that large diatoms and a smaller proportion of medium diatoms respond to artificial Fe addition with an increase in biomass (Table 4; top half). This increased biomass both becomes available to higher trophic levels and leads to significant export of biogenic material to the deep ocean (De La Rocha and Passow, 2007; Poulton et al., 2007). Outside of locally Fe-fertilized areas, however, nannoplankton (2–20 µm) contribute significantly to biomass (sections 1.1.2.1.1 and 3.4.2). Few direct measurements of the effect of Fe on this phytoplankton size class have been recorded (Gall et al., 2001; Crawford et al., 2003), however, the observational results of chapter 3 indicate that nannoplankton community structure may also be affected by dFe concentrations (section 3.4.1).

Here, both microplankton and nannoplankton community responses to Fe fertilization were characterized using bioassay experiments initiated in naturally Fe-fertilized and Fe-depleted regions near the island masses of South Georgia and the South Orkney Islands to expand upon this potential nannoplankton Fe effect within the context of the microplankton Fe response, addressing the fourth hypothesis in section 1.3:

4. Adding Fe to phytoplankton communities in controlled experiments will produce an increase in overall biomass and a taxonomic shift towards medium and large diatoms with their higher Fe requirements and away from the nannoplankton size

fraction with their lower Fe requirements. *E. huxleyi*, small diatoms, and chrysophyte abundances, therefore, will not increase in Fe treatments.

4.2 Methods

4.2.1 Sampling

Cruise tracks, dates, and data constraints are detailed in chapter 3 (section 3.2.1). Collection of SEM samples (JR200 bioassay samples) and calculation of biomass were as in chapter 3 (section 3.2.2). Collection of seawater for underway dFe measurements and for initial filling of bioassay bottles was performed using a trace metal clean tow fish (Bowie et al., 2001; Nielsdóttir et al., 2009). Analysis of dFe concentrations was performed by M. Nielsdottir for JR161 and JR177, and by S. Steigenberger for JR200. Microplankton community data collected from CTD bottles on cruise JR177 have been presented previously (Korb et al., 2010) and the authors' large-scale survey of the Scotia Sea in summer was used to provide a broader context for the initial bioassay microplankton community samples taken using the tow fish (Figure 36).

Physiological data were collected underway, during bioassay experiments, and on-station using fast repetition rate fluorometry (FRRf). Two types of FRRf instruments were used to measure F_v/F_m and σ_{PSII}, the FAST*tracka*™ I, manufactured by Chelsea Technologies Group (CTG) (UK), and the bench top FIRe™ system (Fluorescence Induction and Relaxation of Emission Spectrometer), manufactured by Satlantic (Canada). FRRf protocols were similar to those detailed in several articles by Moore et al. (2005; 2006; 2007b) and in Bibby et al. (2008). The FIRe instrument was used in flow-through mode throughout, including with discrete samples. Underway samples, used to assess physiology in the study region on cruises JR161 and JR177 (JR161 – FIRe instrument, Figure 37d; JR177 - Chelsea instrument, Figure 37e), were collected from the ship's non-toxic sea-water supply. Discrete samples, used to assess physiology in the study region on cruise JR200 (Chelsea instrument, Figure 37f) were collected using the stainless steel CTD (CTD as in chapter 3; 10-m Niskin bottles). Discrete samples were also collected from bioassay experiments for analysis of bioassay physiology (FIRe instrument data shown).

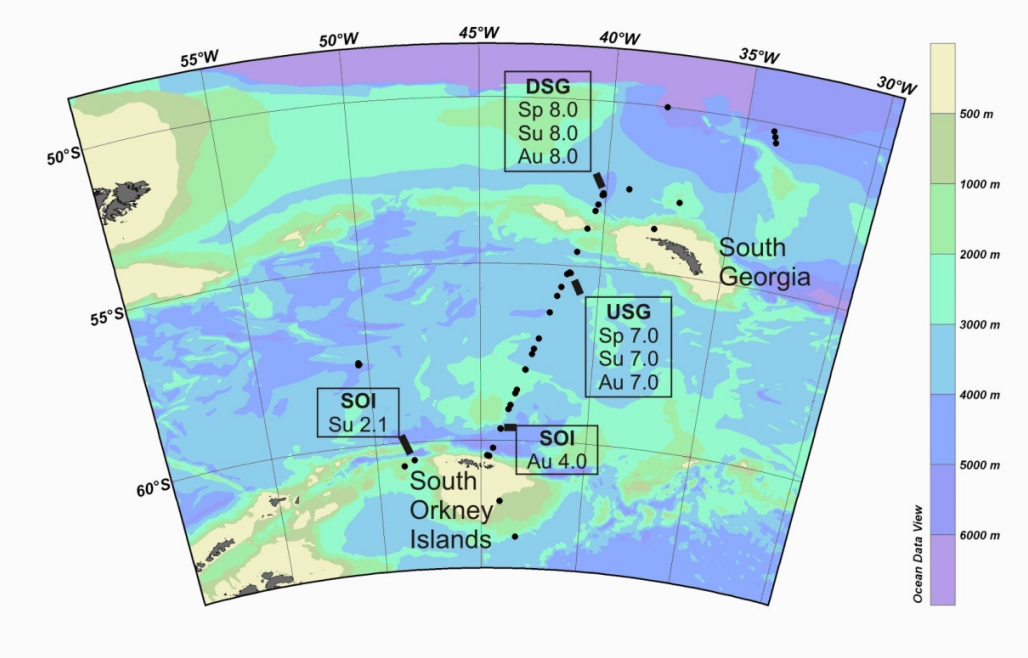

Figure 36. Map of cruise stations and bioassay experiment sites for austral spring (Sp), summer (Su), and autumn (Au) cruises overlaid on the benthic topography of the Scotia Sea (scale bar at right represents depth in meters). Regions where water was collected for onboard bioassay incubations were region 1: DSG (Sp/Su/Au 8.0), region 2: USG (Sp/Su/Au 7.0), and region 3: SOI (Su 2.1 and Au 4.0) (section 4.2.2).

As often as possible, underway and discrete measurements on cruise JR177 were analyzed with both instruments (Chelsea bioassay data not shown), allowing a comparison to be made between F_v/F_m values returned by each FRRf. Chelsea F_v/F_m values averaged 0.43 ±0.099 while FIRe F_v/F_m values averaged 0.36 ±0.096, therefore Chelsea values are 0.075 units higher on average than FIRe values. Discrete samples were dark-adapted for a minimum of 30 minutes at *in situ* temperatures before analysis (Moore et al., 2007b). Filtrates were analyzed for discrete samples after every set of samples and for underway sampling daily to allow correction using a blank measurement (Cullen and Davis, 2003; Moore et al., 2007b; Bibby et al., 2008). Fluorescence data were processed using either manufacturer-supplied software (JR161 underway FIRe F_v/F_m data) or Matlab® (JR177 underway FRRf F_v/F_m data, JR200 discrete FRRf F_v/F_m data, and all bioassay F_v/F_m data). The Matlab processing routine used was developed by C. M. Moore (2007b) and was based on the model of Kolber et al. (1988). During JR161, physiological data was collected by T. Bibby, and during JR177 and JR200 data were collected by D. J. Hinz.

Ancillary data is described in chapter 3 (section 3.2.1) with the addition of the extinction coefficient for downwards irradiance (K_d) and average daily irradiance at the surface (E_{avg}). K_d and E_{avg} were provided by M. Nielsdóttir (pers. comm.). The hydrographic sensors used included a SeaBird 9/11+ CTD with 2π irradiance sensor and an Oceanlogger SeaBird Electronics SBE45 CTD. MODIS/Aqua Chl-*a* monthly composite images were provided by the NERC Earth Observation Data Acquisition and Analysis Service (NEODAAS) for the cruise periods.

4.2.2 **Bioassays**

Locations for grow-out bioassay experiments were selected through the *in situ* analysis of phytoplankton biomass, as measured by Chl-*a* concentration, and of phytoplankton physiology, as measured by the photosynthetic energy conversion efficiency, F_v/F_m. Both of these measurements were monitored continuously from surface sea water sampling. The data (section 4.3.1) were compared to MODIS/Aqua Chl-*a* monthly composite images for the region at corresponding times of year (data not shown), and three contrasting regions of the Southern Ocean were identified. These locations were: (1) a high-chlorophyll, Fe-fertilized region DSG (Korb et al., 2010), (2) a low-chlorophyll, Fe-deplete region USG (Korb et al., 2010), and (3) a high-chlorophyll, Fe-fertilized region off the South Orkney Islands (SOI). On-deck, controlled Fe addition bioassay experiments were conducted in these regions to demonstrate the role and magnitude of Fe in controlling the phytoplankton community in the Scotia Sea. Water was collected for Fe addition bioassay experiments on each cruise using the towfish while steaming to stations 7.0 (Sp/Su/Au 7.0), region 2, and 8.0 (Sp/Su/Au 8.0), region 1, off the South Georgia shelf. In addition, on cruises JR177 and JR200, a third bioassay was set up on the South Orkney Island shelf at stations Su 2.1 and Au 4.0, respectively (region 3; Figure 36). Nannoplankton biomass values (chapter 3; Table 19) corresponded to the three study regions outlined here in the following way: (1) DSG – summer samples 18A and 20A; autumn samples B4 and 26, (2) USG - summer samples 15B and 16A; autumn samples 23A and B3, and (3) SOI - summer samples 8B and 11A; autumn samples 19B, 20B, and B2.

Bioassay set-up was similar to that of Moore et al. (2007b; Kerguelen Islands, Southern Ocean), and Nielsdóttir et al. (2009; Northeast Atlantic). Four experimental treatments were compared, with five replicates of each condition: (1) High Light Control (HLC), (2) High Light, Fe Added (HLFe), (3) Low Light Control (LLC), and

(4) Low Light, Fe Added (LLFe). Fe added bottles were acidified with $FeCl_3$ to a final concentration ~2 nM above ambient. No other nutrients were added, however, and the bottles were closed systems once sealed. Light levels were maintained using neutral density and blue lagoon filters (Lee Ltd.; Andover, UK) at 60% (HL) and 30% (LL) of ambient surface irradiance for cruise JR161, at 40% (HL) and 22% (LL) of ambient surface irradiance for cruise JR177, and at 15% (HL) and 2.5% (LL) of ambient surface irradiance for cruise JR200. Originally, an analysis of the effect of light was envisioned, however, the light levels maintained for the HL and LL conditions were reduced each year as previous light levels were deemed too high following each cruise. This inconsistency prevented comparison of light effects between seasons, thus light manipulation effects were not analyzed, and HL and LL measurements were pooled according to Fe treatment.

Three of the five replicates from each condition were sampled only at the endpoint of the bioassay to minimize the chances of contamination, while two replicates from each condition were sub-sampled at either 24- or 48-hours after setup and then every 48 hours through the completion of the experiment to monitor the development of the experiments. With the combination of HL and LL groups, the number of endpoint replicates and sub-sampled replicates doubled (N = 6 and N = 4, respectively). Initial samples (N = 3) were taken using the towfish during the process of filling bioassay bottles at the start, when halfway-filled, and at the finish. Because these samples were taken underway (using a trace metal clean method and analyzed with the FIRe instrument), they serve as further *in situ* discrete samples and can be compared to the underway samples from the non-toxic supply (analyzed with the Chelsea instrument). Sub-samples (N = 4) were collected for physiology, dFe, macronutrients, and Chl-*a* analysis, though macronutrient and Chl-*a* samples were not collected on every sub-sampling day. Samples for physiology, dFe, macronutrients, Chl-*a*, and phytoplankton community analysis were collected at endpoints only. At endpoints, therefore, two sets of data were available: (1) the set from sub-sampled bottles (N = 4), and (2) the set from endpoint bottles (N = 6). In statistical analyses, sub-sampled bottles were considered for 24- and 48-hour time points (N = 4; only bottle available), while endpoint bottles were considered at final time points (N = 6; both N = 4 and N = 6 available). The choice of endpoint bottles over sub-sampled bottles was made at final endpoints because endpoint bottles were not opened until the final bioassay time points and were therefore less subject to contamination. Determination of Fe-limited bioassays was made using the

earliest time point available from sub-sampled bottles (24 to 48 hours for the majority of bioassays; 72 hours for the spring DSG bioassay). The earliest F_v/F_m measurements available were used because changes in F_v/F_m at 24- to 48-hour time points are indicative of nutrient stress (a fast response), while changes after 48 hrs are indicative of shifts in phytoplankton community composition (a slower response; Moore et al., 2007b; Suggett et al., 2009).

The duration of bioassays was not standardized for the 3 seasons, creating a discrepancy between bioassay final time points. The JR161 USG, JR161 DSG, and JR177 SOI bioassays ran for 10 days, 8 days, and 8 days, respectively (long-running bioassays), while JR177 USG, JR177 DSG, JR200 USG, JR200 DSG, and JR200 SOI bioassays each ran for 4-5 days (short-running bioassays). The available day 3 and 4 sub-sampling measurements (N = 4) from the 3 long-running bioassays, therefore, were compared to the day 4 and 5 final endpoint measurements from the 5 short-running bioassays (N = 6). Lugols community analysis data, however, could not be presented in this way as Lugols samples were only taken at bioassay initial time points and final time points. It should therefore be noted that, when comparing JR161 microplankton community data to JR177 microplankton community data, the endpoints differed.

4.2.3 **Statistical analysis**

Minitab® 15 was used to identify significant differences in F_v/F_m, physiology, Chl-*a*, abundance, and nutrient concentrations between Fe treatment groups in bioassay experiments (one-way ANOVA test). Control bottles (the 3 HLC and 3 LLC bottles were combined as one group, C, for Lugols samples; 2 HLC bottles were used as the C group for SEM samples) were compared with Fe-treated bottles (the 3 HLFe and 3 LLFe bottles were combined as one group, Fe, for Lugols samples; 2 HLFe bottles were used as the Fe group for SEM samples), regardless of light level. The same test was used to identify significant differences in diversity indices between bioassay microplankton samples; however, too few nannoplankton species were included to warrant a comparison of diversity for the nannoplankton community.

For the microplankton community, diversity indices were calculated and multivariate statistical analysis were carried out using PRIMER-E version 6.1.6 (Clarke and Gorley, 2006) on species biomass. From this point, the calculation of a Bray-Curtis similarity matrix, CLUSTER and Multidimensional scaling analyses, and ANOSIM significance analyses were as in chapter 3 (section 3.2.3). For these multivariate

analyses, the 4 experimental groups were left separate, to aid visualization of the similarity between replicate samples. In ANOSIM tests and all following statistical tests, C bottles were compared with Fe bottles regardless of light level. *A priori* groupings based on sampling season (spring - summer), sampling geography (SOI - South Georgia and USG - DSG), bioassay time point (initial - C and initial - Fe), and Fe treatment (C - Fe) were tested for significance using either a one-way or a two-way ANOSIM with replicates routine. The contribution of individual species to overall dissimilarity between groups was analyzed using the SIMPER routine, which ranks the species with the largest changes in biomass between groups by their contribution to the overall dissimilarity. The top 50% of the ranked species were then compared between groups (season or geography *in situ*; time point or Fe treatment in bioassays) using a two-tailed, unpaired homoscedastic Student's *t*-Test. The associated probability values that the test returned were used to assess the significance of individual species changes in biomass between the groups tested for microplankton community differentiation in the ANOSIM test.

4.3 **Results**

4.3.1 **Contrasting regions of the Scotia Sea**

Study region 1, the area DSG, was characterized by high phytoplankton biomass as measured by Chl-*a* concentration (mg m^{-3}), which was lowest in spring and highest in summer (0.86 ± 0.38 mg Chl-*a* m^{-3}, 3.75 ± 1.75 mg Chl-*a* m^{-3}, and 1.05 ± 0.76 mg Chl-*a* m^{-3}, spring, summer, and autumn respectively; Figure 37a-c); in contrast, the photosynthetic physiology of the phytoplankton community (F_v/F_m) was high over all seasons (averages of 0.46 ± 0.13, 0.51 ± 0.24, and 0.60 ± 0.08, for spring, summer, and autumn, respectively; Figure 37d-f). Study region 2, the area USG, was characterized by lower phytoplankton biomass than DSG (0.28 ± 0.09 mg Chl-*a* m^{-3}, 1.15 ± 0.44 mg Chl-*a* m^{-3}, and 0.45 ± 0.07 mg Chl-*a* m^{-3}, for spring, summer, and autumn, respectively (Figure 37a-c) and F_v/F_m measurements were lower here than DSG (0.32 ± 0.09, 0.38 ± 0.22, and 0.30 ± 0.07, spring, summer, and autumn respectively; Figure 37d-f). Study region 3, the SOI, developed high phytoplankton biomass in summer and autumn (1.74 ± 1.17 mg Chl-*a* m^{-3} and 1.22 ± 0.50 mg Chl-*a* m^{-3}, respectively) but F_v/F_m (0.46 ± 0.009 and 0.45 ± 0.08, for summer and autumn, respectively; Figure 37b-c, e-f) was lower than DSG in summer.

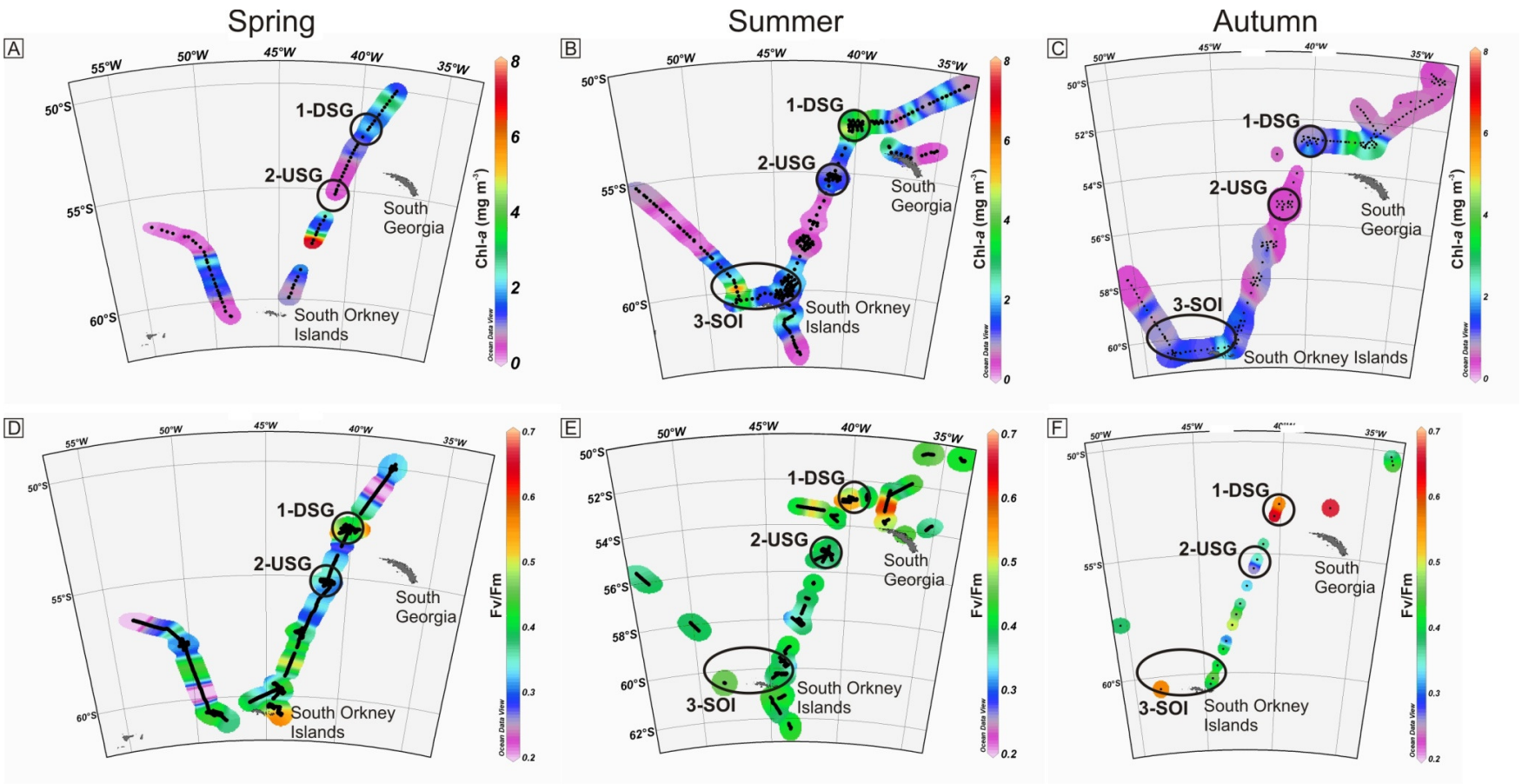

Figure 37a-f. Underway (a-c) Chl-*a* and (d-f) F_v/F_m for austral (a, d) spring, (b, e) summer, and (c, f) autumn cruises with regions identified for initiation of bioassay experiments, labelled: 1-DSG (downstream of South Georgia), 2-USG (upstream of South Georgia), and 3-SOI (off the South Orkney Island shelf). The spring and summer images are modifications of those provided by M. Nielsdóttir (pers. comm.).

A high-chlorophyll region midway between South Georgia and the South Orkney Islands (at approximately 57.4°S and 42.6°W) was present in the spring sampling season and was likely associated with a frontal region (according to corresponding satellite imagery; data not shown).

While there was considerable meso-scale variability within each study region, the initial bioassay data presented in Table 23 agreed well with the regional hydrographic data and suggest that the locations of bioassay experiments were representative of the regions shown on a broad scale in Figure 37, with the exception of the SOI. In initial samples, phytoplankton biomass DSG was high in all three seasons (1.27 mg Chl-*a* m^{-3}, 3.59 mg Chl-*a* m^{-3}, and 0.82 mg Chl-*a* m^{-3}, in spring, summer, and autumn, respectively). There were large differences between nitrate and silicate concentrations in summer and autumn compared to spring (25.9 mmol NO_3^- m^{-3} and 24.0 mmol $Si(OH)_4$ m^{-3}; 15.1 mmol NO_3^- m^{-3} and 14.2 mmol $Si(OH)_4$ m^{-3}; 14.1 mmol NO_3^- m^{-3} and 2.6 mmol $Si(OH)_4$ m^{-3}; in spring, summer, and autumn, respectively), suggesting strong nutrient drawdown in summer, and even stronger drawdown in autumn. Dissolved Fe concentrations DSG were high in all three seasons (0.4 nM, 0.25 nM, and 0.24 nM, in spring, summer, and autumn, respectively) and F_v/F_m ranged from moderate values in spring to high values in summer and autumn (0.39, 0.56, and 0.50, in spring, summer, and autumn, respectively). The maximum PSII effective absorption cross section (σ_{PSII}) remained moderate in spring and summer DSG (454.8 and 462.5, respectively) and increased in autumn (513.8).

Phytoplankton biomass USG was lower than DSG, but was higher USG in the summer season relative to the spring and autumn USG (0.42 mg Chl-*a* m^{-3}, 1.43 mg Chl-*a* m^{-3}, and 0.34 mg Chl-*a* m^{-3}, in spring, summer, and autumn, respectively) with concomitant low macronutrient concentrations in summer relative to spring and autumn (27.5 mmol NO_3^- m^{-3} and 20.1 mmol $Si(OH)_4$ m^{-3}; 16.6 mmol NO_3^- m^{-3} and 1.5 mmol $Si(OH)_4$ m^{-3}; 24 mmol NO_3^- m^{-3} and 7.4 mmol $Si(OH)_4$ m^{-3}; in spring, summer, and autumn, respectively). Dissolved Fe concentrations USG, while measureable in spring (0.05 nM), were reduced to below detection limits by the summer. F_v/F_m remained moderate in spring and summer (0.41 and 0.38 in spring and summer respectively), with F_v/F_m USG lower than DSG in summer. In summer USG σ_{PSII} was at its highest value (634.3), while moderate values, were observed in spring (532.0). The pattern of low dFe USG was not apparent in autumn, when dFe remained high (0.23 nM) and σ_{PSII} was moderate (450.1); although F_v/F_m in autumn was similar to spring and summer (0.36).

Table 23. Initial conditions for bioassay experiments with standard deviations shown in parentheses (based on the average of 3 samples over the course of filling bioassay bottles). BD indicates below detectable limit.

	Spring 2006		Summer 2008			Autumn 2009		
	USG	DSG	SOI	USG	DSG	SOI	USG	DSG
Sampling date	18 Nov	23 Nov	4 Jan	26 Jan	31 Jan	20 Mar	30 Mar	4 Apr
Latitude	-55.21	-52.88	60.41	-55.38	-52.81	-59.92	-55.30	-52.88
Longitude	-41.25	-40.09	47.90	-41.54	-39.69	-44.01	-41.11	-40.51
Sample depth (m)	3	3	3	3	3	3	3	3
MLD (m)	109	87	41	67	63	47	63	
K_d (m^{-1})	0.058	0.081	0.24	0.09	0.15			
E_{avg} (%E_0)	15.9	14.2	10.3	15.7	10.5			
SST (°C)	2.21	1.69	-0.01 ±0.06	3.28 ±0.01	3.26 ±0.02	1.61	4.42	5.24
Salinity	33.92	33.88	33.38	33.82	33.81	33.94	33.68	33.65
dFe (nM)	0.05 ±0.01	0.4 ±0.02	0.28 ±0.07	BD	0.25±0.12	0.09 ±0.14	0.23 ±0.05	0.24 ±0.04
Silicic acid (mmol m^{-3})	20.14 ±0.01	23.98 ±0.78	70.15 ±0.91	1.50 ±0.37	14.21 ±1.03	71.58 ±0.46	7.39 ±01.30	2.61 ±0.56
Nitrate (mmol m^{-3})	27.53 ±0.17	25.86 ±0.2	20.55 ±0.36	16.59 ±0.08	15.11 ±0.30	24.85 ±0.3	24.0 ±0.06	14.08 ±0.41
σ_{PSII}	532.0 ±40.3	454.8 ±27.8	404.1 ±10.6	634.3 ±22.3	462.5 ±36.6	475.7 ±35.5	450.1 ±29.1	513.8 ±62.7
F_v/F_m	0.41 ±0.03	0.39 ±0.04	0.39 ±0.09	0.38 ±0.03	0.56 ±0.03	0.48 ±0.02	0.36 ±0.01	0.50 ±0.05
Chlorophyll (mg m^{-3})	0.42 ±0.00	1.27 ±0.08	6.90 ±1.27	1.43 ±0.08	3.59 ±0.62	0.10 ±0.07	0.34 ±0.02	0.82 ±0.12

At the SOI (where sampling was only possible in the summer and autumn seasons owing to ice cover in spring), the initial bioassay conditions were dominated at the more westerly site used in summer (Figure 37b, e) by a very large phytoplankton bloom (6.90 mg Chl-*a* m^{-3}) and available macronutrient (20.55 mmol NO_3^- m^{-3} and 70.15 mmol $Si(OH)_4$ m^{-3}) and micronutrient (0.28 nM dFe) concentrations. At the SOI, F_v/F_m was lower (0.39) than in the phytoplankton community DSG in the same season, however σ_{PSII} was also lower (404.1). In contrast, biomass was very low at the more easterly SOI site (Figure 37c, f) in autumn (0.10 mg Chl-*a* m^{-3}) where macronutrient values remained high (24.85 mmol NO_3^- m^{-3} and 71.58 mmol $Si(OH)_4$ m^{-3}), but micronutrient concentrations (0.09 nM dFe) were very low. Data from neither summer nor autumn bioassay initiation sites agreed well with the average biomass for region 3 (1.22 ± 0.50 mg Chl-*a* m^{-3}), suggesting that the SOI regions was considerably more spatially variable than regions 1 and 2.

Graphical representations of F_v/F_m versus σ_{PSII} allowed a better visualization of the interaction between nutrient stress and taxonomy in initial bioassay samples than mean values alone (Figure 38a). Trends found in previous FRRf observations and experiments, including (1) higher F_v/F_m and lower σ_{PSII} in nutrient replete conditions (24- to 48-hr response) and when phytoplankton communities were made up of larger cells (>48-hr response), and (2) lower F_v/F_m and higher σ_{PSII} in nutrient-limited conditions (24- to 48-hr response) and when phytoplankton communities were made up of smaller species (>48-hr response) (Figure 38a; Suggett et al., 2009), were assessed in the context of location and season. Differences between instruments and methodology prevented a quantitative comparison of Sugget et al.'s findings and the current bioassay findings, however, the trends can be extrapolated from Suggett et al. to the bioassay results. Higher values of F_v/F_m and lower values of σ_{PSII} in summer DSG, autumn SOI, and autumn DSG suggest that the phytoplankton community was shifted towards larger species and/or was higher in nutrients. Lower values of F_v/F_m and higher values of σ_{PSII} in JR161 and JR177 USG suggest that the phytoplankton community was shifted towards smaller species and/or was lower in nutrients. In JR161 DSG, JR177 SOI, and JR200 USG, however, values of F_v/F_m and σ_{PSII} followed neither of these trends, potentially due to unexpected effects of taxonomy or the interaction between phytoplankton taxonomy effects and nutrient stress effects.

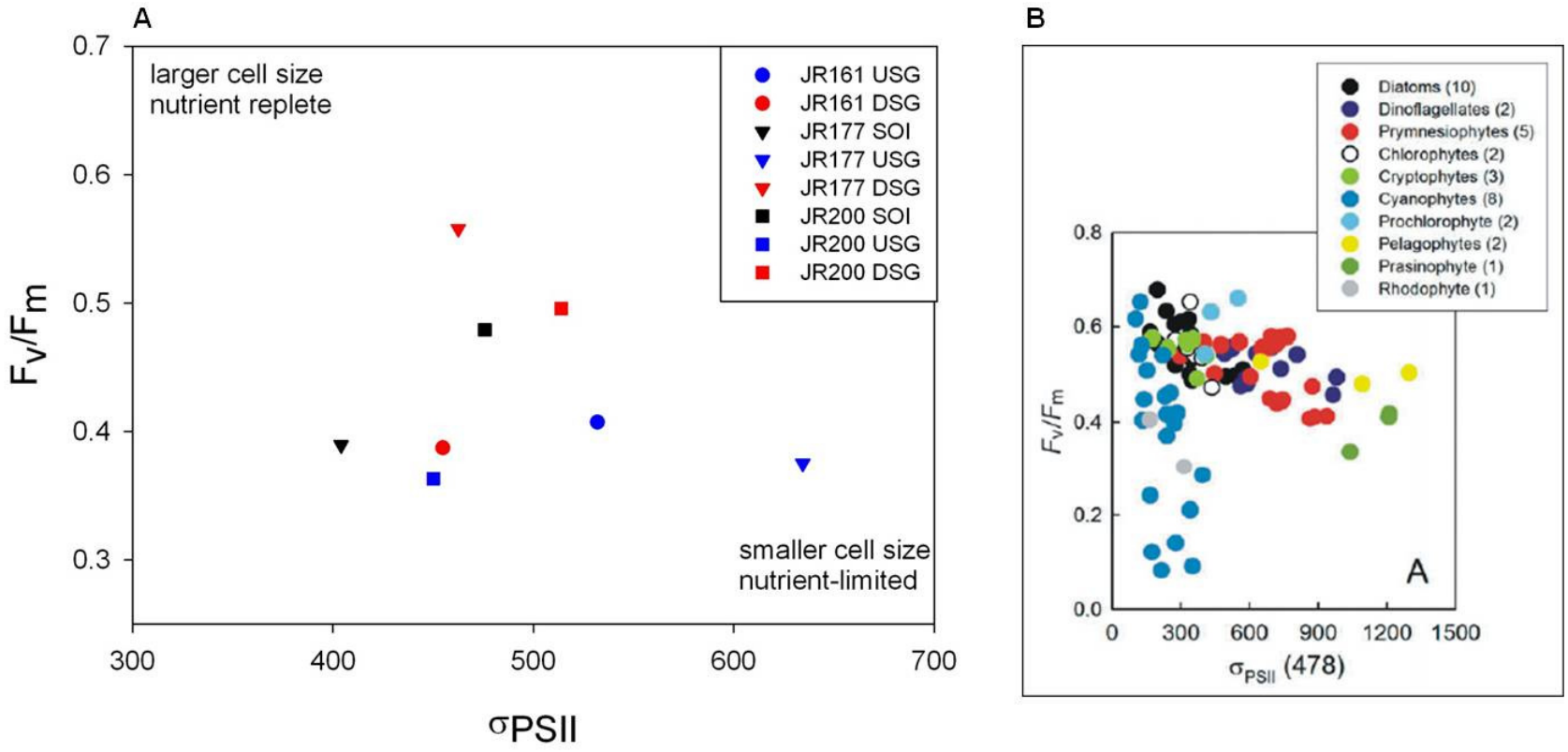

Figure 38a-b. Physiological changes (a) occurring in initial bioassay samples and (b) found in previous FRRf observations and experiments of a wide range of phytoplankton species (Suggett et al., 2009). Trends summarized by Suggett et al. (2009) were added on to plot (a) for reference.

4.3.2 **Initial phytoplankton community structure**

4.3.2.1 Microplankton community

The microplankton community from initial bioassay samples was analyzed to determine the starting microplankton communities in bioassay experiments. Microplankton community biomass was highest in summer (R. E. Korb, pers. comm.; section 3.3.3), therefore the summer microplankton community data covers the height of the microplankton growing season, while the spring microplankton community data covers the early phase of the growing season. Initial microplankton community structure was dominated by diatoms near South Georgia (SG) (which comprised 57.5% to 93.9% of biomass), and cryptophytes near the SOI (92.8% to 93.9% of biomass). Species diversity (Shannon-Weiner diversity index; H') and the evenness of species abundance (Pielou's evenness; J') were significantly lower ($p \leq 0.05$) near the SOI (means of 1.23 and 0.50, for H' and J' respectively) than at either USG or DSG (means of 2.67 and 0.89 for H' and J', respectively USG; and means of 3.01 and 0.86 for H' and J', respectively DSG) (Table 24). Shannon-Weiner diversity over both seasons was significantly lower DSG relative to USG ($p \leq 0.032$).

A CLUSTER analysis found that the largest difference between initial bioassay microplankton communities was between the SOI microplankton community and the SG microplankton communities (approximately 80% dissimilarity), followed by differences between the spring and summer SG microplankton communities (approximately 70% dissimilarity), and finally between the USG and DSG microplankton communities within each season (approximately 40–50% dissimilarity) (Figure 39). MDS analysis agreed well with the CLUSTER hierarchy (data not shown; 2-D stress level of 0.06) and confirmed the CLUSTER representation was reasonable.

Table 24. Diversity indices calculated using the Lugols microplankton counts. S= total species, (N), J'= Pielou's evenness, and H'= Shannon-Weiner diversity (logs to base e). Abbreviation for "Site" are USG (Upstream of South Georgia), DSG (Downstream of South Georgia), and SOI (South Orkney Islands).

Sample	S	Dominant Functional Group (% Total Biomass)	Dominant Species (% Total Biomass)	J'	H'	Cruise	Site	Season
161_3_I1	28	Diatoms (57.5%)	Medium naked dinoflagellates (20 – 40 µm) (19.4%)	0.9	3.1	161	USG	Spring
161_3_I2	32	Diatoms (58.7%)	Small naked dinoflagellates (20 µm) (17.7%)	0.9	3.2	161	USG	Spring
161_3_I3	29	Diatoms (59.4%)	Medium naked dinoflagellates (20 – 40 µm) (21.2%)	0.9	3.1	161	USG	Spring
161_4_I1	19	Diatoms (59%)	*Corethron pennatum* (34.5%)	0.8	2.4	161	DSG	Spring
161_4_I2	17	Diatoms (70.2%)	*Corethron pennatum* (58.5%)	0.8	2.2	161	DSG	Spring
161_4_I3	22	Diatoms (72%)	*Corethron pennatum* (24.9%)	0.9	2.7	161	DSG	Spring
177_2_I1	13	Cryptophytes (92.5%)	Cryptophyte *(possibly Geminigera cryophila)* (92.7%)	0.5	1.4	177	SOI	Summer
177_2_I2	13	Cryptophytes (93.4%)	Cryptophyte *(possibly Geminigera cryophila)* (93.4%)	0.5	1.3	177	SOI	Summer
177_2_I3	10	Cryptophytes (91.9%)	Cryptophyte *(possibly Geminigera cryophila)* (91.9%)	0.5	1.1	177	SOI	Summer
177_4_I1	27	Diatoms (92.9%)	*Pseudonitzschia* spp. (M) (48.4%)	0.9	2.9	177	USG	Summer
177_4_I2	26	Diatoms (93.9%)	*Pseudonitzschia* spp. (M) (41.6%)	0.9	2.8	177	USG	Summer
177_4_I3	31	Diatoms (92.8%)	*Pseudonitzschia* spp. (M) (41.4%)	0.9	3.0	177	USG	Summer
177_5_I1	29	Diatoms (58.5%)	Medium naked dinoflagellates (20 – 40 µm) (33.5%)	0.9	2.9	177	DSG	Summer
177_5_I2	26	Diatoms (57.587.3%)	*Thalassiothrix antarctica* (21.4%)	0.9	2.9	177	DSG	Summer
177_5_I3	22	Diatoms (84%)	*Odontella* (19.6%)	0.9	2.9	177	DSG	Summer

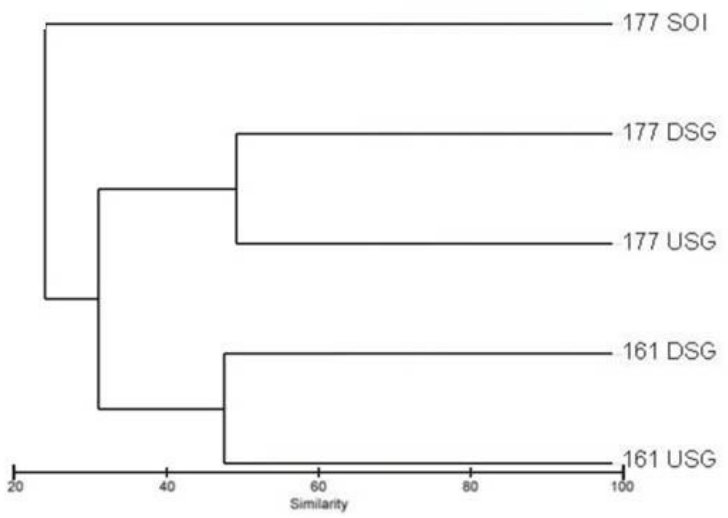

Figure 39. CLUSTER diagram created using a Bray-Curtis similarity matrix for all microplankton samples showing microplankton community relationships between bioassays. Spring and summer samples are labelled by their respective cruise numbers 161 and 177.

4.3.2.2 Nannoplankton community

The *in situ* biogeography of the nannoplankton in the Scotia Sea is presented for summer and autumn in chapter 3. Nannoplankton samples could only be collected from bioassays in the autumn, however, the higher biomass experienced by the nannoplankton community in autumn relative to summer (33 mg C m^{-3} in autumn versus 30 mg C m^{-3} in summer; data not included in Table 19), suggest that the autumn bioassays represented the height of the nannoplankton growth season. The nannoplankton community from initial bioassay samples was analyzed to determine the starting nannoplankton communities in bioassay experiments, though small sample sizes prevented using diversity indices or CLUSTER analysis. As occurred with the microplankton communities, nannoplankton communities in autumn were also defined by region, with *E. huxleyi* present USG (160 cells ml^{-1}) and DSG (80 cells ml^{-1}), but not off the SOI. The two other representative nannoplankton species, *Tetraparma* spp. and small (<20 µm) *Fragilariopsis* spp. (see chapter 3 for further explanation of nannoplankton choice) occurred in very high abundances in the SOI (1570 cells ml^{-1} and 1370 cells ml^{-1}, respectively), and in very small abundances DSG (4 cells ml^{-1} and 5 cells ml^{-1}, respectively). USG, *Tetraparma* was absent whereas *Fragilariopsis* was present (110 cells ml^{-1}) at similar abundance to *E. huxleyi*. The counterintuitive higher

abundance of *E. huxleyi* relative to *Fragilariopsis* in the Fe-replete region DSG (given the results of chapter 3) was expected to be the result of succession following summer diatom blooms in the region.

4.3.3 **Controlled Fe addition grow out experiments**

Controlled grow-out experiments were then conducted at each sampling site to determine the effect of Fe addition on phytoplankton communities over two growing seasons; Fe-added samples (Fe) were compared with control samples (C) with no Fe addition. Bioassays which showed a large significant increase in F_v/F_m after 24- and 48-hours were determined to be Fe-limited (the earliest data available for JR161 DSG was 72 hrs). Only the summer USG and summer DSG bioassays experienced a significant increase in F_v/F_m in the Fe treatment relative to the C treatment (USG: 0.35 ±0.02 and 0.49 ±0.01, for the C and Fe treatments respectively; DSG: 0.55 ±0.006 and 0.58 ±0.02, for the C and Fe treatments respectively). These early positive responses to relief from Fe limitation indicate *in situ* Fe limitation, however the very small magnitude of the summer DSG response suggests that the summer USG bioassay is the only bioassay which is legitimately Fe-limited initially.

Microplankton and nannoplankton community responses, changes in biomass, macronutrient concentrations, and physiology between C and Fe samples were analyzed after 3-10 days, a period long enough to develop a significant change in phytoplankton community composition in response to iron manipulation. Differences in phytoplankton community composition between initial and final samples (Initial - C; Initial - Fe) were also investigated after the same period. Broadly, Fe addition caused an increase in phytoplankton biomass (as assessed by Chl-*a* concentration) and a drawdown of available macronutrients relative to control experiments in all bioassays in the summer and in the SOI in autumn (Figure 41i-y). However, in the SG bioassays in autumn, and in all bioassays in the spring, Fe addition had little effect on the biomass or macronutrient uptake in the experiments (Figure 41a-h, z-gg). Significant changes in F_v/F_m and σ_{PSII} for Fe bottles relative to C bottles occurred as follows: an increase in F_v/F_m alone in spring DSG, summer SOI, and autumn DSG; a decrease alone in σ_{PSII} in autumn USG; and an increase in F_v/F_m with a decrease in σ_{PSII} in summer USG, summer DSG, and autumn SOI.

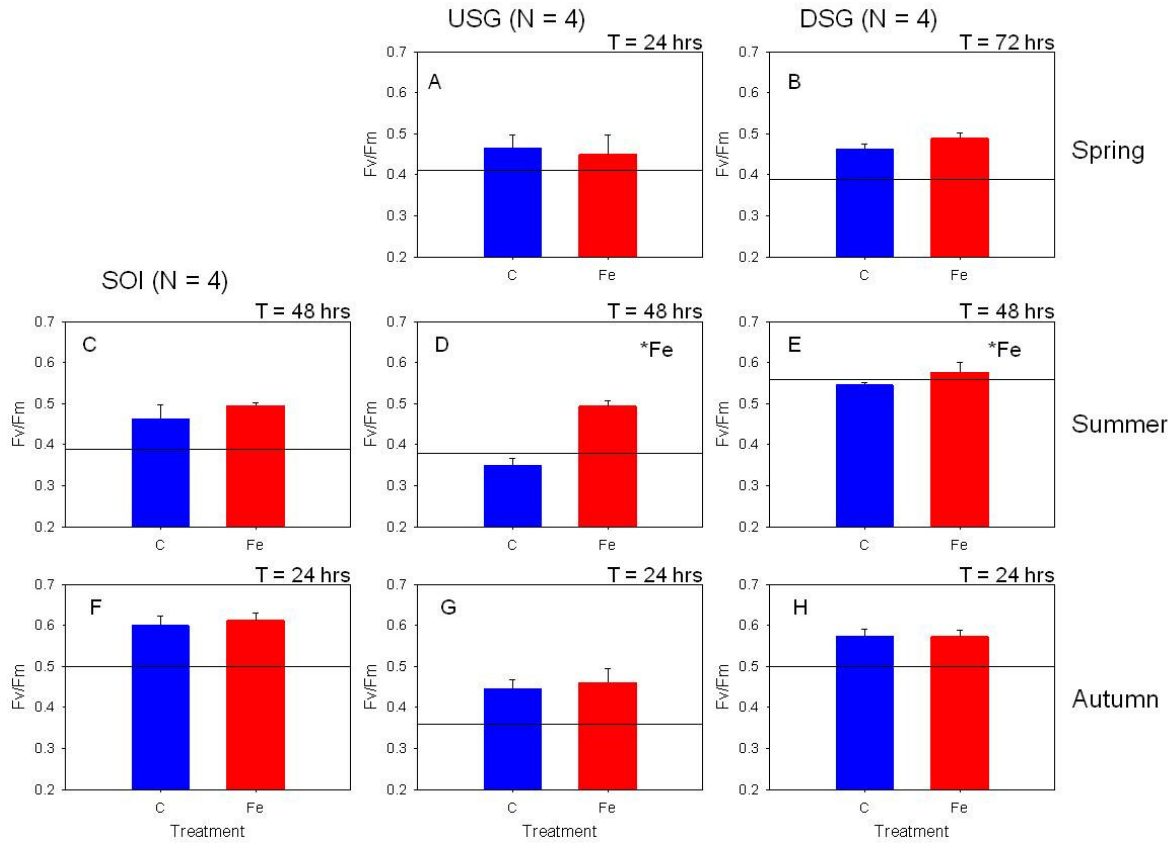

Figure 40a-h. Early responses in F_v/F_m for (a, b) spring, (c-e) summer, and (f-h) autumn. Fe-treated bottles are shown in red, and controls are shown in blue. Sampling time points are noted in the upper right corner of each graph. Initial values are indicated by the solid black reference line on each graph, and significant differences between Fe treatment groups are indicated by "*Fe". Error bars are based on the standard deviation for each replicate group.

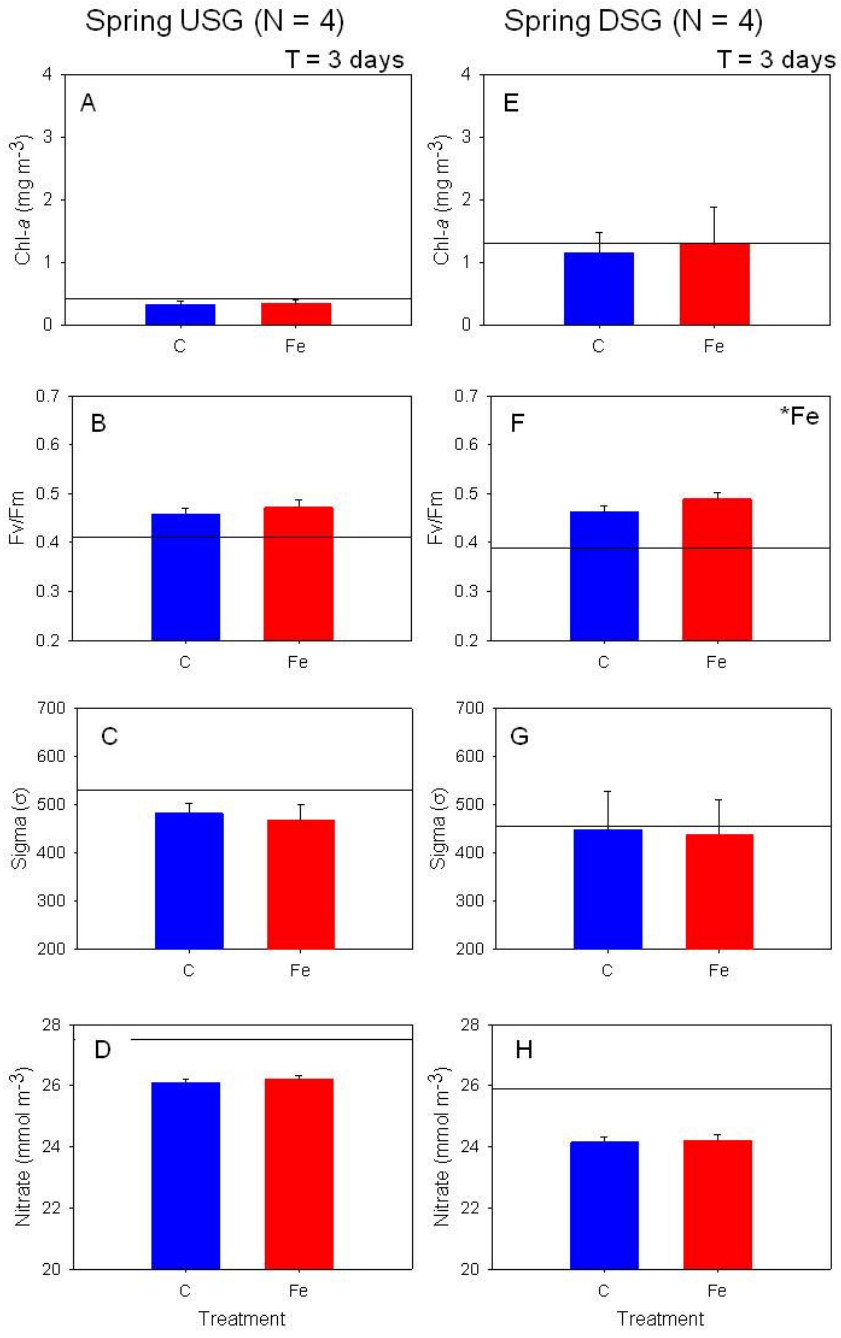

Figure 41a-h. Results from final sampling of spring bioassays.

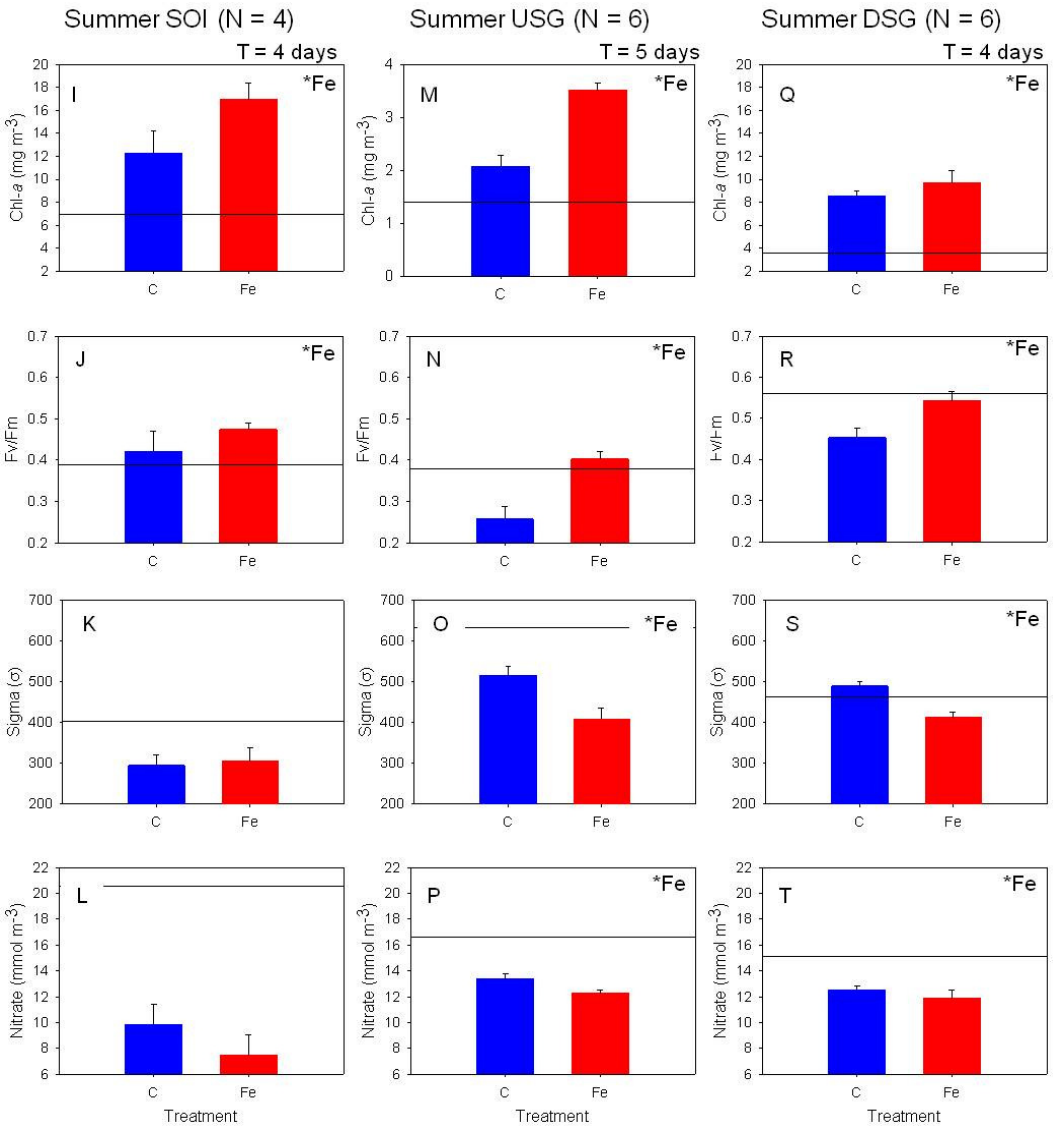

Figure 41i-t. Results from final sampling of summer bioassays.

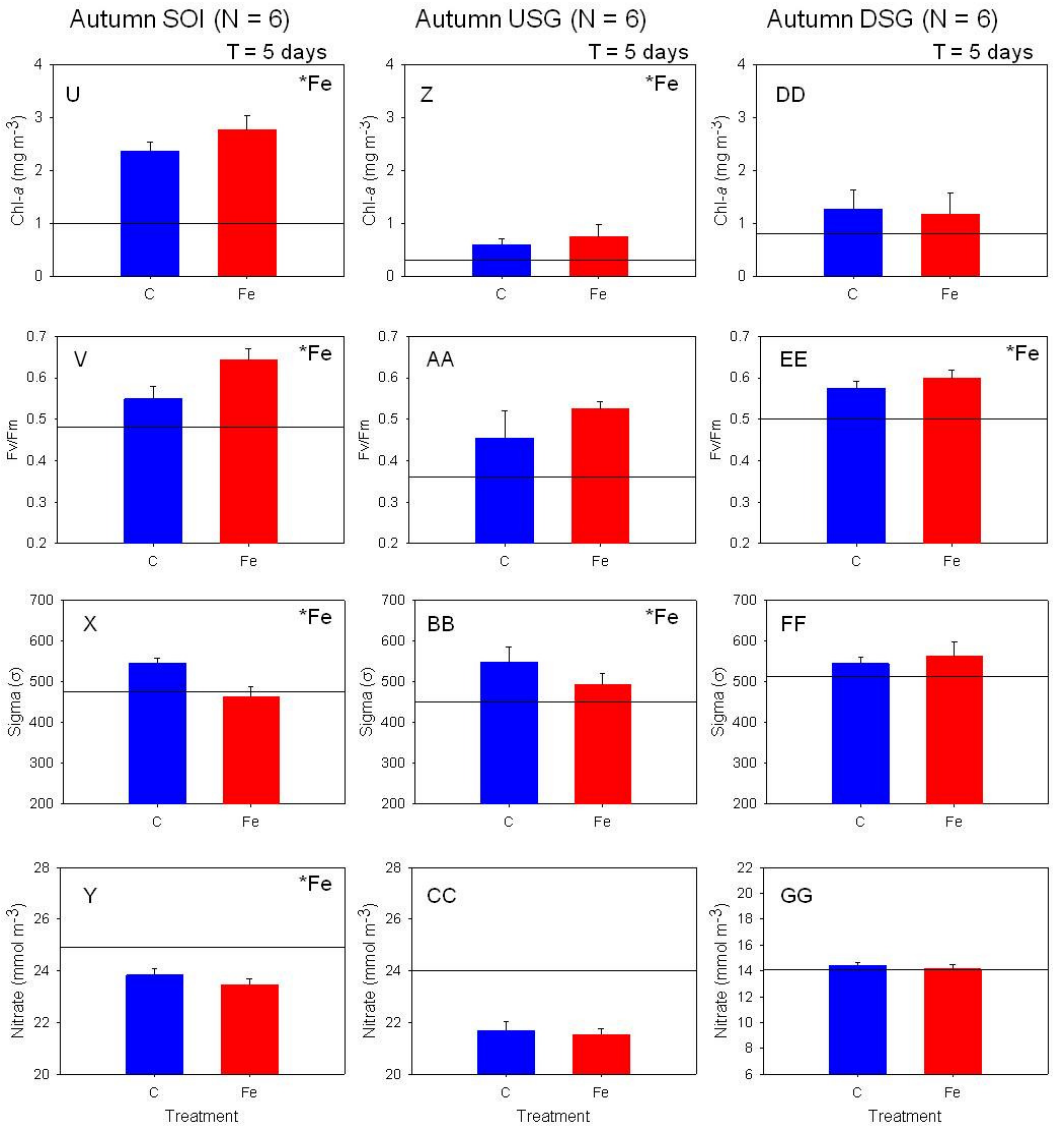

Figure 41a-gg. Measurements from final sampling of (a-h) spring, (i-t) summer, and (u-gg) autumn bioassays, including Chl-*a* concentration, F_v/F_m, σ_{PSII}, and nitrate concentration. Fe-treated bottles are shown in red, and controls are shown in blue. Initial values are indicated by the solid black reference line on each graph, and significant differences between Fe treatment groups are indicated by "*Fe". Sampling time points are noted in the upper right corner of each graph. Note scale changes for Chl-*a* and nitrate and differences in replicate numbers between short-running bioassays and long-running bioassays.

At these later time points (3-5 days) increases in F_v/F_m and decreases in σ_{PSII} are indicative of both a shift in the taxonomy of the phytoplankton community towards larger cell size ('taxonomic signature') and nutrient limitation (Fe or macronutrients as communities sealed in bottles may have rapidly depleted any nutrients originally in excess).

Graphical representations of physiology were again used to visualize trends in phytoplankton nutrient stress and taxonomy as bioassays progressed (Figure 42). Summer USG, the bioassay Fe-limited *in situ*, did not follow either of the 2 simple trends (section 4.3.1) after 48 hrs, suggesting that the steadily decreasing F_v/F_m and σ_{PSII} observed was due to a combination of nutrient and taxonomic signatures (Figure 42e). Bioassays in spring USG, summer SOI, autumn USG, and autumn DSG also failed to show simple trends in F_v/F_m and σ_{PSII}, providing further evidence of combined signatures after 48 hrs (Figure 42). Only C bottles in the summer DSG and autumn SOI bioassays showed the expected trend of decreasing F_v/F_m and increasing σ_{PSII}, while only Fe bottles in the autumn SOI bioassay showed the expected trend of increasing F_v/F_m and decreasing σ_{PSII} (Figure 42f, g).

According to a multivariate analysis of the microplankton community, Fe addition in spring and summer altered microplankton community structure significantly (ANOSIM test) in spring USG ($p<0.02$; 100 permutations) and in summer both USG ($p<0.02$; 100 permutations) and DSG ($p<0.04$; 100 permutations). Differences in individual species biomass occurred across all 3 bioassays (Figure 43) and were cumulatively responsible for the significant differences in community structure observed in the multivariate statistical analysis. Although significant in aggregate, only two of the individual species biomass changes were significant in isolation, both in summer USG. In this bioassay, two diatom species increased significantly in biomass with Fe addition, *Pseudonitzschia* spp. (M) (by 24 mg C m^{-3}; $p\leq0.002$) and *Cylindrotheca* spp. (S) (by 1.8 mg C m^{-3}; $p\leq0.0003$). Within the nannoplankton community in autumn, significant changes occurred in *E. huxleyi* abundance both USG (80 cells ml^{-1} and 91 cells ml^{-1} in C and Fe bottles, respectively; $p\leq0.04$) and DSG (44 cells ml^{-1} and 113 cells ml^{-1} in C and Fe bottles, respectively; $p\leq0.01$) (Figure 44).

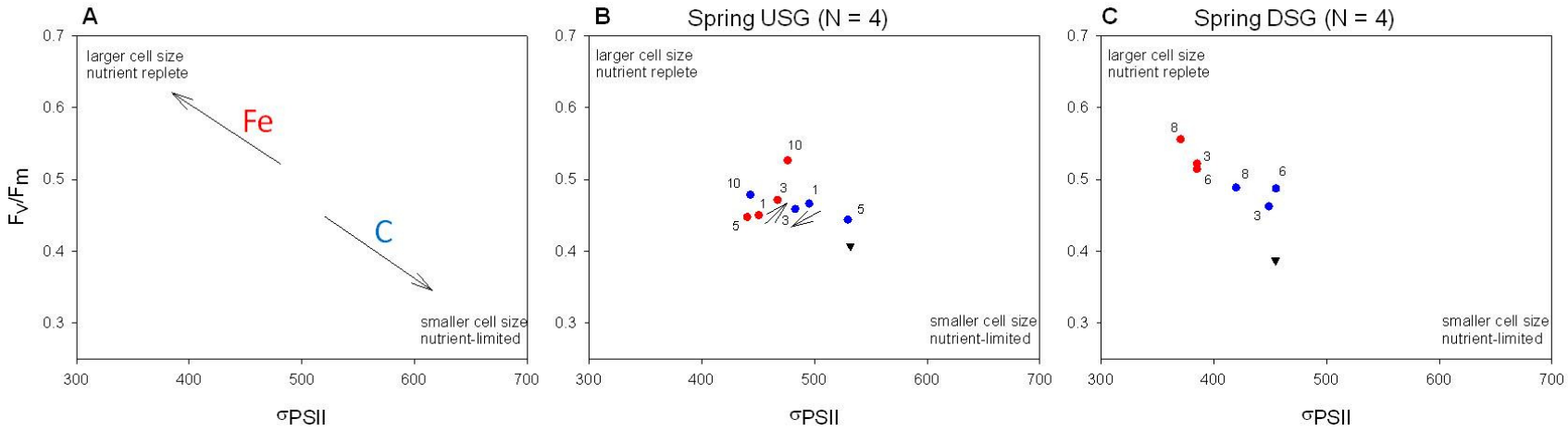

Figure 42a-c. Physiological changes (a) expected for bioassay experiments and (b, c) occurring in bioassay experiments at all sampling points for spring bioassays.

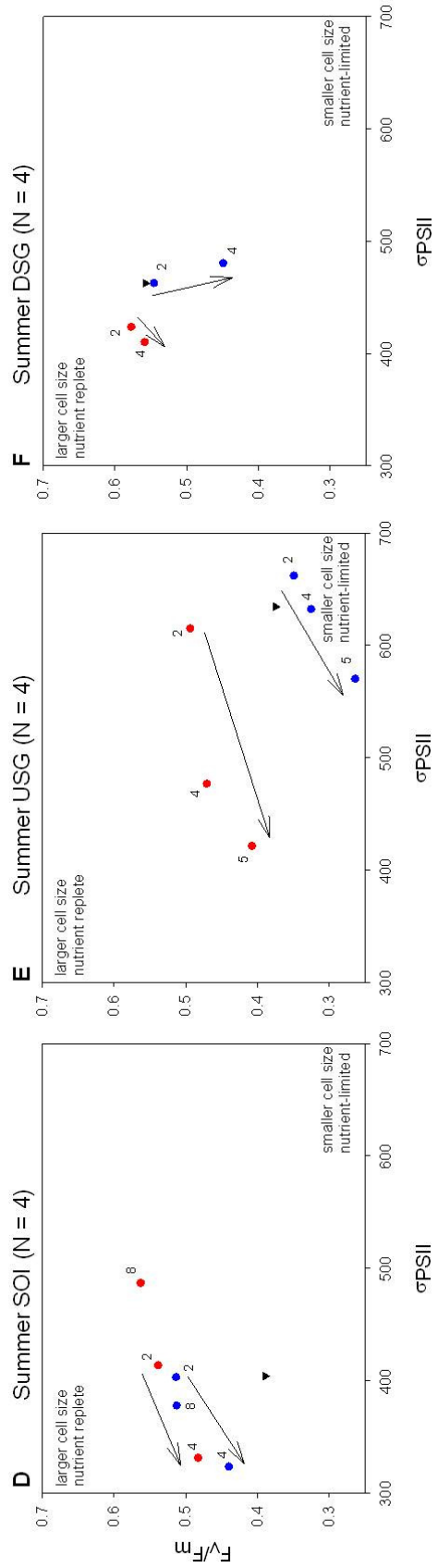

Figure 42d-f. Physiological changes for bioassay experiments at all sampling points for summer bioassays.

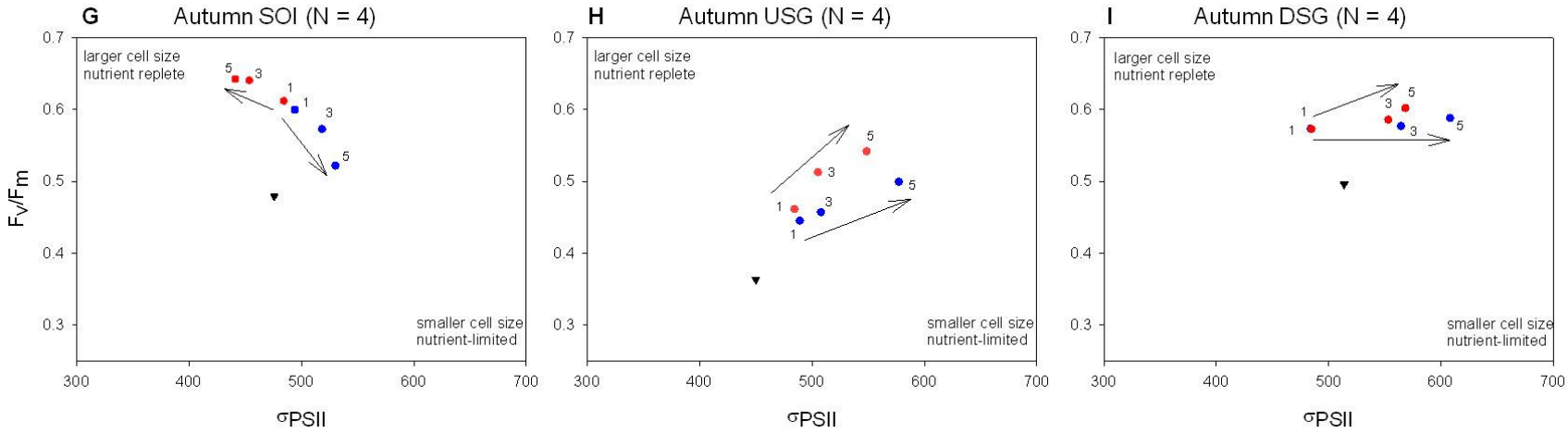

Figure 42a-i. Physiological changes (a) expected for bioassay experiments based on Suggett et al. (2009) and (b-i) occurring in bioassay experiments at all sampling points for (b, c) spring, (d-f) summer, and (g-i) autumn bioassays, showing early and late responses. Average values for each day shown for Fe-treated bottles with red circles, and controls with blue circles. Initial values are indicated by the black triangles and each bioassay data point is labelled with sampling day. Arrows indicate the trend of the data points over the period between the early sub-sampling (24- to 48-hrs; no data this early for spring DSG) and the final sub-sampling (3-5 day; same final day as that used in Figure 41; long-running bioassay data points after this cut-off were not used for the trend line; section 4.2.2). Trends found in previous FRRf observations and experiments (Suggett et al., 2009) were added on to the plots for reference.

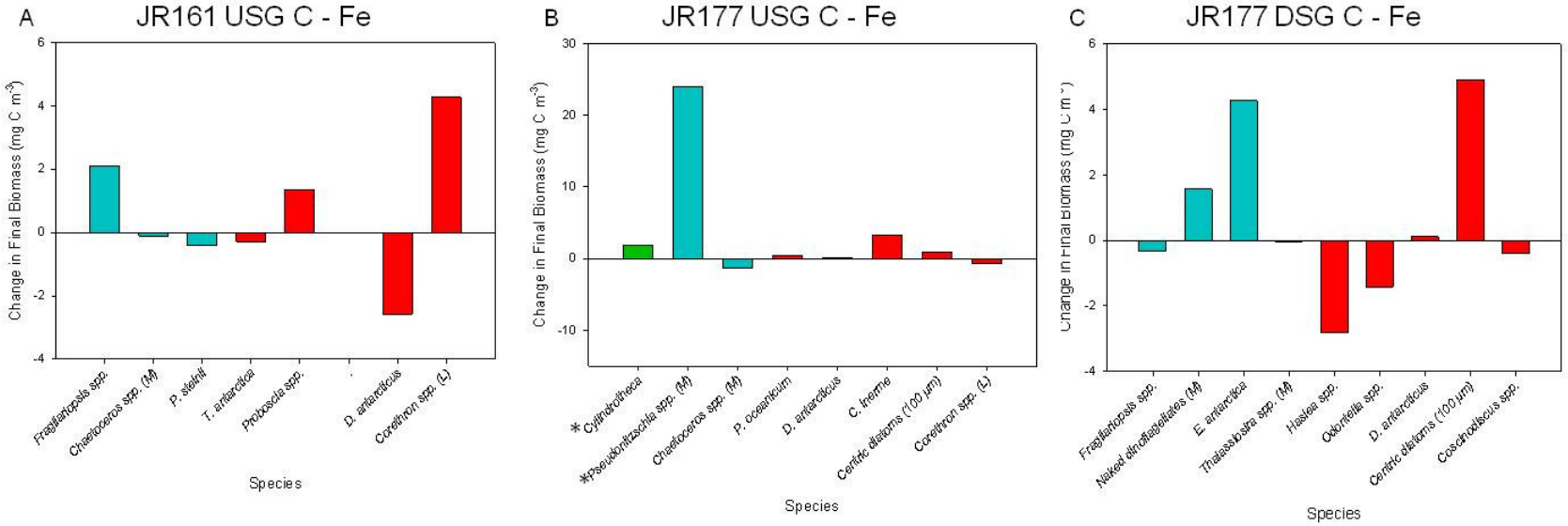

Figure 43a-c. Changes in biomass for the microplankton species with the highest changes in biomass between iron treatment groups in bioassay experiments (cumulatively responsible for 50% of dissimilarity between the groups), for (a) spring USG, (B) summer USG, and (3) summer DSG. Changes in biomass are calculated as Fe group minus C group. Species are ordered from smallest to largest, with 'small' species <100 pg C cell^{-1} in green, 'medium' species 100-1000 pg C cell^{-1} in blue, and 'large' species >1000 pg C cell^{-1} in red. Significant differences between group averages are marked with an asterisk "*".

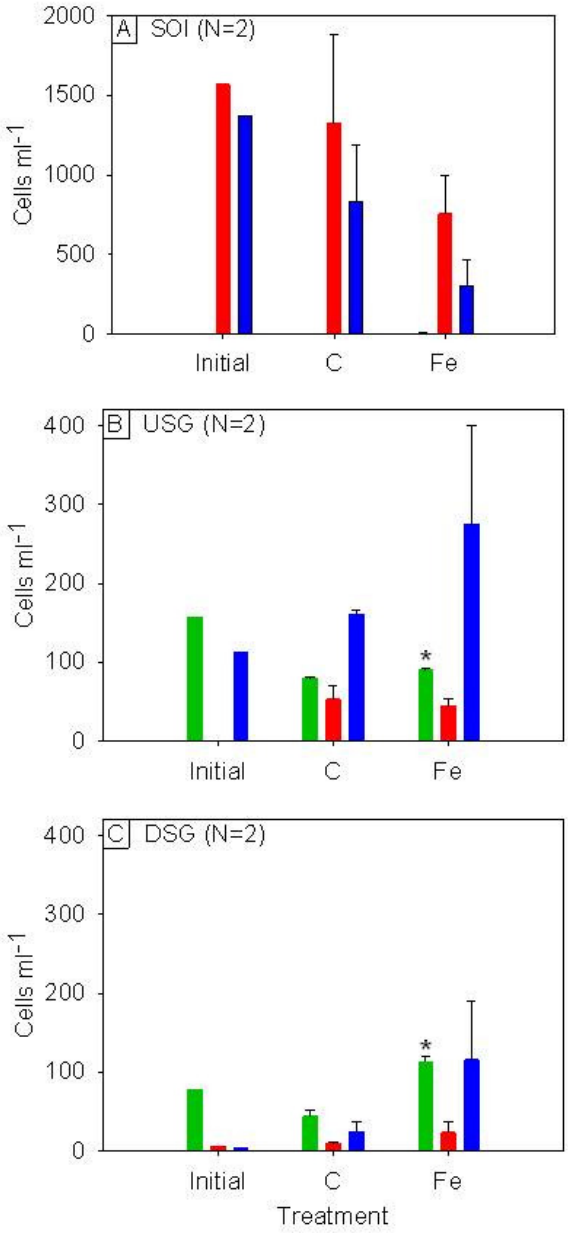

Figure 44a-c. Autumn cell counts for initial, C, and Fe treatments from (a) the SOI bioassay, (b) USG, and (c) DSG, showing *E. huxleyi* (green), *Tetraparma* spp. (red), and *Fragilariopsis* spp. (blue) abundances. Significant differences between treatment groups are marked with an asterisk "*". Error bars are based on the standard deviation for each replicate group. Note the scale change between (a) and (b)/(c).

Comparison of initial and final bioassay community structure

A more general comparison was then made between initial samples and final samples taken from the bottles after Fe manipulation at all of the sample sites, to investigate the similarity in community structure between initial samples and final

bioassay samples. In all but one case, initial Lugols bioassay samples could be classified into groups significantly different from the final Lugols samples for the same bioassay (SIMPROF test in the CLUSTER analysis) (Figure 45). ANOSIM tests used to define the significance of the factors identified through differentiation in CLUSTER groups confirmed significant differences between initial and final phytoplankton communities in 4 of the 5 bioassays with Lugols samples ($p \leq 0.05$), but not for the spring bioassay DSG, which was therefore dropped from statistical analysis of individual species. Species that significantly increased in biomass ($p \leq 0.05$ in Student's *t*-test) in both control and Fe addition bottle incubations included: *Pseudonitzschia* spp. (M) (Spring USG; Summer USG; Summer DSG); centric diatoms (30-60 µm; M) and *Haslea* spp. (L) (Spring USG); *Fragilariopsis* spp. (M), *Corethron* spp. (L), and *Cryptophyte* spp. (S) (Summer SOI); and *Melosira* spp. (S), *Odontella* spp. (L), and *Proboscia* spp. (L) (Summer DSG). The species that significantly increased in biomass ($p \leq 0.05$ in Student's *t*-test) in Fe bottles included: *Fragilariopsis* spp. (M) and *Corethron* spp. (L) (Spring USG); *Pseudonitzschia* spp. (M), *C. inerme* (L), and *Pseudonitzschia* spp. (S) (Summer USG); and *E. antarctica* (M) (Summer DSG). The species that significantly increased in biomass ($p \leq 0.05$ in Student's *t*-test) in C bottles included: *C. neglectus* (S) (Spring USG) and *Chaetoceros* spp. (M) (Summer USG) (Figure 46).

Bioassay initial and final Lugols samples, however, were more similar to each other than they were to initial or final Lugols samples from other bioassays, i.e., communities differed significantly between the start and finish of a bioassay, but they formed a single community when compared with other bioassays. At the bioassay level, therefore, relationships between final samples were the same as those for initial samples (section 4.3.2). Initial SEM samples differed from final SEM samples in only one of the three autumn bioassays ($p \leq 0.05$), USG, where *E. huxleyi* numbers dropped sharply following bottle incubation (by 77 cells ml^{-1} and 66 cells ml^{-1} in C and Fe bottles, respectively; Figure 44b).

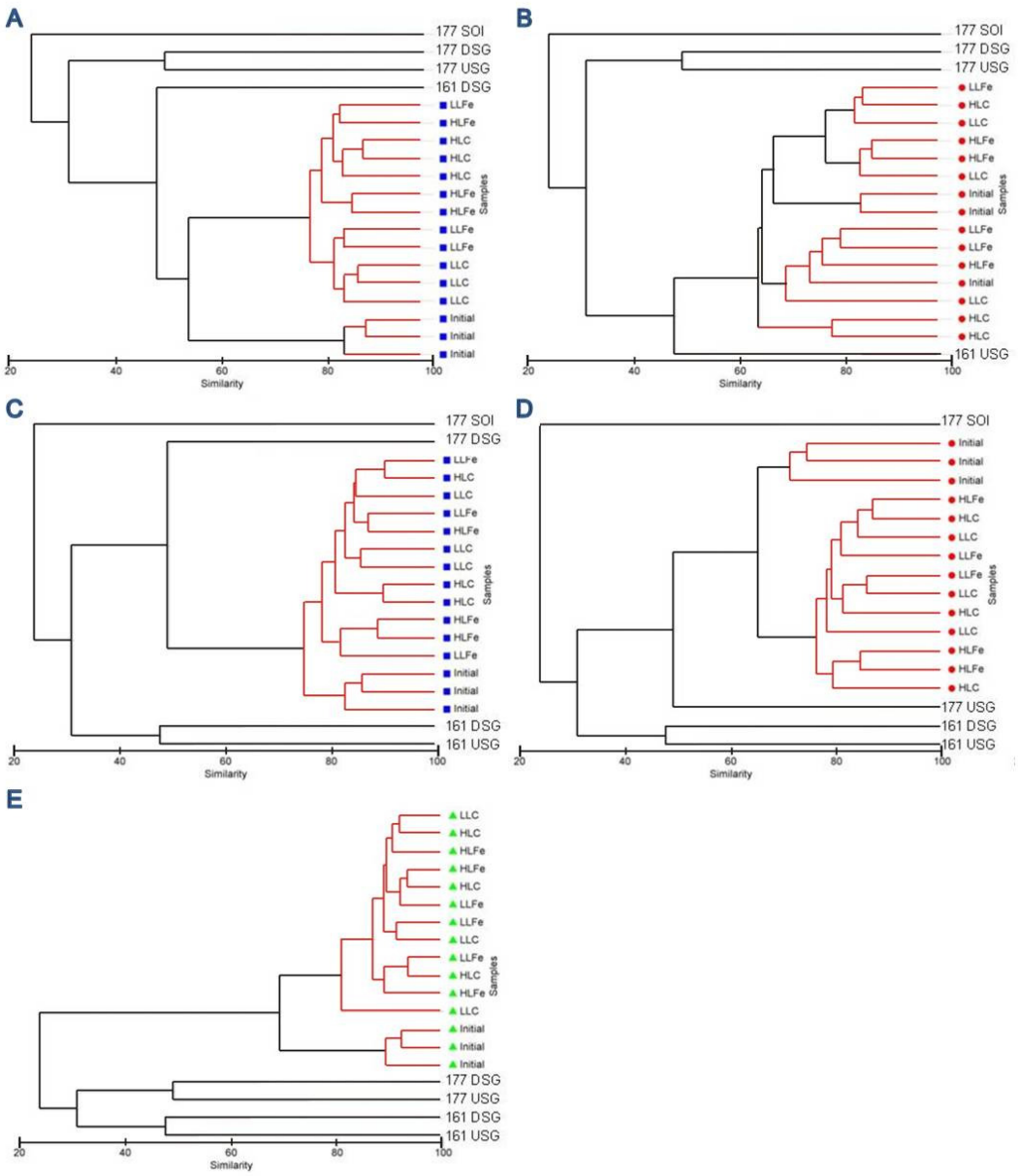

Figure 45a-e. CLUSTER diagrams based on Figure 39, with bioassay data expanded to show microplankton community relationships within bioassay treatments, for (a) spring USG, (b) spring DSG, (c) summer USG, (d) summer DSG, and (e) summer SOI. USG samples are represented by blue squares, DSG samples by red circles, and SOI samples by green triangles. All spring and summer samples are labelled by their respective cruise numbers 161 and 177. All four experimental conditions (HLC, HLFe, LLC, LLFe) are presented to allow correct interpretation of the groupings, and significant branches are shown in black (SIMPROF test). See methods for how the 4 experimental groups were combined to form 2 groups in subsequent analyses (section 4.2.3).

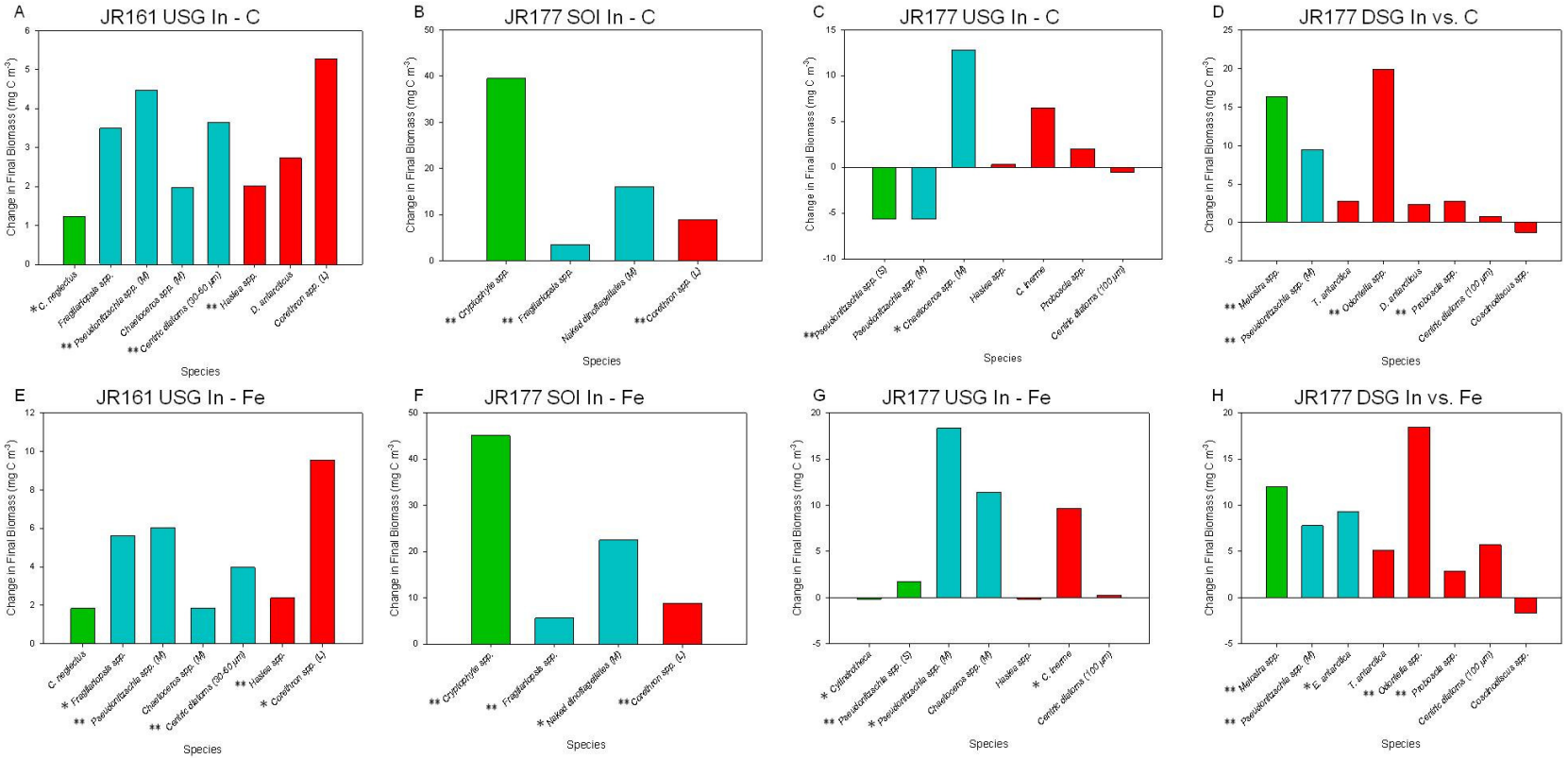

Figure 46a-h. Changes in biomass for the microplankton species with the highest changes in biomass between initials and finals in bioassay experiments (cumulatively responsible for 50% of dissimilarity between the groups), broken down into: (a-d) initials and the C bottles and (e-h) initials and the Fe bottles. Changes in biomass are calculated as finals minus initials. Species are ordered from smallest to largest, with 'small' species <100 pg C cell^{-1} in green, 'medium' species 100-1000 pg C cell^{-1} in blue, and 'large' species >1000 pg C cell^{-1} in red. Significant differences between group averages are marked with an asterisk "*" if they occur in either C or Fe groups, and with two "" if they occur in both C and Fe groups.**

4.4 Discussion

4.4.1 Regional differences in the Scotia Sea

Over three successive phases of the growing season, bioassays were initiated in three contrasting regions of the Scotia Sea. The three regions considered, (1) DSG, (2) USG, and (3) the SOI, differed in terms of biomass, physiological stress, and micronutrient concentrations; Chl-*a* was consistently higher DSG relative to USG in all seasons, F_v/F_m was higher DSG relative to USG in summer and autumn, and dFe was consistently higher DSG relative to USG in spring and summer (Figure 37; Table 23). Off the SOI both Chl-*a* and dFe were high and similar to DSG in summer, while in autumn both variables decreased considerably and were well below DSG levels. Combined with the observations of lower nitrate, silicate, and dFe concentrations within each site in summer relative to spring, these findings were consistent with the conclusions of Korb et al. (2010) of seasonal Fe limitation USG (Fe limitation in summer, but not spring), which prevents large, sustained phytoplankton blooms, and a continuous source of Fe DSG capable of supporting high biomass over many months. In the autumn, some recycling of nutrients USG appeared to occur; however, biomass remained low compared with DSG. Additionally the results support the categorization of the SOI as an Fe-fertilized region in summer.

The complications presented by regional and seasonal trends in macronutrient availability and ecological pressures prevented a clear resolution, however, of the effects of natural Fe limitation on phytoplankton community structure. Observational studies in the Scotia Sea based on *in situ* comparisons of Fe-limited regions (such as USG) and Fe-fertilized regions (such as DSG), therefore, were not sufficient to determine specifically Fe effects on phytoplankton species responses, necessitating artificial Fe addition experiments to aid in interpretation of phytoplankton community results and validating the need to confirm the observational conclusion of Fe-limited nannoplankton in chapter 3 with controlled experiments.

4.4.2 Fe effects on phytoplankton species ecology

The bioassay USG in summer was identified as the only bioassay Fe-limited *in situ* using significant 24- and 48-hour physiology changes of reasonable magnitude (section 4.3.3), supporting the suggestion of M. Nielsdóttir (pers. comm.) that a natural

source of Fe exists across the Scotia Sea in spring and in the DSG and SOI regions in summer. Significant physiological changes in spring DSG, summer SOI, summer DSG, autumn SOI, autumn USG, and autumn DSG bioassays may the result of taxonomic shifts, Fe limitation (in C bottles) once the link to a continuous source of Fe was removed, or a combination of the two.

The spring USG, summer USG, and summer DSG bioassays exhibited significant differences in microplankton community structure between Fe and C conditions at the community level (Figure 43). Biomass increased in all three bioassays in a number of microplankton species. Although not all of the species changes were significant, they cumulatively equated to a difference in community structure between Fe treatment groups. The occurrence of significant community level shifts without significant species changes is not unexpected given that the multivariate community analysis is based on even small changes across the entire array of microplankton species analyzed. The community shifts occurred as increases in medium and large diatoms, a result consistent with previous results from Fe addition experiments and observational studies of Fe-fertilized regions (section 3.1). Significant species responses occurred in summer USG only, where *Cylindrotheca* spp. (a small diatom) and *Pseudonitzschia* spp. (M) biomass increased significantly in Fe-treated bottles (Figure 43b). Importantly, this was also the only bioassay determined to be Fe-limited *in situ*, suggesting that the increase in *Cylindrotheca* spp. and *Pseudonitzschia* spp. (M) biomass with Fe addition was due to relief from *in situ* Fe limitation. *Pseudonitzschia* spp. also responded to Fe addition in bioassays carried out in the Kerguelen Islands region of the Southern Ocean (Moore et al., 2007a), however, in those bioassays the responding *Pseudonitzschia* spp. were small (<100 pg C cell^{-1}), while in these bioassays they were medium in size (100-1000 pg C cell^{-1}). Generally the microplankton response, therefore, was characterized by a taxonomic shift to medium and large diatoms, however, the significant response of one small diatom demonstrates that small phytoplankton do in some cases manifest an Fe response when relieved from Fe limitation *in situ*, contrary to expectations (hypothesis 4).

The nannoplankton bioassay results are less representative of a natural Fe fertilization event because none of the autumn bioassays were found to be initially Fe-limited (Figure 40), however, all 3 of the bioassays showed significant changes in F_v/F_m or σ_{PSII} indicative of Fe limitation or taxonomic shifts in Fe bottles. An effect of Fe addition was not apparent for the siliceous taxa, which showed no significant changes in

biomass in Fe bottles as expected (hypothesis 4), and suggesting that complicating regional or seasonal trends were responsible for the Fe effect observed on siliceous phytoplankton in chapter 3 (section 3.4.1). *E. huxleyi*, however, did increase in biomass in Fe bottles (section 4.3.3; Figure 44). An *E. huxleyi* Fe response has been observed previously in the North Atlantic (Nielsdóttir et al., 2009), however the observational evidence from chapter 3 did not suggest that Southern Ocean *E. huxleyi* populations would respond to Fe (section 3.4.1).

Another effect, unrelated to treatment type was apparent in the microplankton bioassays, and may have been responsible for unexpected responses of small diatoms and *E. huxleyi* to Fe addition; the effect of initial phytoplankton community composition, which has been found previously in the Southern Ocean (Moore et al., 2007a) as well as in the Gulf of Alaska (Martin et al., 1989). Species responses to Fe addition in the three bioassays with significant community changes involved different species in each case; only three species, *Corethron* spp., *Chaetoceros* spp., and centric diatoms (100 µm), appeared in the top 50% of discriminating species between treatment groups for two bioassays, and only one species, *D. antarcticus*, appeared for all three bioassays (Figure 43). The most likely reason for the lack of homogeneity in species responding across regions was the significant differences in initial phytoplankton community composition between the bioassays (section 4.3.1). For example, high Fe species from DSG including *E. antarctica* and large centric diatoms, which responded in the DSG bioassay (non-significantly) and have been shown in previous experiments to proliferate in high Fe environments, may not have been sufficiently present USG in the Fe-limited summer bioassay, and thus a response was not recorded.

4.4.3 **Bottle effects**

The variability in species responses between bioassays may also be due to bottle effects, such as further nutrient limitation (section 4.3.3) or high grazing pressures. *In situ*, a complicated set of environmental and ecological factors appeared to determine the phytoplankton community (section 4.3.2) and removal from this dynamic environment could strongly affect the phytoplankton community in bottle incubations. All but one of the spring and summer bioassays and one autumn bioassay showed significant differences between final samples and initial samples (Figure 46), suggesting that some species present *in situ* grew well in both C and Fe bottles. Again, the individual species responses differed between bioassays, with a number of species

appearing to favour conditions within bioassays relative to *in situ*. One species, however, demonstrated a particularly strong bottle response; *Pseudonitzschia* spp. (M) increased in biomass in three of the four bioassays and in both C and Fe groups (Figure 46a, d-e, g-h). The recent discovery of an Fe storage protein, ferritin (Marchetti et al., 2009), in several species of the genus *Pseudonitzschia* offers a potential explanation of the group's success in bioassays (sections 4.4.2 and 4.4.3). According to Marchetti et al. (2009), ferritin serves in the short-term as an agent to reduce oxidative stress and its transcription increases after a 'pulse of iron,' while in the long-term it serves an Fe storage role, allowing acclimation to low Fe environments. This Fe-storage mechanism revises the expectations of how low dFe concentrations will affect this diatom species and suggests that unknown physiological abilities may affect the biogeography of Southern Ocean phytoplankton in unpredicted ways.

4.4.4 Conclusions

To the author's knowledge, this is the first study of both microplankton and mineralizing nannoplankton responses to Fe addition in the Scotia Sea using on-deck bioassay incubations. The major findings of this work were that regional and seasonal trends prevented observational studies from separating the effects of dFe concentrations out from other environmental factors (as expected given the significant covariances between environmental variables observed in chapter 3), the expected response of medium and large diatoms generally to Fe addition, the unexpected response of *Cylindrotheca* (a small diatom) and *E. huxleyi* to Fe addition, and the high success of medium *Pseudonitzschia* in bioassays.

The implications of these findings are that in some cases phytoplankton with small cell sizes do respond to Fe addition, despite the low Fe requirements expected as a result of their cell size. The questions raised by these results are whether dFe affects *E. huxleyi* distributions in the Southern Ocean *in situ*, and whether these Fe effects are obscured by the physical effects of frontal boundaries and the biological effects of competition with siliceous nannoplankton, (as observed in chapter 3), which are likely to be substantially larger, and whether low-Fe adapted diatoms in the Southern Ocean, such as *Pseudonitzschia*, crowd the low-nutrient, K-selected niche that *E. huxleyi* are expected to exploit in the region, adding a further biological factor to consider in studies of the ecology of *E. huxleyi* in the Southern Ocean.

5 Synthesis and future work

5.1 Synthesis

The field and laboratory research reported in this thesis, undertaken with the aim of expanding biologists' understanding of ecological processes for the model coccolithophorid *Emiliania huxleyi* (section 1.3), has contributed substantially to the knowledge of *E. huxleyi's* fine-scale population genetic diversity in a Norwegian model bloom system, and its broad-scale biogeography in the natural case study of the Southern Ocean. The genetic variability and population differentiation observed between *E. huxleyi* isolates within a single summer bloom, the association of Southern Ocean *E. huxleyi*-dominated nannoplankton communities with lower nutrient concentrations (particularly silicate), the occurrence of *E. huxleyi* blooms in three regions of the Scotia Sea, and the potential response of Southern Ocean *E. huxleyi* to higher iron (Fe) inputs all demonstrate the opportunistic nature of this ubiquitous coccolithophore in the context of the larger phytoplankton community. The thesis research further highlights the importance of *E. huxleyi* and other mineralizing nannoplankton taxa in the rapidly changing Southern Ocean, where biomass estimates were on par with larger phytoplankton groups and blooms of all 3 taxa studied occurred.

In population genetic studies, using a newly-applied flow cytometry single-cell sorting method capable of isolating large numbers of single *E. huxleyi* cells with low mortality (section 2.3.3), it appeared that a genetically diverse background population of *E. huxleyi* reproduced rapidly and asexually, with diversity maintained most likely through culling of faster-growing *E. huxleyi* clones by *E. huxleyi*-specific virus (EhV) (section 2.4.1). Following the rapid proliferation of viruses, *E. huxleyi* numbers were reduced to pre-bloom concentrations, and a new background population of *E. huxleyi* was produced, genetically distinct from the pre-bloom background population, yet similar to it in overall genetic diversity (as indicated by the average gene diversity H_E that did not vary significantly between bloom stages; sections 2.3.4 and 2.3.5). *E. huxleyi* population differentiation under conditions of viral attack suggests that the species' high genetic variability may be related to the presence of more rare resistant strains, while the low frequency of resampling and the large uncertainty in clonal richness suggest that the genetic diversity found are only lower estimates of the potential diversity within an *E. huxleyi* bloom. This large genetic adaptive potential

appears to be maintained year after year and even within a single bloom, and implies that different *E. huxleyi* clones may respond differently to future climate changes.

The distribution of nannoplankton including *E. huxleyi* in the rapidly changing Southern Ocean has traditionally been overlooked due to sampling protocols, however, *in situ* evidence of high-latitude *E. huxleyi* blooms in 3 regions of the Scotia Sea (up to 23% of total phytoplankton biomass; chapter 3), and the substantial biomass of *Tetraparma* spp. in austral autumn, and of small *Fragilariopsis* spp. (<20 µm) in both austral summer and autumn (of up to 36% of total phytoplankton biomass; chapter 3), argue for their inclusion in estimates of current and future productivity, and suggest that studies including only estimates of microplankton biomass underestimate Southern Ocean productivity, as previously suggested by (Komuro et al., 2005). Particularly for mineralizing nannoplankton, which are capable of efficiently exporting biomass from the surface ocean to depth through the formation of aggregates with their calcareous and siliceous skeletons (Passow, 2002; De La Rocha and Passow, 2007), this underestimation of productivity may also be a significant underestimation of export in the Southern Ocean.

High *E. huxleyi* cell numbers and high coccolith to cell ratios (section 3.3.2) off the Falkland Island shelf and South Georgia Island coincide well with predicted bloom in the Scotia Sea from satellite images. Overall *E. huxleyi* distributions were correlated to a range of environmental variables, including frontal boundaries, lower macronutrient concentrations relative to siliceous nannoplankton, and lower dFe concentrations relative to siliceous nannoplankton. The inverse relationship between *E. huxleyi* biogeography and more favourable nutrient regimes supported the conclusions that, even within the nannoplankton size fraction, *E. huxleyi* abundances are in part determined by the biogeography of siliceous taxa, and that *E. huxleyi* is better-adapted to low nutrient conditions than other nannoplankton species within the size class. While the first outcome suggests that competition even in low nutrient regions is fierce in the small size range, the second outcome suggests that the increase in stratified, low nutrient regions expected to occur with increased SST in the future, are favourable environments for the proliferation of *E. huxleyi*. No significant relationship was found between *E. huxleyi* biogeography and pCO_2, suggesting that ocean acidification may not be as strong a driver for the distribution of this particular calcareous species in future climate scenarios.

In bioassay experiments, *E. huxleyi* increased in biomass in a single bioassay, complicating the simplistic view of *E. huxleyi* restriction to low Fe regions. Medium *Pseudonitzschia* spp. also increased in biomass in one bioassay (most likely due to a capacity for Fe storage), further complicating the idea that medium and large diatoms are succeeded by nannoplankton in low dFe regions. While these deviations from expectations are interesting, they are species-specific responses. Rather than altering the general expectation of succession to *E. huxleyi* in low dFe regions, they serve to reiterate the plasticity of various phytoplankton taxa, including *E. huxleyi*, to changing environments.

The conclusions of high adaptability to low nutrients, proliferation when diatom competition is relieved, and significant biomass in sensitive regions drawn from the thesis research suggests that *E. huxleyi* will continue to be a major model phytoplankton species in the warmer, more stratified, and more acidic future ocean. Given the high molecular diversity of the species, these climate change effects have the potential to select for different *E. huxleyi* strains which are more competitive in high pCO_2 oceans.

5.2 Future Work

The major challenge of this work has been relating the *potential* for 'adaptability' expected given the maintenance of high genetic diversity through *E. huxleyi* blooms (chapter 2), and the *observed* 'adaptability' found *in situ* (chapter 3) and in bioassay experiments (chapter 4) carried out in the Southern Ocean. The molecular findings of high diversity in chapter 2 support the 'adaptability' observed in chapter 3 and experimentally tested in chapter 4 and suggest that while future climate scenarios may select for different strains of *E. huxleyi*, they are unlikely to discriminate against the species as a whole; however, this relationship has not been directly tested. Further work should therefore focus on functional experiments, particularly of viral resistance, interspecific competition, and nutrient ranges, which would conclusively demonstrate whether the observed genetic diversity and population differentiation translate into physiological adaptive potential relevant for future climate scenarios. The extension of genetic and functional studies to *E. huxleyi* morphotypes from different geographic locations including the Southern Ocean would maximize the applicability of the studies to *E. huxleyi* populations found in a wide range of environments and subject to a wide range of biological and environmental factors. Another limitation of the genetic work in this research were the sample sizes available. Although 143 *E. huxleyi* strains were

analyzed, sampling was not sufficient to fully represent the *in situ* population. A repeat of the mesocosm experiment with the capacity to sort and culture a larger number of isolates would strengthen the population genetic analyses. The characterization of genetic diversity for blooms of a range of *E. huxleyi* morphotypes would further strengthen the application of the genetic analyses results to the species as a whole.

Relating genetic diversity and functional diversity with functional experiments must also take into account flexibility within a strain, i.e. phenotypic plasticity, which may also have a strong effect on the role of phytoplankton in biogeochemical cycling in the present and future ocean. The correlations between environmental variables and nannoplankton biogeography would benefit from experiments testing the physiological responses and range of the various nannoplankton taxa. The Fe addition bioassays employed in chapter 4 were carried out along these lines, and experimentation should be expanded to include macronutrients. The bioassays in chapter 4 were limited by both a low number of replicates for the nannoplankton community and the existence of bottle effects. More replicates are available and could be analyzed at some point in the future.

Finally, the importance of the nannoplankton size fraction suggests that future studies of the Southern Ocean should include estimates of nannoplankton production and export. Longer time-series data are also necessary to determine whether nannoplankton populations are responding to changes in temperature and pCO_2 contingent with climate change. In summary, there is a great deal still to learn about *E. huxleyi* and Southern Ocean nannoplankton ecology, however, the promising results in terms of genetic diversity, population differentiation, biogeographic range, and biomass reveal a complicated interplay of ecological, physical, and biological factors well worth exploring further.

,

Appendix Figures

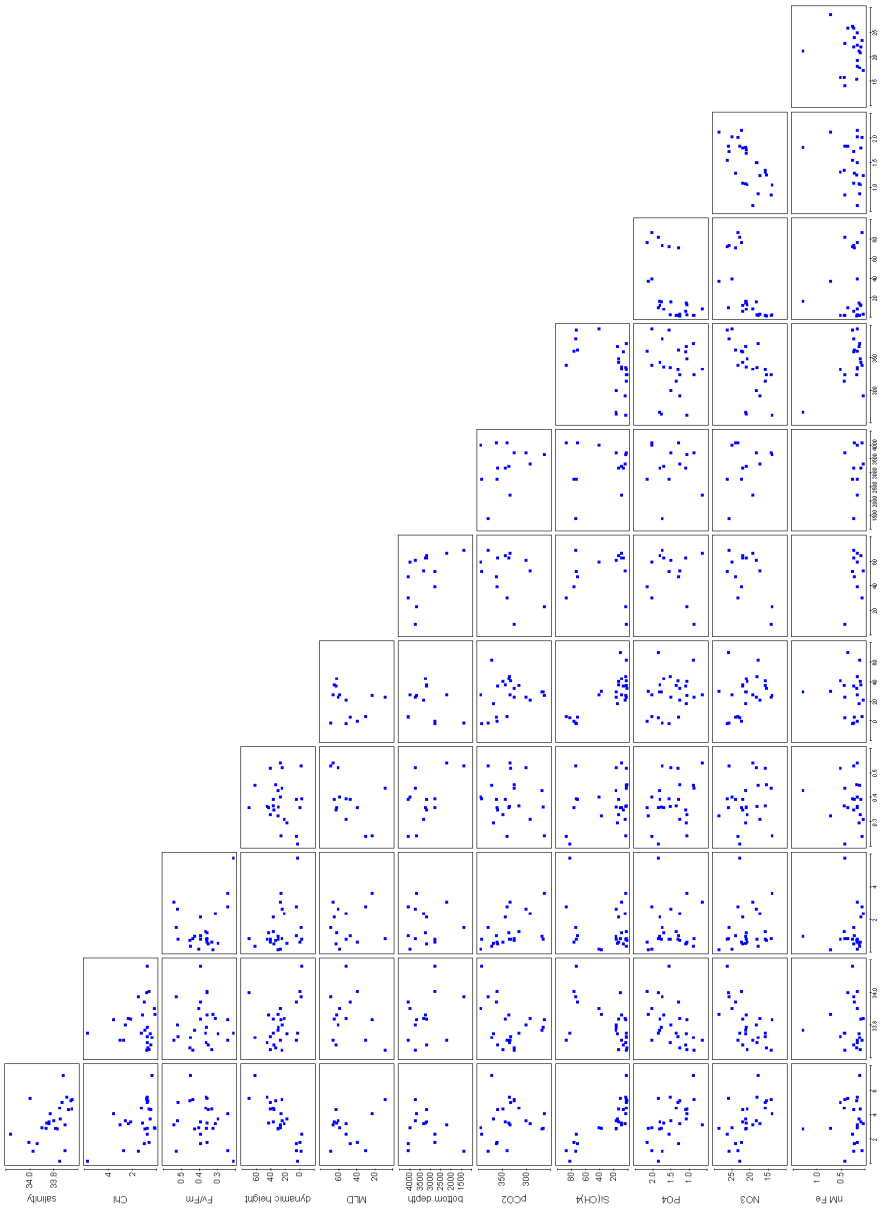

Appendix Figure 1. Draftsman's plot of all environmental variables used to judge appropriate transformations for individual variables. Scatter should appear distributed across the range of values. If 'skew' was observed variables were transformed (Table 17).

List of References

Alderkamp, A.-C., de Baar, H.J.W., Visser, R.J.W., and Arrigo, K.R., 2010. Can photoinhibition control phytoplankton abundance in deeply mixed water columns of the Southern Ocean? Limnology and Oceanography 55 (3), 1248-1264.

Andersen, R.A., 2004. Biology and systematics of heterokont and haptophyte algae. Am. J. Bot. 91 (10), 1508-1522.

Armstrong, R.A., Lee, C., Hedges, J.I., Honjo, S., and Wakeham, S.G., 2001. A new, mechanistic model for organic carbon fluxes in the ocean based on the quantitative association of POC with ballast minerals. Deep Sea Research Part II: Topical Studies in Oceanography 49 (1-3), 219-236.

Balch, W.M., 2004. Re-evaluation of the physiological ecology of coccolithophores, in: H.R. Thierstein and J.R. Young (Eds.), Coccolithophores: from molecular processes to global impact. Springer Berlin Heidelberg, New York. pp. 165-190.

Barnola, J.M., Raynaud, D., Korotkevich, Y.S., and Lorius, C., 1987. Vostok ice core provides 160,000-year record of atmospheric CO2. Nature 329 (6138), 408-414.

Behrenfeld, M.J., O/'Malley, R.T., Siegel, D.A., McClain, C.R., Sarmiento, J.L., Feldman, G.C., Milligan, A.J., Falkowski, P.G., Letelier, R.M., and Boss, E.S., 2006. Climate-driven trends in contemporary ocean productivity. Nature 444 (7120), 752-755.

Belkhir, K., Borsa, P., Chikhi, L., Raufaste, N., and Bonhomme, F. (1996-2004). GENETIX 4.05, logiciel sous Windows TM pour la génétique des populations. Montpellier (France), Laboratoire Génome, Populations, Interactions, CNRS UMR 5171, Université de Montpellier II.

Bell, G.A.C., 1997. Experimental evolution in Chlamydomonas. I. Short-term selection in uniform and diverse environments. Heredity 78 (5), 490-497.

Berge, G., 1962. Discolouration of the sea due to *Coccolithus huxleyi* "bloom". Sarsia 6 27-40.

Bibby, T.S., Gorbunov, M.Y., Wyman, K.W., and Falkowski, P.G., 2008. Photosynthetic community responses to upwelling in mesoscale eddies in the subtropical North Atlantic and Pacific Oceans. Deep Sea Research Part II: Topical Studies in Oceanography 55 (10-13), 1310-1320.

Bijma, J., Spero, H.J., Lea, D.W., and Bemis, B.E., 1999. G. Fischer and G. Wefer (Eds.), Use of proxies in paleoceanography: examples from the South Atlantic. Springer, Berlin. pp. 489-512.

Billard, C., 1994. Life cycles, in: J.C. Green and B.S.C. Leadbeater (Eds.), The Haptophyte algae. Systematics Association Special Volume51, pp. 161-167.

Blain, S., Queguiner, B., Armand, L., Belviso, S., Bombled, B., Bopp, L., Bowie, A., Brunet, C., Brussaard, C., Carlotti, F., Christaki, U., Corbiere, A., Durand, I., Ebersbach, F., Fuda, J.-L., Garcia, N., Gerringa, L., Griffiths, B., Guigue, C., Guillerm, C., Jacquet, S., Jeandel, C., Laan, P., Lefevre, D., Lo Monaco, C., Malits, A., Mosseri, J., Obernosterer, I., Park, Y.-H., Picheral, M., Pondaven, P., Remenyi, T., Sandroni, V., Sarthou, G., Savoye, N., Scouarnec, L., Souhaut, M., Thuiller, D., Timmermans, K., Trull, T., Uitz, J., van Beek, P., Veldhuis, M., Vincent, D., Viollier, E., Vong, L., and Wagener, T., 2007. Effect of natural iron fertilization on carbon sequestration in the Southern Ocean. Nature 446 (7139), 1070-1074.

Blain, S., Sarthou, G., and Laan, P., 2008. Distribution of dissolved iron during the natural iron-fertilization experiment KEOPS (Kerguelen Plateau, Southern Ocean). Deep Sea Research Part II: Topical Studies in Oceanography 55 (5-7), 594-605.

Blain, S., Tréguer, P., Belviso, S., Bucciarelli, E., Denis, M., Desabre, S., Fiala, M., Martin Jézéquel, V., Le Fèvre, J., Mayzaud, P., Marty, J.-C., and Razouls, S., 2001. A biogeochemical study of the island mass effect in the context of the iron hypothesis: Kerguelen Islands, Southern Ocean. Deep Sea Research Part I: Oceanographic Research Papers 48 (1), 163-187.

Booth, B.C., Lewin, J., and Norris, R.E., 1980. Siliceous nanoplankton I. Newly discovered cysts from the Gulf of Alaska. Marine Biology 58 (3), 205-209.

Booth, B.C., Lewin, J., and Norris, R.E., 1982. Nanoplankton species predominant in the subarctic Pacific in May and June 1978. Deep Sea Research Part A. Oceanographic Research Papers 29 (2), 185-200.

Booth, B.C., and Marchant, H.J., 1987. Parmales, a new order of marine chrysophytes, with descriptions of three new genera and seven new species. Journal of Phycology 23 (s2), 245-260.

Bopp, L., Kohfeld, K.E., Le Quéré, C., and Aumont, O., 2003. Dust impact on marine biota and atmospheric CO2 during glacial periods. Paleoceanography 18 (2), 1046.

Bopp, L., Monfray, P., Aumont, O., Dufresne, J.-L., Le Treut, H., Madec, G., Terray, L., and Orr, J.C., 2001. Potential impact of climate change on marine export production. Global Biogeochem. Cycles 15 (1), 81-99.

Bowie, A.R., Maldano, M.T., Frew, R.D., Croot, P.L., Achterberg, E.P., Mantoura, R.F.C., Worsfold, P.J., Law, C.S., and Boyd, P.W., 2001. The fate of added iron during a mesoscale fertilisation experiment in the Southern Ocean. Deep Sea Research Part II: Topical Studies in Oceanography 48 (11-12), 2703-2743.

Boyd, P.W., 2002. Environmental factors controlling phytoplankton processes in the Southern Ocean. Journal of Phycology 38 (5), 844-861.

Boyd, P.W., and Doney, S.C., 2002. Modelling regional responses by marine pelagic ecosystems to global climate change. Geophys. Res. Lett. 29 (16), 1806.

Boyd, P.W., Jickells, T., Law, C.S., Blain, S., Boyle, E.A., Buesseler, K.O., Coale, K.H., Cullen, J.J., de Baar, H.J.W., Follows, M., Harvey, M., Lancelot, C., Levasseur, M., Owens, N.P.J., Pollard, R., Rivkin, R.B., Sarmiento, J., Schoemann, V., Smetacek, V., Takeda, S., Tsuda, A., Turner, S., and Watson, A.J., 2007. Mesoscale Iron Enrichment Experiments 1993-2005: Synthesis and Future Directions. Science 315 (5812), 612-617.

Brand, L.E., 1981. Genetic Variability in Reproduction Rates in Marine Phytoplankton Populations. Evolution 35 (6), 1117-1127.

Brand, L.E., 1991. Minimum iron requirements of marine phytoplankton and the implications for the biogeochemical control of new production. Limnology and Oceanography 36 (8), 1756-1771.

Brand, L.E., 1994. Physiological ecology of marine coccolithophores, in: A. Winter and W.G. Siesser (Eds.), Coccolithophores. Cambridge University Press, Cambridge. pp. 39-49.

Brand, L.E., and Guillard, R.R.L., 1981. The effects of continuous light and light intensity on the reproduction rates of twenty-two species of marine phytoplankton. Journal of Experimental Marine Biology and Ecology 50 (2-3), 119-132.

Bratbak, G., Egge, J.K., and Heldal, M., 1993. Viral mortality of the marine alga *Emiliania huxleyi* (Haptophyceae) and termination of algal blooms. Marine Ecology Progress Series 93 39-48.

Bratbak, G., Wilson, W., and Heldal, M., 1996. Viral control of *Emiliania huxleyi* blooms? Journal of Marine Systems 9 (1-2), 75-81.

Brzezinski, M.A., 1985. The Si:C:N ratio of marine diatoms: interspecific variability and the effect of some environmental variables. Journal of Phycology 21 (3), 347-357.

Buck, K.R., and Garrison, D.L., 1983. Protists from the ice-edge region of the Weddell Sea. Deep Sea Research Part A. Oceanographic Research Papers 30 (12), 1261-1277.

Castberg, T., Larsen, A., Sandaa, R.A., Brussaard, C.P.D., Egge, J.K., Heldal, M., Thyrhaug, R., Hannen, E.J.V., and Bratbak, G., 2001. Microbial population dynamics and diversity during a bloom of the marine coccolithophorid *Emiliania huxleyi* (Haptophyta). Marine Ecology Progress Series 221 39-46.

Chao, A., 1984. Non-parametric estimation of the number of classes in a population. Scandinavian Journal of Statistics 11 265-270.

Chao, A., 1987. Estimating the population size for capture-recapture data with unequal catchability. Biometrics 43 783-791.

Chisholm, S.W., 2000. Oceanography: Stirring times in the Southern Ocean. Nature 407 (6805), 685-687.

Clarke, K.R., 1993. Non-parametric multivariate analyses of changes in community structure. Australian Journal of Ecology 18 117-143.

Clarke, K.R., and Gorley, R.N. (2006). PRIMER v6: User Manual/Tutorial. Plymouth, PRIMER-E.

Clarke, K.R., and Warwick, R.M., 2001. Change in marine communities: an approach to statistical analysis and interpretation. PRIMER-E, Plymouth.

Colwell, R.K. (2009). EstimateS: Statistical estimation of species richness and shared species from samples, http://purl.oclc.org/estimates.

Crawford, D.W., Lipsen, M.S., Purdie, D.A., Lohan, M.C., Statham, P.J., Whitney, F.A., Putland, J.N., Johnson, W.K., Sutherland, N., Peterson, T.D., Harrison, P.J., and Wong, C.S., 2003. Influence of zinc and iron enrichments on phytoplankotn growth in the northeastern subarctic Pacific. Limnology and Oceanography 48 (4), 1583-1600.

Cubillos, J.C., Wright, S.W., Nash, G., de Salas, M.F., Griffiths, B., Tilbrook, B., Poisson, A., and Hallegraeff, G.M., 2007. Calcification morphotypes of the coccolithophorid *Emiliania huxleyi* in the Southern Ocean: changes in 2001 to 2006 compared to historical data. Marine Ecology Progress Series 348 47-54.

Cullen, J.J., and Davis, R.F., 2003. The blank can make a big difference in oceanographic measurements. Limnology and Oceanography Bulletin 12 (2), 29-35.

Daly, K.L., Smith, W.O., Jr., Johnson, G.C., DiTullio, G.R., Jones, D.R., Mordy, C.W., Feely, R.A., Hansell, D.A., and Zhang, J.-Z., 2001. Hydrography, nutrients, and carbon pools in the Pacific sector of the Southern Ocean: Implications for carbon flux. J. Geophys. Res. 106 (C4), 7107-7124.

de Baar, H.J.W., Boyd, P.W., Coale, K.H., Landry, M.R., Tsuda, A., Assmy, P., Bakker, D.C.E., Bozec, Y., Barber, R.T., Brzezinski, M.A., Buesseler, K.O., Boyé, M., Croot, P.L., Gervais, F., Gorbunov, M.Y., Harrison, P.J., Hiscock, W.T., Laan, P., Lancelot, C., Law, C.S., Levasseur, M., Marchetti, A., Millero, F.J., Nishioka, J., Nojiri, Y., van Oijen, T., Riebesell, U., Rijkenberg, M.J.A., Saito,

H., Takeda, S., Timmermans, K.R., Veldhuis, M.J.W., Waite, A.M., and Wong, C.-S., 2005. Synthesis of iron fertilization experiments: From the Iron Age in the Age of Enlightenment. J. Geophys. Res. 110 (C9), C09S16.

De La Rocha, C.L., and Passow, U., 2007. Factors influencing the sinking of POC and the efficiency of the biological carbon pump. Deep Sea Research Part II: Topical Studies in Oceanography 54 (5-7), 639-658.

Deacon, G.E.R., 1933. A general account of the hydrology of the South Atlantic Ocean. Discovery Reports 7 171-238.

Deacon, G.E.R., 1979. The Weddell gyre. Deep Sea Research Part A. Oceanographic Research Papers 26 (9), 981-995.

Deacon, G.E.R., 1982. Physical and biological zonation in the Southern Ocean. Deep Sea Research Part A. Oceanographic Research Papers 29 (1), 1-15.

Des Marais, D.J., 2000. Evolution: When Did Photosynthesis Emerge on Earth? Science 289 (5485), 1703-1705.

Di Rienzo, A., Donnelly, P., Toomajian, C., Sisk, B., Hill, A., Petzl-Erler, M.L., Haines, G.K., and Barch, D.H., 1998. Heterogeneity of Microsatellite Mutations Within and Between Loci, and Implications for Human Demographic Histories. Genetics 148 (3), 1269-1284.

Doty, M.S., and Oguri, M., 1965. The Island Mass Effect. Journal du Conseil 22 33-37.

Dugdale, R.C., and Wilkerson, F.P., 1998. Silicate regulation of new production in the equatorial Pacific upwelling. Nature 391 (6664), 270-273.

Eichert, W. (1999). WhichRun Version 4.1 written for Michael Banks, Bodega Marine Lab, U. C. Davis.

Ellstrand, N.C., and Roose, M.L., 1987. Patterns of Genotypic Diversity in Clonal Plant Species. American Journal of Botany 74 (1), 123-131.

Evans, K.M., Bates, S.S., Medlin, L.K., and Hayes, P.K., 2004. Microsatellite marker development and genetic variation in the toxic marine diatom *Pseudo-nitzschia multiseries* (Bacillariophyceae)1. Journal of Phycology 40 (5), 911-920.

Evans, K.M., and Hayes, P.K., 2004. Microsatellite markers for the cosmopolitan marine diatom *Pseudo-nitzschia pungens*. Molecular Ecology Notes 4 (1), 125-126.

Evans, K.M., Kuhn, S.F., and Hayes, P.K., 2005. High levels of genetic diversity and low levels of genetic differentiation in North Sea *Pseudo-nitzschia pungens* (Bacillariophyceae) populations1. Journal of Phycology 41 (3), 506-514.

Eynaud, F., Giraudeau, J., Pichon, J.J., and Pudsey, C.J., 1999. Sea-surface distribution of coccolithophores, diatoms, silicoflagellates and dinoflagellates in the South Atlantic Ocean during the late austral summer 1995. Deep Sea Research Part I: Oceanographic Research Papers 46 (3), 451-482.

Falkowski, P.G., Katz, M.E., Knoll, A.H., Quigg, A., Raven, J.A., Schofield, O., and Taylor, F.J.R., 2004. The Evolution of Modern Eukaryotic Phytoplankton. Science 305 (5682), 354-360.

Feng, Y., Warner, M.E., Zhang, Y., Sun, J., Fu, F.-X., Rose, J.M., and Hutchins, D.A., 2008. Interactive effects of increased pCO2, temperature and irradiance on the marine coccolithophore *Emiliania huxleyi* (Prymnesiophyceae). European Journal of Phycology 43 (1), 87 - 98.

Fernández, E., Boyd, P., Holligan, P.M., and Harbour, D.S., 1993. Production of organic and inorganic carbon within a large-scale coccolithophore bloom in the northeast Atlantic Ocean. Marine Ecology Progress Series 97 271-285.

Field, C.B., Behrenfeld, M.J., Randerson, J.T., and Falkowski, P., 1998. Primary Production of the Biosphere: Integrating Terrestrial and Oceanic Components. Science 281 (5374), 237-240.

Findlay, C.S., and Giraudeau, J., 2000. Extant calcareous nannoplankton in the Australian Sector of the Southern Ocean (austral summers 1994 and 1995). Marine Micropaleontology 40 (4), 417-439.

Foster, C., Aswath, K., Chanock, S., McKay, H., and Peters, U., 2006. Polymorphism analysis of six selenoprotein genes: support for a selective sweep at the glutathione peroxidase 1 locus (3p21) in Asian populations. BMC Genetics 7 (1), 56.

Frada, M., Not, F., Probert, I., and de Vargas, C., 2006. CaCO3 optical detection with fluorescent in situ hybridization: a new method to identify and quantify calcifying microorganisms from the oceans. Journal of Phycology 42 (6), 1162-1169.

Frada, M., Probert, I., Allen, M.J., Wilson, W.H., and de Vargas, C., 2008. The "Cheshire Cat" escape strategy of the coccolithophore *Emiliania huxleyi* in response to viral infection. Proceedings of the National Academy of Sciences 105 (41), 15944-15949.

Francois, R., Honjo, S., Krishfield, R., and Manganini, S., 2002. Factors controlling the flux of organic carbon to the bathypelagic zone of the ocean. Global Biogeochem. Cycles 16 (4), 1087.

Fuhrman, J.A., 1999. Marine viruses and their biogeochemical and ecological effects. Nature 399 (6736), 541-548.

Fuhrman, J.A., and Schwalbach, M., 2003. Viral Influence on Aquatic Bacterial Communities. Biol Bull 204 (2), 192-195.

Gadagkar, R., 1998. How to gain the benefits of sexual reproduction without paying the cost: a worm shows the way. Trends in Ecology & Evolution 13 (6), 220-221.

Gall, M.P., Boyd, P.W., Hall, J., Safi, K.A., and Chang, H., 2001. Phytoplankton processes. Part 1: Community structure during the Southern Ocean Iron RElease Experiment (SOIREE). Deep Sea Research Part II: Topical Studies in Oceanography 48 (11-12), 2551-2570.

Gattuso, J.P., Frankignoulle, M., Bourge, I., Romaine, S., and Buddemeier, R.W., 1998. Effect of calcium carbonate saturation of seawater on coral calcification. Global and Planetary Change 18 (1-2), 37-46.

Geider, R.J., Greene, R.M., Kolber, Z., MacIntyre, H.L., and Falkowski, P.G., 1993. Fluorescence assessment of the maximum quantum efficiency of photosynthesis in the western North Atlantic. Deep Sea Research Part I: Oceanographic Research Papers 40 (6), 1205-1224.

Geisen, M., Billard, C., Broerse, A., Cros, L., Probert, I., and Young, J., 2002. Life-cycle associations involving pairs of holococcolithophorid species: intraspecific variation or cryptic speciation? European Journal of Phycology 37 531-550.

Gervais, F., Riebesell, U., and Gorbunov, M.Y., 2002. Changes in primary productivity and chlorophyll a in response to iron fertilization in the Southern Polar Frontal Zone. Limnology and Oceanography 47 (5), 1324-1335.

Gill, A.E., 1973. Circulation and bottom water production in the Weddell Sea. Deep Sea Research and Oceanographic Abstracts 20 (2), 111-140.

Gordon, A.L., 1967. Structure of Antarctic waters between 2O°W and 17O°W, in: V.C. Bushnell (Eds.), Antarctic map folio series, Folio 6. American Geography Societypp. 10 pp.

Gordon, A.L., 1988. Spatial and temporal variability within the Southern Ocean, in: D. Sahrhage (Eds.), Antarctic ocean and resources variability. Springer-Verlag, Berlin. pp. 41-56.

Gordon, A.L., Molinelli, E., and Baker, T., 1978. Large-Scale Relative Dynamic Topography of the Southern Ocean. J. Geophys. Res. 83 (C6), 3023-3032.

Gordon, R.M., Martin, J.H., and Knauer, G.A., 1982. Iron in north-east Pacific waters. Nature 299 (5884), 611-612.

Goudet, J. (1999). PCA-GEN for Windows TM. Lausanne (Switzerland), Institute of Ecology Biology Building, UNIL CH-1015.

Goudet, J., Raymond, M., de-Meeus, T., and Rousset, F., 1996. Testing Differentiation in Diploid Populations. Genetics 144 (4), 1933-1940.

Green, J.C., Course, P.A., and Tarran, G.A., 1996. The life-cycle of *Emiliania huxleyi*: A brief review and a study of relative ploidy levels analysed by flow cytometry. Journal of Marine Systems 9 (1-2), 33-44.

Greene, R.M., Geider, R.J., and Falkowski, P.G., 1991. Effect of iron limitation on photosynthesis in a marine diatom. Limnology and Oceanography 36 (8), 1772-1782.

Greene, R.M., Kolber, Z.S., Swift, D.G., Tindale, N.W., and Falkowski, P.G., 1994. Physiological limitation of phytoplankton photosynthesis in the eastern equatorial Pacific determined from variability in the quantum yield of fluorescence. Limnology and Oceanography 39 (5), 1061-1074.

Guillard, R.R.L., 1975. Culture of phytoplankton for feeding marine invertebrates, in: W.L. Smith and M.H. Chaney (Eds.), Culture of marine invertebrate animals. Plenum Press, New York. pp. 29-60.

Guo, S., and Thompson, E., 1992. Performing the exact test of Hardy-Weinberg proportion for multiple alleles. Biometrics 48 361-372.

Haldane, J., 1954. An exact test for randomness of mating. Journal of Genetics 52 (3), 631-635.

Hare, C.E., Leblanc, K., DiTullio, G.R., Kudela, R.M., Zhang, Y., Lee, P.A., Riseman, S., and Hutchins, D.A., 2007. Consequences of increased temperature and CO_2 for phytoplankton community structure in the Bering Sea. Marine Ecology Progress Series 352 9-16.

Hasle, G.R., 1960. Plankton coccolithophorids from the Subantarctic and Equatorial Pacific. Nytt Magasin for Botanikk 8 77-92.

Hasle, G.R., 1965. *Nitzschia* and *Fragilariopsis* species studied in the light and electron microscopes III, in: (Eds.), The genus *Fragilariopsis*. Skrifter utgitt av Det Norske Videnskaps-Akademi I. Matematisk-Naturvitenskapelige Klasse. Ny Serie21, pp. 1-49.

Heck, K.L., van Belle, G., and Simberloff, D., 1975. Explicit Calculation of the Rarefaction Diversity Measurement and the Determination of Sufficient Sample Size. Ecology 56 (6), 1459-1461.

Hoffmann, L.J., Peeken, I., Lochte, K., Assmy, P., and Veldhuis, M., 2006. Different reactions of Southern Ocean phytoplankton size classes to iron fertilization. Limnology and Oceanography 51 (3), 1217-1229.

Holligan, P.M., Charalampopoulou, A., and Hutson, R., 2010. Seasonal distributions of the coccolithophore, *Emiliania huxleyi,* and of particulate inorganic carbon in surface waters of the Scotia Sea. Journal of Marine Systems 82 (4), 195-205.

Holligan, P.M., Fernandez, E., Aiken, J., Balch, W.M., Boyd, P., Burkill, P.H., Finch, M., Groom, S.B., Malin, G., Muller, K., Purdie, D.A., Robinson, C., Trees, C.C., Turner, S.M., and Wal, P.v.d., 1993. A Biochemical study of the

coccolithophore, *Emiliania huxleyi*, in the North Atlantic. Global Biogeochemical Cycles 7 879-900.

Holmen, C.S., 1992. The global carbon cycle, in: S.S. Butcher, R.J. Charlson, G.H. Orians and G.V. Wolfe (Eds.), Global Biogeochemical Cycles. Academic Press, London. pp. 239-262.

Honjo, S., 1980. Material fluxes and modes of sedimentation in the mesopelagic and bathypelagic zones. Journal of Marine Research 38 53-97.

Honjo, S., 1996. Fluxes of particles to the interior of the open oceans, in: V. Ittekkot, P. Schäfer, S. Honjo and P.J. Depetris (Eds.), Particle Flux in the Ocean, SCOPE. Wiley, New York. pp. 91-254.

Houdan, A., Billard, C., Marie, D., Not, F., Saez, A.G., Young, J.R., and Probert, I., 2003. Holococcolithophore - heterococcolithophore (Haptophyta) life cycles: flow cytometric analysis of relative ploidy levels. Systematics and Biodiversity 1(4) 453-465 (DOI 410.1017/S1477200003001270).

Huber, B.T., Hodell, D.A., and Hamilton, C.P., 1995. Middle–Late Cretaceous climate of the southern high latitudes: Stable isotopic evidence for minimal equator-to-pole thermal gradients. Geological Society of America Bulletin 107 (10), 1164-1191.

Ichinomiya, M., Yoshikawa, S., Kamiya, M., Ohki, K., Takaichi, S., and Kuwata, A., 2010. Isolation and characterization of Parmales (Heterokonta/Heterokontophyta/Stramenopiles) from the Oyashio region, western North Pacific. Journal of Phycology no-no.

Iglesias-Rodríguez, D., Saez, A.G., Groben, R., Edwards, K.J., Batley, J., Medlin, L.K., and Hayes, P.K., 2002. Polymorphic microsatellite loci in global populations of the marine coccolithophorid *Emiliania huxleyi*. Mol. Ecol. Notes 2 495-497.

Iglesias-Rodríguez, M.D., Halloran, P.R., Rickaby, R.E.M., Hall, I.R., Colmenero-Hidalgo, E., Gittins, J.R., Green, D.R.H., Tyrrell, T., Gibbs, S.J., von Dassow, P., Rehm, E., Armbrust, E.V., and Boessenkool, K.P., 2008. Phytoplankton Calcification in a High-CO_2 World. Science 320 (5874), 336-340.

Iglesias-Rodríguez, M.D., Schofield, O.M., Batley, J., Medlin, L.K., and Hayes, P.K., 2006. Intraspecific genetic diversity in the marine coccolithophore *Emiliania huxleyi* (Prymnesiophyceae): the use of microsatellite analysis in marine phytoplankton population studies. Journal of Phycology 42 (3), 526-536.

IPCC. (2007a). "Climate Change 2007: Synthesis Report." from http://www.ipcc.ch/ipccreports/ar4-syr.htm.

IPCC (2007b). Contribution of Working Group I to the Fourth Assessment Report of the Intergovernmental Panel on Climate Change. Climate Change 2007: The physical science basis. S. Solomon, D. Qin, M. Manning*et al*. Cambridge, Cambridge University Press.

Jacquet, S., Heldal, M., Iglesias-Rodríguez, D., Larsen, A., Wilson, W., and Bratbak, G., 2002. Flow cytometric analysis of an *Emiliana huxleyi* bloom terminated by viral infection. Aquatic Microbial Ecology 27 (2), 111-124.

Jarne, P., and Lagoda, P.J.L., 1996. Microsatellites, from molecules to populations and back. Trends in Ecology and Evolution 11 424-429.

JGI. (2008). "Emiliania huxleyi CCMP1516 Main Genome Assembly v1.0." from http://genome.jgi-psf.org/Emihu1/Emihu1.home.html.

Jochem, F.J. (2007). "Biogeochemical Mineral Cycles." Retrieved September 19, 2010, from http://www.jochemnet.de/fiu/OCB3043_28.html.

Kalinowski, S.T., 2005. Do polymorphic loci require large sample sizes to estimate genetic distances? Heredity 94 (1), 33-36.

Kang, S.-H., Kang, J.-S., Lee, S., Chung, K.H., Kim, D., and Park, M.G., 2001. Antarctic Phytoplankton Assemblages in the Marginal Ice Zone of the Northwestern Weddell Sea. J. Plankton Res. 23 (4), 333-352.

Klaas, C., and Archer, D.E., 2002. Association of sinking organic matter with various types of mineral ballast in the deep sea: Implications for the rain ratio. Global Biogeochem. Cycles 16 (4), 1116.

Klaveness, D., 1972. *Coccolithus huxleyi* (Lohm.) Kamptn II. The flagellate cell, aberrant cell types, vegetative propagation and life cycles. European Journal of Phycology 7 (3), 309-318.

Kleypas, J.A., Buddemeier, R.W., Archer, D., Gattuso, J.-P., Langdon, C., and Opdyke, B.N., 1999. Geochemical Consequences of Increased Atmospheric Carbon Dioxide on Coral Reefs. Science 284 (5411), 118-120.

Koester, J., Swalwell, J., von Dassow, P., and Armbrust, E.V., 2010. Genome size differentiates co-occurring populations of the planktonic diatom *Ditylum brightwellii* (Bacillariophyta). BMC Evolutionary Biology 10 (1), 1.

Kolber, Z., Wyman, K.D., and Falkowski, P.G., 1990. Natural variability in photosynthetic energy conversion efficiency: A field study in the Gulf of Maine. Limnology and Oceanography 35 (1), 72-79.

Kolber, Z., Zehr, J., and Falkowski, P., 1988. Effects of Growth Irradiance and Nitrogen Limitation on Photosynthetic Energy Conversion in Photosystem II. Plant Physiol. 88 (3), 923-929.

Kolber, Z.S., Barber, R.T., Coale, K.H., Fitzwateri, S.E., Greene, R.M., Johnson, K.S., Lindley, S., and Falkowski, P.G., 1994. Iron limitation of phytoplankton photosynthesis in the equatorial Pacific Ocean. Nature 371 (6493), 145-149.

Komuro, C., Narita, H., Imai, K., Nojiri, Y., and Jordan, R.W., 2005. Microplankton assemblages a Station KNOT in the subarctic western Pacific, 1999-2000. Deep Sea Research II 52 2206-2217.

Korb, R., Whitehouse, M., Atkinson, A., and Thorpe, S., 2008. Magnitude and maintenance of the phytoplankton bloom at South Georgia: a naturally iron-replete environment. Marine Ecology Progress Series 368 75-91.

Korb, R.E., and Whitehouse, M., 2004. Contrasting primary production regimes around South Georgia, Southern Ocean: large blooms versus high nutrient, low chlorophyll waters. Deep Sea Research Part I: Oceanographic Research Papers 51 (5), 721-738.

Korb, R.E., Whitehouse, M.J., Gordon, M., Ward, P., and Poulton, A.J., 2010. Summer microplankton community structure across the Scotia Sea: implications for biological carbon export. Biogeosciences 7 (1), 343-356.

Korb, R.E., Whitehouse, M.J., Thorpe, S.E., and Gordon, M., 2005. Primary production across the Scotia Sea in relation to the physico-chemical environment. Journal of Marine Systems 57 (3-4), 231-249.

Korb, R.E., Whitehouse, M.J., and Ward, P., 2004. SeaWiFS in the southern ocean: spatial and temporal variability in phytoplankton biomass around South Georgia. Deep Sea Research Part II: Topical Studies in Oceanography 51 (1-3), 99-116.

Kosman, C.A., Thomsen, H.A., and Østergaard, J.B., 1993. Parmales (Chrysophyceae) from Mexican, Californian Baltic, Arctic and Antarctic waters with the description of new subspecies and several new forms. Phycologia 32 116-128.

Langdon, C., Takahashi, T., Sweeney, C., Chipman, D., Goddard, J., Marubini, F., Aceves, H., Barnett, H., and Atkinson, M.J., 2000. Effect of calcium carbonate saturation state on the calcification rate of an experimental coral reef. Global Biogeochem. Cycles 14 (2), 639-654.

Larsen, A., Castberg, T., Sandaa, R.A., Brussaard, C.P.D., Egge, J., Heldal, M., Paulino, A., Thyrhaug, R., Hannen, E.J.V., and Bratbak, G., 2001. Population dynamics and diversity of phytoplankton, bacteria and viruses in a seawater enclosure. Marine Ecology Progress Series 221 47-57.

Larsen, A., Flaten, G.A.F., Sandaa, R.-A., Castberg, T., Thyrhaug, R., Erga, S.R., Jacquet, S., and Bratbak, G., 2004. Spring phytoplankton bloom dynamics in Norwegian coastal waters: Microbial community succession and diversity. Limnology and Oceanography 49 (1), 180-190.

Li, Y.-C., Korol, A.B., Fahima, T., Beiles, A., and Nevo, E., 2002. Microsatellites: genomic distribution, putative functions and mutational mechanisms: a review. Molecular Ecology 11 (12), 2453-2465.

Lohmann, H., 1902. Die Coccolithophoridae, eine Monographie der coccolithen bildenden flagellaten, zugleich ein Betrag zur Kenntnis des Mittelmeerauftriebs. Arch. Protistenk 1 89-165.

Long, S.P., Humphries, S., and Falkowski, P.G., 1994. Photoinhibition of Photosynthesis in Nature. Annual Review of Plant Physiology and Plant Molecular Biology 45 (1), 633-662.

MacArthur, R., and Wilson, E.O., 1967. The Theory of Island Biogeography. Princeton University Press, Princeton.

Marchetti, A., Parker, M.S., Moccia, L.P., Lin, E.O., Arrieta, A.L., Ribalet, F., Murphy, M.E.P., Maldonado, M.T., and Armbrust, E.V., 2009. Ferritin is used for iron storage in bloom-forming marine pennate diatoms. Nature 457 (7228), 467-470.

Margalef, R., 1978. Life-forms of phytoplankton as survival alternatives in an unstable environment. Oceanologica Acta 1 493-509.

Martin, J.H., 1990. Glacial-interglacial CO_2 change: the iron hypothesis. Paleoceanography 5 (1), 1-13.

Martin, J.H., and Gordon, M.R., 1988. Northeast Pacific iron distributions in relation to phytoplankton productivity. Deep Sea Research Part A. Oceanographic Research Papers 35 (2), 177-196.

Martin, J.H., Gordon, R.M., Fitzwater, S., and Broenkow, W.W., 1989. Vertex: phytoplankton/iron studies in the Gulf of Alaska. Deep Sea Research Part A. Oceanographic Research Papers 36 (5), 649-680.

Martínez-Martínez, J., Norland, S., Thingstad, T.F., Schroeder, D.C., Bratbak, G., Wilson, W.H., and Larsen, A., 2006. Variability in microbial population dynamics between similarly perturbed mesocosms. Journal of Plankton Research 28 (8), 783-791.

Martinez, J.M., Schroeder, D.C., Larsen, A., Bratbak, G., and Wilson, W.H., 2007. Molecular Dynamics of *Emiliania huxleyi* and Cooccurring Viruses during Two Separate Mesocosm Studies. Appl. Environ. Microbiol. 73 (2), 554-562.

Matsumoto, K., Sarmiento, J.L., and Brzezinski, M.A., 2002. Silicic acid leakage from the Southern Ocean: A possible explanation for glacial atmospheric pCO2. Global Biogeochem. Cycles 16 (3), 1031.

McCave, I.N., 1975. Vertical flux of particles in the ocean. Deep Sea Research and Oceanographic Abstracts 22 (7), 491-502.

McIntyre, A., and Bé, A.W.H., 1967. Modern coccolithophoridae of the atlantic ocean--I. Placoliths and cyrtoliths. Deep Sea Research and Oceanographic Abstracts 14 (5), 561-564, IN563-IN568, 565-566, IN569-IN520, 567-597.

Medlin, L.K., Barker, G.L.A., Campbell, L., Green, J.C., Hayes, P.K., Marie, D., Wrieden, S., and Vaulot, D., 1996. Genetic characterisation of *Emiliania huxleyi* (Haptophyta). Journal of Marine Systems 9 (1-2), 13-31.

Meredith, M.P., Naveira Garabato, A.C., Stevens, D.P., Heywood, K.J., and Sanders, R.J., 2001. Deep and Bottom Waters in the Eastern Scotia Sea: Rapid Changes in Properties and Circulation. Journal of Physical Oceanography 31 (8), 2157-2168.

Minitab (2006). Minitab Statistical Software, Release 15 for Windows. State College, Pennsylvania. Minitab® is a registered trademark of Minitab Inc.

Mohan, R., Mergulhao, L.P., Guptha, M.V.S., Rajakumar, A., Thamban, M., AnilKumar, N., Sudhakar, M., and Ravindra, R., 2008. Ecology of coccolithophores in the Indian sector of the Southern Ocean. Marine Micropaleontology 67 (1-2), 30-45.

Moore, C.M., Hickman, A.E., Poulton, A.J., Seeyave, S., and Lucas, M.I., 2007a. Iron-light interactions during the CROZet natural iron bloom and EXport experiment (CROZEX): II--Taxonomic responses and elemental stoichiometry. Deep Sea Research Part II: Topical Studies in Oceanography 54 (18-20), 2066-2084.

Moore, C.M., Lucas, M.I., Sanders, R., and Davidson, R., 2005. Basin-scale variability of phytoplankton bio-optical characteristics in relation to bloom state and community structure in the Northeast Atlantic. Deep Sea Research Part I: Oceanographic Research Papers 52 (3), 401-419.

Moore, C.M., Seeyave, S., Hickman, A.E., Allen, J.T., Lucas, M.I., Planquette, H., Pollard, R.T., and Poulton, A.J., 2007b. Iron-light interactions during the CROZet natural iron bloom and EXport experiment (CROZEX) I: Phytoplankton growth and photophysiology. Deep Sea Research Part II: Topical Studies in Oceanography 54 (18-20), 2045-2065.

Moore, C.M., Suggett, D.J., Hickman, A.E., Kim, Y.-N., Tweddle, J.F., Sharples, J., Geider, R.J., and Holligan, P.M., 2006. Phytoplankton photoacclimation and photoadaptation in response to environmental gradients in a shelf sea. Limnology and Oceanography 51 (2), 936-949.

Morel, F.M.M., Rueter, J.G., and Price, N.M., 1991. Iron nutrition of phytoplankton and its possible importance in the ecology of ocean regions with high nutrient and low biomass. Oceanography 4 (2), 56-61.

Morris, J.J., Kirkegaard, R., Szul, M.J., Johnson, Z.I., and Zinser, E.R., 2008. Facilitation of Robust Growth of Prochlorococcus Colonies and Dilute Liquid Cultures by "Helper" Heterotrophic Bacteria. Appl. Environ. Microbiol. 74 (14), 4530-4534.

Nagai, S., Lian, C., Hamaguchi, M., Matsuyama, Y., Itakura, S., and Hogetsu, T., 2004. Development of microsatellite markers in the toxic dinoflagellate *Alexandrium tamarense* (Dinophyceae). Molecular Ecology Notes 4 (1), 83-85.

Nagai, S., Lian, C., Yamaguchi, S., Hamaguchi, M., Matsuyama, Y., Itakura, S., Shimada, H., Kaga, S., Yamauchi, H., Sonda, Y., Nishikawa, T., Kim, C.-H., and Hogetsu, T., 2007. Microsatellite markers reveal population genetic structure of the toxic dinoflagellate *Alexandrium tamarense* (Dinophyceae) in Japanese coastal waters. Journal of Phycology 43 (1), 43-54.

Nei, M., 1987. Molecular Evolutionary Genetics. Columbia University Press, New York.

Nielsdóttir, M.C., Moore, C.M., Sanders, R., Hinz, D.J., and Achterberg, E.P., 2009. Iron limitation of the postbloom phytoplankton communities in the Iceland Basin. Global Biogeochemical Cycles 23

Nishida, S., 1986. Nannoplankton flora in the southern oceans, with special reference to siliceous varieties. Memoirs of the National Institute Polar Research Special Issue 40 56-68.

Olseth, J.A., Cleveland, F., and Lange, T.d., 2008. Radiation Yearbook No. 44. Universitetet i Bergen, Geogysisk Institutt, Avdeling for Meteorologi, Bergen.

Orr, J.C., Fabry, V.J., Aumont, O., Bopp, L., Doney, S.C., Feely, R.A., Gnanadesikan, A., Gruber, N., Ishida, A., Joos, F., Key, R.M., Lindsay, K., Maier-Reimer, E., Matear, R., Monfray, P., Mouchet, A., Najjar, R.G., Plattner, G.-K., Rodgers, K.B., Sabine, C.L., Sarmiento, J.L., Schlitzer, R., Slater, R.D., Totterdell, I.J., Weirig, M.-F., Yamanaka, Y., and Yool, A., 2005. Anthropogenic ocean acidification over the twenty-first century and its impact on calcifying organisms. Nature 437 (7059), 681-686.

Orsi, A.H., Nowlin Jr, W.D., and Whitworth Iii, T., 1993. On the circulation and stratification of the Weddell Gyre. Deep Sea Research Part I: Oceanographic Research Papers 40 (1), 169-203.

Orsi, A.H., Whitworth, T., and Nowlin, W.D., 1995. On the meridional extent and fronts of the Antarctic Circumpolar Current. Deep Sea Research Part I: Oceanographic Research Papers 42 (5), 641-673.

Paasche, E., 1966. Adjustment to Light and Dark Rates of Coccolith Formation. Physiologia Plantarum 19 (2), 271-278.

Passow, U., 2002. Transparent exopolymer particles (TEP) in aquatic environments. Progress In Oceanography 55 (3-4), 287-333.

Patterson, S.L., and III, T.W., 1990. Physical oceanography of the Pacific sector of the Southern Ocean, in: G.P. Glasby (Eds.), Antarctic sector of the Pacific. Elsevier Oceanography Series, Amsterdam. 51, pp. 55-93.

Pianka, E.R., 1970. On r- and K-Selection. The American Naturalist 104 (940), 592.

Pollard, R.T., Salter, I., Sanders, R.J., Lucas, M.I., Moore, C.M., Mills, R.A., Statham, P.J., Allen, J.T., Baker, A.R., Bakker, D.C.E., Charette, M.A., Fielding, S., Fones, G.R., French, M., Hickman, A.E., Holland, R.J., Hughes, J.A., Jickells, T.D., Lampitt, R.S., Morris, P.J., Nedelec, F.H., Nielsdottir, M., Planquette, H., Popova, E.E., Poulton, A.J., Read, J.F., Seeyave, S., Smith, T., Stinchcombe, M., Taylor, S., Thomalla, S., Venables, H.J., Williamson, R., and Zubkov, M.V., 2009. Southern Ocean deep-water carbon export enhanced by natural iron fertilization. Nature 457 (7229), 577-580.

Poulton, A.J., Charalampopoulou, A., Young, J.R., Tarran, G.A., Lucas, M.I., and Quartly, G.D., 2010. Coccolithophore dynamics in non-bloom conditions during late summer in the central Iceland Basin (July-August 2007). Limnology and Oceanography 55 (4), 1601-1613.

Poulton, A.J., Mark Moore, C., Seeyave, S., Lucas, M.I., Fielding, S., and Ward, P., 2007. Phytoplankton community composition around the Crozet Plateau, with emphasis on diatoms and *Phaeocystis*. Deep Sea Research Part II: Topical Studies in Oceanography 54 (18-20), 2085-2105.

Price, N.M., Andersen, L.F., and Morel, F.M.M., 1991. Iron and nitrogen nutrition of equatorial Pacific plankton. Deep Sea Research Part A. Oceanographic Research Papers 38 (11), 1361-1378.

Purdie, D.A., and Finch, M.S., 1994. Impact of a coccolithophorid bloom on dissolved carbon dioxide in sea water enclosures in a Norwegian fjord. Sarsia 79 (4), 379-387.

Ragni, M., Airs, R.L., Leonardos, N., and Geider, R.J., 2008. Photoinhibition of PSII in *Emiliania huxleyi* (*Haptophyta*) under high light stress: the roles of photoacclimation, photoprotection, and photorepair. Journal of Phycology 44 (3), 670-683.

Raven, J., Caldeira, K., Elderfield, H., Hoegh-Guldberg, O., Liss, P., Riebesell, U., Shepherd, J., Turley, C., Watson, A., Heap, R., Banes, R., and Quinn, R. (2005). Ocean Acidification due to increasing atmospheric carbon dioxide. London, The Royal Society, Policy Document.

Raven, J.A., 1988. The iron and molybdenum use efficiencies of plant growth with different energy, carbon and nitrogen sources. New Phytologist 109 (3), 279-287.

Raven, J.A., 1990. Predictions of Mn and Fe use efficiencies of phototrophic growth as a function of light availability for growth and of C assimilation pathway. New Phytologist 116 (1), 1-18.

Raymond, M., and Rousset, F., 1995. GENEPOP (version 1.2): population genetics software for exact tests and ecumenicism Journal Heredity 86 248-249.

Redfield, A.C., 1958. The biological control of chemical factors in the environment. American Scientist 46 205-221.

Riebesell, U., Zondervan, I., Rost, B., Tortell, P.D., Zeebe, R.E., and Morel, F.M.M., 2000. Reduced calcification of marine plankton in response to increased atmospheric CO_2. Nature 407 (6802), 364-367.

Robertson, J.E., Robinson, C., Turner, D.R., Holligan, P., Watson, A.J., Boyd, P., Fernandez, E., and Finch, M., 1994. The impact of a coccolithophore bloom on oceanic carbon uptake in the Northeast Atlantic during summer 1991. Deep Sea Research I 41 (2), 297-314.

Rodman, M.R., and Gordon, A.L., 1982. Southern Ocean Bottom Water of the Australian-New Zealand Sector. J. Geophys. Res. 87 (C8), 5771-5778.

Rost, B., and Riebesell, U., 2004. Coccolithophores and the biological pump: responses to environmental changes, in: H.R. Thierstein and J.R. Young (Eds.), Coccolithophores: from molecular processes to global impact. Springer Berlin Heidelberg, New York. pp. 99-125.

Rousset, F., 2008. genepop'007: a complete re-implementation of the genepop software for Windows and Linux. Molecular Ecology Resources 8 (1), 103-106.

Rynearson, T.A., and Armbrust, E.V., 2000. DNA fingerprinting reveals extensive genetic diversity in a field population of the centric diatom *Ditylum brightwellii*. Limnology and Oceanography 45 (6), 1329-1340.

Rynearson, T.A., and Armbrust, E.V., 2005. Maintenance of clonal diversity during a spring bloom of the centric diatom *Ditylum brightwellii*. Molecular Ecology 14 (6), 1631-1640.

Rynearson, T.A., and Armbrust, V.E., 2004. Genetic differentiation among populations of the planktonic marine diatom *Ditylum brightwellii* (Bacillariophyceae). Journal of Phycology 40 (1), 34-43.

Rynearson, T.A., Lin, E.O., and Armbrust, E.V., 2009. Metapopulation Structure in the Planktonic Diatom *Ditylum brightwellii* (Bacillariophyceae). Protist 160 (1), 111-121.

Rynearson, T.A., Newton, J.A., and Armbrust, E.V., 2006. Spring bloom development, genetic variation, and population succession in the planktonic diatom *Ditylum brightwellii*. Limnology and Oceanography 51 (3), 1249-1261.

Sabine, C.L., Feely, R.A., Gruber, N., Key, R.M., Lee, K., Bullister, J.L., Wanninkhof, R., Wong, C.S., Wallace, D.W.R., Tilbrook, B., Millero, F.J., Peng, T.-H., Kozyr, A., Ono, T., and Rios, A.F., 2004. The Oceanic Sink for Anthropogenic CO_2. Science 305 (5682), 367-371.

Sambrook, J., and Russell, D.W., 2001. Molecular cloning: a laboratory manual. Cold Spring Harbor Laboratory Press, Cold Spring Harbor.

Sandgren, C.D., Smol, J.P., and Kristiansen, J., 1995. Chrysophyte Algae: Ecology, phylogeny and development. Cambridge University Press, Cambridge.

Sarmiento, J.L., and Gruber, N., 2006. Ocean Biogeochemical Dynamics. Princeton University Press, Princeton.

Sarmiento, J.L., Slater, R., Barber, R., Bopp, L., Doney, S.C., Hirst, A.C., Kleypas, J., Matear, R., Mikolajewicz, U., Monfray, P., Soldatov, V., Spall, S.A., and Stouffer, R., 2004. Response of ocean ecosystems to climate warming. Global Biogeochem. Cycles 18 (3), GB3003.

Schlotterer, C., and Tautz, D., 1992. Slippage synthesis of simple sequence DNA. Nucl. Acids Res. 20 (2), 211-215.

Schroeder, D.C., Biggi, G.F., Hall, M., Davy, J., Martinez, J.M., Richardson, A.J., Malin, G., and Wilson, W.H., 2005. A genetic marker to separate *Emiliania huxleyi* (Prymnesiophyceae) morphotypes. Journal of Phycology 41 (4), 874-879.

Scott, F.J., and Marchant, H.J., 2005. Antarctic Marine Protists. Australian Biological Resources Study, Canberra.

Seeyave, S., Lucas, M.I., Moore, C.M., and Poulton, A.J., 2007. Phytoplankton productivity and community structure in the vicinity of the Crozet Plateau during austral summer 2004/2005. Deep Sea Research Part II: Topical Studies in Oceanography 54 (18-20), 2020-2044.

Sigman, D.M., and Boyle, E.A., 2000. Glacial/interglacial variations in atmospheric carbon dioxide. Nature 407 (6806), 859-869.

Silver, M.W., Mitchell, J.G., and Ringo, D.L., 1980. Siliceous nanoplankton. II. Newly discovered cysts and abundant choanoflagellates from the Weddell Sea, Antarctica. Marine Biology 58 (3), 211-217.

Smetacek, V., 1999. Diatoms and the Ocean Carbon Cycle. Protist 150 (1), 25-32.

Smetacek, V., Assmy, P., and Henjes, J., 2004. The role of grazing in structuring Southern Ocean pelagic ecosystems and biogeochemical cycles. Antarctic Science 16 (04), 541-558.

Steinke, M., Wolfe, G.V., and Kirst, G.O., 1998. Partial characterisation of dimethylsulfoniopropionate (DMSP) lyase isozymes in 6 strains of Emiliania huxleyi. Marine Ecology Progress Series 175 215-225.

Stevenson, B.S., Eichorst, S.A., Wertz, J.T., Schmidt, T.M., and Breznak, J.A., 2004. New Strategies for Cultivation and Detection of Previously Uncultured Microbes. Appl. Environ. Microbiol. 70 (8), 4748-4755.

Suggett, D.J., Le Floc'H, E., Harris, G.N., Leonardos, N., and Geider, R.J., 2007. Different strategies of photoacclimation by two strains of *Emiliania huxleyi* (Haptophyta)1. Journal of Phycology 43 (6), 1209-1222.

Suggett, D.J., Moore, C.M., Hickman, A.E., and Geider, R.J., 2009. Interpretation of fast repetition rate (FRR) fluorescence: signatures of phytoplankton community structure versus physiological state. Marine Ecology Progress Series 376 1-19.

Symes, J.L., and Kester, D.R., 1985. The distribution of iron in the Northwest Atlantic. Marine Chemistry 17 (1), 57-74.

Thierstein, H.R., Geitzenauer, K.R., Molfino, B., and Shackleton, N.J., 1977. Global synchroneity of late Quaternary coccolith datum levels Validation by oxygen isotopes. Geology 5 (7), 400-404.

Thingstad, T.F., and Lignell, R., 1997. Theoretical models for the control of bacterial growth rate, abundance, diversity and carbon demand. Aquatic Microbial Ecology 13 (1), 19-27.

Tozzi, S., Schofield, O., and Falkowski, P., 2004. Historical climate change and ocean turbulence as selective agents for two key phytoplankton functional groups. Marine Ecology Progress Series 274 123-132.

Tyrell, T., Holligan, P.M., and Mobley, C.D., 1999. Optical impacts of oceanic coccolithophore blooms. Journal of Geophysical Research-Oceans 104 3223-3241.

Tyrell, T., and Merico, A., 2004. *Emiliania huxleyi*: bloom observations and the conditions that induce them, in: H.R. Thierstein and J.R. Young (Eds.), Coccolithophores: from molecular processes to global impact. Springer Berlin Heidelberg, New York. pp. 75-98.

Ury, H.K., 1976. A Comparison of Four Procedures for Multiple Comparisons among Means (Pairwise Contrasts) for Arbitrary Sample Sizes. Technometrics 18 (1), 89-97.

Vardi, A., Van Mooy, B.A.S., Fredricks, H.F., Popendorf, K.J., Ossolinski, J.E., Haramaty, L., and Bidle, K.D., 2009. Viral Glycosphingolipids Induce Lytic Infection and Cell Death in Marine Phytoplankton. Science 326 (5954), 861-865.

Verbeek, J.W., 1989. Recent calcareous nannoplankton in the southernmost Atlantic. Polarforschung 59 (1/2), 45-60.

Verhulst, P.F., 1838. Notice sur la loi que la population pursuit dans son accroissement. Corresp. Math. Phys.

von Dassow, P., Ogata, H., Probert, I., Wincker, P., Silva, C.D., Audic, S., Claverie, J., and Vargas, C.d., 2009. Transcriptome analysis of functional differentiation between haploid and diploid cells of *Emiliania huxleyi*, a globally significant photosynthetic calcifying cell. Genome Biology 10 R114.111-R114.133.

Watson, A.J., Bakker, D.C.E., Ridgwell, A.J., Boyd, P.W., and Law, C.S., 2000. Effect of iron supply on Southern Ocean CO2 uptake and implications for glacial atmospheric CO2. Nature 407 (6805), 730-733.

Weir, B.S., and Cockerham, C.C., 1984. Estimating F-statistics for the analysis of population structure. Evolution 38 1358-1370.

Whitworth, T., III, and Nowlin, W.D., Jr., 1987. Water Masses and Currents of the Southern Ocean at the Greenwich Meridian. J. Geophys. Res. 92 (C6), 6462-6476.

Wilson, W.H., Schroeder, D.C., Allen, M.J., Holden, M.T.G., Parkhill, J., Barrell, B.G., Churcher, C., Hamlin, N., Mungall, K., Norbertczak, H., Quail, M.A., Price, C., Rabbinowitsch, E., Walker, D., Craigon, M., Roy, D., and Ghazal, P., 2005. Complete Genome Sequence and Lytic Phase Transcription Profile of a Coccolithovirus. Science 309 (5737), 1090-1092.

Wilson, W.H., Tarran, G., and Zubkov, M.V., 2002. Virus dynamics in a coccolithophore-dominated bloom in the North Sea. Deep Sea Research Part II: Topical Studies in Oceanography 49 (15), 2951-2963.

Wilson, W.H., Tarran, G.A., Schroeder, D., Cox, M., Oke, J., and Malin, G., 2002. Isolation of viruses responsible for the demise of an *Emiliania huxleyi* bloom in the English Channel. Journal of the Marine Biological Association of the United Kingdom 82 (3), 369-377.

Wilson, W.H., Turner, S., and Mann, N.H., 1998. Population Dynamics of Phytoplankton and Viruses in a Phosphate-limited Mesocosm and their Effect on DMSP and DMS Production. Estuarine, Coastal and Shelf Science 46 (2), 49-59.

Winter, A., Elbrächter, M., and Krause, G., 1999. Subtropical coccolithophores in the Weddell Sea. Deep Sea Research Part I: Oceanographic Research Papers 46 (3), 439-449.

Winter, A., Jordan, R.W., and Roth, P.H., 1994. Biogeography of living coccolithophores in ocean waters, in: A. Winter and W.G. Seisser (Eds.), Coccolithophores. Cambridge University Press, Cambridge. pp. 161-177.

Wright, S., 1965. The interpretation of population structure by F-statistics with special regard to systems of mating. Evolution 19 (395-420),

Young, J., Geisen, M., Cros, L., Kleijne, A., Sprengel, C., Probert, I., and Østergaard, J., 2003. A guide to extant Coccolithophore taxonomy. Journal of Nannoplankton Research Special Issue 1 1-125.

Young, J.R., and Westbroek, P., 1991. Genotypic variation in the coccolithophorid species *Emiliania huxleyi*. Marine Micropaleontology 18 5-23.

Yu, Y., Breitbart, M., McNairnie, P., and Rohwer, F., 2006. FastGroupII: A web-based bioinformatics platform for analyses of large 16S rDNA libraries. BMC Bioinformatics 7 (1), 57.

Zane, L., Bargelloni, L., and Patarnello, T., 2002. Strategies for microsatellite isolation: a review. Molecular Ecology 11 (1), 1-16.

Zondervan, I., Zeebe, R.E., Rost, B., and Riebesell, U., 2001. Decreasing marine biogenic calcification: a negative feedback on rising atmospheric pCO_2. Global Biogeochemical Cycles 15 (2), 507-516.